Heinrich Heine
Universität
Düsseldorf

Functional Calix[n]arenes as Building Blocks for the Solid-Phase Polymer Synthesis of Multivalent Glycocalix[n]arenes

Inaugural-Dissertation

To obtain the academic degree Doctor rerum naturalium (Dr. rer. nat.) of the faculty of Mathematics and Natural Science of Heinrich Heine University Düsseldorf

Submitted by

Alisa Isabel Kayser

Düsseldorf, September 2025

In liebevoller Erinnerung an diejenigen, die die Vervollständigung dieser Arbeit nicht mehr mit mir feiern können.

From the Institute of Organic Chemistry and Macromolecular Chemistry at the Heinrich Heine University Düsseldorf.

Published by permission of the

Faculty of Mathematics and Natural Sciences

Heinrich Heine University Düsseldorf

Supervisor: Laura Hartmann

Second reviewer: Guillaume Delaittre

Date of oral examination: 28.11.2025

This thesis was accomplished in the period between September 2020 and June 2024 in the Institute of Organic Chemistry and Macromolecular Chemistry at Heinrich Heine University in Düsseldorf under the supervision of Prof. Dr. Laura Hartmann.

I hereby declare that the thesis submitted is my own work without making use of impermissible aids, considering the "Rules on the Principles for Safeguarding Good Scientific Practice at Heinrich Heine University Düsseldorf". All direct or indirect sources used are acknowledged in the bibliography as references. I further declare that I have not submitted this nor a similar thesis at any other examination board in order to obtain a degree.

Düsseldorf, 25.09.2025

_____

Alisa Kayser

Acknowledgement

An dieser Stelle möchte ich mich bei allen jenen bedanken, die mich während der Entstehung dieser Arbeit begleitet und unterstützt haben.

Mein besonderer Dank gilt meiner Doktormutter, Frau Prof. Dr. Laura Hartmann. Ich danke ihr herzlich für die Möglichkeit, dieses spannende Thema zu bearbeiten, für die wertvolle fachliche Begleitung und dafür, dass sie stets ein offenes Ohr für Fragen und Probleme hatte. Ihre Unterstützung und ihr Vertrauen haben wesentlich zum Gelingen dieser Arbeit beigetragen.

Ebenso danke ich meinem Zweitgutachter Prof. Dr. Guillaume Delaittre für die Bereitschaft, diese Arbeit zu begutachten.

Ein herzliches Dankeschön geht an Frau Dr. Monir Tabatabai, die mir mit ihrer Expertise im Bereich der Calixaren Chemie, vielen hilfreichen Ratschlägen und tatkräftiger Unterstützung nicht nur während der Zeit dieser Promotion zur Seite stand, sondern auch mit großer Leidenschaft und Einsatz stets die Interessen der Studierenden vertritt.

Ein großer Dank geht zudem an Dr. Ulla Gerling-Driessen, von der ich sehr viel lernen durfte. Mit großer Geduld und Leidenschaft hat sie uns nicht nur ihr Wissen vermittelt, sondern stand auch jederzeit mit einem offenen Ohr zur Seite.

Ebenso möchte ich mich beim gesamten Arbeitskreis für das kollegiale und inspirierende Arbeitsklima bedanken. Ich bin sehr dankbar nicht nur für die tollen Arbeitskollegen, die ich hier kennenlerne durfte, sondern auch für die großartigen Freundschaften, die sich hieraus entwickelt haben. Ihr alle habt einen großen Beitrag dazu geleistet, dass ich immer gerne an diese Zeit zurückdenken werde. Im Besonderen möchte ich mich auch für die gute Zusammenarbeit im gemeinsamen Labor bei Dr. Serap Üclue, Melanie Schmidt und Sandra Mücke bedanken. Darüber hinaus möchte an dieser Stelle Melina Feldhof, Nina Jahnke und Dr. Theresa Seiler hervorheben, die sowohl auf fachlicher als auch auf persönlicher Ebene im besonderen Maße zum Erfolg dieser Arbeit beigetragen haben. Mein Dank gilt ebenso Stephanie Scheelen und Michaela Kitza, die immer mit Rat und Tat zur Seite standen.

Ich danke dem CeMSA@HHU (Center for Molecular and Structural Analytics an der Heinrich-Heine-Universität) für die Aufnahme der massenspektrometrischen und NMR-spektroskopischen Daten.

Vielen Dank auch an meine Bachelor- und Masterstudierenden, mit denen die Zusammenarbeit eine große Freude war. Einen großen Anteil an dieser Arbeit haben Daria Babushkina und Cleo Macke.

Schließlich danke ich meiner Familie und meinen Freunden, die mich in all den Jahren unermüdlich unterstützt haben. Mein Dank gilt meinem Freund Oliver Kubina, der mir mit Geduld, Zuspruch und Rückhalt in allen Phasen dieser Arbeit zur Seite stand. Zum Abschluss danke ich meinen liebsten Eltern, Anette und Günther Kayser, denen ich so vieles zu verdanken habe. Ihre Unterstützung, ihr Vertrauen und ihre Liebe haben mir stets den Rückhalt gegeben, meinen Weg zu gehen.

Parts of this thesis have already published or were presented at professional conferences:

Publications:

Alisa Kayser, Kai Klein, Daria Babushkina, Anna Sakse, Gisele Mouafo Kenne, Ulla I.M. Gerling-Driessen, Monir Tabatabai, Matthias Epple, and Laura Hartmann, "A Modular Solid Phase Synthesis Approach for Glycocalix[4]arene Derivatives and their Multivalent Presentation on Ultrasmall Gold Nanoparticles" Chemistry, A European Journal, **2025**, *31*, e202500497.

Own contribution: Synthesis of the calix[4]arene building block. Optimization of a solid phase synthesis strategy toward the glycocalix[4]arene derivatives C1-C3. The synthesis of the derivatives C1-C3 following the optimized route has been performed by Gisele Mouafo Kenne. The synthesis of the second set of glycocalix[4]arenes C4-C7 was performed with support from Daria Babushkina and Narges Irani. Characterization of the calix[4]arene-gold nanoparticle conjugates. Performance of the bacteria assay and fluorescence microscopy. Writing of the first manuscript draft. Collaborative writing of the final manuscript.

Conference Poster:

Alisa Kayser, Kai Klein, Daria Babushkina, Gisele Mouafo Kenne, Hajo Bösche, Anna Sakse, Matthias Epple, Laura Hartmann, „Glycocalix[4]arene Derivatives for the Functionalization of Ultrasmall Gold Nanoparticles", 32nd Joint Glycobiology Meeting, September 18-20, **2022**, Utrecht, Netherlands,

Abstract

Carbohydrates play a pivotal role in nature as recognition markers, mediating a variety of biological processes such as cell-cell communication, immune responses, and pathogen-host interactions. Their counterparts are carbohydrate-binding proteins, including lectins and enzymes, which specifically recognize glycans. However, the individual carbohydrate-protein interactions are typically weak, which is why multivalency, a simultaneous binding of multiple carbohydrate ligands to a protein receptor, is employed by nature to achieve sufficient binding avidity. The principle of multivalency is also explored by scientists generating so-called multivalent glycomimetic compounds. These types of compounds can help to gain a deeper understanding of the complex glycan-protein interactions. Furthermore, they are promising candidates as drug substances and diagnostic tools. The use of synthetic glycomimetics allows to apply tailored scaffolds for the multivalent presentation of carbohydrate epitopes, thereby achieving high binding affinities and selectivity. Additionally, pharmacological throwbacks of natural glycan-based therapeutics, such as poor metabolic stability, can be improved. Among these, calix[n]arenes have emerged as promising scaffolds due to their structural versatility and synthetic accessibility, allowing for the functionalization with carbohydrate ligands in a multivalent fashion.

This thesis focused on integrating calix[n]arene motifs into the solid-phase polymer synthesis (SPPoS) approach established by Hartmann et al., enabling the sequence-defined synthesis of glycocalix[n]arene-polymer conjugates. By combining the unique structural features of calix[n]arenes with the modularity and precision of SPPoS, this work introduced a new synthetic route to develop tailor-made multivalent glycocalix[n]arene conjugates with precisely adjustable ligand properties, such as valency, scaffold rigidity, linker length, and functional group positioning. Figure 1 gives an overview of the different topics addressed in this thesis and shows systematically depicted structures of the targeted molecules as well as their potential application field.

The first part of this thesis (see Figure 1, highlighted in blue) established the foundation for this work by synthesizing a calix[4]arene building block CBB1 compatible with the SPPoS method. A robust and straightforward synthetic strategy was developed, allowing for the preparation of versatile glycocalix[4]arenes. The synthetic route was demonstrated for a first set of homo- and heteromultivalent glycocalix[4]arene derivatives bearing eight carbohydrate residues on the upper rim. These compounds were further evaluated in a bacterial adhesion inhibition assay, supporting their potential as antibacterial agents.

Compared to monovalent ligands, the glycocalix[4]arene ligands exhibited significantly enhanced binding affinities, highlighting the advantageous cluster-like presentation of ligands on the calix[4]arene scaffold.

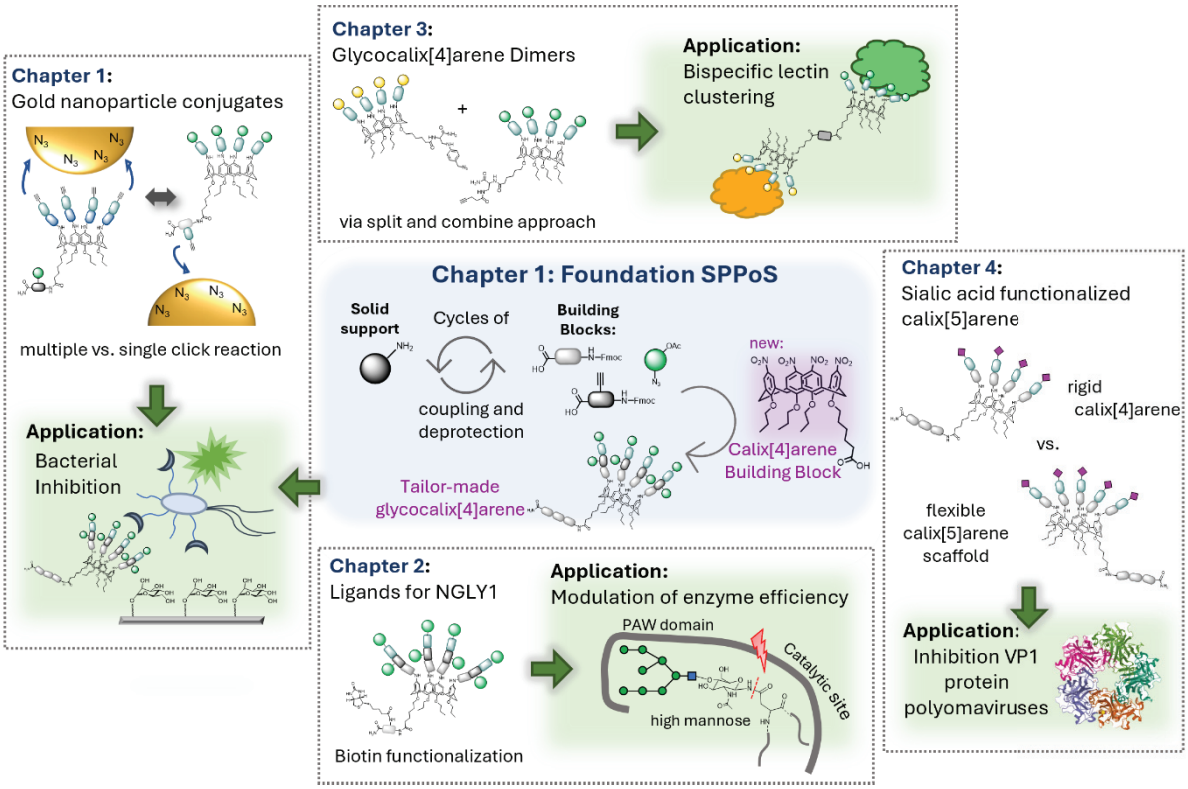

Figure 1: Overview of the topics addressed in this thesis: The development of a Solid-Phase Polymer Synthesis approach (chapter 1), shown in the middle (highlighted in blue), builds the foundation for all further projects/chapters (1-4), which are represented in the grey boxes. For each chapter, a systemically depicted target calix[n]arene derivative and the potential application field (highlighted in green) is shown.

Based on this, an advanced application of the modular glycocalix[4]arenes by attaching them onto ultrasmall gold nanoparticles (GNPs) was explored (see Figure 1, chapter 1). This approach leveraged the concept of "multivalency of multivalency," wherein the multivalency of the glycocalix[4]arene scaffold was further amplified by its presentation on a larger NP platform. It was reasoned that this could result in an even increased inhibitory potential against bacterial adhesion. Additionally, a key aspect of this part of the project was to achieve control over the ligand arrangement on the nanoparticle surface. To do so, a targeted ligand design was developed and successfully implemented by making only small alterations to the established SPPoS methodology. A second set of glycocalix[4]arenes was synthesized, exhibiting alkyne functionalities positioned either at the upper or lower rim, allowing for an attachment to the azide-functionalized GNPs via copper-catalyzed azide-alkyne cycloaddition (CuAAC) in a single or multiple fashion. The functionalized GNPs were

then evaluated in a bacterial adhesion inhibition assay and fluorescence microscopy. The results indicated the occurrence of large GNP-bacteria clusters, supporting the initial hypothesis.

The second part of this thesis (see Figure 1, chapter 2) expanded the scope of target proteins beyond lectins to carbohydrate-processing enzymes. While multivalent ligands have already been extensively explored for lectin targeting, their potential as regulators or inhibitors of enzymes remains relatively unexplored. In this work, the de-*N*-glycosylating enzyme *N*-glycanase-1 (NGLY1) was investigated as a potential target. NGLY1 contains a so-called lectin-like PAW domain that is known to interact with high-mannose glycans, suggesting that a synthetic multivalently mannose-functionalized calix[4]arenes could act as an artificial ligand and potentially affect enzymatic efficiency. To test this hypothesis, the mannose-functionalized glycocalix[4]arene derivatives were additionally equipped with a biotin tag to facilitate bioanalytical studies. The ligands were evaluated in different binding studies, such as a pull-down assay and an enzymatic activity test, comparing their effects on NGLY1 and related glycosidases, such as PNGase F. As no selective binding was observed, these studies suggest that further ligand optimization, such as adjusting the spatial arrangement of mannose residues, may be necessary to enhance binding affinity. The modularity of the SPPoS approach provides an ideal platform for further refinement in subsequent studies, making it possible to systematically vary ligand structures for future enzyme-targeting studies.

The SPPoS-based synthetic strategy was further enhanced with a split-and-combine approach to generate bispecific glycocalix[4]arene dimers. This approach allowed for the combination of two distinct glycocalix[4]arene units in a single structure, offering the ability to simultaneously target different carbohydrate-binding proteins. Such heterobifunctional ligands, also referred to as Janus-like structures, are of interest for biomedical and biotechnological applications, as they can be used for selective targeting or bridging interactions between different biomolecules. To explore this concept, homo- and heteromultivalent glycocalix[4]arene dimers were synthesized. The heteromultivalent dimer was designed to simultaneously bind two lectins with different specificities. As proof of concept, the model lectins Concanavalin A (Con A), which recognizes mannose, and Peanut Agglutinin (PNA), which binds to galactose, were chosen. To validate the bispecific binding capability, turbidity and precipitation assays were performed, demonstrating that the heteromultivalent dimer induced clustering of both lectins in solution, unlike the homomultivalent analogs. Beyond the presented proof-of-concept studies, these

bispecific glycocalix[4]arene dimers open new possibilities for applications as heterobifunctional ligands for therapeutic strategies, e.g., including lysosome-targeting chimeras (LYTACs). The modularity of the synthetic approach ensures that different carbohydrate epitopes (and other relevant binding motifs) can be integrated into a dimeric construct, expanding the potential for tailored biological interactions.

In the last part of this thesis (see Figure 1, chapter 4) calix[5]arenes, a higher homolog of calix[4]arenes, were explored as building block for SPPoS, thereby further enhancing the variety of available scaffolds for multivalent glycomimetics. Calix[5]arenes introduce additional structural features, including increased conformational flexibility, which may allow ligands to better adapt to the structural environment of their target proteins through a so-called induced fit mechanism. Additionally, their symmetric architecture provides an ideal platform for engaging pentameric protein assemblies, such as viral capsid proteins. To explore these interesting possibilities, a new calix[5]arene building block **CBB2** was synthesized and incorporated into the SPPoS approach, demonstrating the versatility of the method for different macrocyclic scaffolds. The primary focus was on the development of sialic acid-functionalized glycocalix[5]arenes as potential inhibitors of viral attachment proteins, specifically targeting the VP1 capsid protein of polyomaviruses. A series of glycocalix[5]arene derivatives with varying linker lengths and valency were synthesized to evaluate the influence of these parameters on binding interactions.

In conclusion, this thesis presents a versatile and modular synthetic approach to develop tailor-made glycocalix[n]arenes as demonstrated in multiple projects for various target proteins. Additionally, for some compounds, successful binding studies have been demonstrated, underlining the utility of glycocalix[n]arenes, e.g., as antibacterial agents. Moreover, this work provides a strong foundation for future studies on further multivalent calix[n]arene-based glycomimetics and their potential in biomedicine and biotechnology.

Table of Contents

Introduction

1.1 Carbohydrates in Nature

Carbohydrates are one of the pivotal building blocks in all living organisms and exhibit a wide range of biological functions. These include structural support and nutritional storage, while they also hold critical importance in mediating extrinsic and intrinsic cell interactions. For instance, the underlying recognition processes are involved in the mediation of cell communication with other cells and pathogen adhesives, fertilization, immune response, as well as intracellular trafficking and degradation of glycoproteins.[1, 2] Glycans distinguish themselves from other biologically relevant macromolecules, such as DNA, by their immense structural diversity.[3] The smallest units are monosaccharides. Based on the most common monosaccharides glucose, mannose, fucose, *N*-acetylneuraminic acid (Neu5Ac), *N*-acetyl-glucosamine (GlcNAc), and *N*-acetyl-galactosamine (GalNAc), an extensive array of different oligo- and polysaccharides can be linked via glycosidic bonds in a linear or branched fashion.[2] Additionally, in contrast to proteins and DNA, the biosynthesis of glycans is a non-templated, post-translational modification involving a variety of different enzymes. This highly complex and hardly foreseeable biosynthesis, alongside the resulting high structural diversity, makes the investigation and analysis of glycans challenging. For a thorough understanding of the glycan structure-function relationship, the development of analytical and biochemical tools are pursued. [4, 5]

1.1.1 The Role of Glycans in the Glycocalyx and their Interactions with Lectins

In living organisms glycans are present on the cell surface as a dense sugar coat that is also referred to as the glycocalyx. It is a very complex and dynamic environment of various glycoconjugates, mainly glycoproteins, glycolipids, or proteoglycans that are required for the cell-surface interactions, for example, with other cells, antigens, or pathogens (see Figure 2A).[2, 6] Many of these interactions are based on specific glycan-protein interactions. The complementary carbohydrate-recognizing proteins are called lectins. Lectins are defined as carbohydrate-recognizing proteins that are neither immunoglobulins nor have an enzymatic activity.[7] Since the presumed first discovery of a lectin by Stillmark in 1888, various lectins widely distributed in nature, from animals and plants to bacteria and viruses, have been identified.[8] They can be classified into lectin families, including legume lectins (plant lectins), C-type lectins and galectins (animal lectins), as well as viral agglutinins and toxins.[2, 7, 9, 10] The interaction between lectins and carbohydrates relies primarily on hydrogen bonding, as commonly occurring for carbohydrates due to their hydroxyl groups. They can act as both donors and acceptors towards the complementary protein surface.

The hydrogen bonds formed can be either direct or indirect with water molecules as a moderator.[2, 10, 11] Additionally, van der Waals interactions, hydrophobic interactions, electrostatic interactions, and metal coordination can contribute.[12] For the latter Concanavalin A (Con A) from the jack bean can be used as an example. Con A was the first pure lectin that was isolated by Sumner in 1919 and is a very well-studied model lectin from the legume class.[10] Each Con A monomer has one conserved carbohydrate-binding domain (CBD), favoring α-D-mannose and α-D-glucose as well as two divalent metal binding sites for Ca^{2+} and Mn^{2+} ions. These metal interactions are crucial for the integrity of protein conformation and therefore required for carbohydrate binding.[13] Interestingly, in solution, the monomer assembles into oligomers depending on the pH value. Above pH 6.9, tetramers are formed, whereas at pH below 5.9, Con A is present as a dimer. Another relevant class to be discussed are lectins derived from pathogens, as they have been shown to play a critical role in adhering to cell surfaces, potentially leading to an infection of the host. Thus, they represent a promising research frontier for the development of antiviral and antibacterial therapeutics. So-called FimH, a fimbrial adhesive lectin from *Escherichia coli* (*E.* coli) bacteria that causes urinary tract infections, serves as a well-known model for such studies. The mannose-binding lectin is found at the tip of type 1 fimbriae of the bacteria.[14, 15] In the last decades, many working groups reported α-D-mannopyranoside-based ligands for the bacterial lectin and additionally demonstrated that the affinity towards FimH was significantly increased when alkyl chains were introduced to the anomeric position at the mannose residues. Structural studies revealed that this can be accounted for by the hydrophobic interactions of the alkyl chains with two tyrosine residues (Tyr48 and Tyr137) that are located at the entrance of the binding site.[12, 16] In the case of many viral families, additionally, electrostatic interactions come into play. The viral lectins interact specifically with charged carbohydrate epitopes on the cell surface for the attachment to the host cell.[17, 18] For instance, some polyomavirus such as human BK virus (BKPyV)[19] and the more recently discovered Merkel cell polyomavirus (MCPyV)[20] were reported to exhibit sialic acid-recognizing binding sites on their major capsid proteins VP1 that are critical for the infectious entry of the viral genome.

However, the non-covalent binding between a lectin and a monovalent carbohydrate epitope is typically weak and often not highly specific (compared to enzymes). Consequently, the question arises of how the concept of the so-called sugar code and the associated transmission of specific information work.[12] A crucial concept that is employed in nature is the principle of multivalency. This means the multiple interactions of a multivalent ligand with a corresponding receptor result in a higher binding avidity and

specificity. It was shown for various lectins that the multivalent interaction with glycans on the cell surface exhibits an even increased affinity than the corresponding single carbohydrate interactions would predict - a phenomenon that was reported by Lee et al. as the *glycoside cluster effect*.[21-23] To account for this observation, several possible mechanisms by which a multivalent ligand can interact with protein receptors were proposed (see Figure 2B).[6, 22, 24-27] For oligomeric receptors a typical chelate effect or alternatively in case of single receptors a clustering mechanism can occur when the multivalent ligand is able to overcome the distance between recognition sites of the proteins. This can lead to a great enhancement of overall avidity and can generally be explained by the lower entropic cost paid for a second binding event. Further, some receptors might possess binding subsites in addition to the primary binding site that can be engaged by a multivalent ligand. Additionally, the locally enriched concentration of binding carbohydrate epitopes can lead to higher affinity for statistical reasons. This can also be considered as a rebinding or sliding mechanism that increases the probability of another epitope to bind to the same or a proximal binding site. Finally, the steric stabilization of the ligand against other opposing binding partners can cause a beneficial effect. Depending on the nature of the lectin and ligand, one or more of the described binding modes may occur simultaneously.[24, 26] In summary, by looking beyond monovalent interactions, a much more complex picture emerges, and it becomes clear that not only valency, but also the overall ligand architecture is critical for a high binding avidity and specificity.[24]

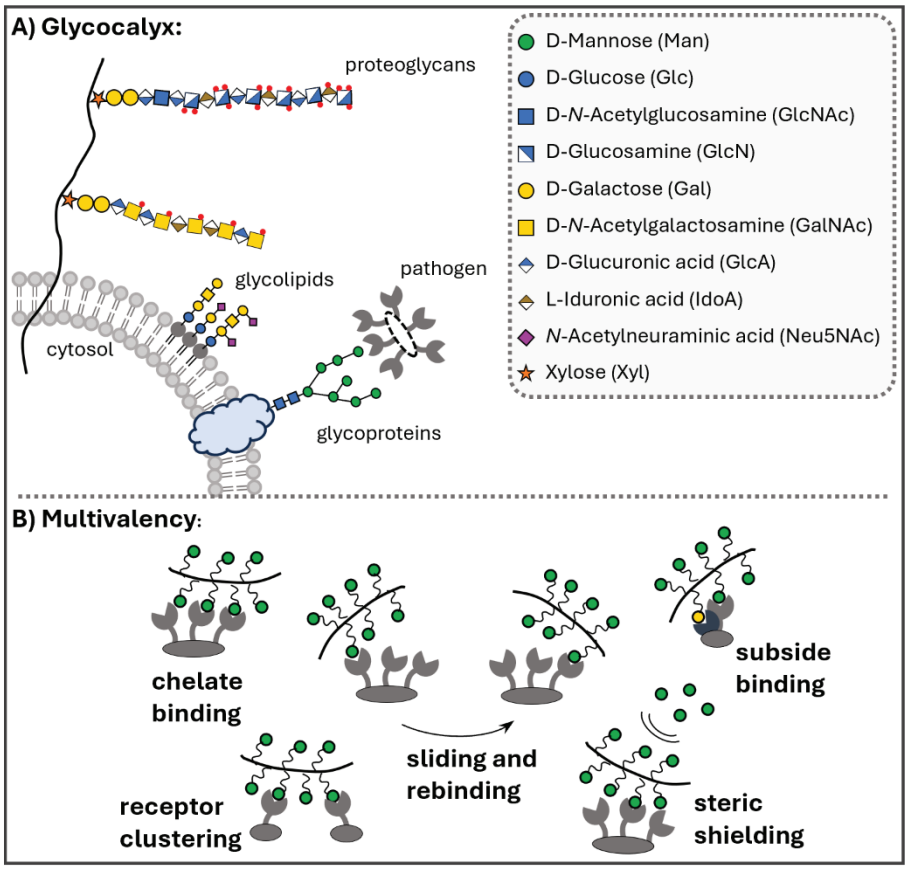

Figure 2: A) Schematic depiction of glycocalyx and pathogen interaction, B) Five mechanisms of multivalent ligand-receptor binding.

1.1.2 The Role of Carbohydrate-processing Enzymes in Biosynthesis.

Carbohydrate-binding domains, which have been discussed above, occur not only on lectins but on other proteins, including carbohydrate-processing enzymes, which are a second topic of interest in this work. In general, enzymes are defined as a class of proteins that catalyze biochemical reactions in living organisms without being consumed or altered themselves within the process.[28] In this chapter, the focus lies especially on enzymes whose substrates and thus natural ligands are glycans. This includes, for example, glycosyltransferases and glycosidases, which are crucial for the biosynthesis and degradation of glycoproteins.[29] Within the class of glycoproteins, it can be distinguished between *O*-linked and *N*-linked glycans as the two most common types of glycans.[3] The glycosylation of proteins has an influence on their proper folding, which is important in order to preserve the biological function.[1] While the synthesis of *O*-linked glycans occurs in the Golgi apparatus by stepwise addition of GalNAc residues to Serine (Ser) or Threonine (Thr) side chains of proteins, the *N*-linked glycans are assembled as a lipid-bound precursor in the endoplasmic reticulum (ER) and transferred in block either post- or co-translational to

proteins containing the amino acid sequence Asn-Xaa-Ser/Thr (Asn = asparagine, Xaa can be any amino acid besides proline). Initially, an oligomer consisting of $(Glc)_3$-$(Man)_9$-$(GlcNAc)_2$ is transferred by the Oligosaccharyltransferase (OST) to the side chain amine of the asparagine to form a *N*-glycosidic bond.[30] The three terminal glucose (Glc) residues play a role in protein quality control in the ER, as they are recognized by chaperones, such as Calnexin and Calreticulin, that act as folding sensors.[31] Correctly folded *N*-glycoproteins can then be translocated to the Golgi apparatus for further glycan modification with additional monosaccharides. In this way, different types of *N*-linked glycans, such as high-mannose, complex, and hybrid types are formed. In contrast, if the protein is revealed to be misfolded, it is translocated to the cytosol, where the degradation of the misfolded glycoprotein by the proteasome is initiated. This process, called ER-associated degradation (ERAD), involves the removal of the glycan residues from the protein backbone by de-*N*-glycosylating enzymes prior to the protein degradation by the proteasome.[32-34]

In this thesis, the focus lies on the de-*N*-glycosylating enzyme peptide-*N*-glycosidase (PNGase) and especially its interactions with multivalent ligands are investigated. PNGase belongs to the enzyme class of amidases (or amidohydrolases) and catalyzes the cleavage of the glycosidic bonding between the innermost GlcNAc residue and the asparagine side chain of *N*-linked glycoproteins. The hydrolysis of the amide bond releases the full glycan intact and results in the formation of aspartic acid (see Figure 3).[34] PNGase is a widely conserved cytosolic enzyme in plants, bacteria, and eukaryotes, including humans.[32, 34-36] In higher eukaryotes, it is also referred to as *N*-Glycanase-1 (NGLY1 for humans or Ngly1 for mouse).[34] Previous studies have investigated the structure of NGLY1 and revealed that the enzyme is composed of three domains: the central transglutaminase domain with the catalytic site, the *C*-terminal PAW domain, and the *N*-terminal PUB domain.[34] While the latter is known to bind to other ERAD components, we here focus on the carbohydrate-binding PAW domain (see Figure 3). High-mannose-type glycans were found to be recognized by this domain and appear to facilitate substrate processing. For yeast PNGase, it was observed that the carbohydrate-binding site (PAW domain) is critical for the enzymatic activity.[37] This was also confirmed for mouse PNGase by Zhou et al, when the enzyme activity of the full-length protein was compared to *C*-terminal truncated mutants without the PAW domain.[32] Even though the exact role of NGLY1 is still not completely understood, it has been shown to be involved in the ER-associated degradation (ERAD) of misfolded glycoproteins, which plays an important role in securing cellular quality control and protein homeostasis.[35, 38] In the case of mutations of the ngly1 gene, a rare genetic disorder called NGLY1 deficiency can occur. Affected patients suffer from various and

oftentimes very severe symptoms.[38] Therefore, high interest arose in a better understanding of the biological function of NGLY1.

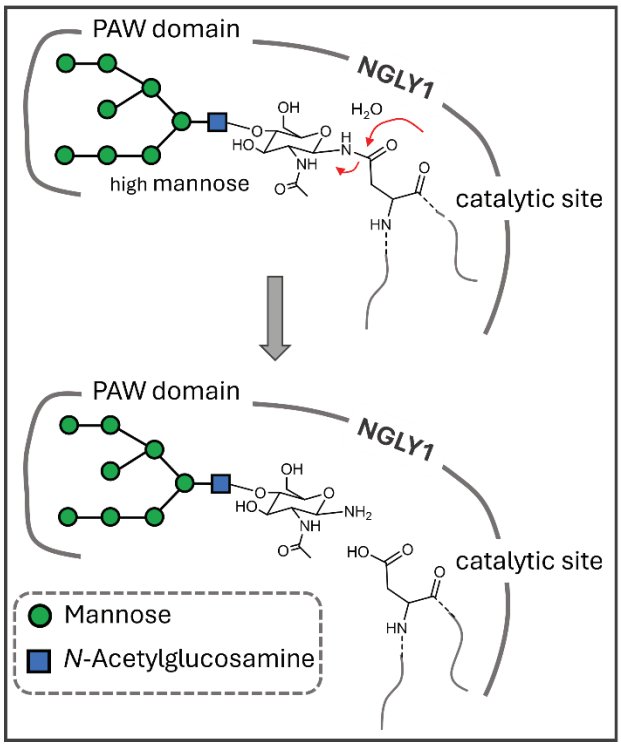

Figure 3: Schematic Depiction of NGLY1 catalyzed hydrolysis of high-mannose-type glycoprotein after Tomlin et al.[33]

1.1.3 Glycomimetics for the Design of Glycan-based Therapeutics.

Carbohydrates are vital for numerous biological processes and are thereby associated with many diseases such as cancer, infections and immune dysfunctions.[39-43] Encouraged by the advances made in the field of glycobiology, chemists embarked upon the development of synthetic carbohydrate ligands with the objective of mimicking the natural carbohydrate ligands, so-called glycomimetics. These types of compounds arouse high interest as they are promising candidates as drug substances and diagnostic tools.[44-46] A major advantage of a chemical approach is the possibility of modifying the molecular structure to improve the drug characteristics of the pharmaceutical active ingredient. In this way, the pharmacological drawbacks such as poor metabolic stability, which is typically linked to carbohydrate-based drugs, can be overcome, and low binding affinities can be improved.[46, 47] Moreover, the synthetic preparation of carbohydrate drugs allows for better control over purity and dispersity compared to compounds derived from biological sources.[48, 49]

The majority of the investigated glycomimetic compounds target extracellular lectins, for example, C-type and I-type lectins, as well as pathogen lectins.[44, 47, 50] Inspired by nature to overcome the weak single carbohydrate interactions (see chapter 1.1.1), a common

approach applied for antiadhesive therapy is the development of multivalent glycomimetics that present the terminal binding epitopes on a non-natural scaffold.[6, 50] In line with the advancements in organic synthesis, a variety of synthetic glycoconjugates have been investigated in search of high-affinity binders and inhibitors for numerous pathogen lectins and toxins.[51-54] To do so, it is crucial to carefully study the receptor structure to create a ligand design that fits the carbohydrate binding sites ideally and reaches multiple sites simultaneously (so-called receptor-based design) whilst minimizing the entropic cost of binding. [12, 47] It has been demonstrated that valency and topology as well as nature of spacer and scaffold can have a pivotal impact on binding affinity and selectivity of the respective glycomimetic.[24, 26, 55-61] Diverse artificial scaffolds like polymers[62, 63 64], dendrimers[65], nanoparticles[66, 67], macrocycles like calix[n]arenes[68] (see chapter 1.2.2) or cyclodextrins[69] as well as small molecule scaffolds (also referred to as glycoclusters)[70, 71] have been explored in the last decades (see Figure 4). Multivalent presentation of carbohydrate epitopes on polymeric backbones often shows an affinity enhancement due to a gain in both binding enthalpy and entropy compared to low-molecular-weight ligands, which usually have lower valency.[63, 72] On the other hand, glycopolymers lack structural precision, even though great advances regarding living polymerization techniques have been made.[72] To give access to detailed studies of the structure-function relationship, monodisperse and defined homo- and heteromultivalent glycomimetics have to be synthesized. An approach using solid-phase polymer synthesis established at the working group of Prof. Hartmann, discussed in more detail in the following chapter 1.3, allows for the synthesis of sequence-defined glycomacromolecules based on oligo(amidoamines) backbones.

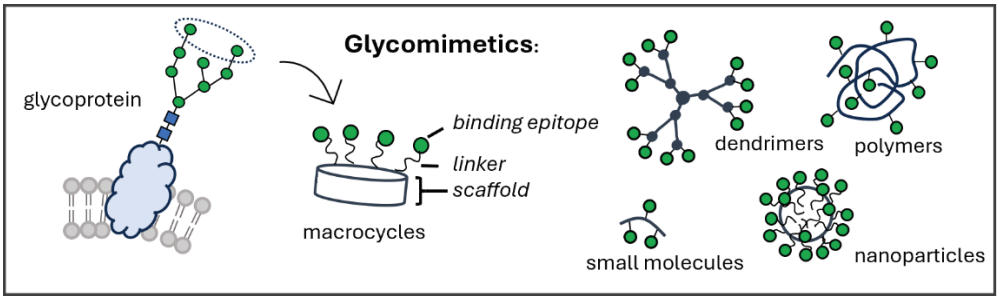

Figure 4: Schematic depiction of glyco-functionalized scaffolds as examples of glycomimetic structures.

Besides lectins, carbohydrate-processing enzymes have been addressed as therapeutic targets since the alteration in the glycocalyx glycan compositions, e.g., hyper sialylation or truncation, can oftentimes be correlated to a diseased state and is a direct consequence of an altered expression of glycosidases and glycosyltransferases.[40, 47] The modification of the regular glycan composition of the glycocalyx has also been used as a therapeutic tool. For

instance, glycomimetic neuraminidase inhibitors, oseltamivir (Tamiflu®) and zanamivir (Relenza®), have successfully been established for influenza treatment.[73, 74] The mode of operation is the inhibition of the cleavage of terminal sialic acid residues on the host cells, preventing the propagation of the virus and thus the progression of the disease. Besides these well-known examples, several other glycomimetic enzyme inhibitors have already been approved for the treatment of various diseases, such as diabetes or lysosomal storage disorders.[44, 47] However, in contrast to lectins, the multivalent effect as a strategy to enhance enzyme inhibition has only recently been explored for glycosidase inhibitors. This might be accounted for by the single substrate binding sites that are usually linked to enzymes.[45] The groups of Nierengarten and Compain were first to find a significant increase in Jack bean (JB) α-mannosidase inhibition in comparison to the monovalent control structure exploiting a 12-valent fullerene glycocluster.[75] In the following decades several more multivalent structures have been demonstrated to exhibit pronounced multivalent effects for several glycosidases [76-78] To gain a deeper understanding of the underlying binding modii numerous studies have been conducted, including atomic force microscopy (AFM), dynamic light scattering (DLS), electron microscopy imaging (EM), electrospray ionization-mass spectrometry (ESI-MS), analytical ultracentrifugation sedimentation velocity (AUC-SV) and crystallography experiments.[45, 78-80] Different binding modes were proposed depending on the size and shape of the multivalent inhibitor and the investigated glycosidase. For instance, the dimeric JB α-mannosidase crystallographic investigation revealed that sandwich-type complexes can be formed when employing suitable multivalent inhibitors that can reach several binding sites simultaneously.[80] In this case, the observed chelate effect can account for the observed high increase in binding affinity and reminds of the well-studied carbohydrate-lectin interactions. For other investigated glycosidases having rather deep and less accessible active sites, it is assumed that the enzyme inhibition might be due to the steric blocking or a structural modification of the binding site.[81, 82] While multivalency is already well established in the development of glycomimetics targeting lectins, an increasing number of promising results have been reported for multivalent glycosidase inhibition, highlighting the still great potential for drug discovery in this field.[45]

1.2 Calix[n]arenes

Calix[n]arenes are classified as the metacyclophanes, yielding from the condensation of certain p-alkylphenols with formaldehyde.[83, 84] Initially, the first condensation reactions of phenol and formaldehyde were carried out by Adolph von Bayer in the 19th century. However, the analytical methods of the time were not sufficient to determine the chemical structure of the products obtained.[84, 85] A few decades later, in the early 20th century, Leo Baekeland

was working on the phenol-formaldehyde chemistry and patented a process yielding products known as phenoplasts or “Bakelite” achieving great commercial success.[84, 86] In the 1940s and 50s, the research group of Zinke postulated the formation of cyclic tetramers, referred to as "Mehrkernmethylenphenolverbindungen", from p-alkylphenols and formaldehyde using a base-catalyzed one-pot synthesis strategy.[83, 87, 88] Later in the 1970s, C. David Gutsche became aware of this class of compounds and recognized their potential to form host-guest complexes. He especially envisioned the application as a synthetic enzyme mimetic. Furthermore, Gutsche established a general nomenclature and introduced the term calix[n]arene because the structure of the cyclic macromolecules reminds of a Greek chalice [calix (Greek) = chalice]. The prefix "arene" refers to the involvement of aromatic rings, and the number in the brackets refers to the number of units that comprise the macrocycle.[83, 84]

1.2.1 Synthesis and Functionalization of Calix[n]arenes.

Gutsche significantly contributed to the research field of calix[n]arenes by not only establishing a general nomenclature but also elucidating the composition of the product mixture obtained from previous one-pot base-catalyzed methods after Zinke-Cornforth (three-step synthesis) and Petrolite/Munch (one-step synthesis, see Figure 5).[83, 87, 89-91] He demonstrated that for both procedures the mixture consisted mainly of cyclic condensation products with varying numbers of p-alkylphenol units. The main macrocycles were composed of four, six, and eight units. Additionally, the one-step Munch conditions yielded a bishomooxacalix[4]arene derivative, that exhibits one CH_2OCH_2 bridge.[90]

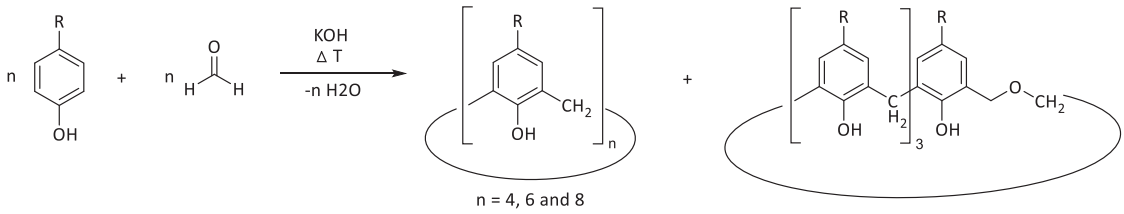

Figure 5: Reaction scheme of calix[n]arenes one-step synthesis after Munch.

Furthermore, Gutsche and coworkers have extensively studied the influence of reaction parameters on the product composition and observed that by particularly varying the reaction temperatures, the equivalents of base and the size of the base cation, it is possible to control the ring size. As an overall trend, it was found that the p-alkyl-calix[8]arene presumably is the kinetically controlled product that was obtained as the main product when p-alkylphenols and formaldehyde were treated with small amount of base in solvents with boiling temperatures lower than 180° C. In contrast, when the amount of base was

increased, and especially larger cations such as rubidium were employed, the hexamer was found to be the main product instead. This was also referred to as the kinetically controlled product involving a template effect from the cation. In order to obtain the tetramer as a main product, higher temperatures (~ 220 °C) had to be applied, as the p-alkyl-calix[4]arene were assumed to be the thermodynamically controlled product.[90-92] Based on these studies, the group was able to optimize the one-pot procedures, which made the calix[4]-, calix[6]-, and calix[8]arene derivatives available in good yields.[92-95] In terms of reaction mechanism, the group came to the conclusion that first linear dimeric, trimeric, and tetrameric mono-hydroxymethylated and/or di-hydroxymethylated derivatives are formed that undergo the cyclisation under the loss of formaldehyde and water in the next step. X-ray crystallographic data showed that the linear tetramers occurred in a conformation that can be described as *zig-zag* conformation. It was therefore assumed that a pathway via an intermolecular association of two linear tetramers through hydrogen bonding to form calix[8]arene derivative is more likely than the direct intramolecular cyclization, as this would perquisite a conformational change. Subsequently, when applying sufficient reaction temperatures (~220 °C), the cyclic octamer is converted to the calix[4]arene derivative. Interestingly, the odd-numbered calix[n]arenes with n = 5 or n = 7 are still not as feasible as the even-numbered homologs using a one-pot synthesis.[96-98] It is assumed that this tendency can be accounted for by better conformational stability due to the formation of hydrogen bonding in the even-numbered homologs. [91, 99] Another procedure is the stepwise synthesis route that was developed by Hayes and Hunter.[100] This approach was further pursued by Kämmerer and later by Böhmer.[101] In this method, fragments are condensed in a stepwise manner, followed by the final cyclization. An advantage of this synthesis route compared to the "one-step method" is the ability to obtain calixarene derivatives with different substituents at the para position.[100, 101] However, this approach is extremely laborious and achieves only low yields.

Due to rotation through the calix[n]arene, the calix[n]arenes can exist in different conformations.[102, 103] Additionally, with respect to the plane of the ring, an upper and lower rim can be defined. For calix[4]arenes, Gutsche established the terms cone, partial cone, 1,2-alternate, and 1,3-alternate conformation as illustrated in Figure 6.[104] Both X-ray structure analyses and thermal NMR analyses showed that *tert*-butyl-calix[4]arene (R=H) exists preferably in the cone conformation at room temperature.[92, 104-107] This finding can be explained by the formation of strong hydrogen bonds between the phenolic hydroxyl groups in the cone conformation.[90, 106, 108, 109] For the larger calix[n]arenes (n = 5, 6 or 7) the energy barrier for rotation around the Ar-CH_2-Ar bonds is lower and the compounds exhibit a higher

flexibility as determined by dynamic NMR spectroscopy. Interestingly, for calix[8]arene, the temperature dependency of the methylene protons in ^{1}H-NMR spectra is very similar to that of the calix[4]arene.[103, 110]

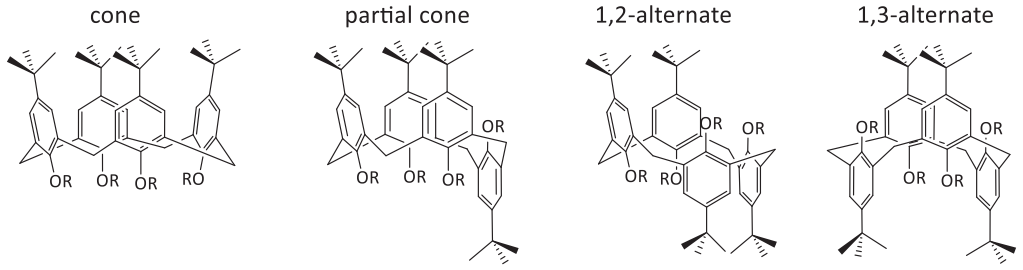

Figure 6: The four conformations of tert-butyl-calix[4]arene after Gutsche.

Since the initial elucidation of their structure and the synthesis of p-alkyl-calix[n]arenes are feasible, functionalization routes to various calix[n]arenes derivatives have been extensively investigated.[92, 111, 112] The *tert*-butyl-calix[4]arene, which is commercially available, has proven to be a suitable precursor and is therefore oftentimes chosen as a starting material.[113, 114] Functionalization routes of larger calix[n]arenes (n = 5, 6, 8) are also known, but are not discussed in further detail here.[115-117] Most commonly, *tert*-butyl-calix[4]arene offers two points of approach for functionalization: On the one hand, functionalities such as alkyl, allyl, ester, ketone, or amide groups can be introduced at the lower rim by alkylation or acylation of the phenolic hydroxyl group.[114-116, 118] Furthermore, at the upper rim, the *tert*-butyl group can be easily removed through trans-alkylation in the presence of aluminum and an acceptor compound (e.g., toluene or phenol), followed by electrophilic substitution at the para-position.[113, 119-121] Furthermore, regioselective reactions are required. For calix[4]arene, it has been shown that regioselective reactions at the phenolic hydroxyl groups can be achieved by varying the reaction conditions, such as base strength, temperature, reaction time, or reactant equivalents.[118, 122, 123] Another approach is to selectively cleave certain ether or ester bonds.[124, 125] To date, mono-, di-, and tri-substituted derivatives can be achieved selectively.[126] This selectivity at the lower rim can also influence the reactivity of the para-position at the upper rim, as phenol ester or ether units are less reactive towards substitution reactions than non-substituted phenol units.[127, 128] Furthermore, by the introduction of larger substituents such as propyl groups at the lower rim, calix[4]arenes can be fixed in all possible conformations, as the substituents sterically hinder the rotation through the cycle.[129-131]

Due to the very extensive and increasingly complex modification opportunities of calix[n]arenes, many fields of application have opened for this substance class. As Gutsche

had already recognized, a particularly intriguing property of calix[n]arenes is their ability to form host-guest complexes with metal ions, smaller guest molecules, as well as proteins.[130, 132-139] Based on this, the implementation of calix[n]arene derivatives for sensor technology[140, 141] wastewater decontamination[142-144], or as catalysts[128, 145] has already been demonstrated. Moreover, calix[n]arene derivatives have been shown to be promising candidates for numerous medicinal applications as therapeutic molecules, drug delivery systems, or for bioimaging.[146-150] In this thesis, the interest lies particularly in the class of glycocalix[n]arenes, which will be discussed in more detail in the next chapter.

1.2.2 Glycocalix[n]arenes

Pioneering work in the field of glycocalix[n]arenes was carried out in the working groups of Ungaro and Dondoni, who first developed synthetic routes to introduce carbohydrate moieties at the wither rim of calix[4]arene derivatives in the mid-1990s.[151, 152] In an initial work, Marra et al. employed a route in which the *O*-glycosylation of the lower rim of a calix[4]arene via a Mitsunobu reaction was achieved. However, this method resulted in low stereoselectivity at the anomeric carbon of the carbohydrate and poor water solubility.[151] Improvements in this regard were achieved through an alternative route in which a 1,3-dihydroxymethyl calix[4]arene derivative was treated with thioethyl glycosides as glycosyl donors in the presence of copper(II) triflate.[152] In the following decade, many more synthetic procedures to obtain calix[n]arene *O*-, *C*-, *N*-, and *S*- glycosides have been studied and successfully implemented.[153] An effective and therefore commonly used synthetic method to prepare multivalent glycocalix[n]arene is amide coupling (see Figure 7A).[154-156] In this approach, carbohydrates equipped with amine linkers are coupled to the carboxyl-functionalized calix[n]arene derivatives or vice versa. For the activation of the carboxyl group, coupling agents[154, 155] or reactive carboxylic acid chlorides[156] were used under alkaline conditions. To avoid steric hindrance, amino acids were coupled first to the calix[4]arene scaffold to act as spacers.[154] For instance, Roy et al. expanded the amid coupling method and were able to obtain dendrimers with up to sixteen carbohydrate units in this way.[156] Further, several studies showed the successful synthesis of glycocalix[4]arenes via the multiple addition of several glycosyl isothiocyanates to amin-functionalized calix[n]arenes via the formation of a thiourea bond at the upper or lower rim (see Figure 7B).[68, 157-159] Moreover, since the introduction of the copper-catalyzed alkyne-azide cycloaddition (CuAAC) and the concept of click reaction in general, also the field of synthetic glycoclusters took advantage of the effectiveness, selectivity and feasibility of this kind of reaction. Dondoni and Marra demonstrated the efficient synthesis of *C*-glycosylated calix[4]arenes using CuAAC (see Figure 7C).[160] Thereby, the click reaction was performed in

both ways: Either a glycosyl azide was attached to an alkyne-functionalized calix[4]arene scaffold or vice versa. Further, Fiore et al. demonstrated that thiol-ene coupling (TEC) can be used for the efficient coupling of glycosyl thiols to both rims of allyl-functionalized calix[4] arene derivatives (see Figure 7D).[161]

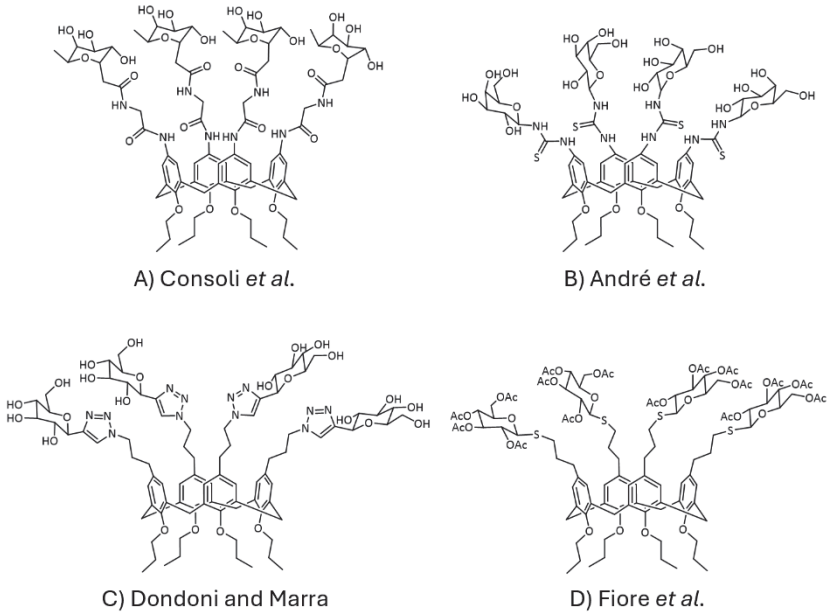

Figure 7: Examples of glycocalix[4]arenes prepared via different synthetic methods.

Exploiting the synthetic methods described, a large number of calix[n]arenes bearing multiple carbohydrate moieties of different kind such as mannose[162], glucose[160, 161], galactose[68, 161], *N*-acetyl-glucosamine[158], *N*-acetyl-galactosamine[156], sialic acid[163, 164], fucose[155] or lactose[68] were prepared and tested for the binding to several medicinal relevant protein targets like bacterial and viral lectins, human galectins and toxins.[53, 68, 155, 158, 162, 164] Thereby, calix[n]arenes revealed to be a particularly interesting platform for ligand presentation as the size and conformation of the macrocycle can be readily varied, providing access to adaptable glycoclusters with increased binding affinities and specificity. For instance, Consoli et al. reported the synthesis of a set of *N*-acetyl-β-D-glucosamine functionalized calix[4]arene analogs, that are conformationally blocked in the cone conformation and mobile calix[8]arene derivatives.[158] The direct binding of the compounds to the *N*-acetyl-β-D-glucosamine specific lectin WGA (wheat germ agglutinin) was proven by turbidity measurements. Interestingly, the performed WGA-dependent hemagglutination inhibition assay showed a higher inhibiting potency of the more rigid calix[4]arene ligands compared to the flexible calix[8]arene ligands. Further, they found that the incorporation of amino acids as spacers between the calix[n]arene scaffold and the terminal carbohydrate moieties was beneficial regarding the inhibition potential. In

contrast, André et al. found that flexible calix[6,8]arene derivatives carrying galactose or lactose residues show especially low IC_{50} (half-maximal inhibitory concentration) values towards the AB toxin Viscum album agglutinin (VAA).[68] Interestingly, they further observed in cell assays that different conformations of the lactosyl-calix[4]arene resulted in the discrimination of galectin-1 and -4 versus galectin-3. In another study, Cecioni et al. investigated the impact of the topological isomerization of calix[4] arene-based glycoclusters towards the bacterial lectin PA-IL from *Pseudomonas aeruginosa* using isothermal titration calorimetry (ITC). They observed that the calix[4]arene in partial cone and 1,3-alternate conformation showed strongly enhanced binding affinity compared to the cone conformation. The authors assumed that a chelating binding mechanism might account for this result.[53] Furthermore, another intriguing structural feature of calix[n]arenes is the possibility to introduce different motifs at the upper and lower rim. In this way, carbohydrate compounds with dual functionalities could be created.[161] Beyond carbohydrate ligands, other binding motifs can be incorporated into the ligand design. For instance, the research group of Geraci employed this strategy for the synthesis of a cancer vaccine.[165] In this approach, a Tn-antigen (Thomsen-nouveau antigen) motif was presented multivalently at the upper rim, while an immunoadjuvant, designed to enhance the immune response, was attached at the lower rim. This method of antigen presentation was intended to mimic the surface of cancer cells. Initial in vivo studies confirmed multiple times increased immune response from the multivalent calix[4]arene derivatives compared to the monovalent derivatives.

The described examples demonstrated the high utility of these platforms to create adaptable glycomimetic compounds to study the complex carbohydrate-protein interactions. Beyond the glycosyl cluster effect, which was observed for calix[n]arene-based glycoclusters, they have also helped to provide further insights into the importance of topology and flexibility of the scaffold, which are crucial for optimizing binding affinity and specificity towards different protein receptors. Further advances in the synthesis of more complex glycocalix[n]arenes are promising to enhance their applications and to fulfill their therapeutic potential.

1.3 Solid-Phase Synthesis

Developed by Bruce Merrifield in the 1960s for the synthesis of peptides and proteins, solid-phase synthesis is now considered an established method (solid-phase peptide synthesis, SPPS).[166, 167] This method is not only suitable for the assembly of amino acids into peptides but has also been extended to the use of various monomers. In particular, other

biomacromolecules, such as polysaccharides[168] and polynucleotides,[169] have been successfully synthesized using solid-phase synthesis. Moreover, the method can be applied to the synthesis of non-natural polymers. For example, Hartmann et al. introduced solid-phase polymer synthesis (SPPoS) for the preparation of monodisperse macromolecules based on poly(amidoamine) (PAA) scaffolds.[170-172]

1.3.1 Solid-Phase Peptide Synthesis (SPPS)

Already in the beginning of the 20th century the first peptide was synthesized in solution by Emil Fischer.[173, 174] However, as the chain length increases, peptide chains are prone to aggregation and become less soluble, which restricted the solution phase peptide synthesis.[166, 167] This issue was circumvented by the development of solid-phase peptide synthesis (SPPS), which enables the synthesis of long peptides and proteins.[175-177] The fundamental methodology of solid-phase peptide synthesis, as proposed by Merrifield, is depicted in Figure 8.[166, 167] A crucial aspect of this approach is that the peptide chain remains firmly anchored to the solid phase during the synthesis. The covalent attachment of amino acids proceeds in a linear fashion, starting from the *C*-terminus elongating toward the *N*-terminus. The initial amino acid, which is protected at its α-amino function with a temporary protecting group, is covalently bound via its carboxyl group to the solid phase. Subsequently, the temporary protecting group is removed, and the next α-protected amino acid is coupled to the free *N*-terminus of the chain. In this way, amino acids are assembled stepwise in repetitive cycles of deprotection and coupling. When the desired sequence is obtained, subsequently the peptide is cleaved from the solid phase in the final step. After each coupling step, a washing step is conducted, whereby an excess of reactants and by-products can be easily separated by filtration. This simplifies purification compared to tedious liquid phase synthesis and allows the use of large excesses of reactants to ensure complete conversion.[166, 178] Nowadays, using standardized protocols, a wide variety of peptides, also so-called difficult sequences, can be prepared manually or automatically by using peptide synthesizers.[179-181]

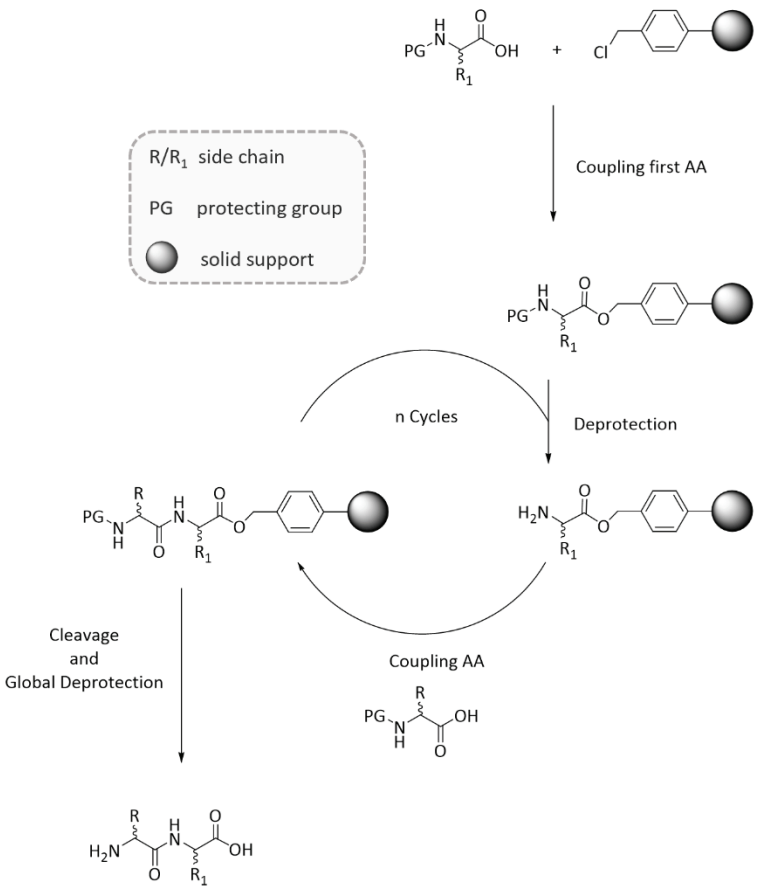

Figure 8: SPPS methodology developed by Merrifield.

The polymeric support material established by Merrifield is a chloromethylated cross-linked copolymer of polystyrene and divinylbenzene (Merrifield resin).[167] Polystyrene with varying amounts of divinylbenzene, allowing to adjust the degree of cross-linking, is still today the most commonly used solid support resin in modern solid phase synthesis.[182] The proper swelling behavior of the support material is crucial for successful solid-phase synthesis, as otherwise the accessibility to the reaction site is hindered. The polystyrene-divinylbenzene copolymer swells in non-polar solvents, preferably dichloromethane.[178] To modify the swelling behavior and to provide an even better accessibility of the reaction site, spacer units, such as polyethylene glycol as applied in the TentaGel® resin, can be grafted onto the polymeric support material.[182, 183] The nature of the linker determines the type of bond, typically amide or ester bonds, formed upon attachment of the first amino acid to the solid support, as well as the cleavage conditions for the release of the final peptide. Both the firm attachment to the polymeric support during the synthesis and the efficient cleavage under defined conditions of the final peptide are important to achieve sufficient yields.[178, 182] As a temporary protecting group of the *N*-terminus, Merrifield employed a *tert*-butyloxycarbonyl (Boc) protecting group strategy, whereby the protecting group can be removed under mild acidic conditions. In these conditions, the bond to the acid-labile

Merrifield resin remains stable. However, the cleavage of the final peptide from the resin requires the use of very strong acids such as hydrofluoric acid.[166] The introduction of the base-labile fluorenylmethyloxycarbonyl (Fmoc) protecting group by Carpino and Han was a major advance in SPPS (see Figure 9C).[184, 185] The Fmoc strategy offers the advantage of using orthogonal linkers and side protection groups that are labile under milder acidic conditions, allowing for the use of less hazardous acids.[186] Some examples of frequently used linkers compatible with the Fmoc strategy are the Wang linker, the chlorotrityl linker, and the Rink linker (see Figure 9A).[187-190] Additional amine functionalities present in the peptide, e.g., in the side chain of lysine, can be protected by use of acid-labile Boc group.[191, 192] This approach allows both the linkers and protecting groups to be cleaved by treatment with trifluoroacetic acid (TFA) solutions in varying concentrations. The cleavage from the resin and removal of the sidechain protecting groups can therefore efficiently be conducted in one step.[193, 194] For a (three-dimensional) selective protection of sidechains, additional orthogonal protecting groups, such as the allyloxy carbonyl (Alloc) group for amines, can be used. The Alloc group is stable under basic and acidic conditions and can be removed with palladium catalysts.[195, 196] An additional advantage of the Fmoc strategy is the UV absorption properties of the fluorene group that can be used to monitor the deprotection conversion.[197]

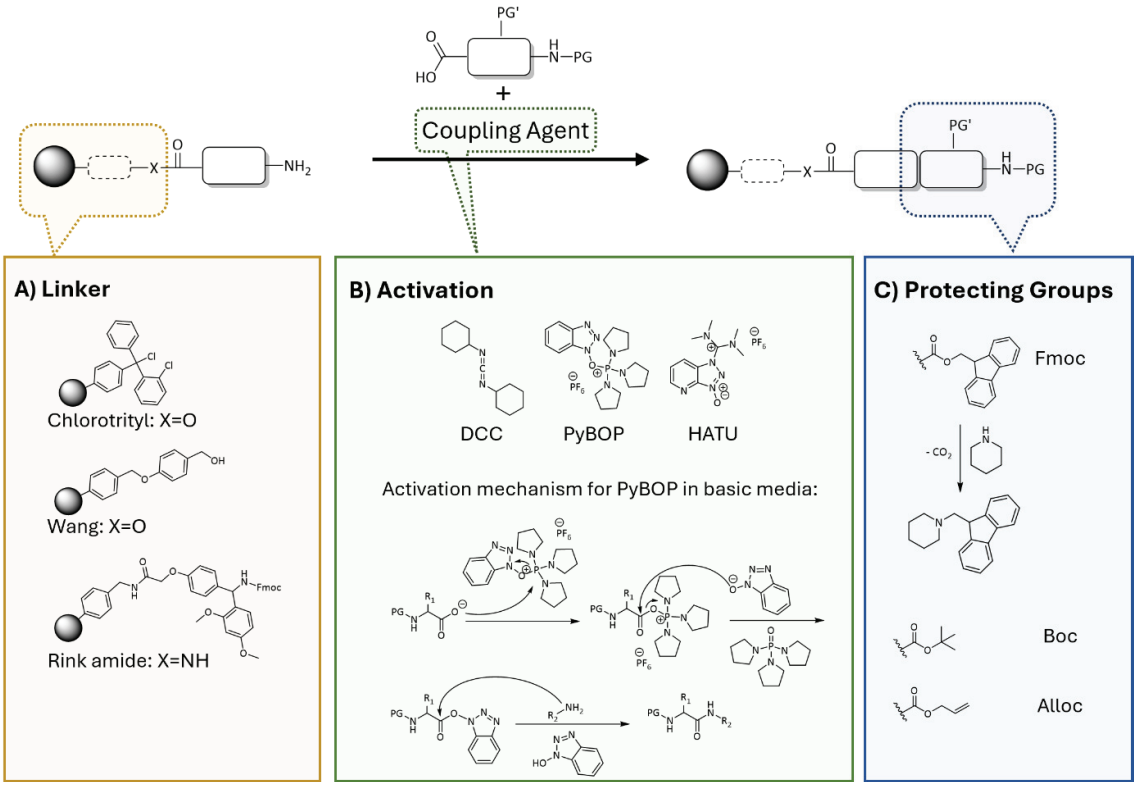

Figure 9: Exemplary overview of frequently used linkers, coupling agents, and protecting groups in SPPS.

A further crucial parameter in SPPS is the selection of coupling reagents (see Figure 9B). Since the condensation of two amino acids occurs at a slow rate at room temperature, it is necessary to activate the carboxyl group by generating a better leaving group.[198] Initially, carbodiimide derivatives were the coupling reactions most commonly used. For instance, Merrifield employed the use of dicyclohexylcarbodiimide (DCC).[167, 199] The driving force of this reaction is the formation of the urea by-product.[200, 201] However, the use of carbodiimides has certain disadvantages, including the formation of unwanted side products, such as a non-reactive *O*-acylurea species, and the racemization of amino acids. For instance, the addition of 1-hydroxybenzotriazole has been shown to suppress the unwanted side reactions.[202] Reagents derived from the class of phosphonium salts have been demonstrated to have significant advantages, as they directly yield the active ester and thus promote the coupling process more rapidly.[190] The initial example discovered by Castro is benzotriazol-1-yloxytris(dimethylamino)phosphonium hexafluorophosphate (BOP).[203] Although BOP exhibits excellent properties as a coupling reagent, the by-product formed during coupling process, hexamethylphosphoramide, is highly toxic. Benzotriazol-1-yloxytris(pyrrolidino)phosphonium hexafluorophosphate (PyBOP) is the preferred alternative today, as the resulting by-product is less toxic, while the reactivity remains undiminished.[204] The generally accepted mechanism of the coupling process of two amino acids with PyBOP as the coupling reagent and diisopropylethylamine (DIPEA) as a non-nucleophilic base is shown in Figure 9B.[205, 206] In an alkaline medium, the deprotonated acid reacts with PyBOP, forming the activated acylphosphonium species and 1-hydroxybenzotriazole (HOBt). This species can then readily react with the OBt anion, resulting in the formation of an active ester. Finally, a nucleophilic attack of the amine on the active ester occurs, forming the desired amide linkage. The formation of phosphoramide is the driving force of the reaction. Furthermore, uronium/aminium salts, such as 2-(1H-benzotriazol-1-yl)-1,1,3,3-tetramethyluronium hexafluorophosphate (HBTU) or *O*-(7-azabenzotriazol-1-yl)-*N*,*N*,*N*',*N*'-tetramethyluronium hexafluorophosphate (HATU) were discovered to be potent reagents for peptide couplings.[207, 208] However, x-ray crystallographic methods revealed that HBTU and related structures rather occur as *N*-oxide salts than uronium species, as originally assumed.[209] In several studies, HATU has been shown to be a particularly potent coupling agent even for difficult sequences.[210-212] On the other hand, a disadvantage of this class is the possibility of undergoing side reactions with the *N*-terminus of the peptide, forming guanidine residues and thereby blocking any further elongation of the peptide.[213, 214]

1.3.2 Solid-Phase Polymer Synthesis (SPPoS)

Solid-phase synthesis methods enable the stepwise assembly of monomers, thereby giving access to the preparation of monodisperse and sequence-defined macromolecules.[166, 169, 215] This advantage can also be exploited for the synthesis of non-natural oligomers and polymers.[216-218] The working group of Hartmann developed a SPPoS strategy for the synthesis of sequence-defined poly(amidoamines) (PAA).[171, 218] To achieve this, monomers that are analogous to amino acids carrying both amine and carboxyl functionalities are employed in the synthesis.[170] The Hartmann group has already established a library of numerous *functional building blocks*, which allow the attachment of additional entities to the PAA scaffold. This includes the conjugation via copper(I)-catalyzed azide-alkyne cycloaddition[170, 219], thiol-ene conjugation[220, 221], and Staudinger ligation[222]. Whereas so-called *spacer building blocks*, such as ethylene glycol diamine succinic acid (EDS, see Figure 10), are useful for customizing the spacing between functional building blocks.

One area of research within the Hartmann group is the development of precision glycomacromolecules to investigate carbohydrate-protein interactions.[170, 219, 223, 224] Figure 10 provides a schematic presentation of the synthesis of a representative linear multivalent glycomacromolecule, which follows the established standard Fmoc protocol.[170, 218, 223, 225] Since the building blocks are temporarily protected by the base-labile Fmoc protecting group, a resin with an acid-labile linker, such as TentaGel® S RAM, is used as the solid phase. For the exemplary sequence, the initial building block EDS is coupled to the solid phase using PyBOP as the coupling reagent under basic conditions. The reagents can be used in large excess to achieve quantitative conversion. In the second step, the coupled building block is deprotected with a 25 % piperidine solution in dimethyl formamide (DMF). Subsequently, triple-bond diethylenetriamine succinic acid (TDS, see Figure 10) can be attached under similar conditions. By repeating the coupling and deprotection steps, selected monomers can be added to elongate the sequence. Once the desired oligomer/polymer is obtained, ligands, in this case carbohydrate residues, can be conjugated via the functional side groups at a specific position and with an adjusted spacing. Furthermore, branched structures[172] with distinct side arm lengths as well as heteromultivalent structures are feasible using an orthogonal approach. [222] In this way, the Hartmann group has already demonstrated the preparation of a variety of glycomacromolecules tailored to targeted protein receptors, such as C-type lectins, galectins, or viral and bacterial lectins.[223, 226-228]

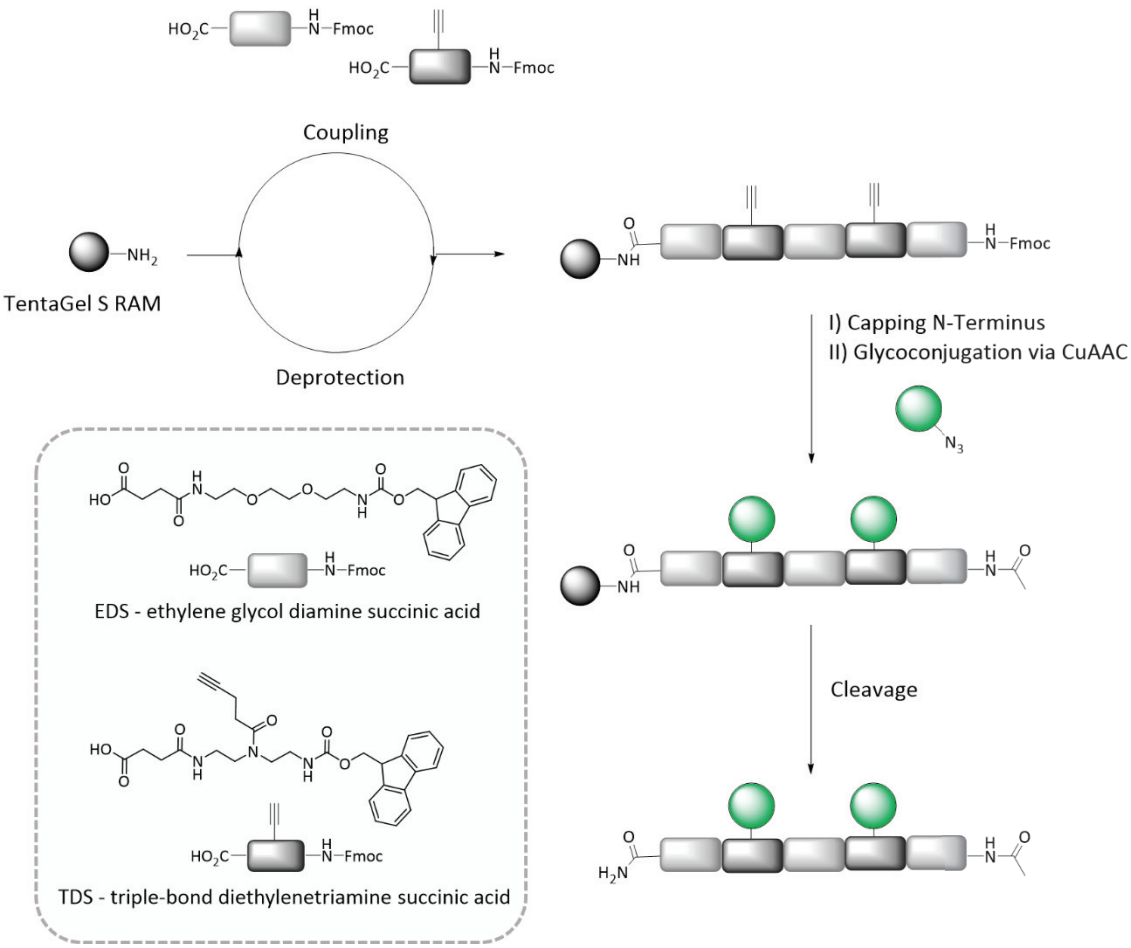

Figure 10: Schematic illustration of SPPoS by Hartmann for the preparation of sequence-defined glycomacromolecules.

1.3.3 Application of Calix[n]arenes in SPS

Despite the great advances in SPS, there have been only a few examples of calix[n]arenes applications in solid-phase synthesis reported. Approaches using an SPS strategy have mainly been reported for the preparation of peptido-calix[n]arene, which arouses interest in supramolecular chemistry as receptors for both small molecules and peptides.[139, 229] Hioki et al. first demonstrated a method for creating a combinatorial peptido-calix[4]arene library (see Figure 11A).[230] To do so, a calix[4]arene building block equipped with an undecanoic acid at the upper rim for the attachment to the solid support and two orthogonal *N*-protected amino-ethyl acetamide linkers at the lower rim for amino acid coupling, was synthesized. After anchoring to a polystyrene resin using HOBt and diisopropylcarbodiimide, the two peptide sequences were constructed individually after sequential deprotection of the amine linkers. Another approach to the synthesis of linear and cyclic peptido-calix[4]arenes on a solid phase was developed by the group of Prof. Ungaro to study the effect of the calix[4]arene motif on the organization of peptides (see Figure 11B).[231] A calix[4]arene amino acid was further modified to yield a calix[4]arene

intermediate with a benzotriazole-activated carboxylic acid and an Fmoc-protected residue at the upper rim. Prior to the attachment of the calix[4]arene intermediate, a peptide chain was built on a Wang resin using Fmoc-protection group strategies. Once the desired sequence was achieved, the calix[4]arene intermediate was incorporated into the sequence using PyBOP and DIPEA. The peptide was then further elongated to the desired peptido-calix[4]arene and cleaved from the solid support. Shuker et al. report on the synthesis of a tetra-peptido-calix[4]arene employing a tetra-nitro-calix[4]arene derivative that was attached via a hexanoic acid linker at the lower rim to an AgroPore solid phase using HATU as coupling reagent (see Figure 11C).[232] Subsequently, the nitro groups are reduced to amines by treatment with tin chloride, making the upper rim available for coupling with Fmoc-protected amino acids.

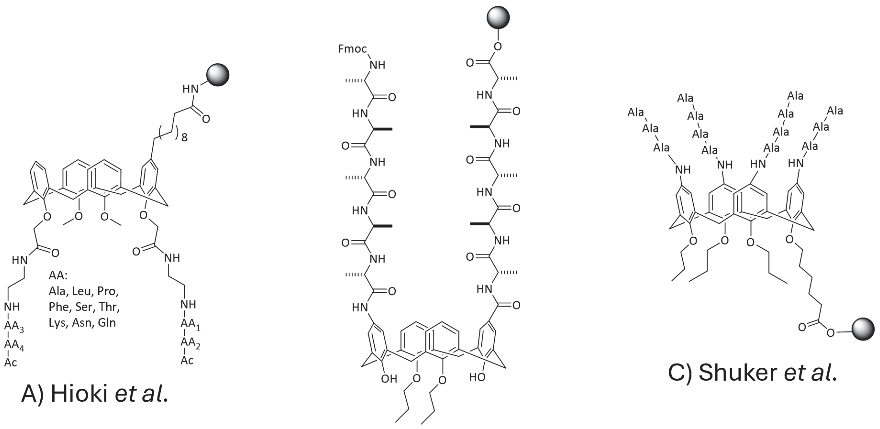

Figure 11: Examples of peptido-calix[4]arenes synthesized on solid phase.

Additionally, nucleotide-calix[4]arene derivatives have been synthesized via a solid-phase approach. Granata et al. used an ethylene glycol linker at the lower rim to anchor the calix[4]arene derivative to a TentaGel® S RAM resin.[233] Prior, the upper rim was functionalized in solution with dimethoxytrityl-protected glycerol building blocks, allowing for an efficient nucleotide coupling via phosphoramidite chemistry, yielding the first upper rim tetra-functionalized nucleotide-calix[4]arene derivative.

The examples presented here show different approaches for anchoring calix[4]arene derivatives to a solid phase at both the lower and upper rim and further efficient functionalization, yielding various peptido- and nucleotide-calix[4]arenes. This approach appears especially promising for the multi-step synthesis of complexly functionalized calix[n]arene structures, as the reactants can be employed in large excess to drive the reaction to completeness, and intermediate washing steps can be significantly simplified

and accelerated. However, the synthesis of glycocalix[n]arene via SPS has not been reported yet.

2. Aims and Outline

Carbohydrates are a prominent example of biologically relevant binding motifs. In nature, they predominantly occur as polysaccharides or glycan conjugates, such as glycoproteins and glycolipids, and play a crucial role as recognition markers mediating numerous biological processes such as cell-cell communication, immune responses, and pathogen-host interactions.[1, 2] Their interaction partners of interest are carbohydrate-recognizing (lectins) and carbohydrate-processing (enzymes) proteins.[7, 81, 234] Since single carbohydrate-protein interactions are typically weak, nature utilizes the principle of multivalency, which enhances both binding avidity and specificity.[21, 22, 45] To investigate these complex multivalent binding events in detail, chemists explored so-called glycomimetic compounds that typically use artificial scaffolds to multivalently present the binding carbohydrate epitopes.[6, 47] Among these, calix[4]arenes have emerged as a well-established platform for the multivalent presentation of carbohydrates. Previous studies have demonstrated their binding to several medically relevant lectins and also their therapeutic potential, for instance, as antiviral inhibitors.[162]

The key aspect of this thesis is the integration of a calix[n]arene motif into the previously established SPPoS approach developed by Hartmann and coworkers.[170] Considering that scaffold properties such as flexibility and polarity, as well as topology, are critical in glycomimetic ligand design[24, 26], the objective is to combine the unique structural features of calix[n]arenes with the advancements of SPPoS. The integration of an inherent rigid and cyclic motif into the PAA scaffold is hypothesized to affect the binding affinity and specificity to carbohydrate-binding proteins. Moreover, compared to currently used synthetic routes in solution, the modularity and precision of SPPoS method offer a straightforward and highly flexible approach, adjusting glycocalix[n]aren ligand properties, such as valency, sequence, and functional group positioning. This allows for the tailored design of glycocalix[n]arenes and conjugates to specific biological targets. To validate these hypotheses, a library of sequence-defined glycocalix[4]arenes is synthesized and evaluated for their binding properties against distinct target proteins. This thesis is structured into four chapters, each addressing a specific aspect of this objective:

The first part lays the key foundation by developing a robust synthetic method to incorporate a calix[4]arene building block, inspired by Shuker et al., into the SPPoS approach by Hartmann.[232] This enables the synthesis of complex glycocalix[4]arenes in a controlled fashion, as should be demonstrated by a first set of homo- and heteromultivalent derivatives. Some initial binding studies to evaluate their potential in pathogen inhibition

should be conducted. To be able to better analyze and assess the results, a binding adhesion inhibition assay, which is already established in the working group, is selected. A second part in the first chapter focuses on enhancing the multivalency of the glycocalix[4]arenes, leveraging the concept of "multivalency of multivalency". This should be achieved in collaboration with the working group of Prof. Epple (University Duisburg-Essen) by their attachment onto ultrasmall gold nanoparticles in a controlled way. The calix[4]arene is designed in a way to give control over the number and density of carbohydrate epitopes attached to nanoparticles and to avoid ligand overcrowding on the surface, which would otherwise hinder binding efficiency or accessibility to target proteins.[235, 236] Again, in a bacterial adhesion inhibition assay, the effect of enhanced multivalency of the glycocalix[4]arene nanoparticle conjugates is evaluated.

The second chapter of this thesis shifts the focus from carbohydrate-recognizing lectins to carbohydrate-processing proteins, exploring the potential of multivalent glycocalix[4]arenes as enzyme regulators or inhibitors. Specifically, the de-*N*-glycosylating enzyme NGLY1, which plays a key role in the endoplasmic reticulum-associated degradation (ERAD) pathway, is investigated.[38] NGLY1 features a lectin-like PAW domain that naturally binds to high-mannose glycans[32], making it an attractive target for synthetic multivalent ligands. In this context, mannose-functionalized glycocalix[4]arenes are hypothesized to interact with the PAW domain, potentially influencing the enzymatic activity of NGLY1. To facilitate detailed binding studies, a biotin tag is introduced into the ligand design, allowing experiments based on the biotin-streptavidin interaction. Further, a gel shift assay to investigate the inhibitory potential on the enzyme activity is performed.

A further development of the previous approach towards higher valent homo- and heteromultivalent glycocalix[4]arenes is presented in the third chapter of this work. This project explores a straightforward split and combined synthesis to synthesize two-sided glycocalix[4]arene dimers. Particular emphasis is placed on the heteromultivalent dimer, derived from the conjugation of two distinct calix[4]arene monomers, and its ability to bi-specifically bind to two different lectins simultaneously. Such kinds of Janus-like or heterobifunctional structures are currently of growing interest for various biomedical and biotechnological applications.[237-239] In this work, turbidity and precipitation studies on model lectins are performed to provide the proof of concept, demonstrating the potential of these innovative ligands.

In the last part of the thesis, the scope of the established SPPoS is expanded to include calix[5]arenes, a higher homolog of the calix[4]arene building block. The larger cycle of

calix[5]arenes are conformationally mobile and thus may allow for an induced fit to protein binding sites.[117] First, the synthesis route to prepare a suitable calix[5]arene building block is developed, and its applicability to SPPoS is tested. It is assumed that the calix[5]arenes building block provides an ideal scaffold to target VP1 capsid proteins of polyomaviruses due to its pentameric architecture.[240] Therefore, a series of sialic acid functionalized calix[5]arene derivatives with varying valency and linker length is synthesized, as these features are known to be critical for an optimized binding. Subsequently, the calix[5]arene derivatives, as well as a calix[4]arene reference structure, are subjected to crystallographic studies performed by the working group of Prof. Stehle (University Tübingen) to investigate the potential ligand-protein complexes.

3. Results and Discussion

3.1 Synthesis of Glycocalix[4]arene Derivatives and Attachment to Gold Nanoparticles

Alisa Kayser, Kai Klein, Daria Babushkina, Anna Sakse, Gisele Mouafo Kenne, Ulla I.M. Gerling-Driessen, Monir Tabatabai, Matthias Epple, and Laura Hartmann, “A Modular Solid Phase Synthesis Approach for Glycocalix[4]arene Derivatives and their Multivalent Presentation on Ultrasmall Gold Nanoparticles”, Chemistry, A European Journal, **2025**, *31*, 202500497.

Publication:

Own contribution: Synthesis of the calix[4]arene building block. Optimization of a solid phase synthesis strategy toward the glycocalix[4]arene derivatives C1-C3. The synthesis of the derivatives C1-C3 following the optimized route has been performed by Gisele Mouafo Kenne. The synthesis of the second set of glycocalix[4]arenes C4-C7 was performed with support from Daria Babushkina and Narges Irani. Characterization of the calix[4]arene-gold nanoparticle conjugates. Performance of the bacteria assay and fluorescence microscopy. Writing of the first manuscript draft. Collaborative writing of the final manuscript.

Check for updates

Chemistry–A European Journal

Research Article
doi.org/10.1002/chem.202500497

Chemistry Europe
European Chemical Societies Publishing

www.chemeurj.org

A Modular Solid Phase Synthesis Approach for Glycocalix[4]Arene Derivatives and Their Multivalent Presentation on Ultrasmall Gold Nanoparticles.

Alisa Kayser,[a] Kai Klein,[b] Daria Babushkina,[a] Anne Sakse,[a] Gisele Mouafo Kenne,[a] Ulla I.M. Gerling-Driessen,[c] Monir Tabatabai,[a] Matthias Epple,[b] and Laura Hartmann*[a, c]

Gold nanoparticles and calix[n]arenes are well-established platforms for creating multivalent carbohydrate ligands that enhance binding avidity and selectivity toward carbohydrate-recognizing receptors, such as bacterial lectins. In this study, we present a modular synthesis protocol for tailor-made and (multi)functional glycocalix[4]arene derivatives using solid-phase polymer synthesis. A calix[4]arene building block with a single carboxyl group on the lower rim and four nitro groups at the upper rim is introduced. This building block is attached to a solid support using standard solid phase peptide coupling conditions, followed by reduction of the upper rim nitro functionalities to yield four amine groups, that are further functionalized through solid-phase polymer synthesis. Using this modular approach, we access a series of glyco-calix[4]arene structures that are then further conjugated onto ultrasmall gold nanoparticles. Conjugation is promoted either via one or via four alkyne groups on the glycocalixarene structure, providing a handle to tune the overall valency of the final glyco[4]calixarene-gold nanoparticle conjugates. Finally, the glycocalix[4]arene derivatives and conjugates are evaluated for their inhibitory potential against bacterial adhesion showing the importance of multivalent carbohydrate presentation to effectively block Escherichia coli (E. coli) adhesion.

1. Introduction

Carbohydrates represent one of the major building blocks of life. Conjugated to proteins or lipids, they are essential components of the glycocalyx, a dense layer that surrounds every eucaryotic cell and plays a crucial role in mediating processes, such as cell communication, tumor metastasis or pathogen infection.[1] While the underlying single carbohydrate-protein interactions are usually weak, the multivalent binding of multiple epitopes of a multivalent carbohydrate ligand binding to one or more binding sites of a protein (e.g., lectins) is leading to an increased binding avidity thereby yielding strong and specific interactions.[2] To study this so-called glycoside cluster effect[3] macromolecular scaffolds such as polymers,[4] dendrimers,[5] calixarenes[6] and nanoparticles,[7] have been employed to create synthetic multivalent carbohydrate ligands.

Gold nanoparticles are of great relevance in various biomedical applications[8] due to their beneficial properties such as biocompatibility,[8b] high cellular uptake properties[8d,9] as well as high accumulation rates in tumor tissue.[10] Furthermore, they exhibit unique magnetic, electronic, and optical properties, that can be useful for therapeutic and diagnostic applications.[11] Glyco-functionalized gold nanoparticles (g-GNPs) are well-established compounds to study and engage binding of carbohydrate recognizing proteins.[7,12] Besides the size[7a,c,12a,b] and shape of the gold core, also, the number and density of the carbohydrates on the particle surface[7d,12a,d,e,13] as well as length and flexibility of the linker between the particle and carbohydrate[7a,c,12a,d] strongly influence the resulting protein binding and enhancement of binding through multivalent effects. Interestingly, it was shown that an excessive crowding of pendant carbohydrates on the nanoparticle surface can lead to sterically hindrance and thus no increase in binding through avidity is accomplished.[12d,14] For these reasons, serval studies dedicated to the synthesis of well-defined (ultrasmall) gold nanoparticles as well as synthetic pathways for a controlled surface functionalization have been reported.[12c,15] Mainly, ultrasmall g-GNPs with a metal core size of 2 nm or less are obtained via a direct synthesis approach (Brust synthesis) that gives access to ultrasmall thiol-derivatized gold nanoparticles with high carbohydrate valency in one step.[6c,15c,16] To enable a controlled variation of carbohydrate ligand density,

[a] A. Kayser, D. Babushkina, A. Sakse, G. M. Kenne, Dr. M. Tabatabai, Prof. Dr. L. Hartmann
Department of Organic Chemistry and Macromolecular Chemistry, Heinrich Heine University Dusseldorf, Universitätsstraße 1, Dusseldorf 40225, Germany
E-mail: laura.hartmann@makro.uni-freiburg.de

[b] Dr. K. Klein, Prof. Dr. M. Epple
Inorganic Chemistry and Center for Nanointegration Duisburg-Essen (CENIDE), University of Duisburg Essen, Universitätsstraße 7, Essen 45141, Germany

[c] Dr. U. I. Gerling-Driessen, Prof. Dr. L. Hartmann
Institute for Macromolecular Chemistry, University of Freiburg, Stefan-Meier Straße 31, Freiburg i.Br. 79104, Germany

Supporting information for this article is available on the WWW under https://doi.org/10.1002/chem.202500497

© 2025 The Author(s). Chemistry – A European Journal published by Wiley-VCH GmbH. This is an open access article under the terms of the Creative Commons Attribution License, which permits use, distribution and reproduction in any medium, provided the original work is properly cited.

© 2025 The Author(s). Chemistry – A European Journal published by Wiley-VCH GmbH

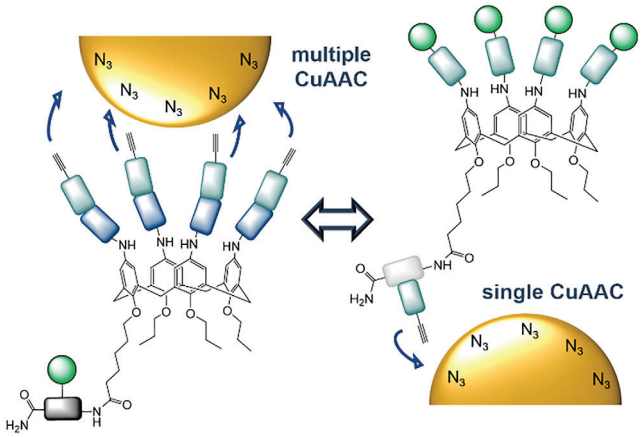

Figure 1. Schematic depiction of multiple versus single click approach depending on the ligand design.

additional noncarbohydrate functionalized components can be incorporated.[12c,d,13] However, this approach meets limits due to different tendencies of chemisorption to the particle surface among thiol-ligands. Furthermore, it must be considered that the additional modulating component can have interactions with the investigated target (e.g., carbohydrate recognizing protein), and that issues regarding water solubility have been reported using this method.[15a] To overcome these disadvantages, van der Meer et al. reported a new strategy using multi-thiol macromolecules allowing for the limitation of ligand crowding on the particle surface without the need of additional modulating components.[17] This approach demonstrates the multiple conjugation to ultrasmall nanoparticle (< 2 nm) giving a handle to tune the degree of surface functionalization.

Herein, we present an advanced strategy to regulate the total number and density of carbohydrate ligands on the surface of ultrasmall gold nanoparticles (< 2 nm) by multivalent, covalent attachment of glycomacromolecules to the particles.[18] In order to do so, we use calix[4]arenes as multivalent component for our macromolecular design. Similar to gold nanoparticles, calixarenes have been studied extensively as scaffolds for the multivalent presentation of carbohydrates and to study multivalent effects as well as their use in biomedicine, for example, in the inhibition of bacterial and viral adhesion as well as for the targeting of cancer cells.[6b,19]

We show a straightforward synthetic route using solid-phase polymer synthesis to gain sequence-defined glycocalix[4]arene (gCs) derivatives carrying four alkyne moieties at the upper rim and one carbohydrate residue at the lower rim or vice versa (Figure 1). This ligand design allows for a conjugation to azide functionalized gold nanoparticles via copper(I)-catalyzed alkyne-azide cycloaddition (CuAAC) through either just one or four alkyne groups simultaneously giving gC-gold nanoparticle conjugates (gC-GNPs) (Figure 1). This approach allows us to tune the density as well as the number of ligands on the particle surface. Based on the use of glycomacromolecules[14] as inhibitors of bacterial adhesion, we investigate the synthesized gCs and gC-GNPs for their inhibitory potential to bacterial adhesion.

2. Results and Discussion

2.1. Ligand Design and Synthesis of First Set of Glycocalix[4]Arenes C1-C3

The focus of this work is the development and synthesis of tailor-made and multifunctional gC derivatives. For this purpose, a solid-phase synthesis previously established by Shuker et al,[20] was combined with the solid-phase polymer approach established in the Hartmann lab.[21] First, a suitable calix[4]arene building block (CBB1) compatible with solid phase polymer synthesis was synthesized according to previously established procedures.[20] CBB1 carries one carboxyl group at the lower rim enabling the selective attachment to the solid support via activation and amide coupling. The upper rim carries four nitro groups, which can be further modified once the CBB1 is attached to the solid support.

Attachment of CBB1 onto the solid support was performed on a TentaGel S RAM. The first three ethylene glycol diamine-succinic acid 1-(9H-fluoren-9-yl)-3,14-dioxo-2,7,10-trioxa-4,13-diazaheptadecan-17-oic acid) (EDS) building blocks were coupled using previously established coupling conditions with DIPEA and PyBOP as activation reagents.[21,22] EDS introduces an ethylene glycol as the main chain motif leading to higher hydrophilicity and therefore facilitates the later analysis of the compound by HPLC-MS. Next, CBB1 was coupled to the EDS_3 oligomer using PyBOP and DIPEA as coupling reagents. After microcleavage, analysis of the formed product by HPLC-MS and MALDI-TOF-MS confirms that CBB1 is coupled with high yields at these standard coupling conditions (see Supporting Information for details). After successful attachment of CBB1 to the solid support, the nitro groups of CBB1 were reduced to amines by treatment with an excess of $Sn(II)Cl_2$ dihydrate followed by excessive washing with methanol, DMF, and DCM. We observed that the successful reduction of all four nitro groups strongly depends on the reaction conditions, especially the reaction temperature. In contrast to previously reported protocols, initial attempts at room temperature showed the formation of by-products due to insufficient reduction of all nitro groups (data not shown).[20] We found that best results were obtained when the reduction was performed with a high excess of $Sn(II)Cl_2$ dihydrate in NMP at 30° C for 24 hours, which we confirmed by HPLC-MS, HR-ESI, and MALDI-TOF-MS (see Supporting Information for analytical data and further details on the reaction conditions). NMP was established as an optimal solvent since harsher reaction conditions, such as increased reaction temperature and longer reaction time yielded a by-product that presumably occurred due to formylation in DMF (see Supporting Information).

After successful formation of the amine functionalities, further building blocks can be coupled via solid phase peptide or polymer synthesis to the upper rim of the calix[4]arene backbone. For different Fmoc-protected building blocks as well as amino acids, N-methyl morpholine, and PyBOP as coupling reagents showed the highest coupling efficiency (see Supporting Information for further details). For the targeted gC derivatives

© 2025 The Author(s). Chemistry – A European Journal published by Wiley-VCH GmbH

15213765, 2025, 40, Downloaded from https://chemistry-europe.onlinelibrary.wiley.com/doi/10.1002/chem.202500497, Wiley Online Library on [13/09/2025]. See the Terms and Conditions (https://onlinelibrary.wiley.com/terms-and-conditions) on Wiley Online Library for rules of use; OA articles are governed by the applicable Creative Commons License

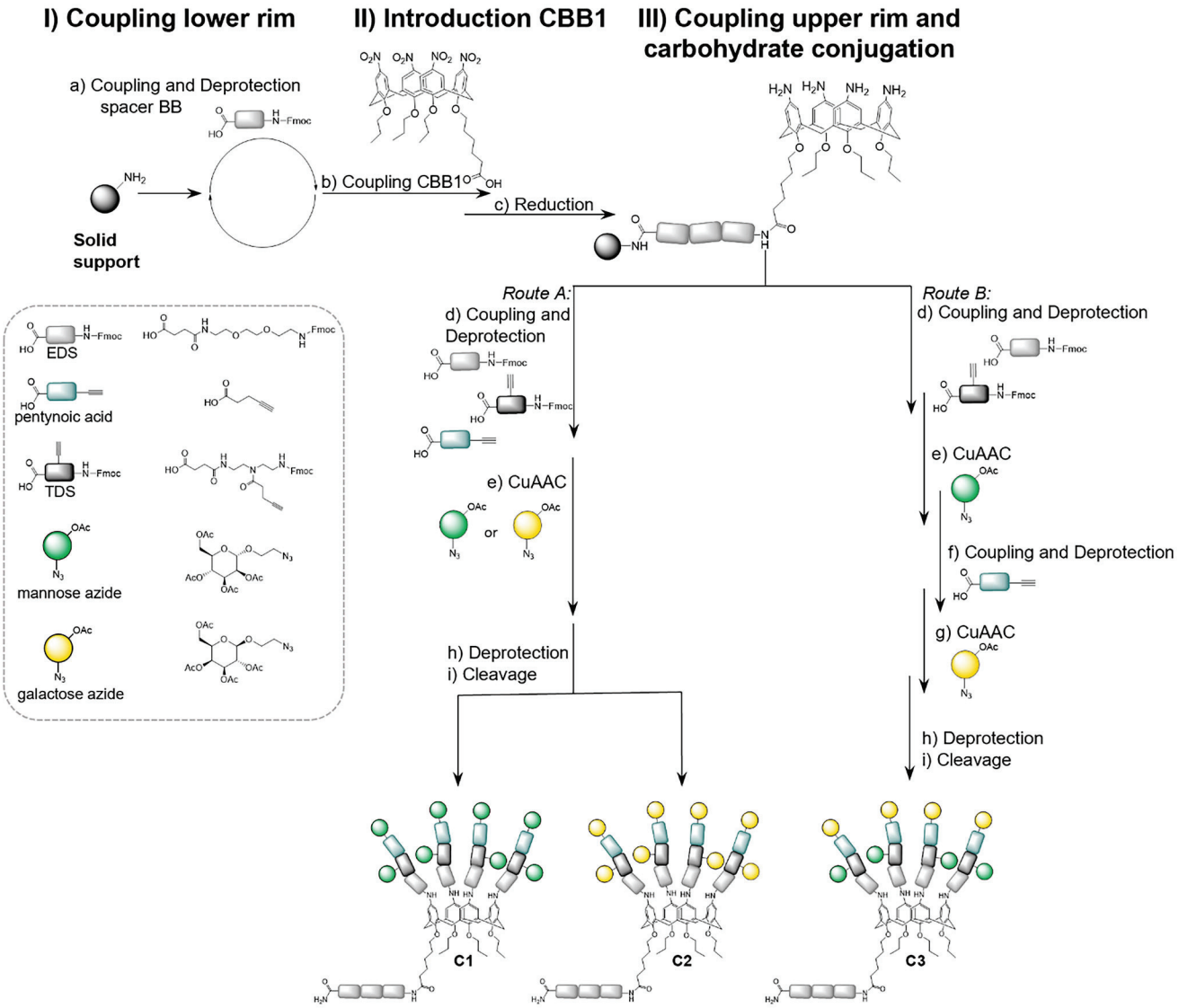

Scheme 1. Solid-phase synthesis of glycocalix[4]arenes C1-C3. Reaction conditions: a) Coupling conditions: 5eq. building block, 5 eq. PyBOP, 10 eq. DIPEA, DMF, 1 hour; for Fmoc deprotection: 20 Vol.% piperidine in DMF was used. b) Coupling conditions: 3 eq. CBB1, 5 eq. PyBOP, 10 eq. DIPEA, DMF, overnight. c) 25 eq. $Sn(II)Cl_2$ dihydrate per nitrogen group, NMP, 24 hours, 30° C. d) and f) Coupling conditions: 5eq. building block per amine, 5eq. PyBOP per amine, 10 eq. N-methyl morpholine per amine, DMF, 1 hours; for Fmoc deprotection 20 Vol.% piperidine in DMF was used. e) and g) 2 eq. carbohydrate azide per alkyne, 20 mol % $CuSO_4$, 20 mol % NaAsc, DMF/water, overnight. h) 0.2 M sodium methanolate, 30 minutes. i) 95/5/5 (vol.%) TFA/TIPS/DCM, 1 hour.

C1-C3, the upper rim was functionalized with an EDS followed by a triple-bond diethylenetriamine-succinic acid, 1-(fluorenyl)-3,11-dioxo-7-(pent-4-ynoyl)-2-oxa-4,7,10-triazatetra-decan-14-oic acid (TDS building block that introduces an alkyne moiety).[21] The incorporation of the alkyne-functionality allows in the next step for the conjugation of azide functionalized carbohydrate residues, here mannose and galactose, via copper-catalyzed azide-alkyne cycloaddition (CuAAC). At this point, different synthetic pathways are possible to either obtain octavalent homo- or heteromultivalent derivatives, as shown in Scheme 1. In route A, pentynoic acid is coupled next to introduce a further, terminal alkyne functionality and subsequently all sugar moieties can be conjugated simultaneously to obtain homomultivalent derivatives C1-C2. Alternatively, in route B, different azide-carbohydrates can be conjugated in a sequential way to accomplish the heteromultivalent derivative C3.[23] The glycocalix[4]arene structures were purified using preparative HPLC (see Supporting Information) and characterized by ^{1}H-NMR (Figure 2) and HPLC-MS and MADLI-TOF-MS (see Supporting Information). The ^{1}H-NMR spectra of all three compounds show the signals of methylene bridge of calix[4]arene motif, which are marked in grey (Figure 2). Additional integrated signals can be assigned to the carbohydrate residues. Comparing the spectra chemical shift of the carbohydrate-related signals can be recognized and validates the mannose conjugation in the case of C1 or galactose residues for C2. Additionally, the intensity of eight protons for each of the carbohydrate-related peaks confirms the successful octavalent conjugation of the carbohydrates to the scaffold. For the heteromultivalent structure C3, signals of both galactose and mannose residues can be observed when

© 2025 The Author(s). Chemistry – A European Journal published by Wiley-VCH GmbH

15213765, 2025, 40, Downloaded from https://chemistry-europe.onlinelibrary.wiley.com/doi/10.1002/chem.202500497, Wiley Online Library on [13/09/2025]. See the Terms and Conditions (https://onlinelibrary.wiley.com/terms-and-conditions) on Wiley Online Library for rules of use; OA articles are governed by the applicable Creative Commons License

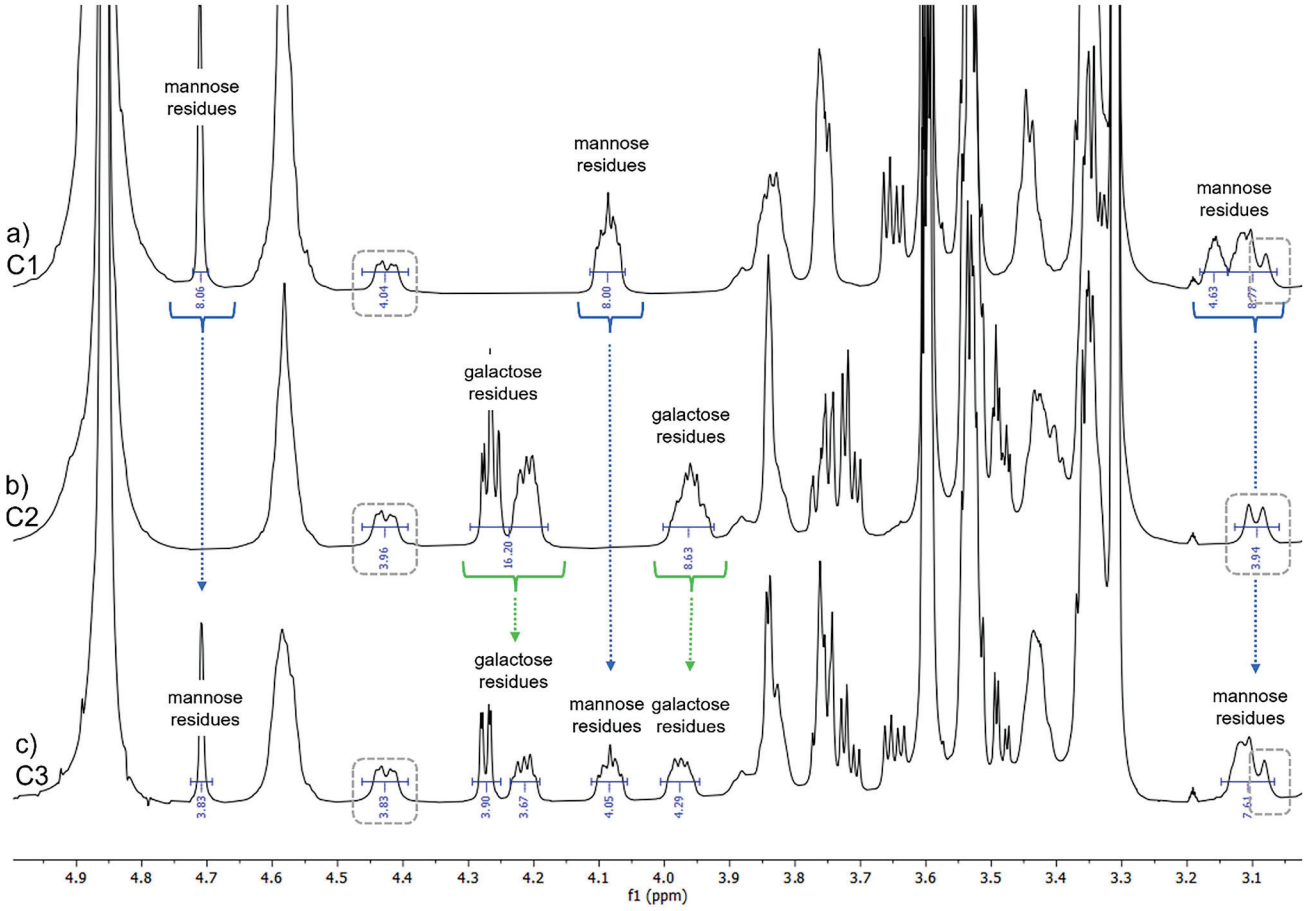

Figure 2. Excerpt from ^{1}H-NMR (600 Hz) spectra of compounds C1-C3 in methanol-$_{d4}$/D_2O. For full spectra see Supporting Information. Signals from calix[4]arene are marked in gray boxes.

compared to the homomultivalent structure, evidencing the successful synthesis of the heteromultivalent compound C3 with four mannose and galactose residues each.

2.2. Synthesis of Second Set of Glycocalix[4]Arenes C4-C7

For the second set of gCs we aimed to incorporate additional alkyne moieties as second functionality into our ligand design. The exhibition of additional alkyne moieties will give access to further conjugation to larger scaffolds like azide-bearing nanoparticles via CuAAC. We reasoned that the increased multivalency and size of the carbohydrate conjugates would result in improved receptor binding, thereby leading to the development of potent pathogen adhesion inhibitors. Several studies showed that the number and density of carbohydrates on the nanoparticle surface effect the binding avidity of the nanoparticles to lectins.[7d,12a,d,e,13,14] We therefore endeavored two different gC derivatives with either four alkyne groups at the upper rim and one carbohydrate group at the lower rim (C4,C5) or vice versa (C6,C7). This approach allows us to conjugate the calix[4]arene ligands to the nanoparticle via CuAAC in either multiple (C4,C5) or single (C6,C7) way and thereby give a handle to the adjust number and density of carbohydrates on the nanoparticle surface. For the synthesis of the alkyne-gC derivative C4-C7, previous reaction conditions were applied again, while the choice of building blocks and the order of their assembly was altered according to the final ligand structure design. Specifically, for the derivatives C4,C5 (Scheme 2, route A) instead of the spacing building blocks (EDS), now one alkyne carrying TDS building block was coupled as an initial building block, immediately followed by coupling of the CBB1 and subsequent reduction of the nitro groups. No notable evidence of a decreased coupling efficiency of CBB1 to TDS compared to EDS was observed. However, we noticed that one prerequisite is that no free amines at the upper rim of the calixarene are present while the sugar azide is attached to TDS at the lower rim via CuAAC as this affected the conjugation efficiency during the click reaction. This could be attributed to a complexation of the catalyzing copper ions by the free amines. Neither is it possible to conjugate the carbohydrate residue before the reduction step has been performed, as the glycosidic bond is not stable under the applied reduction conditions. For these reasons, we decided to react the interfering amines at the upper rim with Fmoc-glycine prior to conjugation of carbohydrate azides. Finally, the remaining alkyne moieties were incorporated by terminal coupling of pentynoic acid to each of the glycine.

© 2025 The Author(s). Chemistry – A European Journal published by Wiley-VCH GmbH

15213765, 2025, 40, Downloaded from https://chemistry-europe.onlinelibrary.wiley.com/doi/10.1002/chem.202500497, Wiley Online Library on [13/09/2025]. See the Terms and Conditions (https://onlinelibrary.wiley.com/terms-and-conditions) on Wiley Online Library for rules of use; OA articles are governed by the applicable Creative Commons License

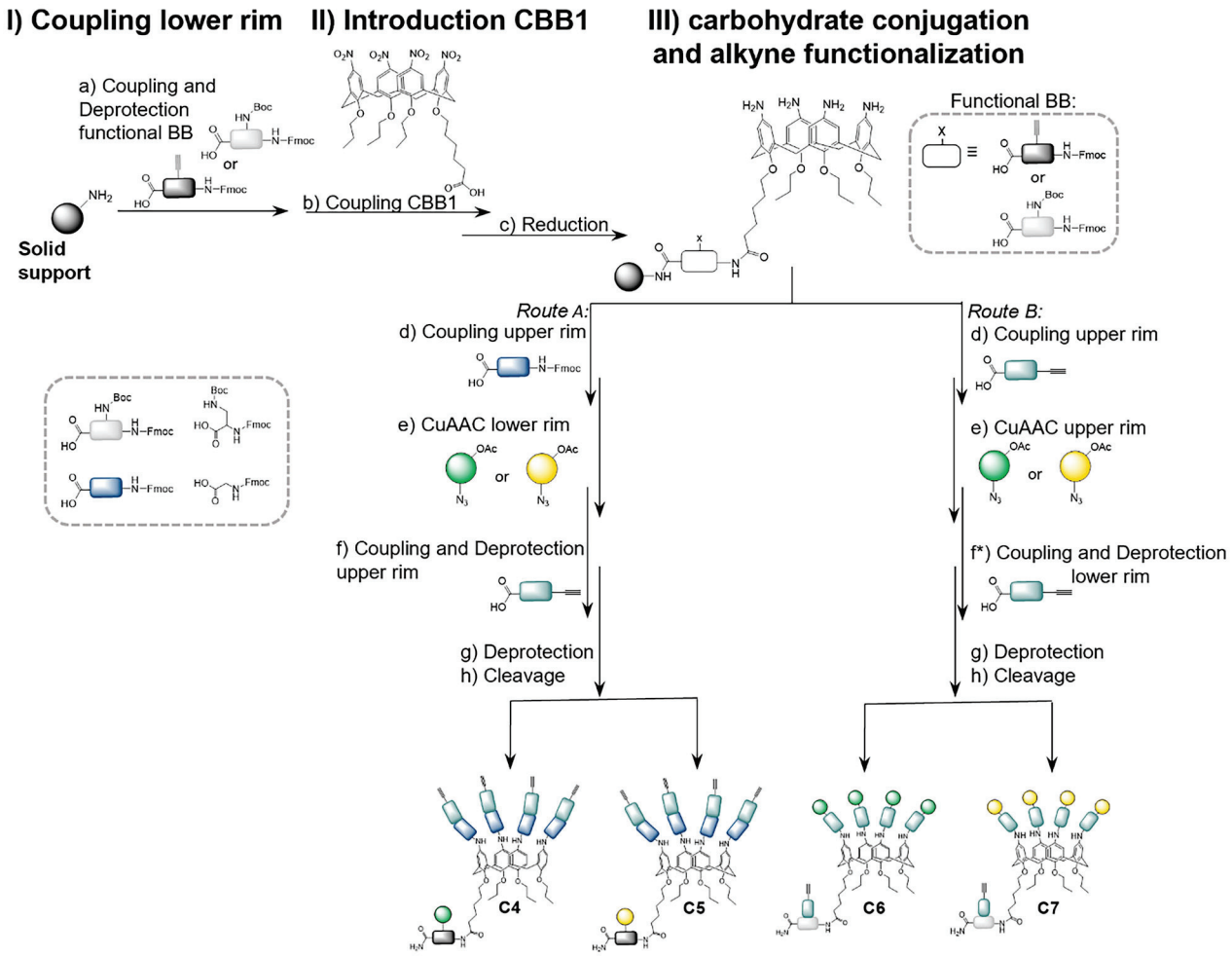

Scheme 2. Solid-phase synthesis of glycocalix[4]arenes C4-C7. Rection conditions: a) 5eq. building block, 5 eq. PyBOP, 10 eq. DIPEA, DMF, 1 hour; for Fmoc deprotection 25% piperidine solution was used. b) 3 eq. CBB1, 5 eq. PyBOP, 10 eq. DIPEA, DMF, overnight. c) 25 eq. $Sn(II)Cl_2$ dihydrate per nitrogen group, NMP, 24 hours, 30° C. d) and f) 5eq. Building block per amine, 5eq. PyBOP per amine, 10 eq. N-methyl morpholine per amine, DMF, 1h¸ for Fmoc deprotection 25% piperidine solution was used. e) 2 eq. carbohydrate azide per alkyne, 20 mol % $CuSO_4$, 20 mol % NaAsc, DMF/water, overnight. f*) 5eq. building block, 5 eq. PyBOP, 10 eq. DIPEA, DMF; for Boc deprotection 4 M HCl in Dioxan was used. g) 0.2 M sodium methanolate, 30 minutes. h) 95/5/5 TFA/TIPS/DCM (vol.%), 1 hour.

The synthesis of C6,C7 was performed in a slightly altered fashion (Scheme 2, route B). Here an orthogonally Fmoc- and Boc-protected diamino propionic acid was coupled instead of TDS as the first building block. Importantly, the Boc group on one amine of the diamino propionic acid can be selectively removed on solid support after functionalization of the upper rim, using 4 M HCl in dioxan. This is followed by coupling of pentynoic acid at the lower rim, which yields the required alkyne moiety at the lower rim without noteworthy effect on the residual structure. Using this method, the desired derivatives C6 and C7 were obtained efficiently. The crude products were purified using preparative HPLC (see Supporting Information) and all structures were analyzed by ^{1}H-NMR (Figure 3), HPLC-MS, and MALDI-TOF-MS (see Supporting Information). Figure 3 shows the ^{1}H-NMR spectra of the alkyne functionalized gCs C4-C7. Marked in gray are the signals assigned to the calix[4]arene motif for all derivatives. In addition, characteristic signals are assigned and integrated for the different derivatives. The downfield shifted signals are attributed to the triazole proton and can be found with an intensity of one proton for C4 and C5 and an intensity of four protons for C6 and C7, confirming the conjugation of one or four carbohydrate residues via CuAAC, respectively. Furthermore, all spectra show the expected signals for the mannose or galactose residues. Also, the signals for the alkyne protons are highlighted in the spectra, and integrals of either one for C4 and C5 or four for C6 and C7 further confirm successful synthesis of the targeted structures. In summary, we successfully established a versatile synthesis route for various calix[4]arene derivatives using solid-phase protocols, as demonstrated by the synthesis of a series of gCs.

2.3. Attachment of C4-C7 to Ultrasmall Gold Nanoparticles and Characterization of gC-GNP

The functionalization of ultrasmall azide-bearing gold nanoparticles (a-GNPs) allowing for an efficient way of covalent nanoparticle functionalization via CuAAC was demonstrated recently by

© 2025 The Author(s). Chemistry – A European Journal published by Wiley-VCH GmbH

15213765, 2025, 40, Downloaded from https://chemistry-europe.onlinelibrary.wiley.com/doi/10.1002/chem.202500497, Wiley Online Library on [13/09/2025]. See the Terms and Conditions (https://onlinelibrary.wiley.com/terms-and-conditions) on Wiley Online Library for rules of use; OA articles are governed by the applicable Creative Commons License

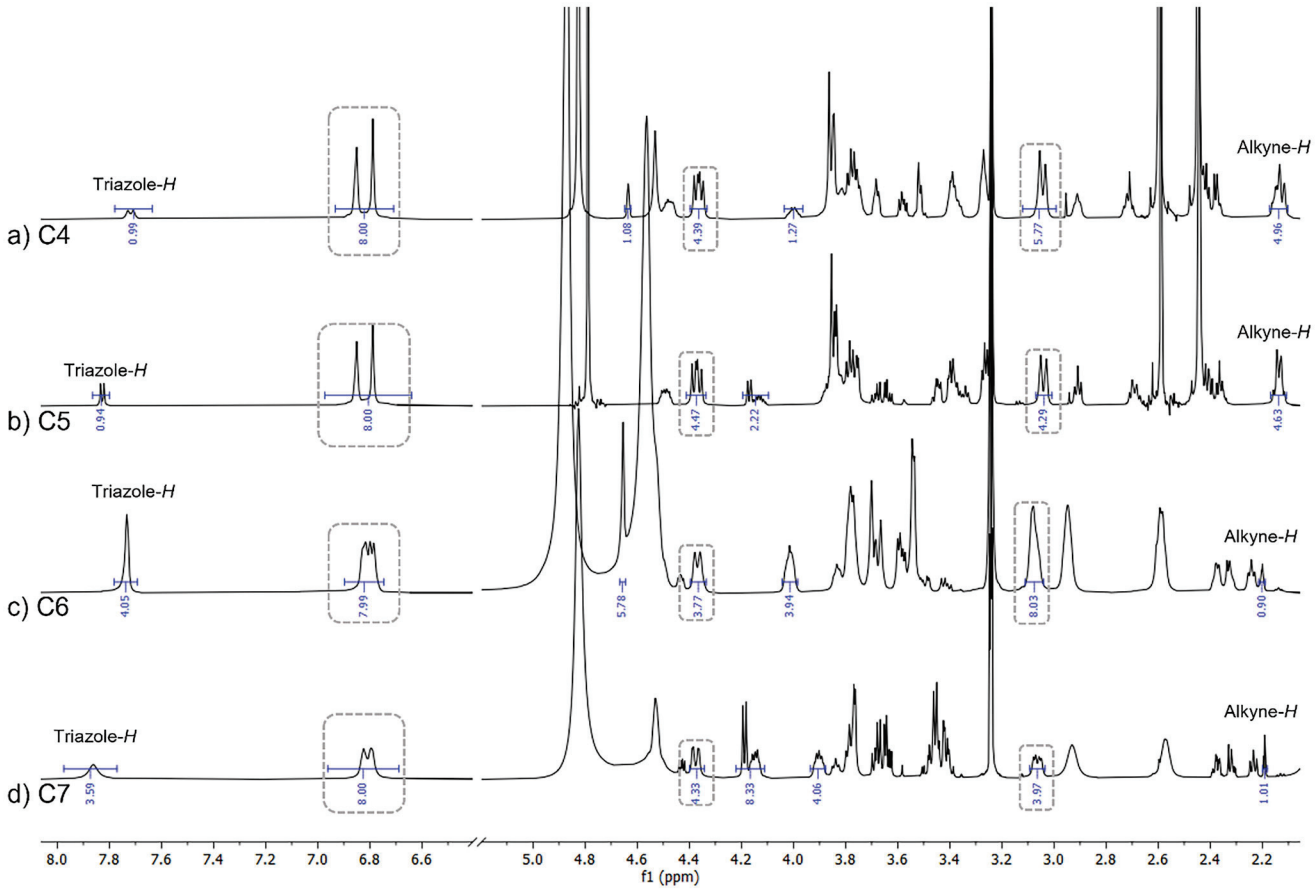

Figure 3. Excerpts from ^{1}H-NMR (600 MHz) spectra of compounds C4-C7 in methanol-*d4*/D_2O. For full spectra see Supporting Information. Signals from calix[4]arene are marked in gray boxes.

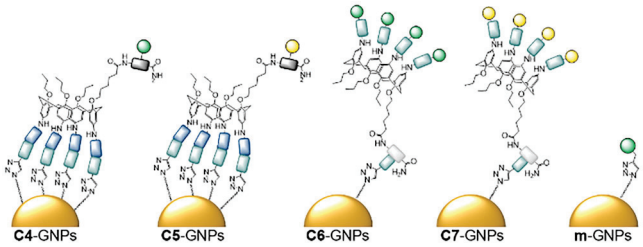

Figure 4. Schematic depiction and nomenclature of mannose-calixarene gold-nanoparticles C4-GNPs, C5-GNPs, C6-GNPs, and C7-GNPs and reference structure m-GNPs.

Klein et al.[24] Here, we wanted to test if the alkyne-bearing gCs C4-C7 are suitable for the conjugation to azide-functionalized ultrasmall GNPs following this protocol. As a reference, we used propargyl mannose without calix[4]arene backbone for conjugation in an analogous fashion, giving mannose-gold nanoparticles (m-GNPs, Figure 4). The GNP conjugates (C4-GNPs–C7-GNPs and m-GNPs, Figure 4) were characterized using differential sedimentation centrifugation (DSC, Table 1 and Supporting Information), ^{1}H-NMR and UV-Vis spectroscopy (see Supporting Information).

They were found to be stable in water as well as in PBS buffer for several months. After approximately six months, we observed some precipitation in the samples, which was presumably attributed to nanoparticle aggregation. Nevertheless, the samples were successfully restored by the addition of 1 M NaOH and ultrasonification.

The absence of surface plasmon resonance in the UV-Vis spectra, which can be observed for gold nanoparticles with a radius of more than 2 nm, indicated that no larger

Table 1. Hydrodynamic diameter d_H and degree of carbohydrate functionalization of the different gC-GNPS as determined by DCS. The concentration of carbohydrates was determined by sulfuric acid phenol method (measurements were performed in triplicates, the error is the standard deviation of the mean value, see Supporting Information for further details) and the carbohydrate to nanoparticle ratio was calculated using the molar concentration of nanoparticles as derived by AAS (see Supporting Information for further details).

Ligand	d_H [nm]	C[carbohydrate] [μM]	N[carbohydrates molecules per nanoparticle][a]
N3-GNPs	1.5 ± 0.2	-	-
C4-GNPs	1.4 ± 0.4	658.2 ± 65	16 ± 2
C5-GNPs	1.5 ± 0.7	236.8 ± 44	6 ± 1
C6-GNPs	1.3 ± 0.2	886.8 ± 30	129 ± 4
C7-GNPs	1.5 ± 0.5	601.1 ± 65	88 ± 9
m-GNPs	n.d.	472 ± 44	11 ± 1

[a] N(carbohydrates molecules per nanoparticle) = c(carbohydrates)/c(NP); for c(NP) see Supporting Information.

© 2025 The Author(s). Chemistry – A European Journal published by Wiley-VCH GmbH

15213765, 2025, 40, Downloaded from https://chemistry-europe.onlinelibrary.wiley.com/doi/10.1002/chem.202500497, Wiley Online Library on [13/09/2025]. See the Terms and Conditions (https://onlinelibrary.wiley.com/terms-and-conditions) on Wiley Online Library for rules of use; OA articles are governed by the applicable Creative Commons License

(plasmonic) gold nanoparticles were present (see Supporting Information).[25] This finding was additionally supported by disc centrifugal sedimentation (DCS), which revealed that the measured hydrodynamic radii of the glycocalixarene-gold nanoparticle conjugates were consistently smaller than 2 nm (Table 1). Furthermore, ^{1}H-NMR spectroscopy indicated the successful conjugation by general broadening of the ligand signals (see Supporting Information).[26] However, to quantitatively assess the surface functionalization of gC-GNPs, these methods were not suitable. The sulfuric acid phenol test was used as a colorimetric method in combination with atomic absorption spectroscopy (AAS) to determine the total carbohydrate concentration of the samples. AAS allows to determine the exact concentration of goldin the given dispersion, which can be further converted to the molar concentration of nanoparticles in the dispersion.[24] Accordingly, the ratio of the molar concentration of carbohydrate molecules to the molar concentration of nanoparticles gives the average number of carbohydrates present on each particle. As shown in Table 1, the obtained results are in good agreement with the theoretically expected values and show that the average number of carbohydrates is around 20 times higher for C6-GNPs in comparison to C4-GNPs. For the galactose-functionalized analogous, we observed a similar trend. Here the amount of carbohydrates was found to be around 15 times higher for C7-GNPs compared to C5-GNPs. Surprisingly, m-GNPs showed a similar amount of carbohydrates in the sulfuric acid-phenol test as C4-GNPs. This might be due to shorter linker length causing reduced click efficiency. In summary, the attachment of gCs either through one or four alkyne groups allows to effectively tune the degree of functionalization on the GNPS and thus to control the overall carbohydrate functionalization for resulting gC-GNPs. The number of carbohydrate molecules per nanoparticle is well in line with earlier results on cysteine-conjugated peptides on ultrasmall gold nanoparticles.[27]

2.4. Bacterial Adhesion-Inhibition Assay

Based on their carbohydrate functionalization and previous studies in literature using both gC as well as GNPs as inhibitors of viral and bacterial infections,[28] we tested the inhibitory potential of the derived gCs C1-C3 as well as gC-GNPs C4-C7 in an adhesion-inhibition assay with the 1-fimbriated *E. Coli* strain pPKL1162 expressing GFP. FimH receptors on the surface of the *E. coli* bacteria show specific binding to α-D-mannopyranoside and adhere well on mannan-coated micro titer plates.[29] This binding can be inhibited by mannose-based compounds such as methyl mannose (MeMan) at high enough concentrations resulting in a decreased number of bacteria on the microtiter plate surface. Thus, the inhibitory potential can be observed by quantifying the GFP fluorescence of the E-coli bacteria that can still adhere to the mannan-coated micro titer plate surface. When applying the examined ligands in a serial dilution series of decreasing concentrations, the half maximum inhibition concertation (IC_{50}) values can be determined. To achieve a better comparability among different assays, the IC_{50} values can be referenced with the IC_{50} value obtained for MeMan of each single experiment leading to the referenced inhibitory potential (RIP). This can further be corrected by the valency of binding mannose epitopes for the investigated multivalent structures (RIP_{VC}).[22b,30]

Table 2. IC_{50}, RIP and RIP_{VC} values for the first set of glyco-calixarenes determined by bacterial adhesion-inhibition assay on mannan coated plates. All measurements were performed in triplicates.

Ligand	IC_{50} [μM]	RIP	RIP_{VC}
C1	97 ± 45	102 ± 55	13 ± 7
C2	n.d[a]	-	-
C3	128 ± 39	77 ± 30	19 ± 7

[a] For the galactosyl functionalized control structure C2 no IC_{50} value could be determined.

Table 2 summarizes the determined IC_{50} and RIP values for C1 and C3 after incubation for 45 minutes at 37° C. For C1 a distinct increase of the inhibitor potential by a factor of 13 per binding sugar can be observed in comparison to MeMan. Additionally, glycomacromolecules with hydrophobic backbone motifs that were previously reported by our group exhibit lower RIP_{VC} values.[30] These findings indicate that not only the incorporation of a hydrophobic motif is beneficial, but also that the cluster-like presentation of the sugar epitopes on the calixarene backbone has a favorable effect on bacteria binding. Interestingly, for the heteromultivalent structure C3 an even higher increase by a factor of 19 per binding sugar was observed. This is consistent with the so-called heterocluster effect, which was previously reported in several studies for various model lectins like Concanavalin A.[23,29a,31] It was proposed that the heterocluster effect can be accounted for by different processes promoted by the nonbinding sugar in heteromultivalent glycoconjugates, such as subside binding, structural preorganization, and sterical effects.[32] As anticipated, for the control structure C2 with galactose residues, no IC_{50} could be determined.

Despite the increased inhibitory potential of C1 and C3, it is not likely to assume that one single gC is able to bind more than one FimH receptor at the same time simply due to their size and spatial arrangement. However, the multivalent display of several gCs on larger scaffolds, such as GNPs in the obtained gC-GNP conjugates, could lead to a further enhanced inhibitory potential. By bridging multiple receptors at the same time, binding avidity might increase further. Since this effect was not expected for the sterically demanding gCs (C1-C3), we conjugated only the sterically less demanding gCs (C4-C7) to the GNPs. However, when performing the adhesion-inhibition assay with gC-GNPs we observed large scattering of the fluorescent measurement, which hampered the assessment of IC_{50} values (data not shown). For the mannose-containing structures C4 and C6-GNP conjugates we observed binding, even though no IC_{50} values could be determined. In contrast, no binding was detected for the monovalent mannose GNP conjugate m-GNP in all experiments. For MeMan as monovalent positive control that was included in each single experiment, we do observe binding. Thus, potentially in the monovalent GNP control, the mannose ligands might be sterically too hindered to bind with the receptor, as similar observations have been made for other GNP systems.[7c] We

© 2025 The Author(s). Chemistry – A European Journal published by Wiley-VCH GmbH

15213765, 2025, 40, Downloaded from https://chemistry-europe.onlinelibrary.wiley.com/doi/10.1002/chem.202500497, Wiley Online Library on [13/09/2025]. See the Terms and Conditions (https://onlinelibrary.wiley.com/terms-and-conditions) on Wiley Online Library for rules of use; OA articles are governed by the applicable Creative Commons License

15213765, 2025, 40, Downloaded from https://chemistry-europe.onlinelibrary.wiley.com/doi/10.1002/chem.202500497, Wiley Online Library on [13/09/2025]. See the Terms and Conditions (https://onlinelibrary.wiley.com/terms-and-conditions) on Wiley Online Library for rules of use; OA articles are governed by the applicable Creative Commons License

hypothesize that the fluctuations observed in our experiment can be accounted for by the formation of bacteria-nanoparticle agglomerates. To further investigate the samples and to support this hypothesis, we engaged fluorescence microscopy (see Supporting Information). Indeed, we found large fluorescent agglomerates after incubating *E. coli* bacteria suspension in PBS buffer for 45 minutes with C6-GNPs. Unexpectedly, the formation of bacteria agglomerates was also observed for bacteria suspension that was not incubated with any glyco conjugate, even though to a smaller extent. Interestingly, after incubation with C1 the formation of agglomerates was notably decreased. Future studies will explore this further, also by using other binding assays such as a fluorescence competition assay for carbohydrate-functionalized GNPs.[7c] Nevertheless, we believe that already our first proof-of-concept study for the combination of gCs and GNPs to derive inhibitors of bacterial adhesion shows the potential of leveraging this dual multivalent presentation.

3. Conclusion

In this study we successfully developed and established solid-phase synthetic protocols for the modular preparation of several gCs, that also allows the incorporation of additional functional groups such as alkyne moieties at both rims of the gC structures. In a second step, gCs were conjugated to ultrasmall GNPs via CuAAC via either one or four pending alkyne residues providing a handle to adapt the number of carbohydrate ligands on the NP surface. Finally, bacterial adhesion-inhibition studies showed the inhibitory potential of mannose bearing gCs and gC-GNPs. Overall, this study presents a versatile synthetic strategy to complex multivalent scaffolds based on the combination of solid-phase synthesis, calixarenes and gold nanoparticles that can now also be used to present other ligands or functional groups for different applications.

Supporting Information

The authors have cited additional references within the Supporting Information.[33]

Acknowledgments

A.K., K.K., M.E. and L.H. thank the DFG for funding by the Collaborative Research Center (CRC) 1093. A.K. and L.H. thank Prof. Stephan Schmidt and Prof. Thisbe Lindhorst for providing the *E. coli* bacteria strain pPKL1162. The authors thank the CeMSA@HHU (Center for Molecular and Structural Analytic at Heinrich Heine University) for recording the mass-spectrometric and NMR-spectroscopic data in the structural analysis of the macromolecules.

Open access funding enabled and organized by Projekt DEAL.

Conflict of Interest

The authors declare no conflict of interest.

Data Availability Statement

The data that support the findings of this study are available in the supplementary material of this article

Keywords: bacterial inhibition · E. coli · glycocalix[n]arenes · gold nanoparticles · multivalency

[1] a) R. D. Cummings, *Glycoconjugate J.* **2019**, *36*, 241; b) R. A. Dwek, *Chem. Rev.* **1996**, *96*, 683; c) G. V. Glinsky, *Cancer Metastasis Rev.* **1998**, *17*, 177; d) K.-A. Karlsson, *Curr. Opin. Struct. Biol.* **1995**, *5*, 622; e) A. Imberty, A. Varrot, *Curr. Opin. Struct. Biol.* **2008**, *18*, 567.
[2] a) C. R. Bertozzi, L. L. Kiessling, *Science* **2001**, *291*, 2357; b) M. Mammen, S.-K. Choi, G. M. Whitesides, *Angew. Chem. Int. Ed.* **1998**, *37*, 2754.
[3] a) Y. C. Lee, R. T. Lee, *Acc. Chem. Res.* **1995**, *28*, 321; b) J. J. Lundquist, E. J. Toone, *Chem. Rev.* **2002**, *102*, 555.
[4] I. Pramudya, H. Chung, *Biomater. Sci.* **2019**, *7*, 4848.
[5] M. Touaibia, T. C. Shiao, A. Papadopoulos, J. Vaucher, Q. Wang, K. Benhamioud, R. Roy, *Chem. Commun.* **2007**, 380.
[6] a) S. André, F. Sansone, H. Kaltner, A. Casnati, J. Kopitz, H. J. Gabius, R. Ungaro, *ChemBioChem* **2008**, *9*, 1649; b) S. Cecioni, R. Lalor, B. Blanchard, J. P. Praly, A. Imberty, S. E. Matthews, S. Vidal, *Chem. Eur. J* **2009**, *15*, 13232; c) S. Francesco, *Chem. Soc. Rev.* **2013**, *42*, 4623.
[7] a) C.-C. Lin, Y.-C. Yeh, C.-Y. Yang, G.-F. Chen, Y.-C. Chen, Y.-C. Wu, C.-C. Chen, *Chem. Commun.* **2003**, 2920; b) C.-C. Lin, Y.-C. Yeh, C.-Y. Yang, C.-L. Chen, G.-F. Chen, C.-C. Chen, Y.-C. Wu, *J. Am. Chem. Soc.* **2002**, *124*, 3508; c) X. Wang, O. Ramstrom, M. Yan, *Anal. Chem.* **2010**, *82*, 9082; d) D. Budhadev, E. Poole, I. Nehlmeier, Y. Liu, J. Hooper, E. Kalverda, U. S. Akshath, N. Hondow, W. B. Turnbull, S. Pöhlmann, *J. Am. Chem. Soc.* **2020**, *142*, 18022.
[8] a) S. B. van der Meer, I. Hadrovic, A. Meiners, K. Loza, M. Heggen, S. K. Knauer, P. Bayer, T. Schrader, C. Beuck, M. Epple, *J. Phys. Chem. B* **2021**, *125*, 115; b) M. Fan, Y. Han, S. Gao, H. Yan, L. Cao, Z. Li, X.-J. Liang, J. Zhang, *Theranostics* **2020**, *10*, 4944; c) A. Leifert, Y. Pan-Bartnek, U. Simon, W. Jahnen-Dechent, *Nanoscale* **2013**, *5*, 6224; d) S. Huo, S. Jin, X. Ma, X. Xue, K. Yang, A. Kumar, P. C. Wang, J. Zhang, Z. Hu, X.-J. Liang, *ACS Nano* **2014**, *8*, 5852.
[9] S. B. van der Meer, K. Loza, K. Wey, M. Heggen, C. Beuck, P. Bayer, M. Epple, *Langmuir* **2019**, *35*, 7191.
[10] K. Huang, H. Ma, J. Liu, S. Huo, A. Kumar, T. Wei, X. Zhang, S. Jin, Y. Gan, P. C. Wang, S. He, X. Zhang, X.-J. Liang, *ACS Nano* **2012**, *6*, 4483.
[11] Y. Ding, Z. Sun, Z. Tong, S. Zhang, J. Min, Q. Xu, L. Zhou, Z. Mao, H. Xia, W. Wang, *Theranostics* **2020**, *10*, 5195.
[12] a) Y. Y. Chien, M. D. Jan, A. K. Adak, H. C. Tzeng, Y. P. Lin, Y. J. Chen, K. T. Wang, C. T. Chen, C. C. Chen, C. C. Lin, *ChemBioChem* **2008**, *9*, 1100; b) I. Papp, C. Sieben, K. Ludwig, M. Roskamp, C. Böttcher, S. Schlecht, A. Herrmann, R. Haag, *Small* **2010**, *6*, 2900; c) Á. G. Barrientos, J. M. de la Fuente, T. C. Rojas, A. Fernández, S. Penadés, *Chem. Eur. J* **2003**, *9*, 1909; d) A. G. Barrientos, J. M. de la Fuente, M. Jiménez, D. Solís, F. J. Cañada, M. Martín-Lomas, S. Penadés, *Carbohydr. Res.* **2009**, *344*, 1474; e) O. Martínez-Ávila, K. Hijazi, M. Marradi, C. Clavel, C. Campion, C. Kelly, S. Penadés, *Chem. Eur. J* **2009**, *15*, 9874.
[13] M. Reynolds, M. Marradi, A. Imberty, S. Penadés, S. Pérez, *Chem. Eur. J* **2012**, *18*, 4264.
[14] S. Boden, K. G. Wagner, M. Karg, L. Hartmann, *Polymers* **2017**, *9*, 716.
[15] a) M. Marradi, F. Chiodo, I. García, S. Penadés, *Chem. Soc. Rev.* **2013**, *42*, 4728; b) M. Brust, J. Fink, D. Bethell, D. Schiffrin, C. Kiely, *J. Chem. Soc. Chem. Commun.* **1995**, 1655; c) M. Brust, M. Walker, D. Bethell, D. J. Schiffrin, R. Whyman, *J. Chem. Soc. Chem. Commun.* **1994**, 801.
[16] a) J. M. de la Fuente, *Angew. Chem.* **2001**, *(International ed. in English) 40*, 2257; b) J. Rojo, V. Díaz, J. M. de la Fuente, I. Segura, A. G. Barrientos, H. H. Riese, A. Bernad, S. Penadés, *ChemBioChem* **2004**, *5*, 291.
[17] S. B. van Der Meer, T. Seiler, C. Buchmann, G. Partalidou, S. Boden, K. Loza, M. Heggen, J. Linders, O. Prymak, C. L. Oliveira, *Chem. Eur. J* **2021**, *27*, 1451.
[18] M. Epple, V. M. Rotello, K. Dawson, *Acc. Chem. Res.* **2023**, *56*, 3369.
[19] a) L. Baldini, A. Casnati, F. Sansone, *Eur. J. Org. Chem.* **2020**, *2020*, 5056; b) S. J. Meunier, R. Roy, *Tetrahedron Lett.* **1996**, *37*, 5469; c) A. Marra, L. Moni, D. Pazzi, A. Corallini, D. Bridi, A. Dondoni, *Org. Biomol. Chem.* **2008**,

© 2025 The Author(s). Chemistry – A European Journal published by Wiley-VCH GmbH

6, 1396; d) G. M. Consoli, G. Granata, V. Cafiso, S. Stefani, C. Geraci, *Tetrahedron Lett.* **2011**, *52*, 5831; e) Y. C. Pan, X. Y. Hu, D. S. Guo, *Angew. Chem. Int. Ed.* **2021**, *60*, 2768; f) A. Palmioli, L. Moretti, C. A. Vezzoni, L. Legnani, P. Sperandeo, L. Baldini, F. Sansone, C. Airoldi, A. Casnati, *Bioorg. Chem.* **2023**, *138*, 106613; g) S. Avvakumova, P. Fezzardi, L. Pandolfi, M. Colombo, F. Sansone, A. Casnati, D. Prosperi, *Chem. Commun.* **2014**, *50*, 11029.

[20] S. B. Shuker, J. Esterbrook, J. Gonzalez, *Synlett* **2001**, *2001*, 0210.

[21] D. Ponader, F. Wojcik, F. Beceren-Braun, J. Dernedde, L. Hartmann, *Biomacromolecules* **2012**, *13*, 1845.

[22] a) M. Ebbesen, C. Gerke, P. Hartwig, L. Hartmann, *Polym. Chem.* **2016**, *7*, 7086; b) S. Igde, S. Röblitz, A. Müller, K. Kolbe, S. Boden, C. Fessele, T. K. Lindhorst, M. Weber, L. Hartmann, *Macromol. Biosci.* **2017**, *17*, 1700198.

[23] D. Ponader, P. Maffre, J. Aretz, D. Pussak, N. M. Ninnemann, S. Schmidt, P. H. Seeberger, C. Rademacher, G. U. Nienhaus, L. Hartmann, *J. Am. Chem. Soc.* **2014**, *136*, 2008.

[24] K. Klein, K. Loza, M. Heggen, M. Epple, *ChemNanoMat* **2021**, *7*, 1330.

[25] R. Yu, L. M. Liz-Marzán, F. J. G. de Abajo, *Chem. Soc. Rev.* **2017**, *46*, 6710.

[26] N. Wolff, C. Beuck, T. Schaller, M. Epple, *Nanoscale Adv.* **2024**, *6*, 3285.

[27] L.-S. Wagner, O. Prymak, T. Schaller, C. Beuck, K. Loza, F. Niemeyer, N. Gumbiowski, K. Kostka, P. Bayer, M. Heggen, *J. Phys. Chem. B* **2024**, *128*, 4266.

[28] a) U. I. M. Gerling-Driessen, M. Hoffmann, S. Schmidt, N. L. Snyder, L. Hartmann, *Chem. Soc. Rev.* **2023**, *52*, 2617; b) P. M. Chaudhary, S. Sangabathuni, R. V. Murthy, A. Paul, H. V. Thulasiram, R. Kikkeri, *Chem. Commun.* **2015**, *51*, 15669.

[29] a) A. K. H. Mirja Hartmann, P. Klemm, T. K. Lindhorst, *Chem. Commun.* **2010**, *46*, 330; b) I. Kalograiaki, M. Abellán-Flos, L. A. n. Fernández, M. Menéndez, S. p. P. Vincent, D. Solís, *Anal. Chem.* **2018**, *90*, 12314; c) S. Kötter, U. Krallmann-Wenzel, S. Ehlers, T. K. Lindhorst, *J. Chem. Soc., Perkin Trans* **1998**, *1*, 2193.

[30] S. Boden, F. Reise, J. Kania, T. K. Lindhorst, L. Hartmann, *Macromol. Biosci.* **2019**, *19*, 1800425.

[31] M. Gómez-García, J. M. Benito, D. Rodríguez-Lucena, J.-X. Yu, K. Chmurski, C. Ortiz Mellet, R. Gutiérrez Gallego, A. Maestre, J. Defaye, J. M. García Fernández, *J. Am. Chem. Soc.* **2005**, *127*, 7970.

[32] C. O. Mellet, J.-F. Nierengarten, J. M. G. Fernández, *J. Mater. Chem. B* **2017**, *5*, 6428.

[33] a) W. Hayes, H. M. Osborn, S. D. Osborne, R. A. Rastall, B. Romagnoli, *Tetrahedron* **2003**, *59*, 7983; b) L. Wu, N. S. Sampson, *ACS Chem. Biol.* **2014**, *9*, 468; c) S. M. Gerchakov, P. G. Hatcher, *Limnol. and Oceanogr.* **1972**, *17*, 938; d) T. Masuko, A. Minami, N. Iwasaki, T. Majima, S.-I. Nishimura, Y. C. Lee, *Anal. Biochem.* **2005**, *339*, 69; e) M. Bergeron-Brlek, T. C. Shiao, M. C. Trono, R. Roy, *Carbohydr. Res.* **2011**, *346*, 1479.

Manuscript received: February 7, 2025
Revised manuscript received: May 27, 2025
Version of record online: June 27, 2025

© 2025 The Author(s). Chemistry – A European Journal published by Wiley-VCH GmbH

15213765, 2025, 40, Downloaded from https://chemistry-europe.onlinelibrary.wiley.com/doi/10.1002/chem.202500497, Wiley Online Library on [13/09/2025]. See the Terms and Conditions (https://onlinelibrary.wiley.com/terms-and-conditions) on Wiley Online Library for rules of use; OA articles are governed by the applicable Creative Commons License

Supporting Information

A Modular Solid Phase Synthesis Approach for Glycocalix[4]arene Derivatives and their Multivalent Presentation on Ultrasmall Gold Nanoparticles.

Alisa Kayser[a], Kai Klein[b], Daria Babushkina[a], Anna Sakse[a], Gisele Mouafo Kenne[a], Hajo Böschen[a], Ulla I.M. Gerling-Driessen[c], Monir Tabatabai[a], Matthias Epple[b] and Laura Hartmann[a][c]

[a] Department of Organic Chemistry and Macromolecular Chemistry, Heinrich Heine University Dusseldorf, Universitätsstraße 1, Dusseldorf, 40225, Germany.
[b] Inorganic Chemistry and Center for Nanointegration Duisburg-Essen (CENIDE), University of Duisburg Essen, Universitätsstraße 7, Essen 45141, Germany.
[c] Institute for Macromolecular Chemistry, University of Freiburg, Stefan-Meier Straße 31, Freiburg i.Br. 79104, Germany

Materials:

The following chemicals were used without further purification: Dimethylformamide (≥99.8%, Biosolve Chemicals) , dichloromethane (≥99.8%, Fisher Scientific), chloroform (≥99.8%, Fisher Chemical), tetrahydrofuran (≥99.9%, Sigma Aldrich), 1,4-dioxane (98%, Sigma Aldrich), N-methyl-2-pyrrolidone (≥99.0%, Acros Organics), methanol (≥99.8% VWR Chemicals), acetonitrile (HPLC grade, ≥99.9%, Honeywell), diethyl ether (≥99.8%, Honeywell), dimethyl sulfoxide (≥ 99%, Carl Roth), N_{β}-boc-N_{α}-Fmoc-L-2,3-diaminopropionic acid (>97%, TCI chemicals), 4-pentynoic acid (95%, Sigma Aldrich), TentaGel S RAM (Rapp Polymere), AG® 1-X8 (Bio-Rad Laboratories), benzotriazole-1-yloxytripyrrolidinophosphonium hexafluorophosphate (≥98%, Carbosynth limited), N,N-diisopropylethylamine (≥99.0%, Carl Roth) N-methyl morpholine (> 99.0% Tokio Chemical Industry), piperidine (99%, Acros Organics), triisopropyl silane (98 %, Sigma Aldrich), sodium methoxide (≥ 97%, Sigma Aldrich), tin(II) chloride dihydrate (≥98%, Carl Roth), sodium ascorbate (≥ 99 %, Carl Roth), copper(II) sulfate (>98%, Acros Organics), sodium diethyldithiocarbamate trihydrate (98%, Alfa Aesar), 4-*tert*-butylcalix[4]arene (≥98%, Biosynth Carbosynth), barium oxide (99.5%, abcr), barium hydroxide octahydrate (≥98%, Sigma Aldrich), 1-iodopropane (99%, Sigma Aldrich), sodium hydride (60% dispersion in mineral oil, Sigma Aldrich), ethyl 6-bromohexanoate (≥97%, Fluorochem), nitric acid (≥99%, Sigma Aldrich), acetic acid (≥99.8%, Sigma Aldrich), hydrochloric acid (37%, Fisher Chemical), trifluoroacetic acid (99.5 %, Acros Organics), potassium hydroxide (≥99.5%, Sigma Aldrich), tris(3-hydroxypropyl-triazoylmethyl) amine (96%, Sigma Aldrich), aminoguanidine hydrogen carbonate (98%, Alfa Aesar), Amberlite IR 120 (Sigma Aldrich), phenol (99%, Fisher Scientific), methyl α-D-mannopyranoside (≥99.0%, Sigma Aldrich), mannan from *Saccharomyces cerevisiae* (Sigma Aldrich), Bovine Serum Albumin (Sigma Life Science),

Milli-Q water was gained by a MicroPure water purification system from ThermoScientific.

Buffer and media: Phosphate-buffered saline (PBS, pH 7.4) was prepared using PBS buffer tablets from Carl Roth for 100 ml. For PBST 0,05 vol.-% Tween® 20 (polyoxyethylen-20-sorbitanmonolaurat, Carl Roth) was added to PBS buffer. For the Carbonate puffer (pH 9.4) 1.59 g sodium carbonate and 2.52 g sodium hydrogen carbonate was dissolved in 1L MQ water. LB-media was prepared by dissolving 25 g LB miller broth from Sigma Aldrich in 1 L MQ water. After sterilization 50,0 mg of ampicillin sodium salt (Sigma Aldrich) and 25,0 mg chloramphenicol (BioChemica, AppliChem) were added. The pH value was adjusted with 0.1 M NaOH using a pH-electrode by Mettler Toledo.

imidazole-1 sulfonyl azide hydrogen sulfate was synthesized according to a previously communicated protocol.[1]

The building blocks TDS ((triple-bond diethylenetriamine-succinic acid, 1-(fluorenyl)-3,11-dioxo-7- (pent-4-ynoyl)-2-oxa-4,7,10-triazatetra-decan-14-oic acid) and EDS (EDS (ethylene glycoldiamine-succinic acid 1-(9H-fluoren-9-yl)-3,14-dioxo-2,7,10-trioxa-4,13-diazaheptadecan-17-oic acid) were synthesized as previously reported.[2]

The synthesis of (2-azidoethyl)-2,3,4,6-tetra-O-acetyl-α-D-mannopyranoside was performed according to literature.[3] (2-azidoethyl)-2,3,4,6-tetra-O-acetyl-β-D-galactopyranoside was synthesized as reported previously.[4]

Instruments:

Reversed Phase – High Pressure Liquid Chromatography (RP-HPLC-MS):

Chromatography measurements were performed on an Agilent 1260 Infinity instrument coupled to a variable wavelength detector at an absorption wavelength of 214 nm and an Agilent Quadrupole mass spectrometer with an electrospray ionization (ESI) source (m/z range from 200-2000). A MZ-Aqua Perfect C18 column (3.0 x 50 nm, 3 µm) was used at 25° C. As mobile phase linear gradients of an eluent system A and B was used: A) H_20/ACN (95/5 vol.%) + 0.1 vol.-% formic acid; B) H_20/ACN (5/95 vol.%) + 0.1 vol.% formic acid). The flow rate was 0.4 ml/min.

Preparative RP-HPLC:

Chromatographic purifications were done on an Agilent 1200 Series instrument with variable wavelength detector at 214 nm and a fraction collector was used. A UG80 C18 RP column (20 x 250 nm, 5 µM) from Shiseido was used at 25° C. A flow rate of 10 ml/min was applied. For all samples an eluent system A and B was used in linear gradients: A) H_2O + 0.1 vol.% formic acid; B) ACN + 0.1 vol.-% formic acid.

Matrix Assisted Laser Desorption Ionization – Time of Flight – Mass Spectrometry (MALDI-TOF-MS):

The MALDI-TOF mass spectra were measured on a Bruker UltrafleXtreme instrument from Bruker Daltonics. The measurements were performed using 2,5-dihydroxybenzoic acid (DHB) or dithranol (DIT) in combination with sodium trifluoroacetate as a matrix in linear or reflector mode.

^{1}H-Nuclear Magnetic Resonance (^{1}H-NMR):

^{1}H-NMR spectra were either recorded on a Bruker Avance III-300 (300 MHz) or 600 (600 MHz). The chemical shifts are reported in delta (δ) expressed in parts per million (ppm). The residual, non-deuterated solvent (δ 3.31 ppm for MeOH-*d4* or δ 2.50 ppm for DMSO-*d6*) were used as an internal reference. The nanoparticles were dispersed in a H_2O/D_2O mixture (90/10 vol.-%) and water signal suppression was used.

Fluorescence Spectroscopy:

All fluorescence emission measurements were acquired on a CLARIOstar® microtiter plate reader from BMG LABTECH at 485/535 nm at ambient temperature. All measurements were performed with black polystyrene 96-wells microtiter plates from Greiner. The data were evaluated with the BMG Mars software.

Fluorescent Microscopy:

The fluorescence microscopy measurements were performed on an inverted microscope IX73 from Olympus with an Olympus 60 x NA 1.35 oil-immersion objective and a CMOS camera (UI-3360CP-M-GL). For the measurement µ-slides 18 wells with glass bottom from ibidi were used. As a light source a collimated LED (530 nm, blue light) from Thorlabs was used.

Atomic Absorption Spectroscopy (AAS):

AAS was done with an Electron M-series spectrometer from ThermoScientific after dissolving the gold nanoparticles in *aqua regia*.

Disc centrifugal sedimentation (DCS):

DCS was done with a DC24000 instrument from CPS. Thereby, the disc was accelerated to 24000 rpm. A gradient of sucrose solution was injected starting 1.6 mL of 24 wt.-% sucrose in water, the gradient increased in steps of 0.2 mL to 1.6 mL of 8 wt.-% sucrose in water. The gradient solution was capped with 0.5 mL of dodecane to avoid evaporation. The instrument was calibrated with a dispersion of stabilized PVC particles with a defined hydrodynamic diameter of 483 nm.

Freeze-dryer:

The final products were freeze-dried with an Alpha 1-4 LD plus instrument from Martin Christ set to -50° C at 0.1 mbar.

Solid phase synthesis protocol:

Coupling and Fmoc-deprotection procedure:

All solid phase reactions were performed on TentaGel S RAM resin in batch sizes up to 0.15 mM in polypropylene syringes with integrated frits. Prior to use, the resin was swollen in DCM for 30 mins followed by washing with DMF five times. The reaction conditions for the coupling of different building blocks are given in the table below (table S1) and differ prior to and subsequent the introduction of CBB2. The coupling steps prior to coupling of CBB1 was performed according to a previously established coupling protocol using 5 eq. PyBOP and 10 eq. DIPEA as coupling reagents.[2b] For the coupling of EDS to CBB1, reaction conditions were optimized. Using DIPEA as a base resulted in relative purities of 83-89%, while N-methyl morpholine yielded purities of 86-95%, depending on the prior coupling sequence. As additional by-product are formed using DIPEA, *N*-methyl morpholine is used as a base as standard procedure. After coupling, the resin was washed 10 times with DMF and DCM. Fmoc deprotection was performed with 20 vol.-% piperidine in DMF for 30 min (fresh solution added after 20 min). The resin was washed 10 times with DMF before the next coupling step.

Table S1. Reaction conditions for coupling steps prior to and subsequent the integration of the calix[4]arene building block CBB1

	Building block	Eq. of building block	Coupling agents	Reaction time
Prior CBB1	EDS/TDS/Dap/ pentynoic acid	5	5 Eq. PyBOP + 10 Eq. DIPEA	1h
-	CBB1	3	5 Eq. PyBOP + 10 Eq. DIPEA	5h
Subsequent CBB1	EDS/TDS/ pentynoic acid	5/amine	5. Eq. PyBOP/amine + 10 Eq. *N*-methyl morpholine/amine	1h

Boc group removal:

The Boc group in the side chain of Dap was removed using 4M HCl in dioxan solution. The resin was first washed five times with dioxan before the HCl solution was added to the syringe and shaken vigorously for 10 min. The resin was then washed three times with dioxan and the procedure was repeated for a further 20 min. For neutralization, the resin was shaken (2x10 min) in 10 vol% DIPEA in DCM. The resin was then washed three times with approximately 2 ml dioxan and DCM and finally ten times with 2 ml DMF. This was followed by a coupling step according to the protocol described above.

Reduction of Aryl-nitro groups:

The nitro groups at the upper rim of CBB1 were reduced to amines by treating the resin with 25 eq. tin(II) chloride dihydrate in NMP (3 ml) for 24 hours at 30° C. To remove excess of tin salt, the resin was washed thoroughly ten times with NMP, methanol, DCM and DMF.

Copper(I)-catalyzed azide-alkyne cycloaddition (CuAAC):

For the cycloaddition 2eq. of the carbohydrate azide was dissolved in 1 ml DMF. In addition, 20 mol-% relative to the azide component of sodium ascorbate as well as copper(II) sulfate was dissolved separately in 0,1 mL of MQ water each. The solutions were then added to the syringe in the mentioned order and shaken overnight in the dark. By washing the resin

alternately with a 0,23 M solution of sodium diethyldithiocarbamate in DMF/water and DMF the excess copper is removed, which can be monitored by color change.

Deacetylation carbohydrate residues:

Approximately 2 ml of a 0.2 M sodium methanolate solution in methanol was added to the syringe and shaken vigorously for 30 mins. Subsequently, the resin was washed ten times with methanol and DMF.

Cleavage from the solid phase:

A solution of TFA/TIPS/DCM (95/2.5/2.5 vol.-%) was used to cleave the final glycocalix[4]arene from the solid support. The resin was treated with the cleavage solution for 1h and subsequently the product was precipitated in ice-cold diethyl ether. After centrifugation at 4000 rpm the supernatant was decanted, and the remaining precipitate was dissolved in water or water/DMSO (for water-insoluble derivative C4 and C5) and finally lyophilized.

To monitor the reactions on the solid support, small amounts of the resin were separated and treated according to the cleavage conditions described above (referred to as micro cleavage). The obtained precipitate was then analyzed via RP-HPLC-MS.

TFA anion exchange:

For the anion exchange of the water-soluble derivatives (C1-C3 and C56-C7) an AG® 1-X8 resin was used. The resin was first washed three times with 1,6 M aqueous acetic acid followed by three times with 0,16 M acetic acid before use. The exchange was performed for two hours.

Sulfuric acid phenol method:

The total concentration of carbohydrates in each sample was determined by the established sulfuric acid phenol method.[5] Here, the reaction is performed in polystyrene microtiter plates, as less sample volume is required. D-mannose in nanoparticle dispersion was used for standard curves. D-mannose was used in a concentration range from 320 to 20 µM, while the nanoparticle concentration was kept constant at 41.11 µM (C4-GNPs, C5-GNPs and m-GNPs) or 6.85 µM (C6-GNPs, C7-GNPs). This procedure was performed because the ultra-small nanoparticles cannot be properly removed from the carbohydrate sample, causing background noise that must be considered. To 35 µL of the sample, 35 µL of a 5 w.-% phenol solution in MQ water was added followed by 180 µL of concentrated sulfuric acid and mixed vigorously with a pipette. The mixture was then incubated for 30 min at 30°C. The absorbance of each sample was detected at 420 nm. All measurements were performed in triplicate. As a reference, the gold nanoparticles were treated analogously before functionalization. By comparing the sample with the standard curve, the carbohydrate concentration was determined.

Bacterial adhesion-inhibition assay:

For the bacterial adhesion inhibition studies, a E. Coli strain pPKL1162, kindly provided by the Lindhorst group from the University of Kiel, Germany, was used. The assay was performed according to literature protocols with slight modifications.[6] The bacteria were cultured from a frozen stock (LB media + AMP + CAM) over night at 37° C in LB media. The bacteria were then washed three times with PBS buffer and subsequently diluted with PBS buffer to obtain a bacterial dispersion with OD(600 nm) = 0.4. The polystyrene microtiter plates were mannan coated with 120 µL of mannan from *Saccharomyces cerevisiae* overnight in carbonate buffer (pH = 9.4) at 37° C. The plates were washed three times with PBST buffer (150 µL, PBS + 0,05% Tween) and then blocked with 120 µL of 0,1% BSA in PBS solution for two hours. Subsequently, the plates were washed three times with PBST (150 µL). Afterwards, the samples were applied to the microtiter plates in a serial dilution in PBS buffer (50 µL) and incubated with bacterial dispersion (50 µL) for 45 min at 45

min. Then, the plates were washed with PBS buffer (100 µL) and the wells were filled with 100 µL PBS. The fluorescence read out was measured at 485/535nm.

Synthesis of nanoparticles and functionalization by CuAAC

The gold nanoparticles Au-GSH were prepared according to an adapted Brust-Schiffrin protocol as previously reported.[1] Subsequently, the azidation of the nanoparticles was performed as reported, except that the equivalents of the imidazole-1 sulfonyl azide hydrogen sulfate were reduced to 15 eq. compared to 50 eq. in the original protocol, with respect to glutathione. CuAAC of the alkyne-functionalized glycocalix[4]arenes **C4-C7** to the AuGSH-N_3 nanoparticles was carried out as follows. The nanoparticle sample containing 7.7 µmol azido groups (68 nmol, 3.15 mg Au) was dispersed in 3 mL of water. Then the glycocalix[4]arenes **C4-C7** were dissolved in 1 mL of water or DMSO (0,4 eq., 3.08 µmol) and added to the nanoparticle dispersion. Subsequently, 630 µL of an aqueous solution of $CuSO_4$, THPTA (50 µmol) and aminoguanidine hydrogen carbonate (10 µmol), previously prepared in 10 mL of water, were added to the reaction mixture. Finally, sodium ascorbate in water (3.15 µmol, 0.63 mg in 100 µL water) was added to start the reaction. The mixture was stirred for 14 h before water was added to give an overall volume of 20 mL, followed by purification by spin filtration (4x) (Amicon spin filters).

The number of carbohydrate molecules was computed as reported earlier, assuming an average diameter of the solid core of a spherical gold nanoparticle of 2 nm, by dividing the concentration of carbohydrate molecules (determined by the sulfuric acid phenol test)[5] in the dispersion by the concentration of gold nanoparticles in the dispersion (determined by AAS).[7]

Analytical Data

α-D-propargyl-mannopyranoside:

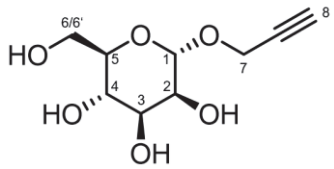

2,3,4,6-Tetra-*O*-acetyl-α-D-propargyl-mannopyranoside was synthesized according to a previously reported protocol.[8] For deacetylation the carbohydrate was dissolved in a 2 mg/mL solution of sodium methoxide in methanol and let stir for 50 minutes. The reaction was stopped by adding Amberlite IR120 Hydrogen Form until the pH is neutral. Subsequently, the resin was filtered off and the product was obtained after concentration under reduced pressure.

^{1}H-NMR (300 MHz, D_2O): δ 5.04 (d, ^{3}J=1.9 Hz, 1H, 1), 4.34 (dd, ^{2}J=5.7 Hz, ^{4}J=2.5 Hz, 2H, 7), 3.96 (dd, ^{3}J = 1.9, 3.4 Hz, 1H, 2), 3.9 (dd, ^{3}J = 1.8, 12.2 Hz, 1H, 4), 3.84-3.65 (m, 4H, 3, 5, 6, 6‘), 2.93 (t, ^{4}J=2.5 Hz, 1H, 8) ppm.

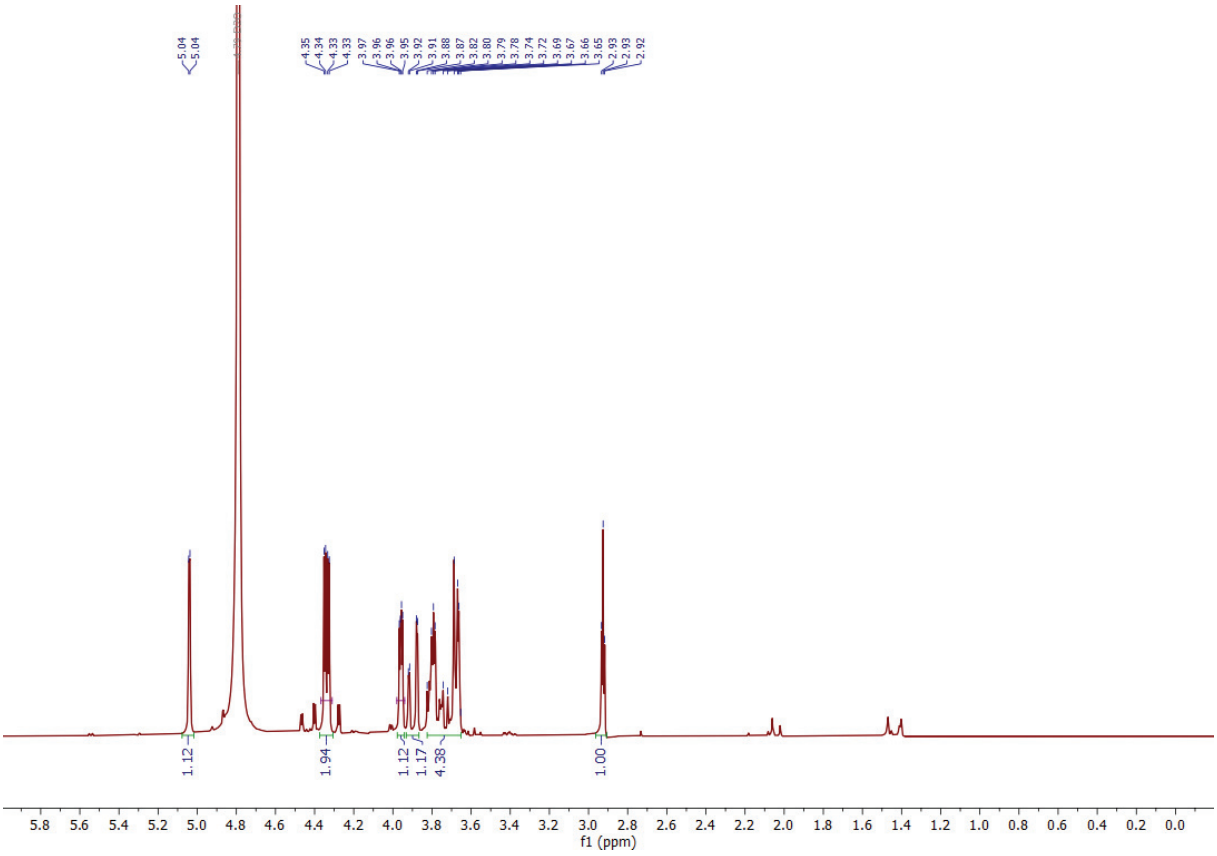

Figure S1. ^{1}H-NMR spectrum (300MHz) of α-D-propargyl-mannopyranoside in D_2O.

Calix[4]arene building block CBB1:

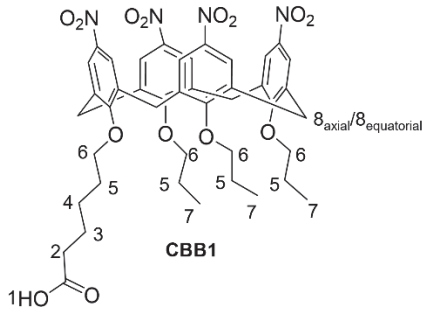

CBB1

The building block was prepared as previously reported.[9]

^{1}H-NMR (300 MHz, DMSO-*d6*): δ 12.04 (s, 1H, 1), 7.65 (s, 8H, Aryl-H), 4.37 (d, ^{2}J= 12.1 Hz, 4H, 8_{axial}), 3.95 (m, 8H, 6), 3.69 (d, ^{2}J=12.1 Hz, 4H, $8_{equatorial}$), 2.24 (t, ^{3}J = 7.2, 2H, 2), 1.85 (m, 8H, 5), 1.58 (p, ^{3}J=7.1 Hz, 2H, 3), 1.41 (m, 2H, 4), 1.05-0.90 (m, 9H, 7) ppm.

MALDI-TOF-MS: m/z calculated for $C_{43}H_{48}N_4O_{14}$: 867.32 $[M+Na]^+$, found: 867.36 $[M+Na]^+$

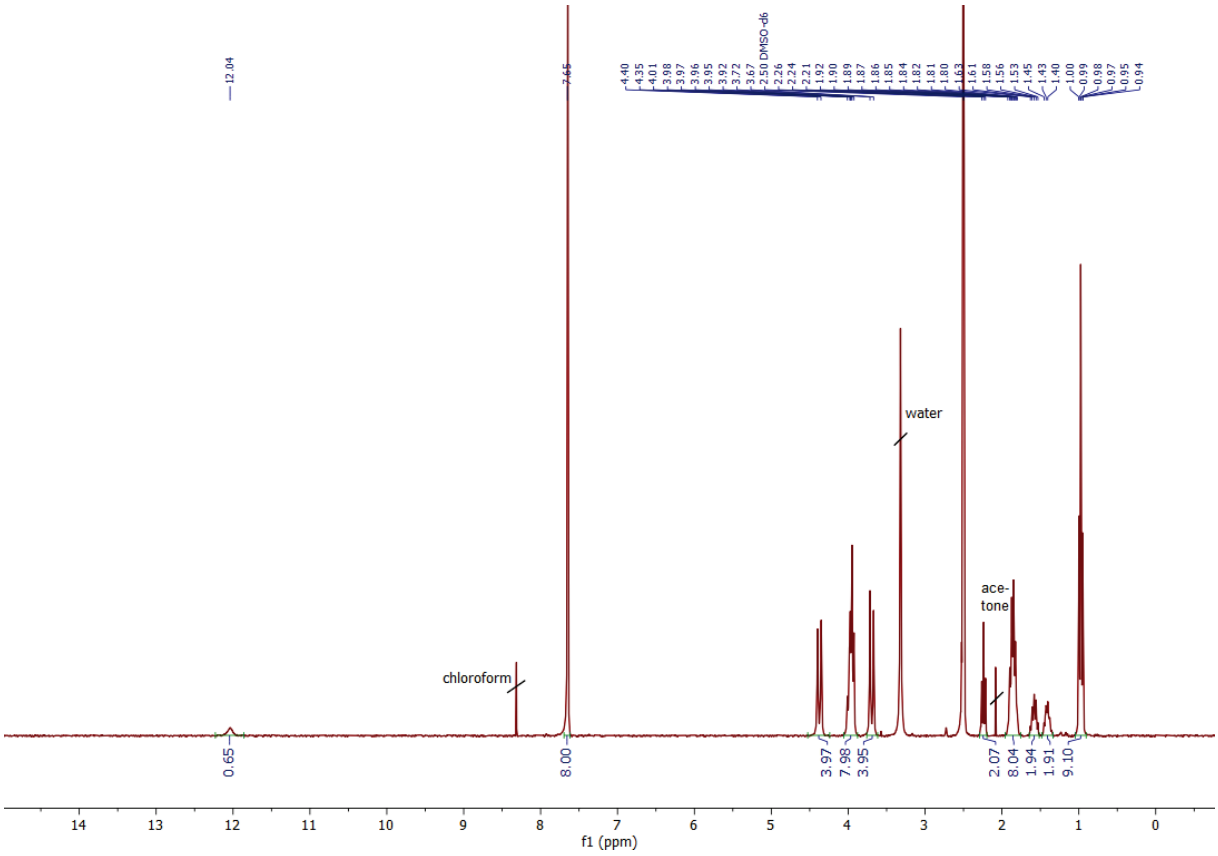

Figure S2. ^{1}H-NMR spectrum (300MHz) of CBB1 in DMSO-*d6*.

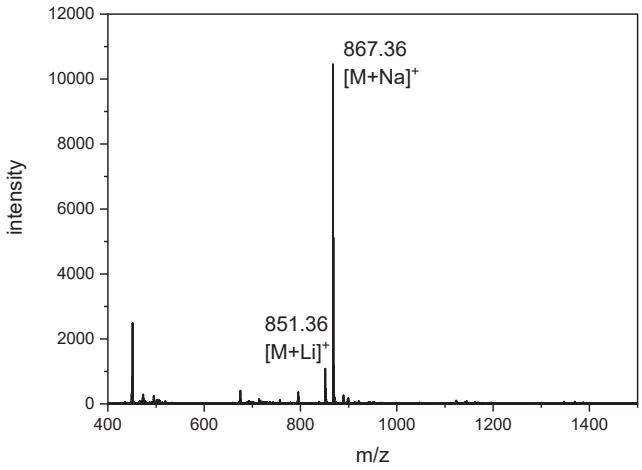

Figure S3: MALDI-TOF-MS spectrum of CBB1.

Compound C1:

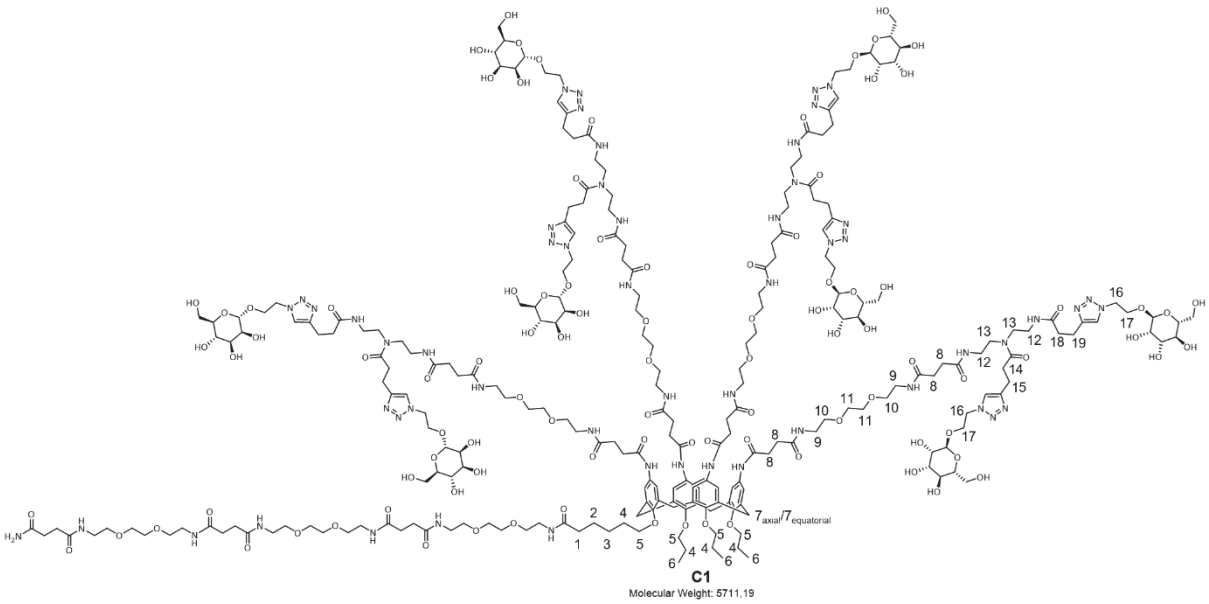

Compound **C1** was purified by preparative HPLC (73% A to 67% A in 13 min) and obtained in a yield of 10%. The relative purity of 90% was determined by integration of the UV signals of the RP-HPLC run at 214 nm. MS analysis suggests that the by-product observed, that could not be separated by preparative purification, is due to EDS-TDS-(man)-pentynoic acid(man) deletion. Additionally, ^{1}H-NMR analysis confirms this.

ESI-MS: m/z calculated for $C_{249}H_{395}N_{55}O_{97}$: 1427.94 $[M+4H]^{4+}$, 1142.55 $[M+5H]^{5+}$, 952.3 $[M+6H]^{6+}$, 816.4 $[M+7H]^{7+}$, 714.47 $[M+8H]^{8+}$, found: 1428.7 $[M+4H]^{4+}$,1143.2 $[M+5H]^{5+}$, 952.8 $[M+6H]^{6+}$, 816.75 $[M+7H]^{7+}$

MALDI-TOF-MS: m/z calculated for $C_{249}H_{395}N_{55}O_{97}$: 5734.19 $[M+Na]^{+}$, found: 5734.0

^{1}H-NMR (600 MHz, MeOH-d_4/D_2O): δ 8.1-7.94 (m, 1H, NH), 7.98-7.71 (m, 8H, Triazole-H), 6.95-6.77 (bs, 8H, Aryl-H), 4.72 (m, 4.71-4.72, 8H, $CH_{mannose}$), 4.45-4.41 (m, 4H, 7_{axial}), 4.14-4.04 (m, 8H, $CH_{mannose}$), 3.93-3.33 (m, 185H, $CH_{mannose}$, 5, 9, 10, 11, 12, 13, 17 overlaps with solvent peak) 3.18-3.06 (m, 12H, $CH_{mannose}$, $7_{equatorial}$) 3.03-2.92 (m, 16H, 15, 19), 2.84-2.73 (m, 8H,14), 2.62-2.41 (m, 54H, 8, 18) 2.25 (t, ^{3}J= 7.4 Hz , 2H, 1), 2.00-1.88 (m, 8H, 4), 1.71 (p, ^{3}J= 7.7 Hz, 2H, 2), 1.51-1.43 (m, 2H, 3), 1.06-0.97 (m, 9H, 6) ppm.
The signals of protons 16 overlap with water peak at 4.59 ppm. Signals from unidentified impurities can be found at 1.29-1.34 ppm.

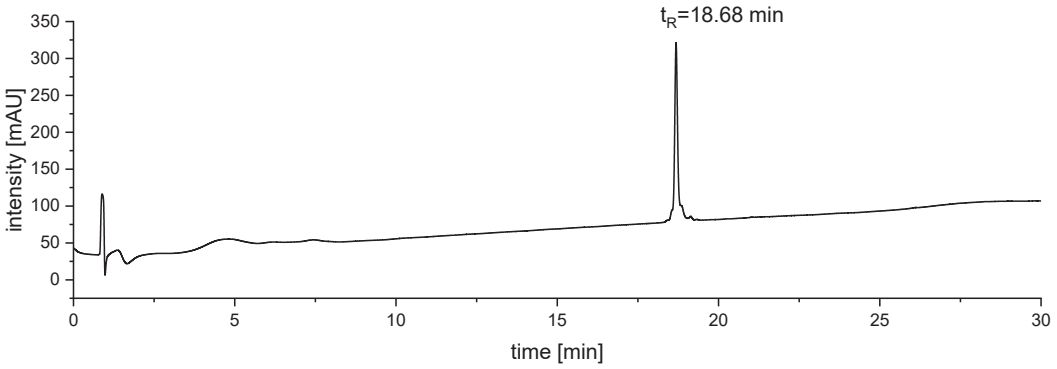

Figure S4. RP-HPLC chromatogram (100% A to 50% A in 30 min at 25° C) of compound C1.

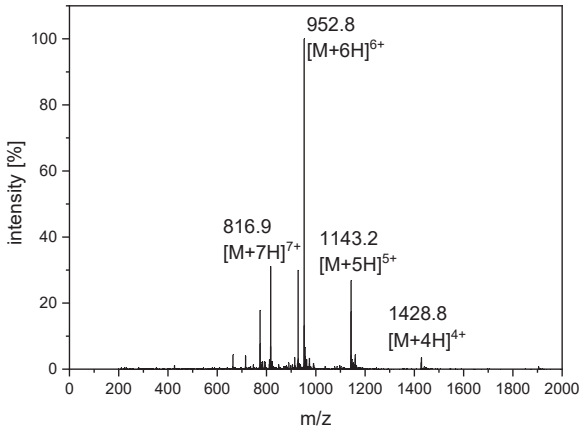

Figure S5. ESI-MS spectrum at t_R = 18.68 min (100% A to 50% A in 30 min at 25° C) of compound C1.

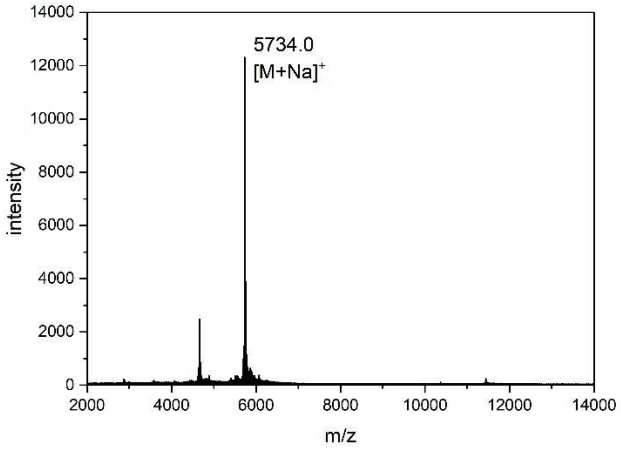

Figure S6. MALD-TOF-MS spectrum of compound C1.

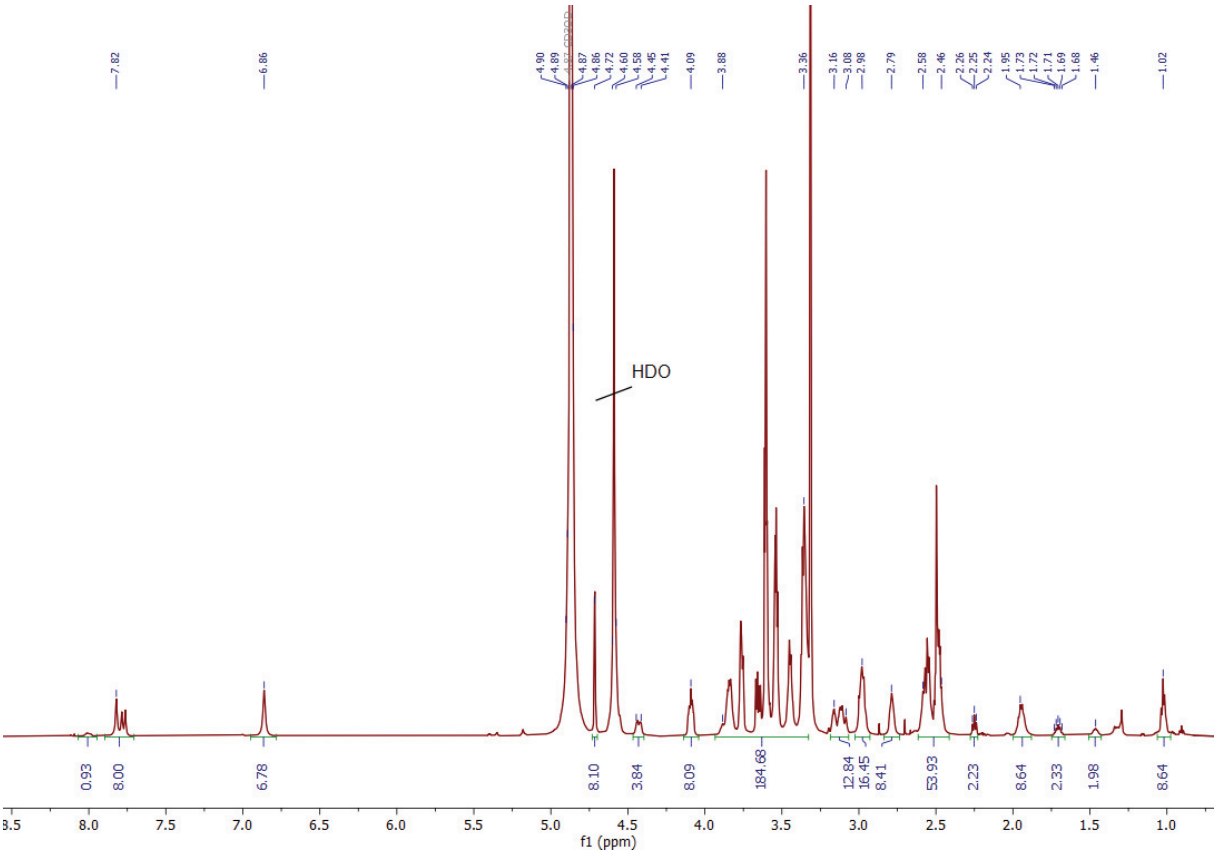

Figure S7: ^{1}H-NMR spectrum (600MHz) of compound C1 in MeOH-*d4*/D_2O.

Compound C2:

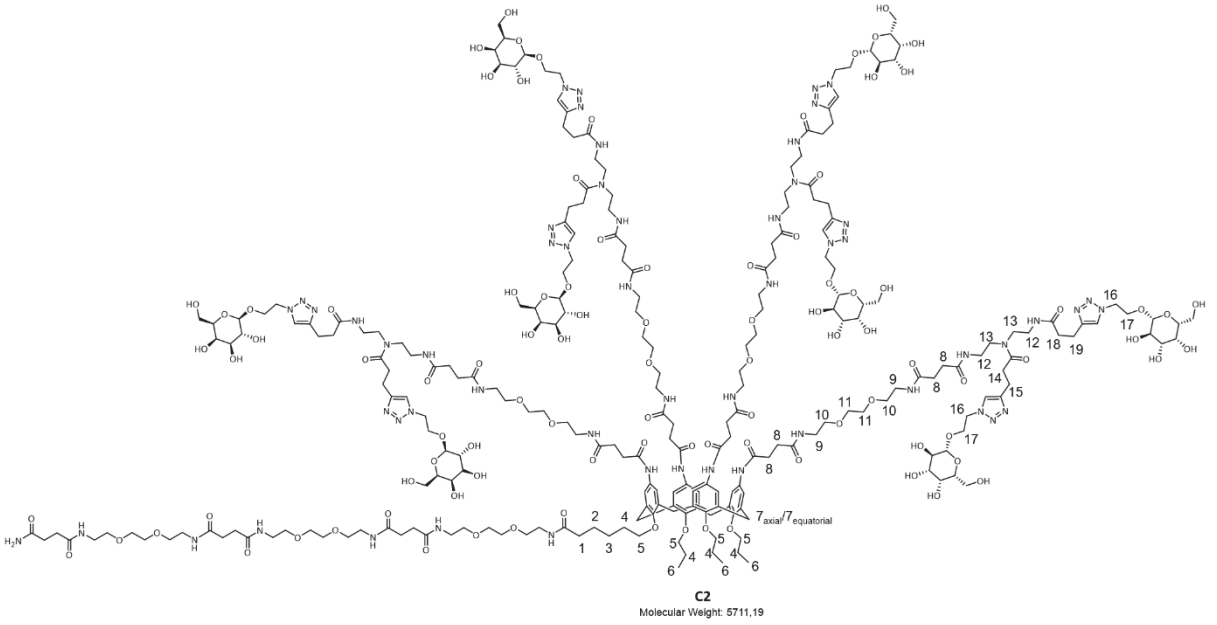

Compound **C2** was purified by preparative HPLC (73% A to 67% A in 13 min) and obtained in a yield of 9%. The relative purity of 90% was determined by integration of the UV signals of the RP-HPLC run at 214 nm. MS analysis suggests that the by-product observed, that could not be separated by preparative purification, is due to EDS-TDS-(man)-pentynoic acid(man) deletion. Additionally, ^{1}H-NMR analysis confirms this.

ESI-MS: m/z calculated for $C_{249}H_{395}N_{55}O_{97}$: 1427.94 $[M+4H]^{4+}$, 1142.55 $[M+5H]^{5+}$, 952.3 $[M+6H]^{6+}$, 816.4 $[M+7H]^{7+}$, 714.47 $[M+8H]^{8+}$, found: 1428.6 $[M+4H]^{4+}$, 1143.2 $[M+5H]^{5+}$, 952.7 $[M+6H]^{6+}$, 816.7 $[M+7H]^{7+}$

MALDI-TOF-MS: m/z calculated for $C_{249}H_{395}N_{55}O_{97}$: 5734.19 $[M+Na]^{+}$, found: 5734.3

^{1}H-NMR (600 MHz, MeOH-d_4/D_2O): δ 8.48 (bs, 0.5H, -NH-), 8.07-7.78 (m, 8H, Triazole-H), 6.89 (bs, 6H, Aryl-H), 4.5-4.4 (m, 4H, 7_{axial}), 4.36-4.14 (m, 16H, $CH_{galactose}$), 4.06-3.33 (m, 182H, $CH_{galactose}$, 5, 9, 10, 11, 12, 13, 17, overlaps with solvent peak), 3.11 (d, 4H, ^{2}J = 13.0, $7_{equatorial}$) 3.05-2.99 (m, 16H, 15, 19), 2.88-2.72 (m, 8H,14), 2.66-2.42 (m, 53H, 8, 18) 2.26 (t, ^{3}J = 7.5 Hz , 2H, 1), 2.01-1.87 (m, 8H, 4), 1.72 (p, ^{3}J = 7.7 Hz, 2H, 2), 1.52-1.43 (m, 2H, 3), 1.07-1.00 (m, 7H, 6) ppm. The signals of protons 16 overlap with water peak at 4.59 ppm. Signals from unidentified impurities can be found at 1.28-1.38, 2.67, 2.71 and 2.88 ppm.

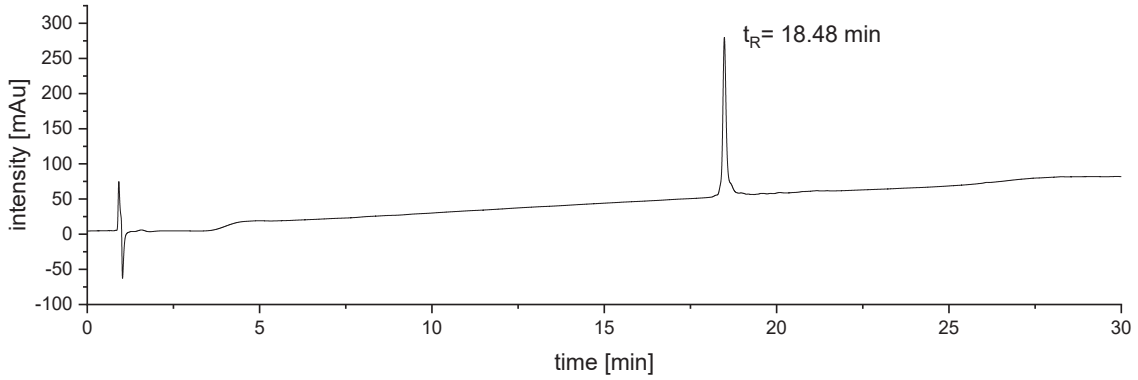

Figure S8. RP-HPLC chromatogram (100% A to 50% A in 30 min at 25° C) of compound C2.

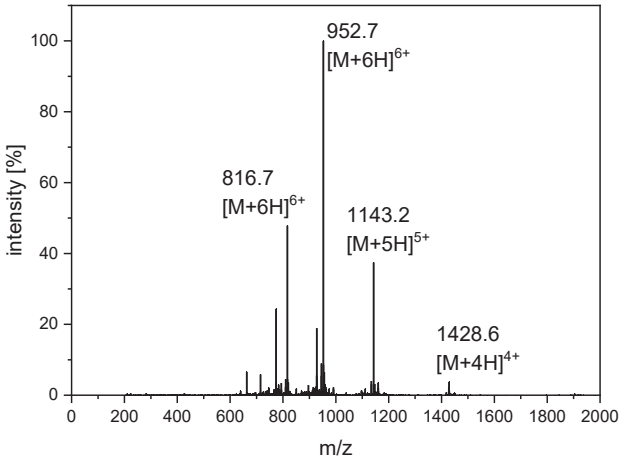

Figure S9. ESI-MS spectrum at t_R = 18.48 min (100% A to 50% A in 30 min at 25° C) of compound C2.

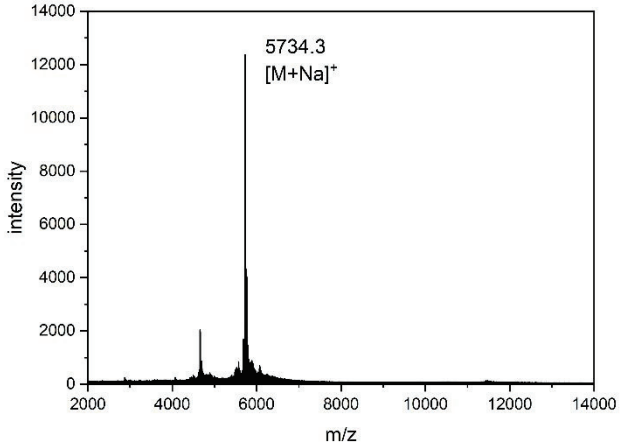

Figure S10. MALDI-TOF-MS spectra of compound C2.

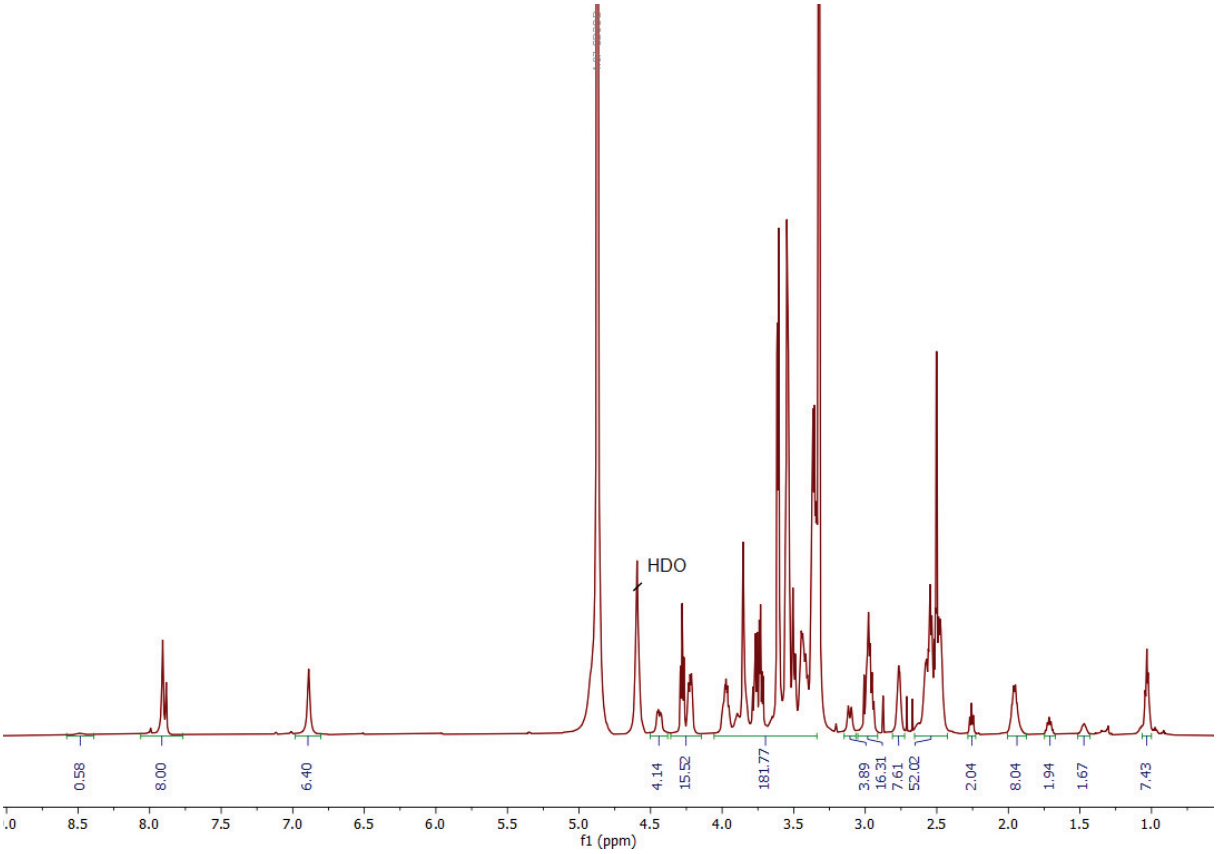

Figure S11. ^{1}H-NMR spectrum (600MHz) of compound C2 in MeOH-*d4*/D_2O. Phase correction was performed.

Compound C3:

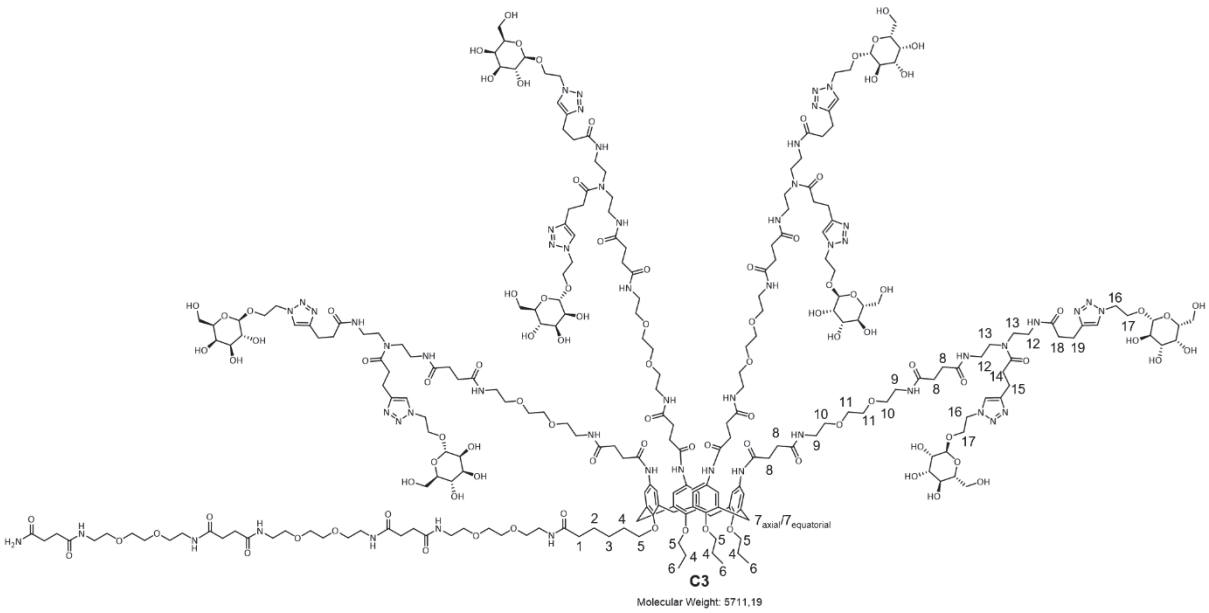

Compound **C3** was purified by preparative HPLC (73% A to 67% A in 13 min) and obtained in a yield of 9%. The relative purity of 95% was determined integration of the UV signals of the RP-HPLC run at 214 nm. MS analysis suggests that the by-product observed, that could not be separated by preparative purification, is due to EDS-TDS-(man)-pentynoic acid(man) deletion. Additionally, ^{1}H-NMR analysis confirms this.

ESI-MS: m/z calculated for $C_{249}H_{395}N_{55}O_{97}$: 1427.94 $[M+4H]^{4+}$, 1142.55 $[M+5H]^{5+}$, 952.3 $[M+6H]^{6+}$, 816.4 $[M+7H]^{7+}$, 714.47 $[M+8H]^{8+}$, found: 1428.6 $[M+4H]^{4+}$, 1143.1 $[M+5H]^{5+}$, 952.8 $[M+6H]^{6+}$, 816.8 $[M+7H]^{7+}$

MALDI-TOF-MS: m/z calculated for $C_{249}H_{395}N_{55}O_{97}$: 5734.19 $[M+Na]^{+}$, found: 5734.0

^{1}H-NMR (600 MHz, MeOH-d_4/D_2O): δ 8.06-7.71 (m, 8H, Triazole-H), 6.88 (s, 7H, Aryl-H), 4.74-4.70(m, 4H, $CH_{mannose}$), 4.65-4.54 (m overlap with water peak, 16) 4.5-4.39 (m, 4H, 7_{axial}), 4.33-4.29 (m, 4H, $CH_{galactose}$), 4.29-4.18 (m, 4H, $CH_{galactose}$), 4.13-4.06 (m, 4H, $CH_{mannose}$), 4.02-3.95 (m, 4H, $CH_{galactose}$), 3.93-3.33 (m, 181H, $CH_{mannose}$, $CH_{galactose}$, 5, 9, 10, 11, 12, 13, 17, overlaps with solvent peak), 3.16-3.07 (m, 8H, $7_{equatorial}$, $CH_{mannose}$,), 2.90-3.04-2.89 (m, 16H, 15, 19), 2.84-2.74 (m, 8H,14), 2.65-2.36 (m, 55H, 8, 18) 2.26 (t, ^{3}J= 7.5 Hz , 2H, 1), 2.00-1.9 (m, 8H, 4), 1.72 (p, ^{3}J= 7.8 Hz, 2H, 2), 1.52-1.43(m, 2H, 3), 1.07-1.0 (m, 8H, 6) ppm.
Signals from unidentified impurities can be found at 1.28-1.38, 2.67, 2.71 and 2.88 ppm.

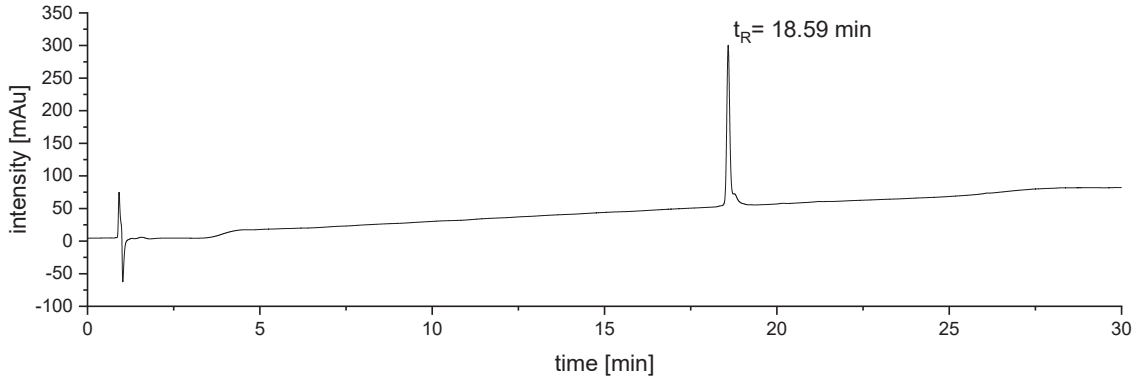

Figure S12. RP-HPLC chromatogram (100% A to 50% A in 30 min at 25° C) of compound C3.

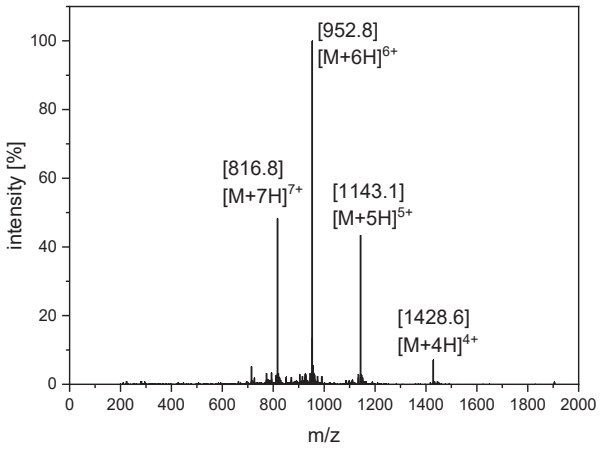

Figure S13. ESI-MS spectrum at t_R = 18.59 min (100% A to 50% A in 30 min at 25° C) of compound C3.

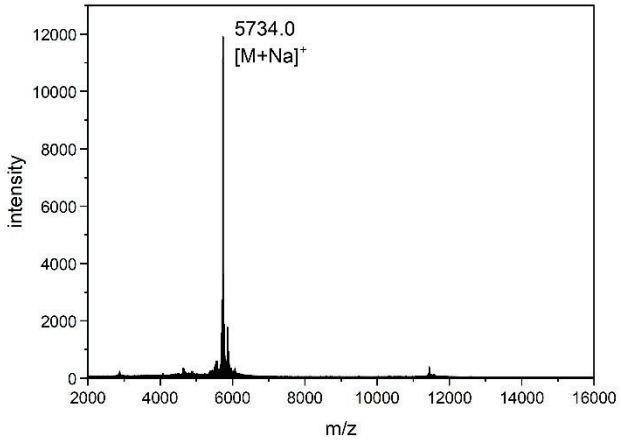

Figure S14. MALDI-TOF-MS spectrum of compound C4.

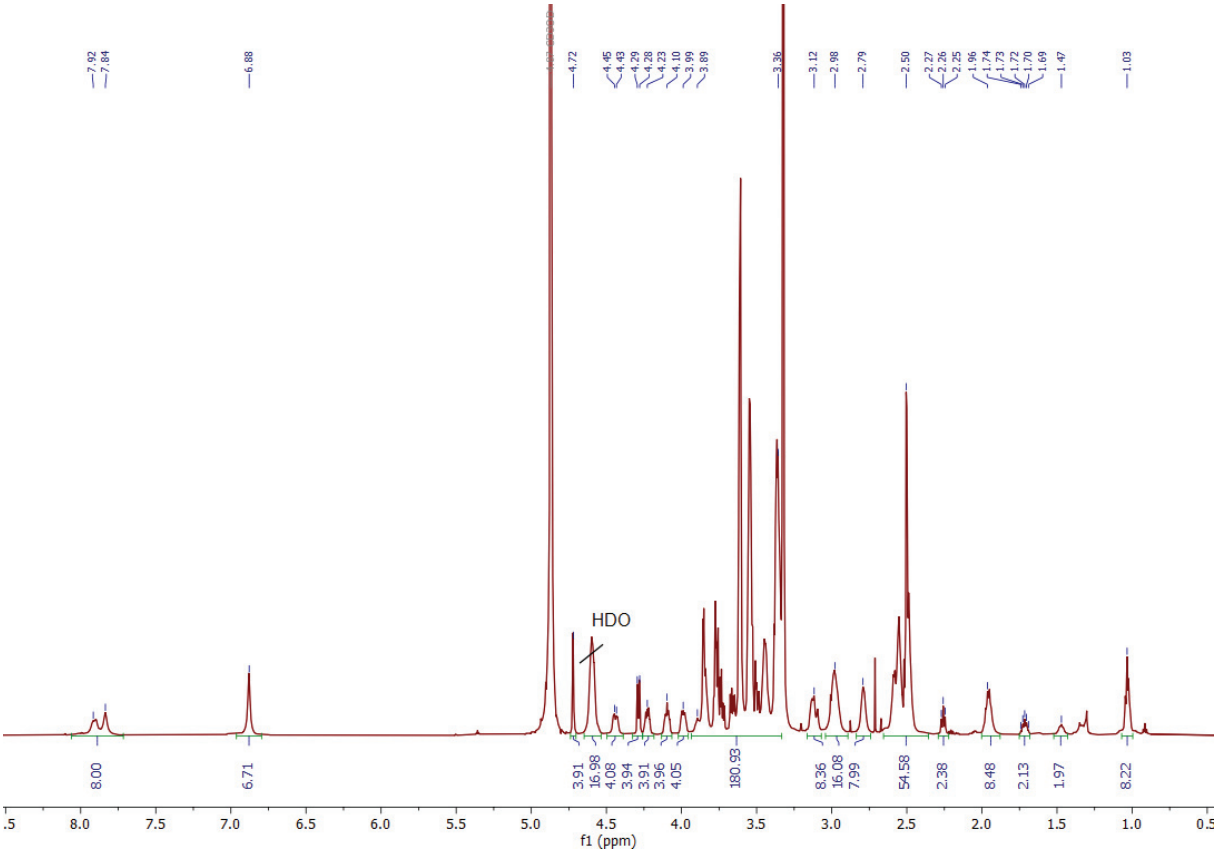

Figure S15. ^{1}H-NMR spectrum (600MHz) of compound C3 in MeOH-*d4*/D_2O.

Compound C4:

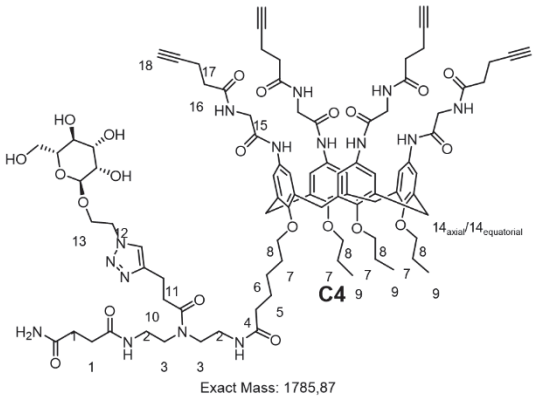

Compound **C4** was purified by preparative HPLC (60% A to 40% A in 15 min) and obtained in a yield of 45%. The relative purity of 89% was determined by integration of the UV signals of the RP-HPLC run at 214 nm.

ESI-MS: m/z calculated for $C_{92}H_{119}N_{15}O_{22}$: 1786.87 $[M+H]^{1+}$, 893.86 $[M+2H]^{2+}$, found: 1786.85 $[M+H]^{+}$, 894.05 $[M+2H]^{2+}$

MADLI-TOF-MS: m/z calculated for $C_{92}H_{119}N_{15}O_{22}$: 1786.87 $[M+H]^{+}$,1808.87 $[M+Na]^{+}$, found: 1810.30 $[M+Na]^{+}$

^{1}H-NMR (600 MHz, DMSO-d_6): δ 9.65-9.45 (m, Aryl-NH-C(O)-), 8.3-8.11 (m, C(O)-NH), 8.02-7.92 (m, C(O)-NH), 7.9-7.83 (m, C(O)-NH), 7.80-7.75 (m ,1H, Triazole-H), 7.42-7.18 (m, C(O)-NH2), 7.0-6.8 (m, 8H, Aryl-H), 6.76-6.64 (m, C(O)-NH2), 4.77 (bs, $OH_{mannose}$), 4.69-4.61 (m, $OH_{mannose}$), 4.61-4.58 (m, 1H, $CH_{mannose}$), 4.56-4.39 (m, 3H, 12, $OH_{mannose}$), 4.36-4.26 (m, 4H, 14_{axial}), 3.95-3.87 (m, 1H, $CH_{mannose}$), 3.85-3.66(m, 18H, 15, 13, 8), 3.61-3.57 (m, 1H, $CH_{mannose}$), 3.56-3.53 (m, 1H, $CH_{mannose}$), 3.52-3.46 (m, 1H, $CH_{mannose}$), 3.20-3.11 (m, 4H, 3), 3.10-3.02 (m, 5H, $14_{equatorial}$, $CH_{mannose}$), 2.83 (t, ^{3}J = 7.2 Hz,

2H, 11), 2.78-2.69 (m, 4H, 1), 2.66-2.60 (m, 2H, 10), 2.39-2.32 (m, 16H, 16, 17), 2.3-2.22 (m, 4H, 18), 2.07 (t, ^{3}J = 7.4 Hz, 2H, 4), 1.92-1.82 (m, 8H, 7), 1.6-1.5 (m, 2H, 5), 1.4-1.3 (m, 2H, 6), 0.85(t, ^{3}J=7.3 Hz, 9H, 9) ppm.
The Signals of 2 and $CH_{mannose}$ overlap with the water peak at 3.3 ppm. Signals from unidentified impurities can be found at 1.2-1.26 ppm.

^{1}H-NMR (600 MHz, MeOH-d_4/D_2O): δ 7.85-7.69 (m, 1H, Triazole-H), 7.15-6.69 (m, 8H, Aryl-H), 4.70-4.40 (m, 1H, $CH_{mannose}$), 4.55-4.49 (m, 2H, 12), 4.44-4.36 (m, 4H, 14_{axial}), 4.08-4.01 (m, 1H, $CH_{mannose}$), 3.97-3.75 (m, 19H, 8, 15, PEG impurities), 3.74-3.70 (m, 2H, 13), 3.64-3.6 (m, 1H, $CH_{mannose}$), 3.58-3.23 (m, 2H, $CH_{mannose}$), 3.48-3.37 (m, 4H, 2), 3.36-3.3 (m, 4H, 3), 3.13-3.09 (m, 5H, $14_{equatorial}$, $CH_{mannose}$), 2.98-2.91 (m, 2H, 11), 2.80-2.73 (m, 2H, 10), 2.51-2.47 (m, 20H, 16, 17, 1), 2.44-2.40 (m, 2H, 4), 2.22-2.14 (m, 4H, 18), 1.98-1.88 (m, 8H, 7), 1.70-1.60 (m, 2H, 5), 1.48-1.38 (m, 2H, 6), 1.03-0.94 (m, 9H, 9) ppm.
Signals from unidentified impurities can be found at 1.2-1.35.

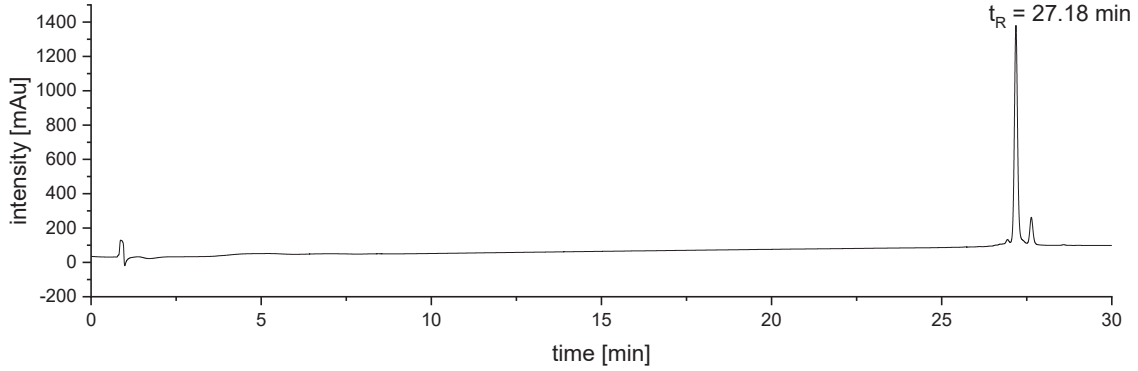

Figure S16. RP-HPLC chromatogram (100% A to 50% A in 30 min at 25° C) of compound C4.

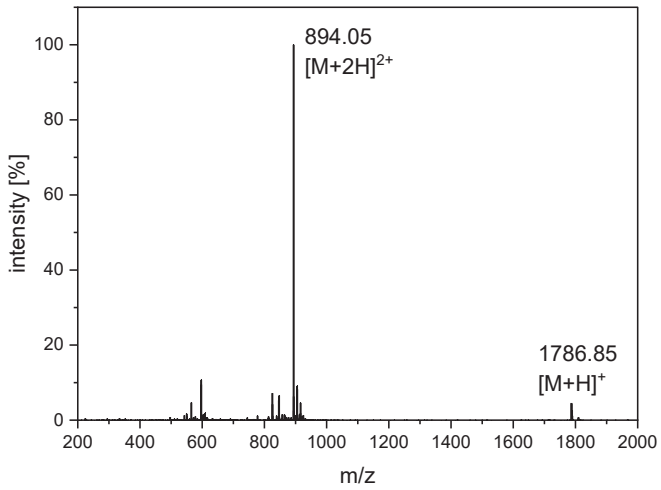

Figure S17. ESI-MS spectrum at t_R = 27.18 min (100% A to 50% A in 30 min at 25° C) of compound C4.

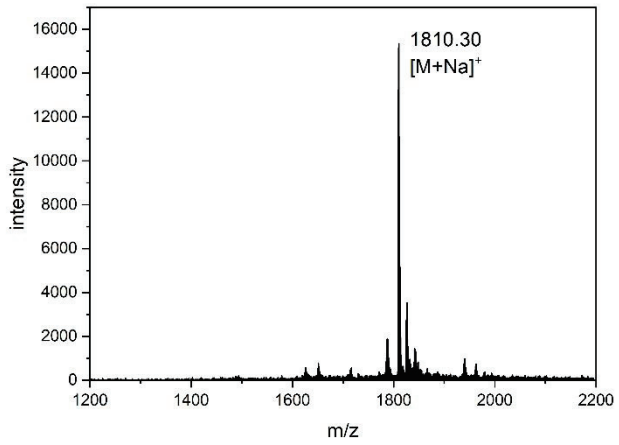

Figure S18. MALDI-TOF-MS spectrum of compound C4.

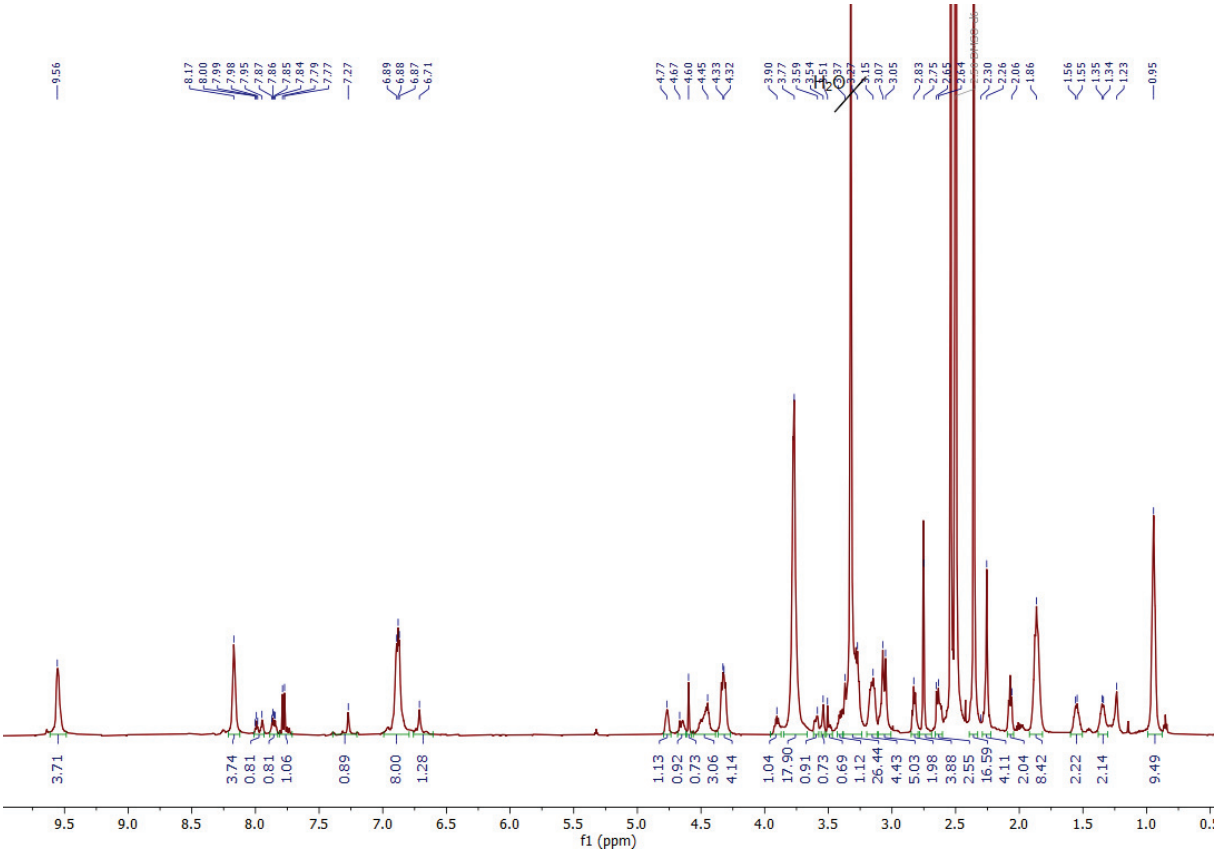

Figure S19. ^{1}H-NMR spectrum (600MHz) of compound C4 in DMSO-*d6*.

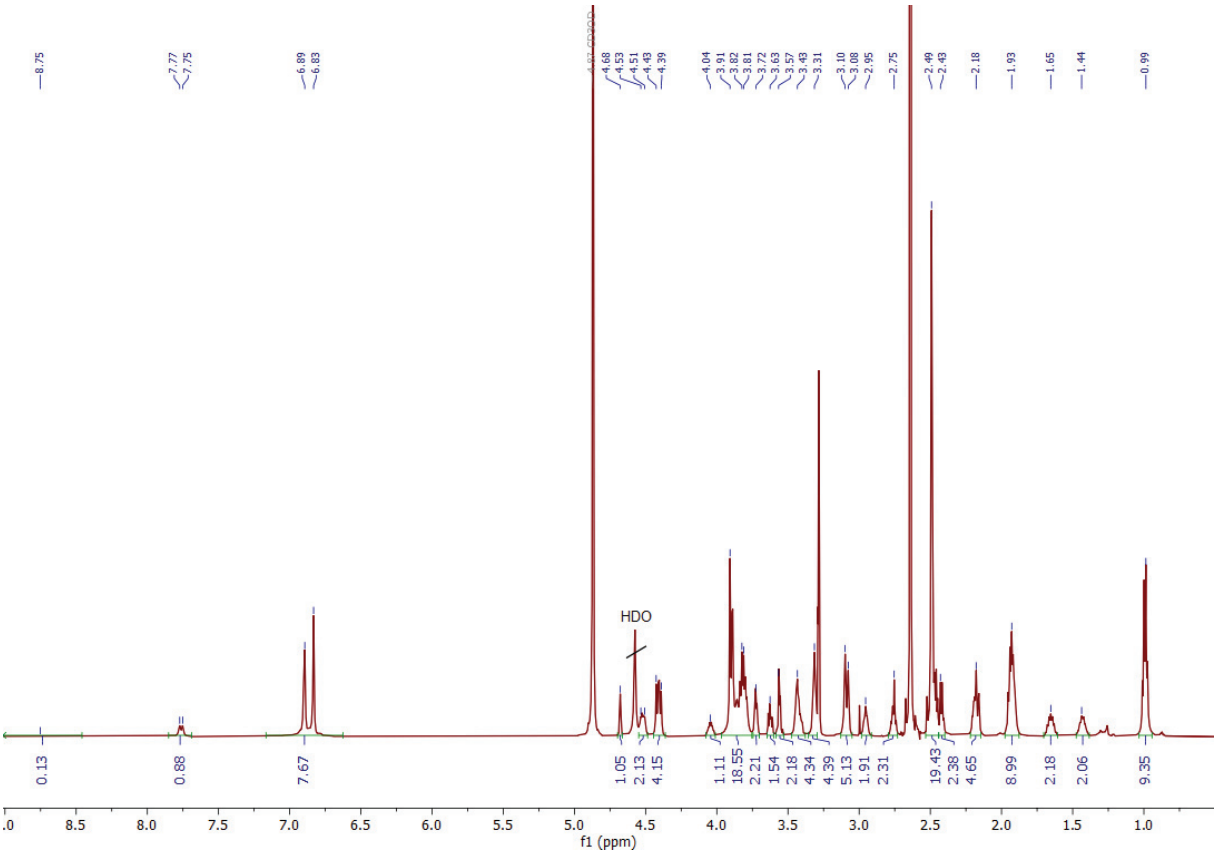

Figure S20. ^{1}H-NMR spectrum (600MHz) of compound C4 in MeOH-*d4*/D_2O.

Compound C5:

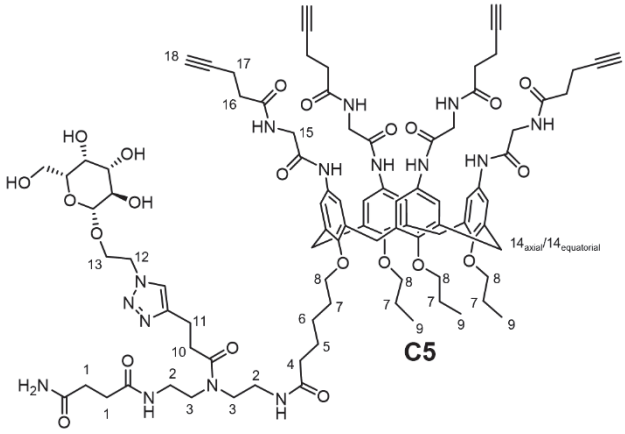

Compound **C5** was purified by preparative HPLC (62% A to 52% A in 15 min) and obtained in a yield of 42%. The relative purity of 89% was determined by integration of the UV signals of the RP-HPLC run at 214 nm.

ESI-MS: m/z calculated for $C_{92}H_{119}N_{15}O_{22}$: 1786.87 $[M+H]^{1+}$, 893.86 $[M+2H]^{2+}$, found: 1787.75 $[M+H]^{+}$, 894.1 $[M+2H]^{2+}$

MADLI-TOF-MS: m/z calculated for $C_{92}H_{119}N_{15}O_{22}$: 1786.87 $[M+H]^{+}$,1808.87 $[M+Na]^{+}$, found: 1810.30 $[M+Na]^{+}$

^{1}H-NMR (600 MHz, DMSO-d_6): δ 9.72-9.46 (m, Aryl-NH-C(O)-), 8.3-8.11 (m, C(O)-NH), 8.00-7.94 (m, C(O)-NH), 7.92-7.82 (m, 2H, Triazole-H, C(O)-NH), 7.28 (s, 1H, C(O)-NH_2), 7.00-6.78 (m, 8H, Aryl-H), 6.71 (s, 1H, C(O)-NH_2), 5.04 (s, 1H, $OH_{galactose}$), 4.86 (m, 1H, $OH_{galactose}$), 4.66 (s, 1H, $OH_{galactose}$), 4.56-4.42 (m, 3H, 12, $OH_{galactose}$), 4.37-4.26 (2d/m, 4H, 14_{axial}), 4.18-4.12 (m, 1H, $CH_{galactose}$), 4.08-3.98 (m, 1H, $CH_{galactose}$) 3.95-3.7 (m, 18H, 15, 13, 8), 3.63 (s, 1H, $CH_{galactose}$), 3.55-3.43 (m, 3H, $CH_{galactose}$) , 3.20-3.11 (m, 4H, 3), 3.06 (d, ^{2}J = 13.4 Hz, 4H, $14_{equatorial}$), 2.83 (t, ^{3}J = 7.4 Hz, 2H, 11), 2.78-2.68 (m,

4H, 1), 2.66-2.60 (m, 2H, 10), 2.4-2.31 (m, 16H, 16, 17), 2.29-2.22 (m, 4H, 18), 2.07 (t, ^{3}J = 7.5 Hz, 2H, 4), 1.92-1.81 (m, 8H, 7), 1.6-1,5 (p, ^{3}J=7.6 Hz, 2H, 5), 1.39-1.3 (m, 2H, 6), 1.00-0.9 (m, 9H, 9) ppm.
The Signals of 2 and $CH_{galactose}$ overlap with the water peak at 3.3 ppm. Signals from unidentified impurities can be found at 1.2-1.26 ppm.

^{1}H-NMR (600 MHz, MeOH-d_4/D_2O): 8.48 (bs, 1H, NH), 7.97-7.85 (m, 1H, Triazole-H), 7.11-6.7 (m, 8H, Aryl-H), 4.62-4.52 (m, 2H, 12), 4.50-4.40 (2d/m, 4H, 14_{axial}), 4.27-4.24 (dd, ^{3}J= 7.6, 1.8 Hz, 1H, $CH_{galactose}$), 4.24-4.18 (m, 1H, $CH_{galactose}$), 4.0-3.80 (m, 20H, 15, 13, 8), 3.78 (dd, ^{2}J = 11.53 Hz, ^{3}J = 6.99 Hz, 1H, $HOCH_{2,galactose}$), 3.72 (dd, ^{2}J = 11.53 Hz, ^{3}J = 5.08 Hz, 1H, $HOCH_{2,\ galactose}$), 3.56-3.33 (12H, m, 2, 3, $CH_{galactose}$, overlap with methanol peak), 3.12 (bd, ^{2}J = 12.56 Hz, 4H, $14_{equatorial}$), 2.99 (t, ^{3}J = 7.4 Hz, 2H, 11), 2.80-2.73 (m, 2H, 10), 2.58-2.39 (m, 22H, 16, 17, 1, 4), 2.25-2.19 (m, 4H, 18), 2.02-1.91 (m, 8H, 7), 1.74-1.64 (m, 2H, 5), 1.52-1.42 (m, 2H, 6), 1.08-0.98 (m, 9H, 9) ppm.
Signals from unidentified impurities can be found at 1.23-1.40 ppm.

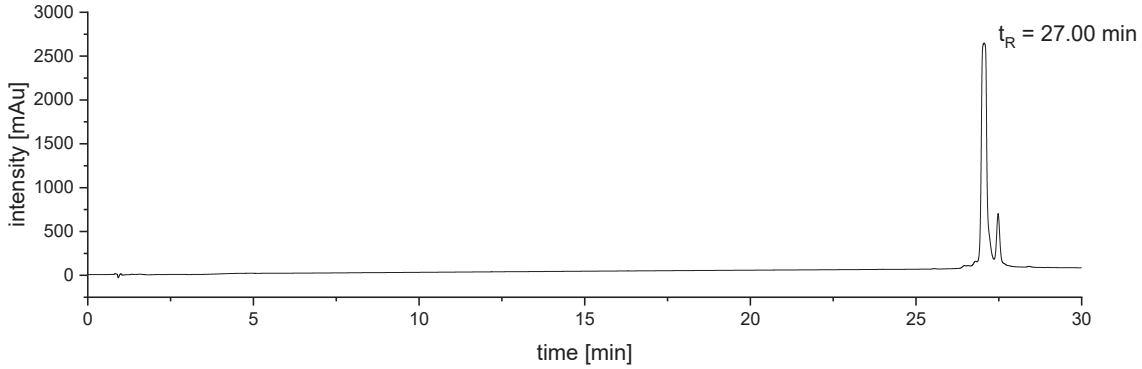

Figure S21. RP-HPLC chromatogram (100% A to 50% A in 30 min at 25° C) of compound C5.

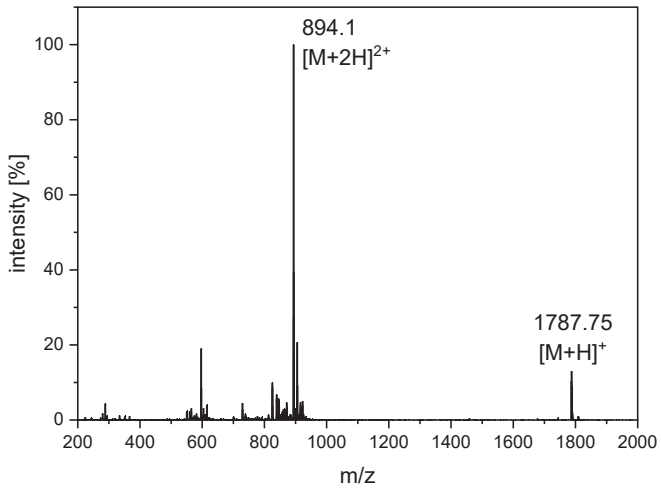

Figure S22. ESI-MS spectrum at t_R = 27.00 min (100% A to 50% A in 30 min at 25° C) of compound C5.

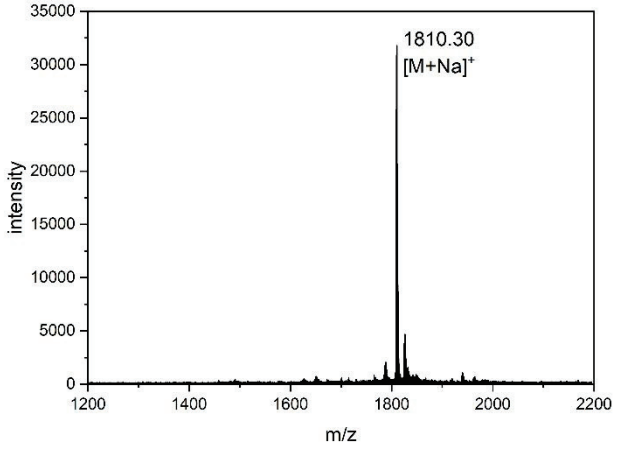

Figure S23. MALDI-TOF-MS spectrum of compound C5.

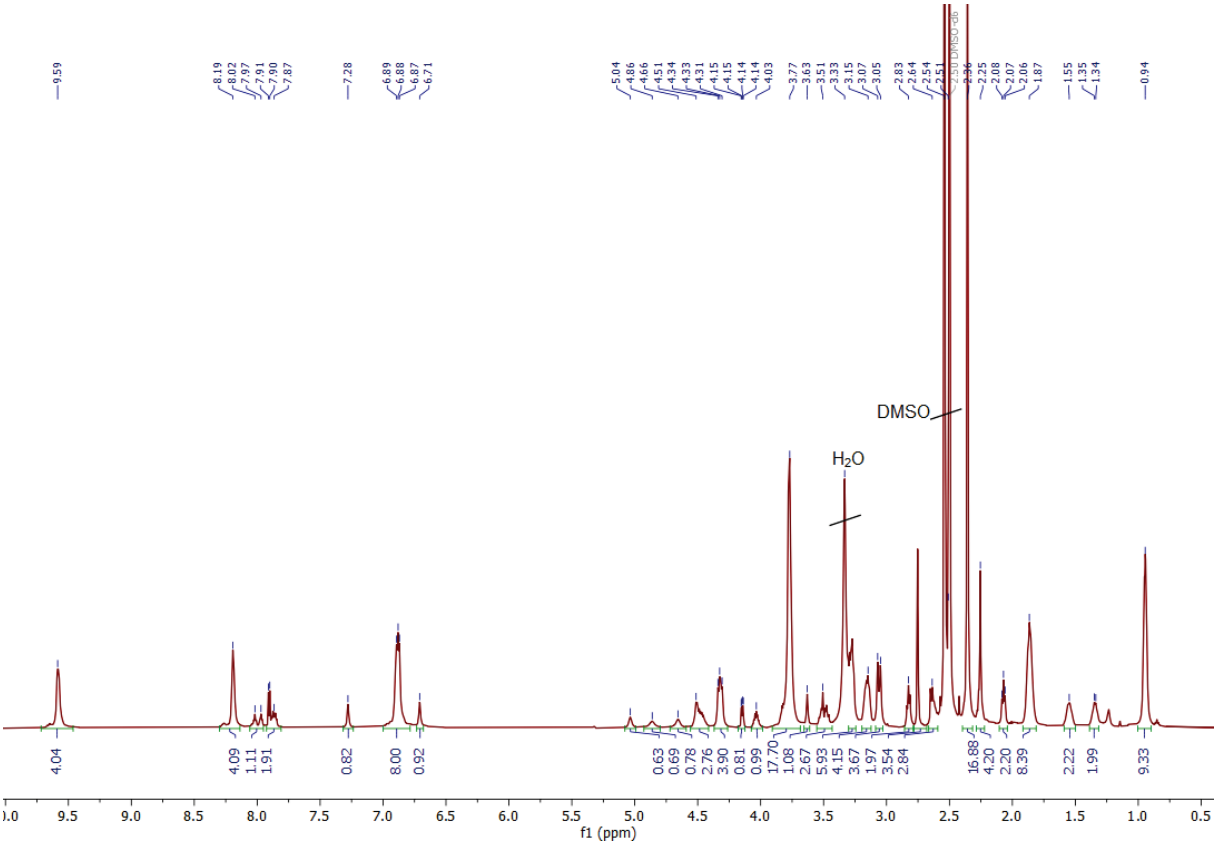

Figure S24: ^{1}H-NMR spectrum (600MHz) of compound C5 in DMSO-*d6*.

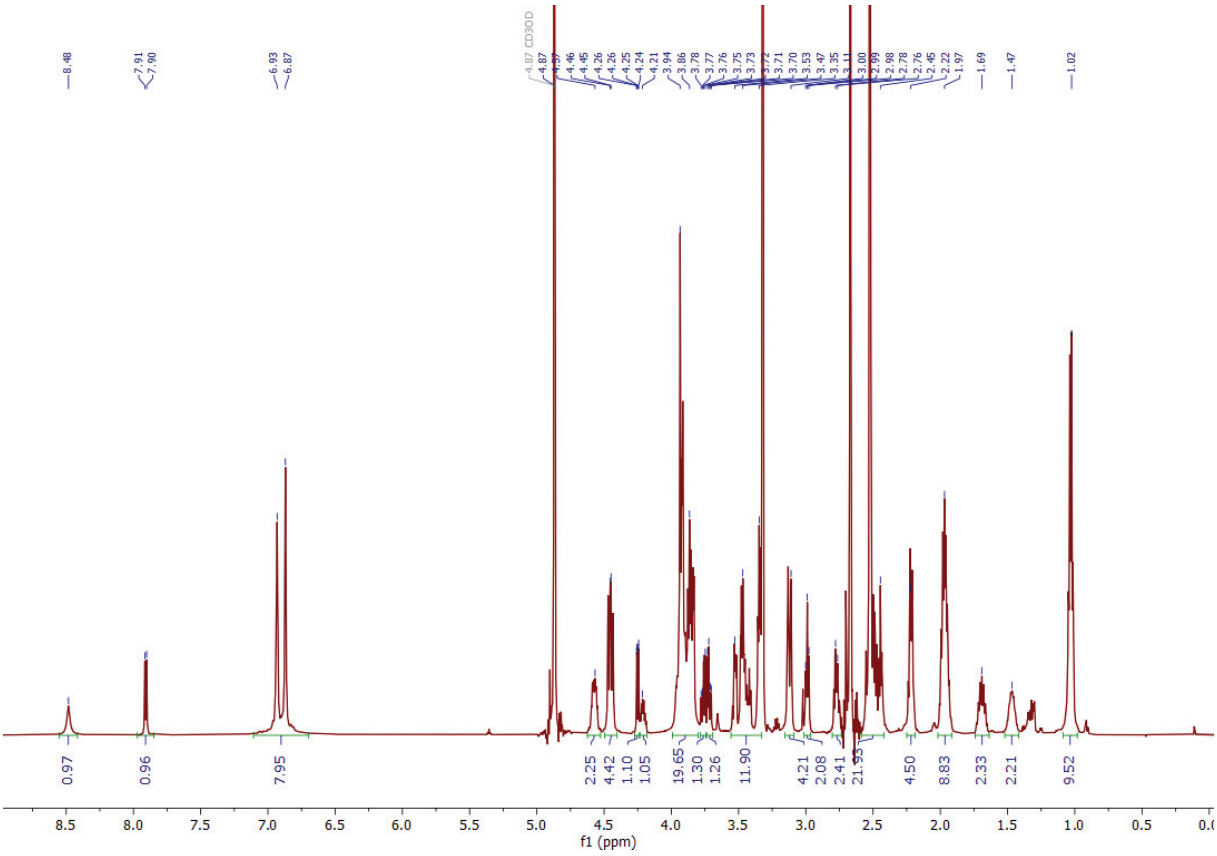

Figure S25: ^{1}H-NMR spectrum (600MHz) of compound C5 in MeOH-*d4*/D_2O.

Compound C6:

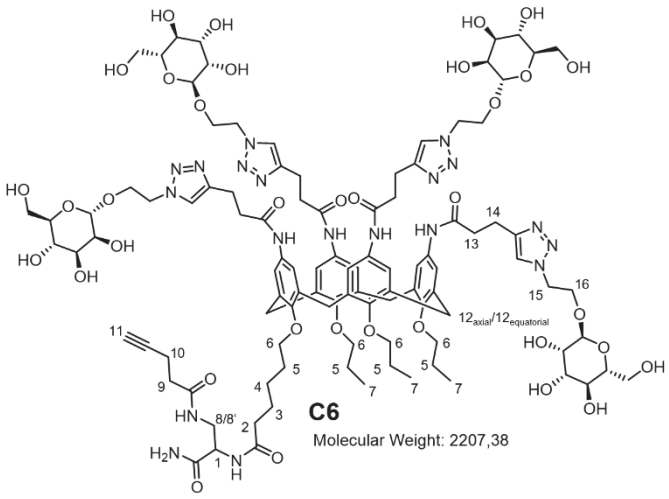

Compound **C6** was purified by preparative HPLC (70% A to 35% A in 15 min) and obtained in a yield of 65%. The relative purity of 94% was determined by integration of the UV signals of the RP-HPLC run at 214 nm.

ESI-MS: m/z calculated for $C_{92}H_{143}N_{19}O_{35}$: 1104.0 $[M+2H]^{2+}$, 736.3 $[M+3H]^{3+}$, found: 1104.55 $[M+2H]^{2+}$, 736.6 $[M+3H]^{3+}$

MALDI-TOF-MS: m/z calculated for $C_{103}H_{143}N_{19}O_{35}$: 2228.99 $[M+Na]^{+}$, found: 2230.18 $[M+Na]^{+}$

^{1}H-NMR (600 MHz, MeOH-*d4*/D_2O): δ 8.58 (bs, -NH-), 7.73(bs, 4H, Triazole-H), 7.09-6.69 (m, 8H, Aryl-H), 4.65 (m overlap with water peak, $CH_{mannose}$), 4.43 (dd, ^{3}J = 8.0, 4.8 Hz, 1H, 1), 4.37 (d, ^{2}J = 12.75 Hz, 12_{axial}), 4.07-3.95 (m, 4H, $CH_{mannose}$), 3.87-3.38 (m, 34H, 6, 8, 8', 16, $CH_{mannose}$), 3.14-3.02 (m, 8H, $12_{equatorial}$, $CH_{mannose}$), 3.00-2.86 (m, 8H, 14), 2.7-2.51-2.7 (m,

8H, 13), 2.42-2.29 (m, 4H, 9, 10), 2.24 (t, ^{3}J=7.6 Hz, 2H, 2), 2.21-2.18 (m, 1H, 11), 1.98-1.81 (m, 13H, 5, overlap with acetate), 1.69-1.60 (m, 2H, 3), 1.46-1.36 (m, 2H, 4), 0.99-0.90 (t, ^{3}J=7.2 Hz, 9H, 7) ppm.

Signals from 15 overlap with water peak at 4.56 ppm. Acetate anions from anion exchange can be found at 1.81-1.98 ppm. Signals from unidentified impurities can be found at 1.2-1.26 ppm.

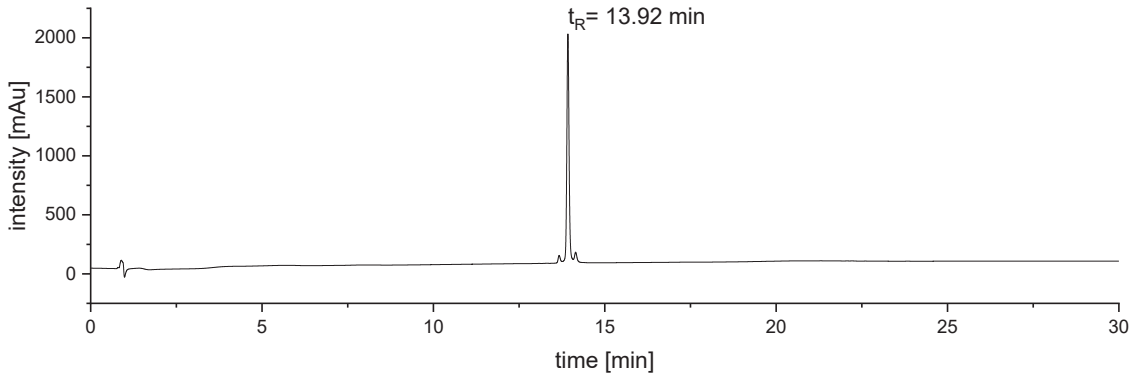

Figure S26. RP-HPLC chromatogram (100% A to 0% A in 30 min at 25° C) of compound C6.

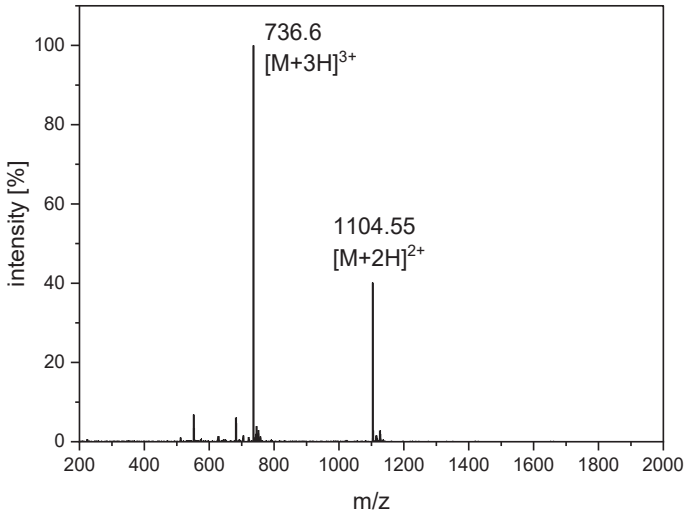

Figure S27. ESI-MS spectrum at t_R = 13.92 min (100% A to 0% A in 30 min at 25° C) of compound C6.

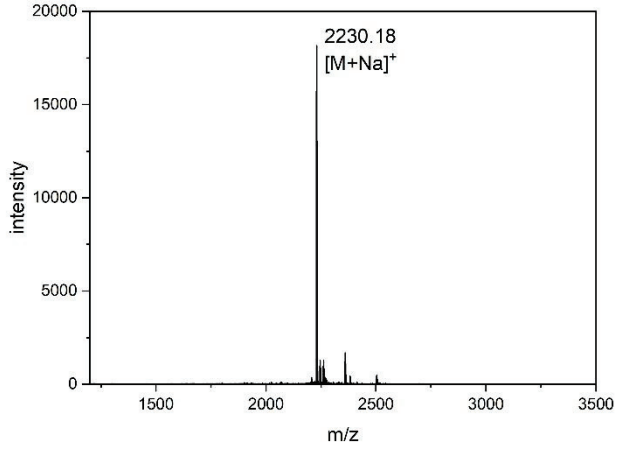

Figure S28. MALDI-TOF-MS spectrum of compound C6.

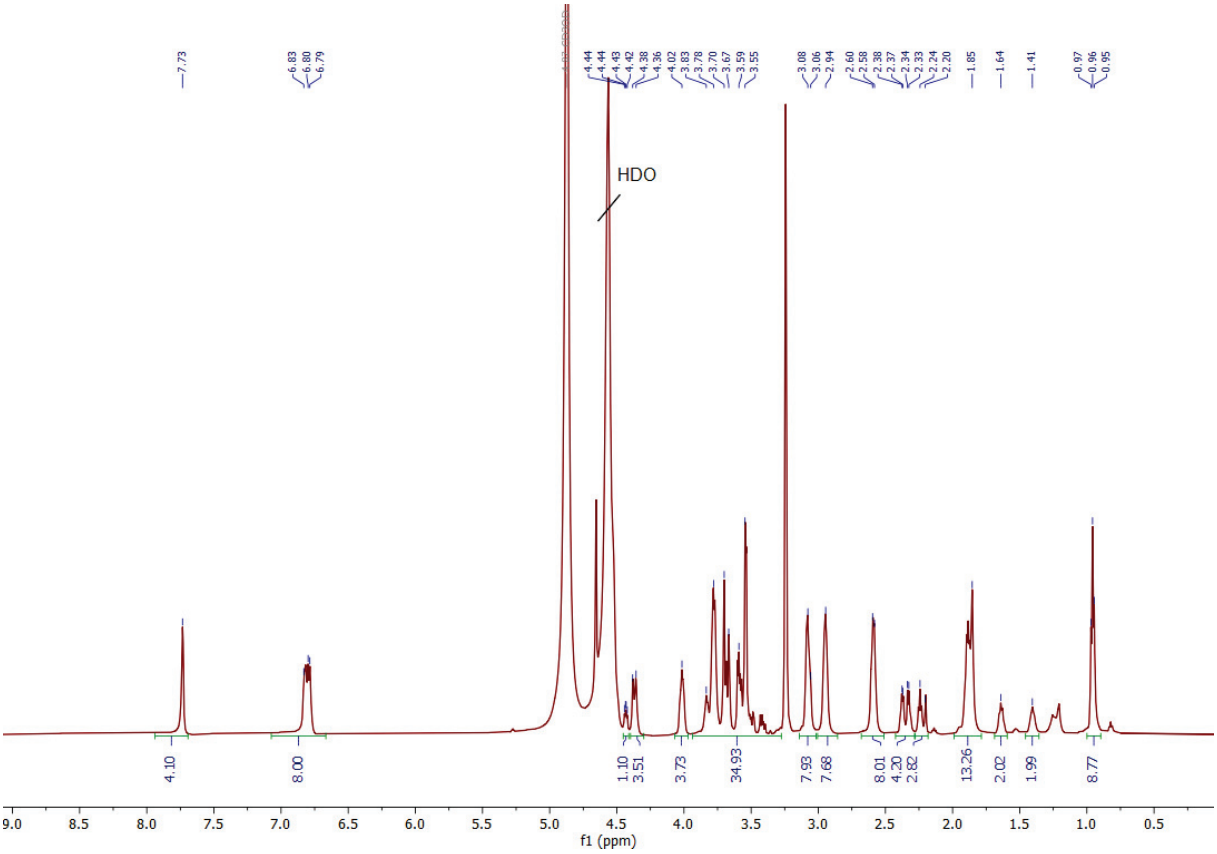

Figure S29. ^{1}H-NMR spectrum (600MHz) of compound C6 in MeOH-*d4*/D_2O.

Compound C7:

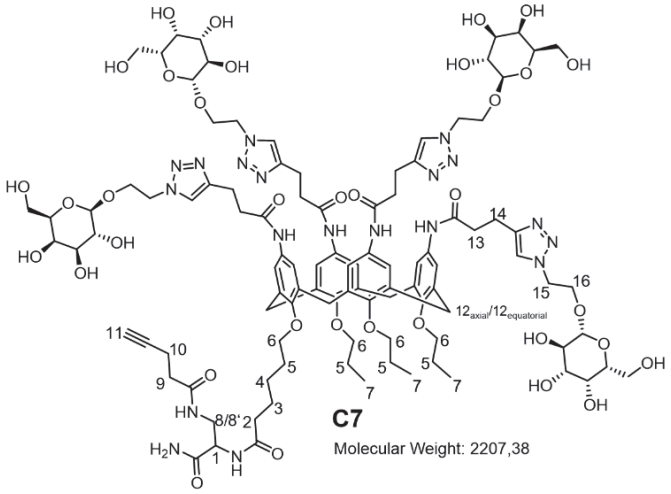

Compound **C7** was purified by preparative HPLC (70% A to 35% A in 15 min) and obtained in a yield of 62%. The relative purity of >95% was determined by integration of the UV signals of the RP-HPLC run at 214 nm.

ESI-MS: m/z calculated for $C_{92}H_{143}N_{19}O_{35}$: 1104.0 $[M+2H]^{2+}$, 736.3 $[M+3H]^{3+}$, found: 1104.3 $[M+2H]^{2+}$, 736.6 $[M+3H]^{3+}$

MALDI-TOF-MS: m/z calculated for $C_{103}H_{143}N_{19}O_{35}$: 2228.99 $[M+Na]^{+}$, found: 2230.18 $[M+Na]^{+}$

^{1}H-NMR (600 MHz, MeOH-d_4/D_2O): δ 7.91 (s, 4H, Triazole-H), 6.94-6.77 (m, 8H, Aryl-H), 4.64-4.52 (m overlaps with water peak, 15), 4.43 (dd, ^{3}J = 7.9, 4.9 Hz, 1H, 1, overlaps with water peak), 4.37 (d, ^{2}J = 12.55, 4H, 12_{axial}), 4.31-4.11 (m, 8H, $CH_{galactose}$), 3.99-3.91 (m, 4H, $CH_{galactose}$), 3.91-3.78 (m, 12H, 6, $CH_{galactose}$), 3.75-3.66 (m, 8H, $HOCH_{2,\ galactose}$), 3.56-3.41 (m, 14H, 16H, $CH_{galactose}$), 3.15-3.07 (2d, 4H, $12_{equatorial}$), 2.97 (bs, 8H, 14), 2.75-2.52 (m, 8H, 13), 2.44-2.32 (m, 4H, 9, 10), 2.28 (t, ^{3}J=7.6 Hz, 2H, 2), 2.23 (t, ^{4}J = 2.6 Hz, , 1H, 11), 1.98-1.88 (m, 8H, 5, overlap with acetate), 1.69 (p, ^{3}J=7.7 Hz, 2H, 3), 1.49-1.41 (m, 2H, 4), 1.01 (t, ^{3}J = 7,27 Hz 9H, 7) ppm.
Signals from unidentified impurities can be found at 1.24-1.31 ppm. Acetate anions from anion exchange can be found at 2.05 ppm.

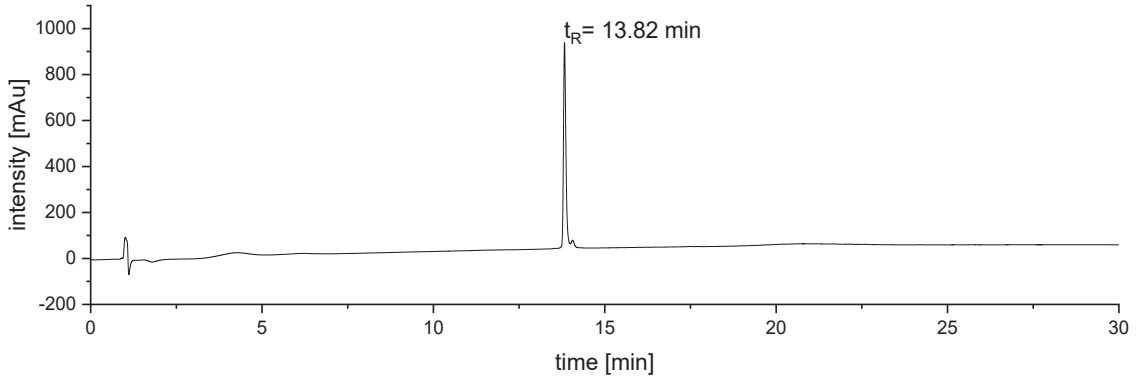

Figure S30. RP-HPLC chromatogram (100% A to 0% A in 30 min at 25° C) of compound C7.

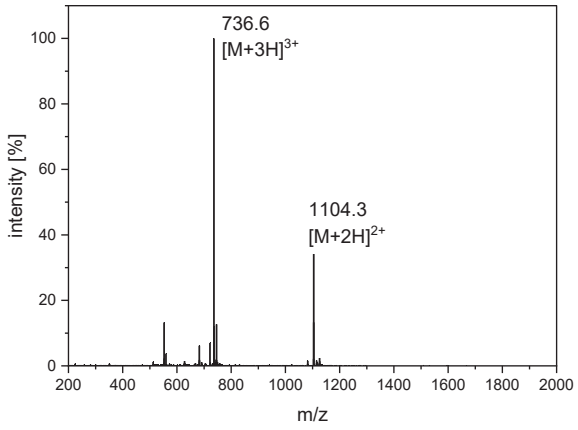

Figure S31. ESI-MS spectrum at t_R = 13.82 min (100% A to 0% A in 30 min at 25° C) of compound C7.

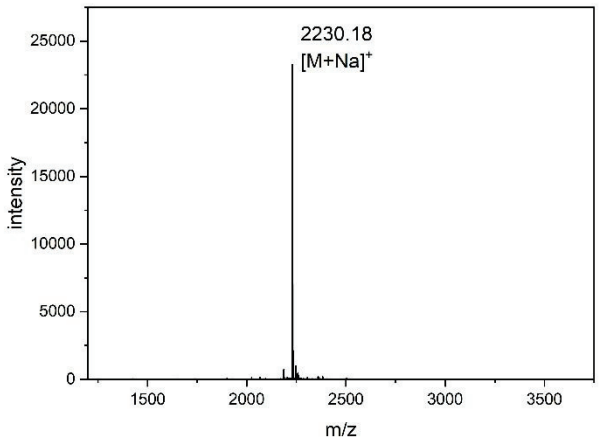

Figure S32. MALDI-TOF-MS spectrum of compound C7.

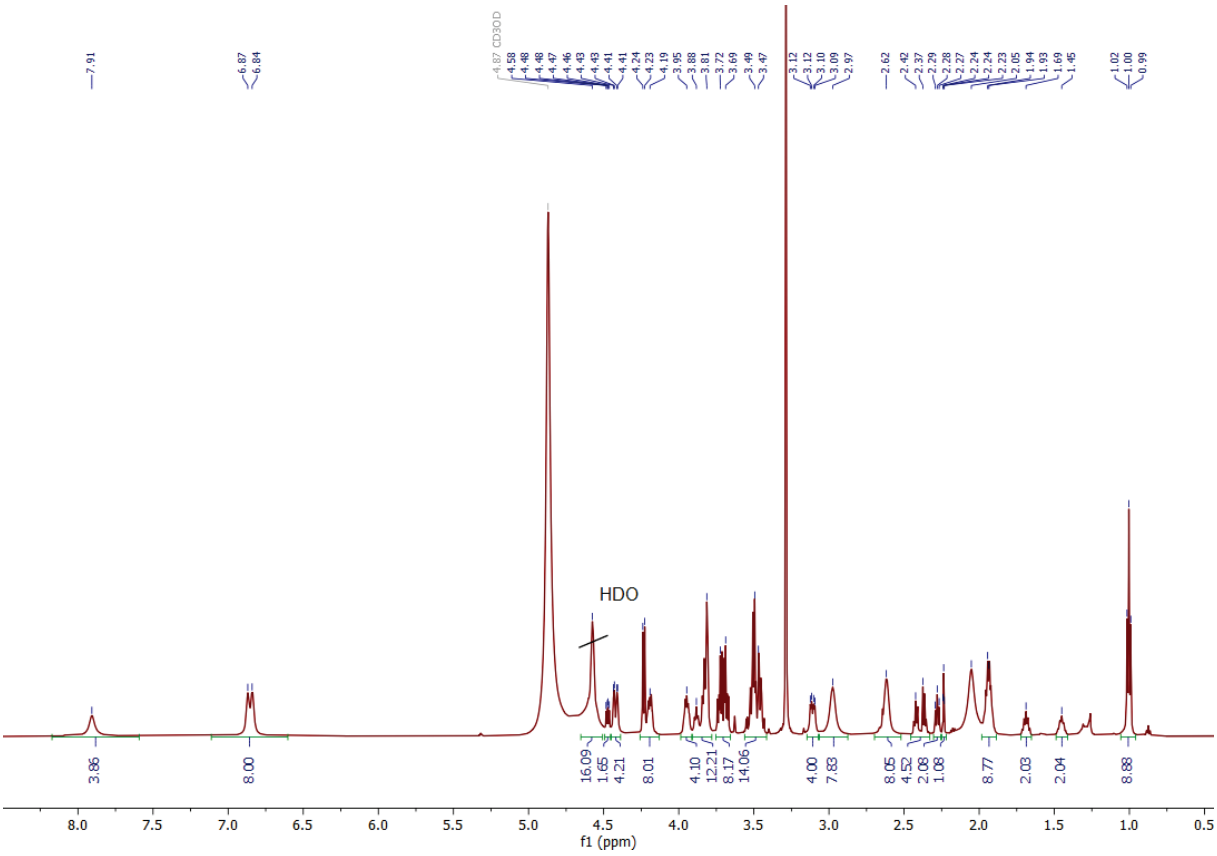

Figure S33. ^{1}H-NMR spectrum (600MHz) of compound C7 in MeOH-*d4*/D_2O.

gold nanoparticles prior to functionalization

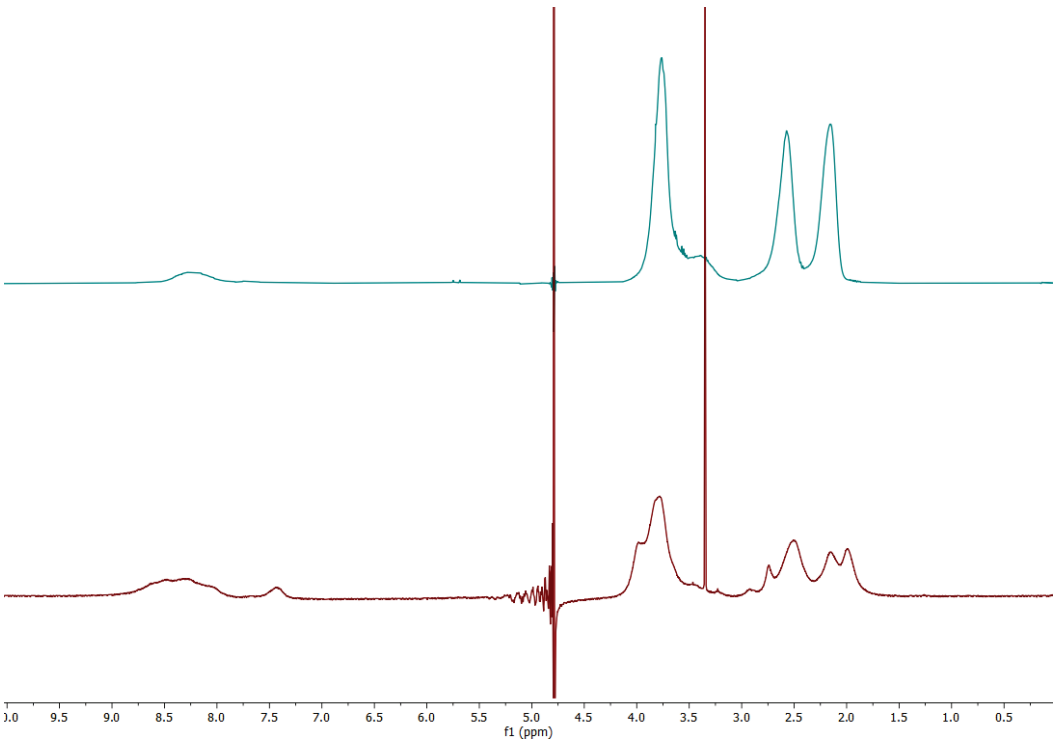

Figure S34. 1H-NMR spectra of AuGSH (blue) and AuN3 (red) in H_2O.

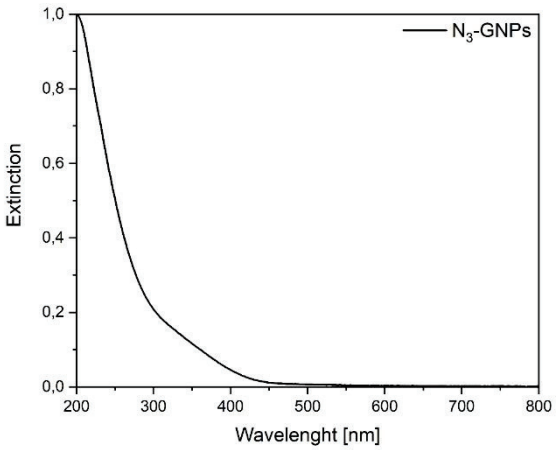

Figure S35. Normalized UV-Vis spectra of N_3-GNPs.

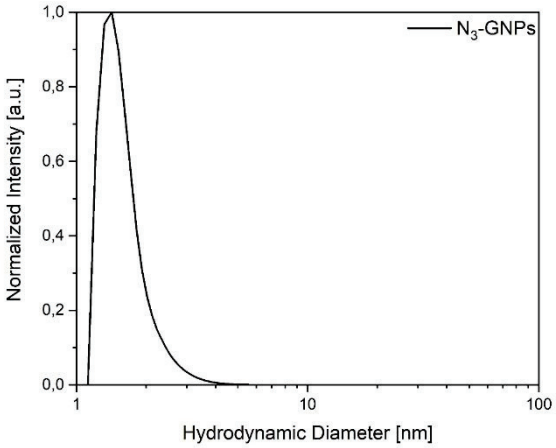

Figure S36. Disc centrifugal sedimentation (DCS) of N_3-GNPs.

glycocalixarene-gold nanoparticle conjugates

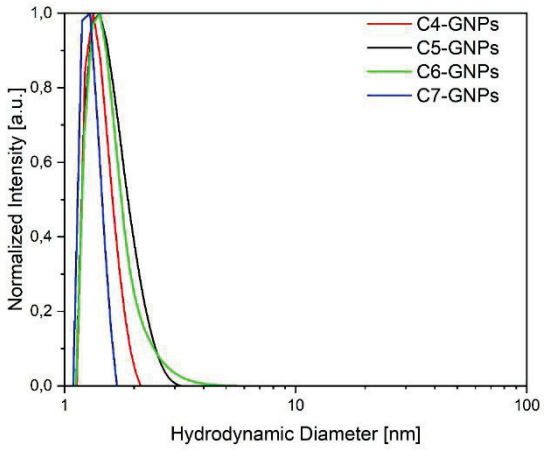

Figure S37. Disc centrifugal sedimentation (DCS) of C4-GNPs (red), C5-GNPs (black), C6-GNPs (green) and C7-GNPs (blue).

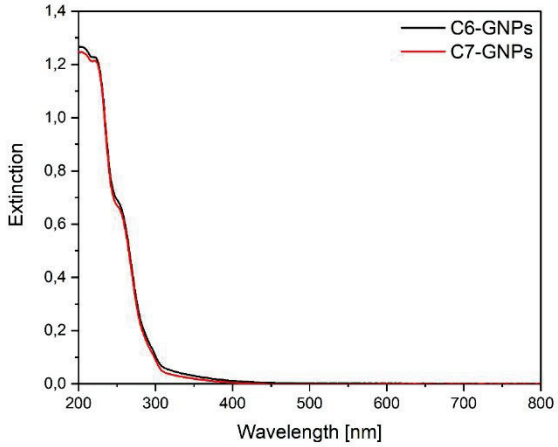

Figure S38. Normalized UV-Vis spectra of C6-GNPs (black) and C7-GNPs (red).

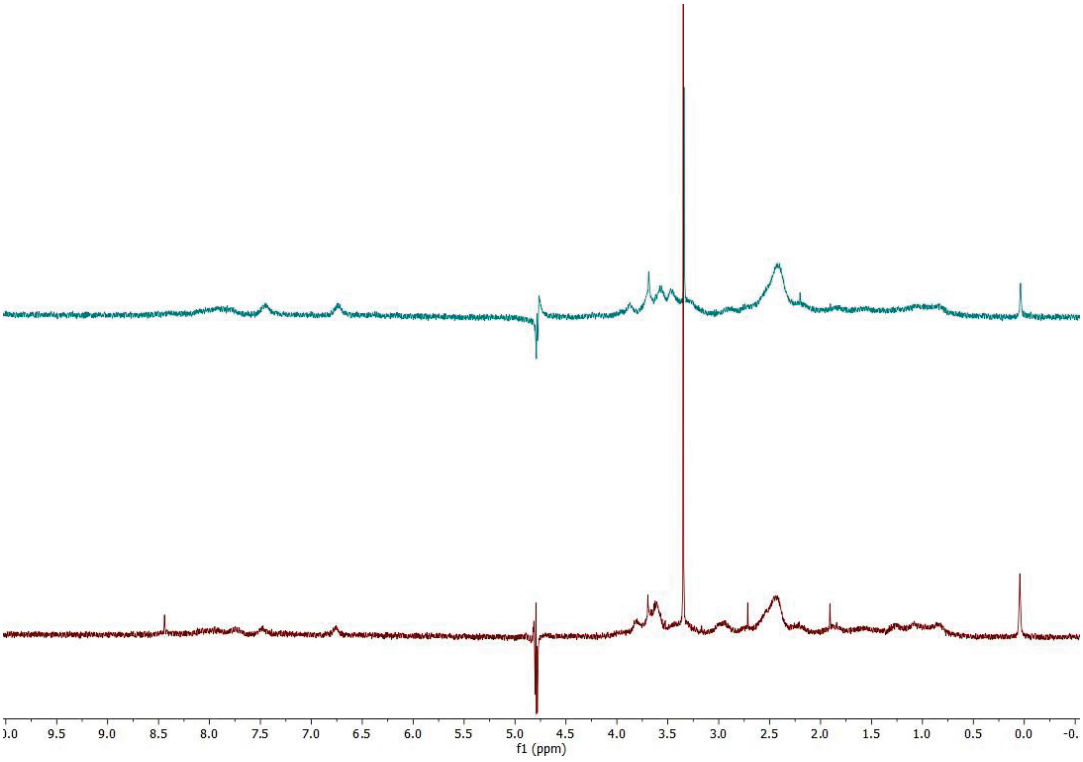

Figure S39. ^{1}H-NMR spectra of C4-GNPs (red) and C5-GNPs (blue).

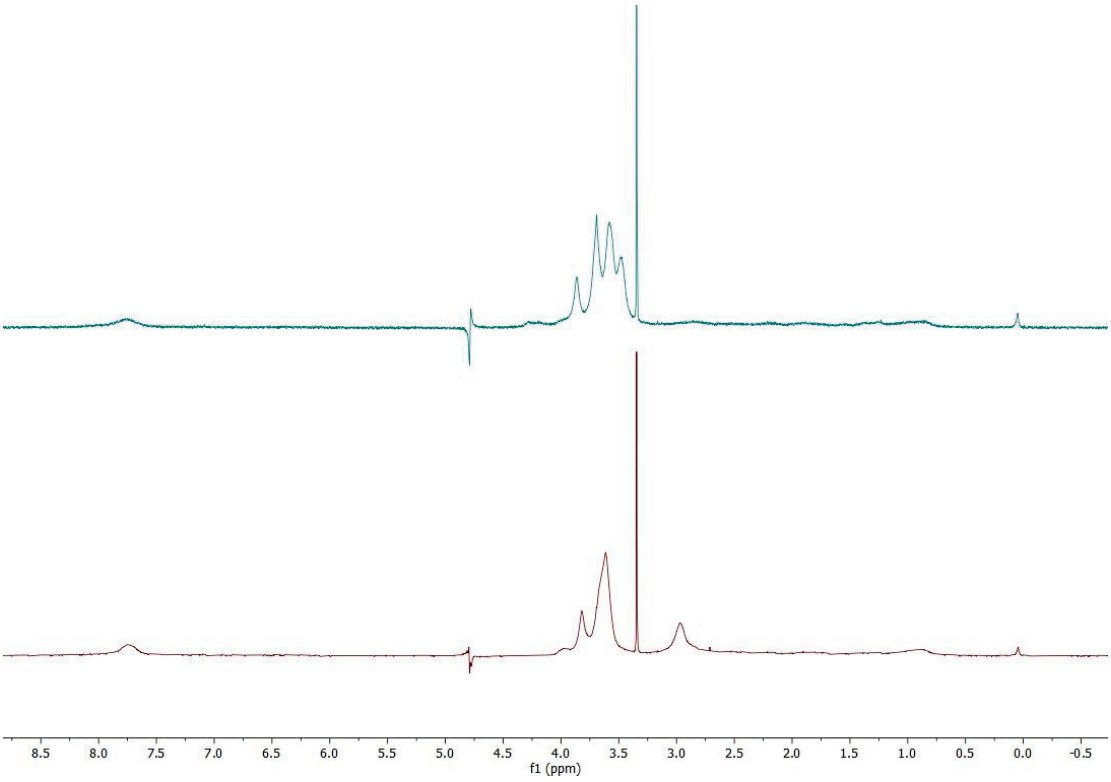

Figure S40. ^{1}H-NMR spectra of C6-GNPs (blue) and C7-GNPS (red).

Bacterial inhibition studies

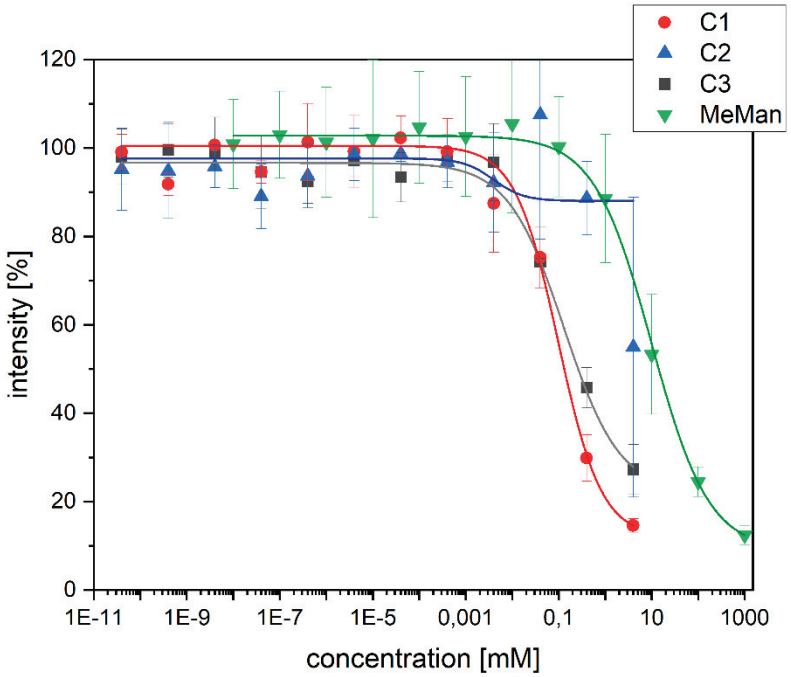

Figure S41. Bacterial adhesin inhibition assay according to protocol described above with compounds C1, C2, C3 and MeMan.

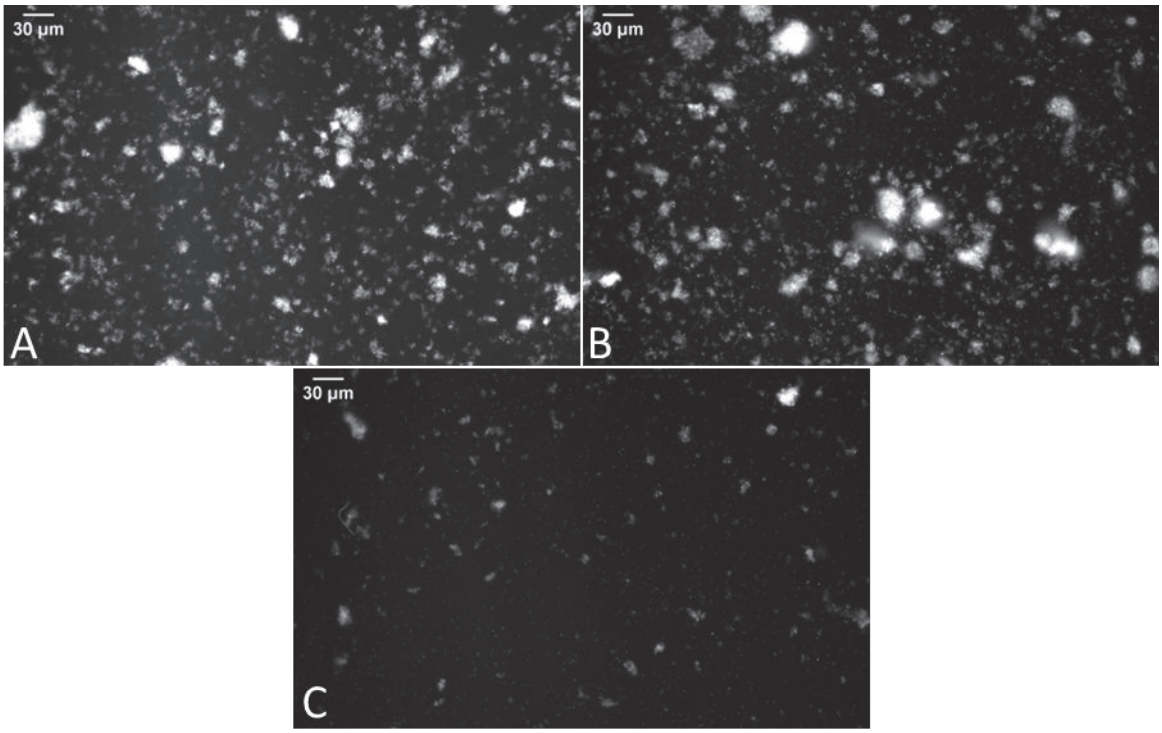

Figure S42. Fluorescence microscopy, A: C6-GNPs (c(NP) = 22.5 µM) + *E.Coli (1mg/ml)* in PBS buffer, B: *E.coli* (1mg/ml) in PBS buffer, C: C1 (c(calix[4]arene) = 22.5 µM) + *E.coli* (1mg/ml) in PBS buffer.

References:

[1] K. Klein, K. Loza, M. Heggen and M. Epple, *ChemNanoMat* **2021**, *7*, 1330-1339.
[2] a) D. Ponader, F. Wojcik, F. Beceren-Braun, J. Dernedde and L. Hartmann, *Biomacromolecules* **2012**, *13*, 1845-1852; b) M. Ebbesen, C. Gerke, P. Hartwig and L. Hartmann, *Polymer Chemistry* **2016**, *7*, 7086-7093.
[3] W. Hayes, H. M. Osborn, S. D. Osborne, R. A. Rastall and B. Romagnoli, *Tetrahedron* **2003**, *59*, 7983-7996.
[4] L. Wu and N. S. Sampson, *ACS chemical biology* **2014**, *9*, 468-475.
[5] a) S. M. Gerchakov and P. G. Hatcher, *Limnology and Oceanography* **1972**, *17*, 938-943; b) T. Masuko, A. Minami, N. Iwasaki, T. Majima, S.-I. Nishimura and Y. C. Lee, *Analytical biochemistry* **2005**, *339*, 69-72.
[6] A. K. H. Mirja Hartmann, Per Klemm, Thisbe K. Lindhorst, *Chemical Communications* **2010**, *46*, 330-332.
[7] L.-S. Wagner, O. Prymak, T. Schaller, C. Beuck, K. Loza, F. Niemeyer, N. Gumbiowski, K. Kostka, P. Bayer and M. Heggen, *The Journal of Physical Chemistry B* **2024**, *128*, 4266-4281.
[8] M. Bergeron-Brlek, T. C. Shiao, M. C. Trono and R. Roy, *Carbohydrate research* **2011**, *346*, 1479-1489.
[9] S. B. Shuker, J. Esterbrook and J. Gonzalez, *Synlett* **2001**, *2001*, 0210-0213.

3.2. Ligands for the Carbohydrate-recognizing Domain of NGLY1

As mentioned above, the *C*-terminal PAW domain of eukaryotic PNGase is known to play an important role in substrate binding and the acceleration of the enzymatic activity. As natural substrates, high-mannose-type glycoproteins have been identified. Zhou et al. reported mannopentaose as a potent binder for mouse PNGase, suggesting that a branched mannose oligomer is the minimal binding motif for this domain.[32, 37] Interestingly, in recent studies, it was reported for several glycosidases that the multivalent presentation of the binding carbohydrate epitope increased binding affinity significantly, in a manner similar to the multivalent effect known from other lectin-domains that are, for instance, present on protein receptors. This was a rather surprising finding since the binding pockets of enzymes are generally considered to be single-substrate binding sites with deep and sterically demanding constitution. [25, 241] Clearly, the binding mechanism between glycans and enzymes is less understood compared to their interactions with lectins, and for NGLY1, a chemical ligand with the ability to bind the *C*-terminal binding site is not known so far. However, it was assumed that the application of multivalent glycomimetics might also be suitable for binding to the lectin-like domain of NGLY1.

To test this, a set of multivalent mannose ligands was synthesized (see Figure 12). Besides some linear compounds with and without branched mannose features (**L1** and **L2**), some glycocalix[4]arene derivatives (**C1b**, **C2b**, and **C8b**) were also prepared. The mannose-functionalized glycocalix[4]arene derivative **C1** has already been shown to bind successfully to the bacterial lectin FimH (see chapter 3.1), presumably benefiting from additional hydrophobic interactions with proteins. Additionally, the branched structure of the calix[4]arene-based ligands has a higher structural resemblance with the natural high-mannose ligands compared to the linear oligo(amidoamine) backbones. For these reasons, it was assumed that **C1b** might be a promising ligand candidate for the PAW domain of NGLY1. An additional interesting feature is that the synthetic structures do not contain the Asn-GlcNAc motif that is present in high-mannose *N*-glycans, which are the natural substrates of NGLY1. During de-glycosylation by NGLY1, it is believed that the hydrolysis of the bond between the asparagine (Asn) residue and the proximal GlcNAc initiates the release of the substrate from the enzyme.[34] Therefore, these synthetic ligands could potentially act as enzyme inhibitors, since the natural release mechanism from the binding pocket may not occur. To give access to a broader range of analytical methods, it was aimed to implement a biotin tag into the ligand design. Since the vitamin biotin is known to bind very strongly and with high stability to the bacterial protein streptavidin, the system has been widely exploited in biotechnology for various applications.[242, 243]

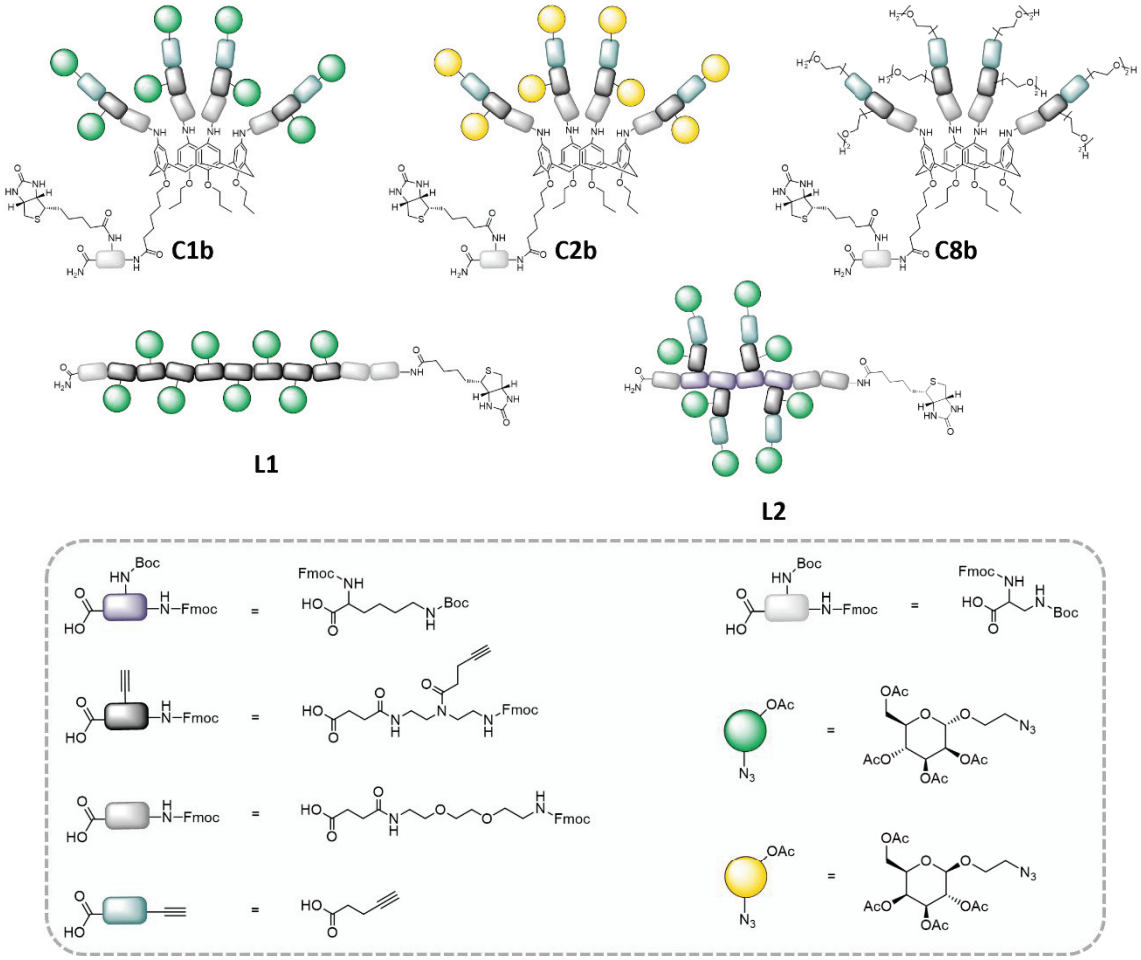

Figure 12: Schematic depiction of biotinylated ligands for the lectin-binding domain of NGLY1 (PAW domain).

3.2.1 Synthesis of Biotinylated Glycocalix[4]arene Ligands

To obtain the desired biotinylated glycocalix[4]arenes, the previously established synthetic approach using solid-phase polymer synthesis was applied. This demonstrates the high versatility of this synthetic procedure towards multifunctional glycocalix[4]arene derivatives for different applications. The synthesis of the structures was executed analogously as described for the derivative **C1-C7** (see chapter 3.1). As has already been shown for the previous structures, it is of high importance to identify the ideal order of assembly, especially when it comes to multifunctional structures. In short, as the first building block, Fmoc-Dap(Boc)-OH, a commercially available orthogonally protected amino acid, was coupled using the standard protocol conditions to implement a branching point. Previous studies within the group of Prof. Hartmann showed the formation of by-products when the lower rim functionality was first introduced before the nitrogen reduction. Therefore, it was decided to directly continue with the attachment of the

calix[4]arene building block **CBB1.** Subsequently, the reduction of the nitrogen groups by treatment with 25 eq. of tin chloride dihydrate per nitrogen group in *N*-methyl-2-pyrrolidone (NMP) at 30 °C for 24h gives the desired tetra-amine-calix[4]arene derivative. In the next steps, EDS, TDS, and finally 4-pentynoic acid were coupled to the upper rim. At this point, it was evaluated whether the next step should be to conjugate the azide moiety via CuAAC or to proceed with the coupling of the biotin residues at the lower rim. For compound **C1b,** first, the copper-catalyzed click reaction (CuAAC) of the tetra-O-acetyl-α-D-mannopyranosyl azide was performed according to the reported protocol.[170] Then, the Boc group at the lower rim was removed following the coupling using 2 eq. Biotin in DMF with 5 eq. PyBOP and 10 eq. DIPEA for 1h. Analysis of the microcleavage after this step showed that several acetyl groups have been removed, presumably due to the exposure to 4 M hydrochloric acid solution during Boc-group removal. Nevertheless, this was neglected as no by-products caused by the unwanted acetyl group removal could be observed. After deprotection of the remaining acetyl groups and subsequent cleavage from the solid support, the crude product **C1b** was obtained with a rel. purity of 66 %. Relative purities of all oligomers were determined by integrating the UV signals of the RP-HPLC chromatogram at 214 nm. The desired product **C1b** can be identified at a retention time (t_R) of 11.4 min in the HPLC spectra (see Figure 13A). In the coupled MS spectra, mass-to-charge ratios (m/z) corresponding to **C1b** were observed. Figure 13B shows the structures of the main by-products identified via HPLC-MS. More hydrophilic byproducts (**BP1**, t_R=11.2 min) at retention times lower than the main product **C1b** were found, indicating that there was no successful coupling of biotin in the last step. Further, by-products **BP2-BP5** (t_R=11.7-12.5 min) were identified as different deletion sequences due to incomplete coupling steps, yielding structures with either one or two mannose residues missing. However, none of the identified by-products suggested that the results of a first qualitative binding study would be significantly affected. Therefore, the product was used without any further purification.

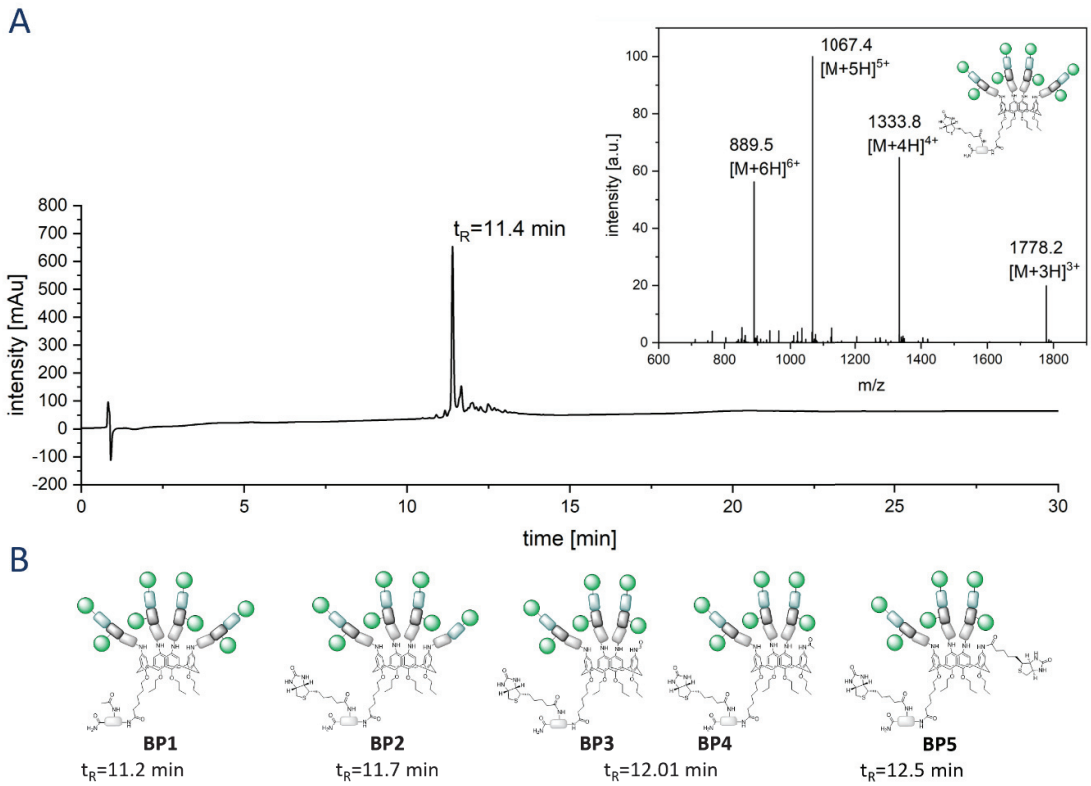

*Figure 13: (A) HPLC chromatogram of compound **C1b** (95/5 to 5/95 vol.-% H_2O/MeCN + 0.1% formic acid in 30 min) and coupled mass spectra at t_R=11.4 min, (B) structure proposal of by-products **BP1-BP5**.*

For compound **C2b,** the opposite approach was tested. Accordingly, Biotin was coupled first, followed by the conjugation of tetra-O-acetyl-galactopyranosyl azide via CuAAC. Besides the altered order of synthesis steps, all steps were performed under the same reaction conditions as described before. After cleavage, the main product **C2b** was found at a t_R of 11.3 min in the HPLC spectra. In the coupled mass spectra, mass-to-charge ratios corresponding to **C2b** were observed (see Figure 14A). However, the product **C2b** was obtained in a lower rel. purity of 53 %. Figure 14B shows the by-products identified with HPLC-MS. Again, some deletion sequences were found (**BP8**, **BP10**), but also by-products indicating that the conjugation of the galactose residues was not complete (**BP7**, **BP9**) were observed. It was assumed that the terminal alkynes might be hydrated under the acidic conditions during the Boc-group removal, resulting in the ketone **BP7**. Additionally, some other by-products were observed that could not be identified. In conclusion, the first synthetic pathway as described for **C1b** appeared to be the more promising approach for future synthesis.

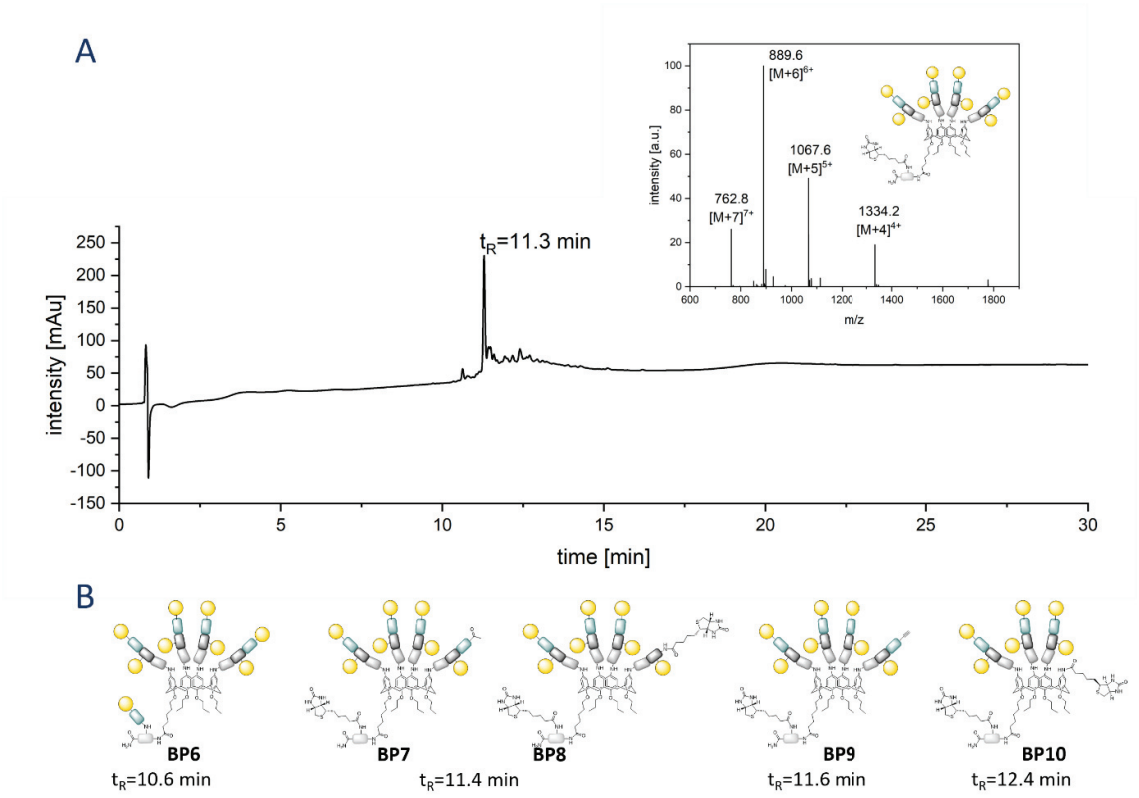

*Figure 14: (A) HPLC chromatogram of compound **C2b** (95/5 to 5/95 vol.-% H_2O/MeCN + 0,1 % formic acid in 30 min) and coupled mass spectra at t_R=11.3 min, (B) structure proposal of by-products **BP6-BP10**.*

In addition to the biotinylated glycocalix[4]arene structures, a non-carbohydrate containing calix[4]arene structure **C8b,** was synthesized as a reference structure. Diethylene glycol was chosen as a motif to compare with carbohydrate residues, as it still allows for engagement with the protein surface by hydrogen bonding, but in contrast, no specific interactions were presumed. Advantageously, azide-functionalized derivatives with different glycol units were commercially available and the required water solubility was still guaranteed upon conjugation to the scaffold via CuAAC. In this case, due to the hydroxyl functionalities of the diethylene glycol azide, the second pathway (analog to **C2b**) appeared to be the more promising approach, as side reactions during Boc-group removal are more likely to occur.[244] Again, the identified by-products in the HPLC chromatogram were explained by deletion sequences due to incomplete coupling steps and incomplete conjugation of the diethylene glycol motif (see Figure 15A and B). However, no by-products that indicated side reactions of the alcohol groups were found. It is worth noting that the HPLC analysis for this compound was performed without formic acid as an additive to the eluent system. Otherwise, additional by-products formed most likely during analysis were observed.

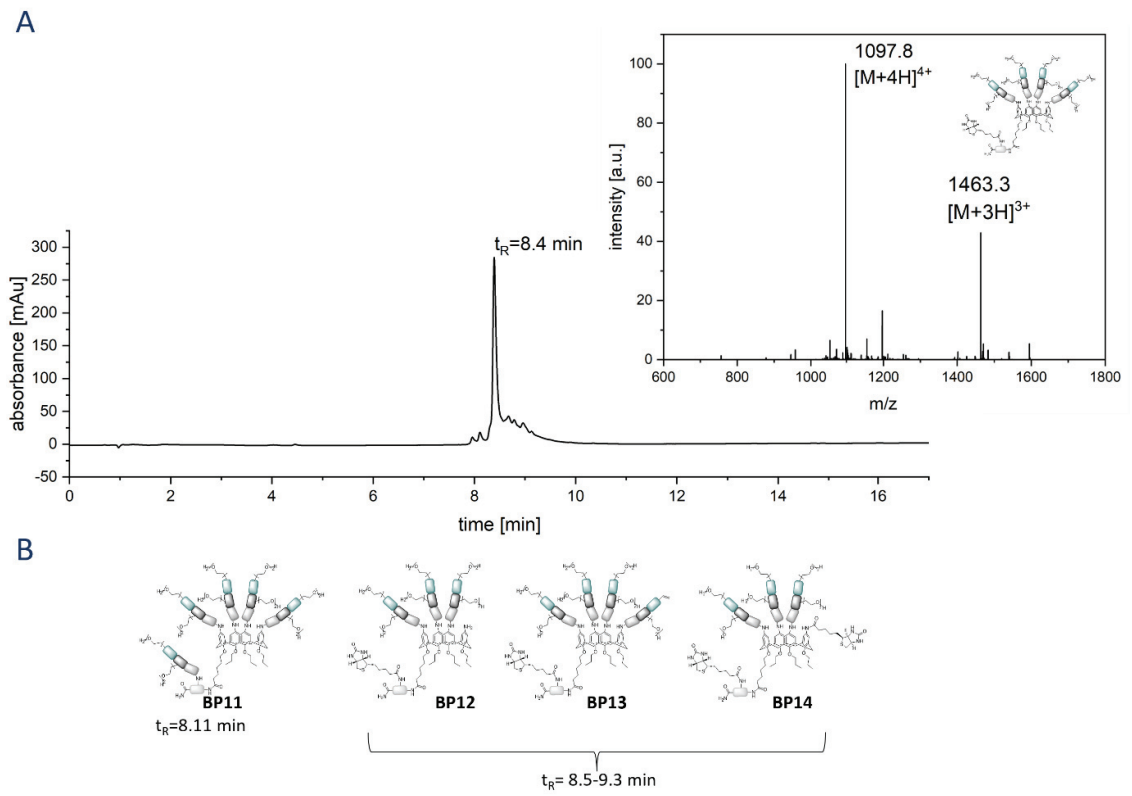

*Figure 15: (A) HPLC chromatogram of compound **C8b** (95/5 to 5/95 vol.-% H_2O/MeCN in 17 min) and coupled mass spectra at t_R=8.4 min, (B) structure proposal of by-products **BP11-BP14**.*

To further analyze the successfully synthesized biotinylated products, ^{1}H-NMR spectroscopy was applied. For example, the spectra of **C1b** and **C8b** are shown in Figure 16. In the following, typical resonances evidencing the successful synthesis of the desired structures are highlighted. The characteristic signals of the scaffold were found for both structures. Signals from the triazole and aryl protons were observed at 7.8 and 6.8 ppm, respectively. Further, resonance caused by the calix[4]arene building block was found at 4.5, 3.1 ppm (methylene bridges 16) and in the aliphatic ppm range, where the occurring signals were assigned to the propyl and the hexyl chains (10, 11, 12, 13, 15). All signals assigned to the biotin motif are highlighted in blue. The biotin linker caused resonance in the area at 2.2 ppm (7) and from 1.3 to 1.7 ppm (4, 5, 6). Other signals evidencing the successful biotin coupling were observed at 2.7 (2') and 2.9 (2) ppm as well as signals at 3.1 ppm (3), 4.5 (1), and 4.3 ppm (1'). Protons related to the ethylene linkers (27 and 28, highlighted in red) overlapped either with the HDO peak (4.-4.71 ppm) or the typical resonances from EDS and TDS building blocks (18, 19, 20, 21, 22). Further resonances related to the diethylene glycol motif of **C8b** (29 and 30, highlighted in red) also overlapped in this ppm area. Additionally, resonances from the mannose residues of **C1b** were observed here. In accordance with the typical resonance caused by the mannose anomeric

position, the signals were found at 4.7 ppm. Further resonances from 4.04 to 4.11 ppm and 3.07 to 3.18 ppm were assigned to the mannose residues. The spectra are in accordance with the spectra of previous comparable structures like **C1** and confirm the successful synthesis of the biotinylated structures C**1b**, C**2b** (see Figure 33, appendix), and C**8b**. Furthermore, the MALDI-TOF-MS was applied and supported the successful synthesis of the desired biotinylated compounds (see Figure 32, Figure 34, and Figure 36, appendix).

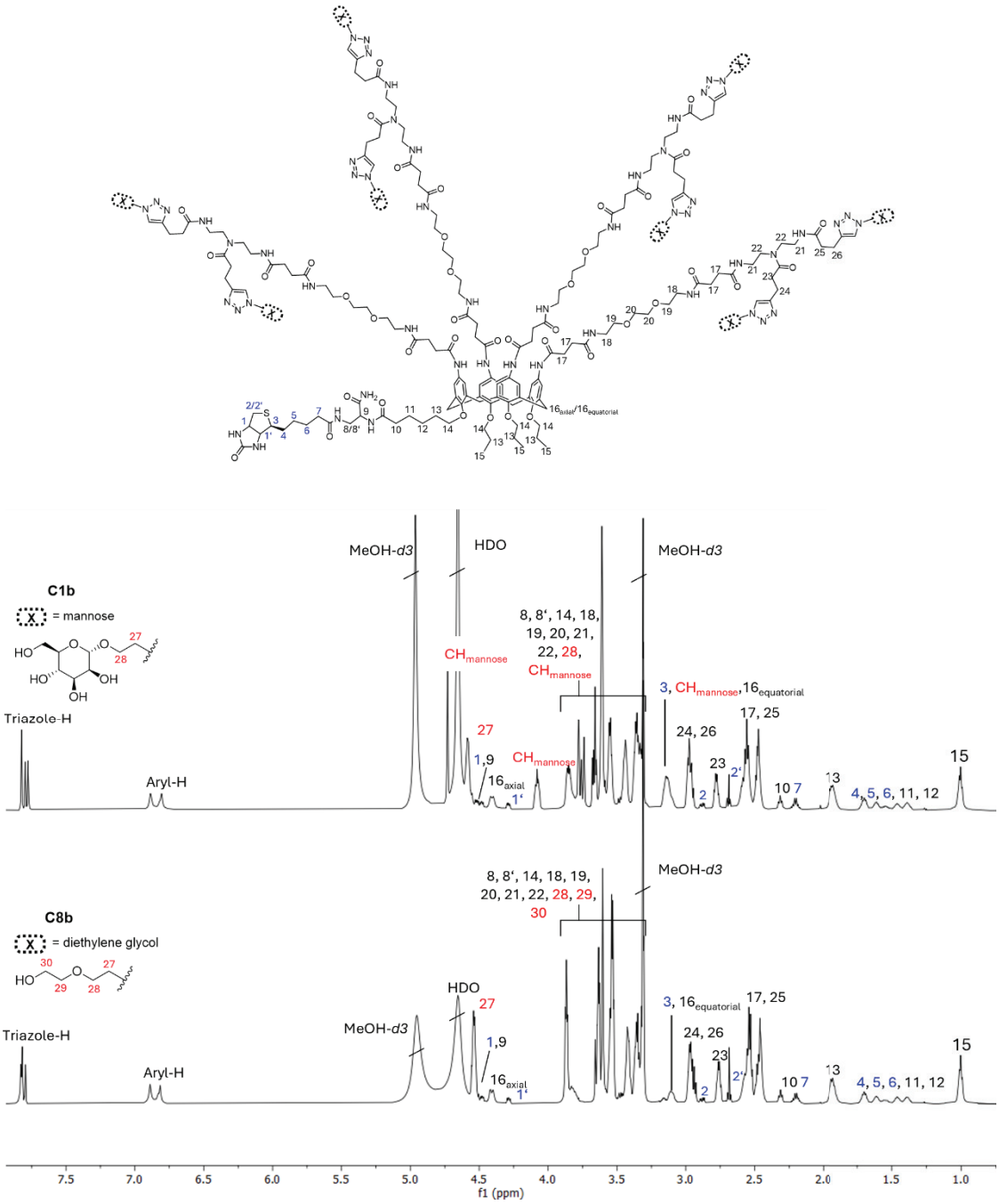

*Figure 16: ^{1}H-NMR (600 MHz, MeOH-d4 and D_2O) of compound **C1b** and **C8b**.*

As further reference structures, the linear analogs **L1** and **L2** were successfully synthesized to assess possible effects of the hydrophobic calix[4]arene scaffold on the interaction with the protein. As the synthesis was performed using the well-established SPPoS protocol, this will not be further discussed here.[219] The compounds were obtained in rel. purity of around 90 % determined by HPLC-MS, respectively. **L1** and **L2** were additionally characterized using ^{1}H-NMR (see Figure 37 and Figure 41, appendix) and MALDI-TOF-MS analytics (see Figure 40 and Figure 44, appendix).

3.2.2 Binding Studies with NGLY1

For initial qualitative evidence of binding between the synthesized ligands and NGLY1, a qualitative pull-down assay was performed using a streptavidin-agarose resin to immobilize the biotin-labeled ligands **C1b**, **C2b**, **C8b**, **L1,** and **L2** (braid molecules). The derivatives **C2b** and **C8b**, which do not exhibit mannosyl residues, were used as negative controls. The assay was performed according to the following procedure depicted in Figure 17A. First, the sample (**C1b**/**C2b**/**C8b**/**L1**/**L2**, 10 mM) was incubated with human NGLY1 (0.91 mg/ml) for one hour at 37 °C (Figure 17A, step 1). Then 100 µL of an agarose-streptavidin resin was added and incubated overnight (Figure 17A, step 2). Due to the strong biotin-streptavidin interaction, the biotin-functionalized ligand, potentially bound to NGLY1, is immobilized on the resin. This is followed by three washing steps with a buffer to remove any excess of NGLY1 protein that may have bound unspecifically to the streptavidin resin (Figure 17A, step 3). The immobilized ligand-protein complex was then eluted and analyzed by SDS-PAGE (Figure 17A, steps 4 and 5). The gel was stained with Coomassie and washed with MQ water overnight. If NGLY1 is successfully bound to the tested ligand (**C1b**/**C2b**/**C8b**/**L1**/**L2**), a band corresponding to the mass of NGLY1 (~ 74 kDa) should be observed on the gel. The obtained gel is shown in Figure 17B. The first lane shows an additional control experiment in which the assay was performed without the addition of any ligand (zero-sample control). As a weak band corresponding to the molecular weight of NGLY1 can be observed, it was assumed that some unspecific interactions between the NGLY1 and the agarose-streptavidin matrix occurred. This might be avoided by using harsher washing conditions like PBST (PBS + tween). However, a very pronounced band corresponding to the molecular weight of NGLY1 was detected on the gel for the sample incubated with **C1b** (Figure 17B, lane 2). This is in line with the expectations since **C1b** was assumed to be the best binder to NGYL1. Interestingly, a high intensity band was also found in lane five, where the non-glycosyl calix[4]arene derivative **C8b** was used as a braid molecule and therefore no binding to NGLY1 was expected. For the linear ligands **L1** and **L2,** as well as the galactosyl-calix[4]arene derivative **C2b,** only low intensity bands were observed, which are

presumably accounted for by unspecific interactions (Figure 17B, lanes 3,4, and 6). Nevertheless, it must also be considered that for this assay design, it cannot be guaranteed that the exact same amount of streptavidin-agarose resin was transferred to each sample, and the experiment can only be evaluated qualitatively.

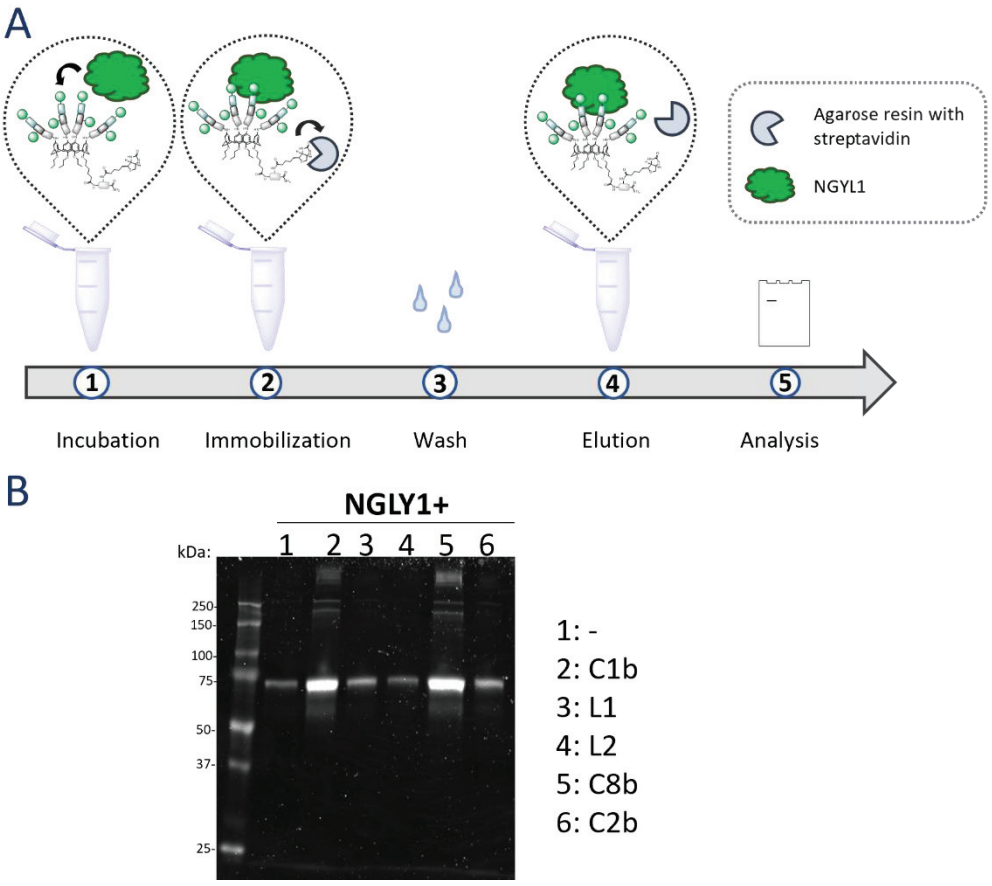

Figure 17: (A) Working steps pull-down assay (B) SDS PAGE gel stained with Coomassie and loading of the wells. Color and contrast of the gel were adjusted using the ImageJ program.

To enable a more accurate and quantitative examination of the ligand-enzyme interaction, an assay design inspired by Enzyme-linked Immunosorbent Assays (ELISA) was developed (see Figure 18A). Therefore, the first step was to immobilize the protein of interest to a suitable surface, such as polystyrene plates, since it is known that proteins can adsorb to polystyrene surfaces due to hydrophobic interactions.[245] As NGLY1 was not available in large amounts, the assay conditions were assessed using Concanavalin A as a mannose-binding model protein, which can be commercially purchased. Initial tests revealed that the most uniform protein coating was achieved when Con A (1 mg/ml in LB buffer) was shaken vigorously overnight at 37 °C. Followed by an intense washing procedure with PBST (5 times) and subsequent blocking with a 1 w.-% Bovine Serum Albumin (BSA) solution to prevent unspecific interactions of the protein with the surface. Additionally, it has been observed

that unspecific hydrophilic interactions between proteins might occur and interfere with the evaluation of the relevant specific interactions. One common way to disrupt these interactions is to treat the protein-coated surface with a carbohydrate solution that does not show any specific interactions with the proteins of interest. A galactose solution (0.1 w. %) was therefore added to the BSA blocking solution. Followed again by a vigorous washing procedure. The ligands (**C1b**/**C2b**/**L1**) were added in serial dilution to the freshly prepared surface in a concentration range from 10 mM to 0.01 pm in lectin binding (LB) buffer, and the plate was shaken for 1 hour at 37 °C. Afterward, the surface was washed again and treated with Horseradish Peroxidase-Streptavidin conjugate (HRP, 125 µL/L, in PBS) for 1 h at room temperature and subsequently treated with a 3,3',5,5'-tetramethylbenzidine (TMB) based substrate solution. HRP is a commonly used enzyme for ELISA applications that gives access to a colorimetric readout when treated with an appropriate substrate like TMB. Upon oxidation TMB becomes a blue dye with an absorbance maximum at 370 nm. As this allows for no proper endpoint determination, concentrated sulfuric acid can be used as a fixation solution, turning the mixture yellow with an absorbance maximum at 450 nm.[246] Hence, the formation of the dye can be used for the determination of the concentration of biotinylated substance by UV/Vis measurement. Figure 18B shows the results of the ELISA-like adhesion assay conducted with Con A-coated microtiter plates. A significant enhancement in absorbance at 450 nm was observed for ligand **L1** with increasing concentration. For the calix[4]arene ligand **C1b**, an increase in absorbance was observed, even though to a lower extent. On the other hand, for the negative control **C2b,** there was no clear concentration-related trend to observe. The values were in a similar range compared to the zero-sample control experiment. The results clearly indicated the successful performance of a concentration-dependent adhesion assay with Con A as the protein of interest. With this suitable assay protocol in hand, it was then proceeded to study the ligands for the binding to NGLY1. The assay was performed according to the procedure described above. Since there were no large amounts of high concentrated stock available, an initial coating attempt was performed with a concentration of 0.35 mg/mL instead of the intended 1 mg/mL NGYL1 buffer solution. However, this attempt did not deliver any reasonable absorbance values for any of the tested ligands. In more detail, for all samples, including the zero-sample control, very similar values were obtained. In previous attempts, when BSA coating was tested as a negative control, HRP appeared to have a high unspecific binding towards BSA, leading to surprisingly high absorbance values for all samples. Therefore, it was reasoned that an insufficient coating with NGLY1, resulting in high amounts of BSA on the surface of the well

plate, might account for the unexpected results. As a consequence, the coating was repeated using a higher concentration of NGLY1 (0.91 mg/mL). In this attempt, the plate surface seemed to be more efficiently coated as the absorbance values obtained for the zero-sample were notably lower compared to all other samples. However, no clear trend within the tested samples (**L1**/**C1b**/**C2b**) was noticeable. Considering the findings of both the pull-down assay and the ELISA-like adhesion assay, there was no clear evidence that the mannosyl ligands (**L1**/**L2**/**C1b**) bind specifically to NGLY1. Accordingly, it was not confirmed that the ligands bind at the targeted *C*-terminal domain of the enzyme, as anticipated, but rather bind randomly to the protein surface.

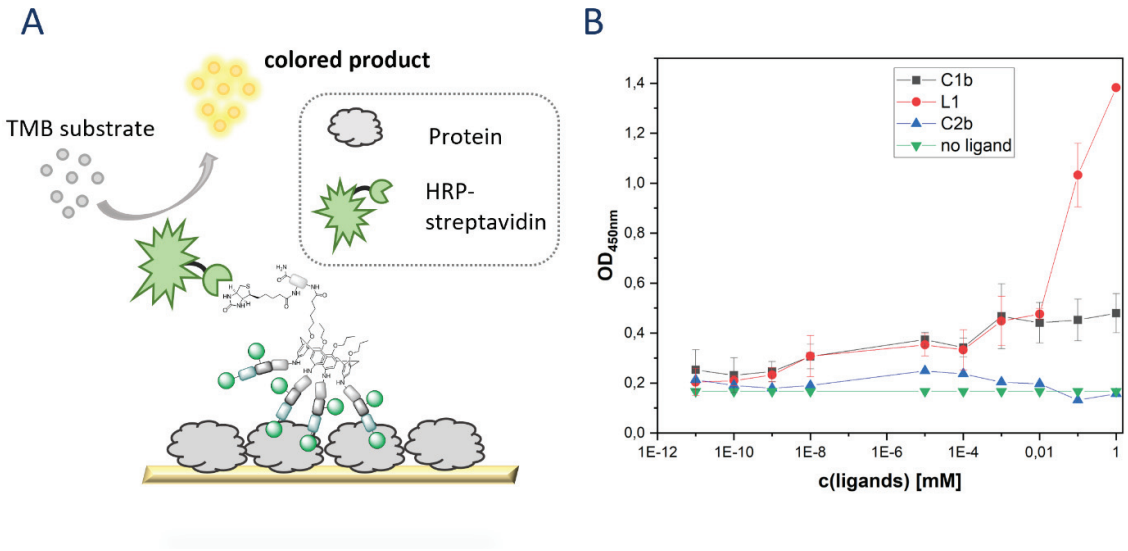

Figure 18: (A) Schematic depiction to illustrate the assay design of ELISA-like adhesion study, (B) absorbance (450 nm) values obtained in ELISA-like adhesion study for C1b, L1, C2b with a Con A-coated surface.

Nevertheless, a further experiment was performed in order to examine whether the enzyme activity was affected by the interactions with the ligands. Recently, the investigation of potential glycosidase regulators and inhibitors has been of high interest for therapeutic applications.[45] Also, for human NGLY1, the Bertozzi group was first to study chemical ligands as NGLY1 inhibitors targeting different severe diseases such as cancer.[33] To test the synthesized ligands, a gel shift assay was performed. Ribonuclease B (RNase B), a high-mannose-type *N*-linked glycoprotein and known substrate for eukaryotic PNGase was investigated using sodium dodecyl sulfate polyacrylamide gel electrophoresis (SDS PAGE). Treatment with an active de-glycosylating enzyme truncates RNase B, resulting in a band shift to lower molecular weights on the SDS-PAGE gel. On the other hand, in case of a reduced or even inhibited enzyme activity due to the addition of a potent inhibitor, the band of lower molecular weight is not observed on the gel. Prior tests with NGLY1 showed no

activity of the available NGLY1 stock towards RNase B as substrate. Therefore, the assay was performed with peptide-*N*-glycosidase F (PNGase F) and endoglycosidase H (Endo H). PNGase F is a bacterial glycanase that, similar to NGLY1, acts as an amidase, cleaving the glycosidic bond between the innermost GlcNAc and the asparagine side chain but is less specific regarding the carbohydrate structure. High-mannose, hybrid-, as well as complex-oligosaccharides can be cleaved.[247, 248] In contrast to PNGase F and NGLY1, Endo H catalyzes the hydrolysis of the glycosidic bond between the GlcNAc residues proximal to the asparagine side chain, leading to a truncated glycoprotein with one GlcNAc residue left. Endo H processes high-mannose oligosaccharides but not highly complex or hybrid types.[249] Additionally, PNGase F and Endo H are less sensitive to protein conformation compared to NGLY1. Gel shift assay kits were commercially purchased for both PNGase F and Endo H. For both enzymes, the ligands **C1b**/**L1**/**L2**/**C2b**/**C8b** were tested as potential enzyme inhibitors. To do so, the ligands were incubated with the enzyme for 30 minutes at 37 °C at different concentrations. Subsequently, freshly denaturized glycoprotein RNase B was added, and the mixture was incubated for another hour at 37 °C. To assess the enzymatic activity of the applied enzymes, a SDS-PAGE was performed. The gels obtained after Coomassie staining are shown in Figure 19A for Endo H and 19B for PNGase F. The results of the SDS-PAGE show that RNase B was successfully cleaved upon addition of both enzymes (see Figure 19A lane 1 and 19B lane 11) as evidenced by the enhanced formation of a band at lower molecular weight compared to the non-truncated RNase B (17 kDa) (see Figure 10A lane 2 and Figure 10B lane 12). However, it was also observed that none of the added ligand acted as an enzyme inhibitor for either Endo H nor PNGase F, as the intensity of the band that can be assigned to the truncated glycoprotein has not changed noticeably (see Figure 19A lane 3-8 and 11-19 and Figure 19B lane 1-10). All in all, it was observed that the tested ligands showed a certain interaction with NGLY1, but the results of the conducted studies did not suggest that a specific binding was dominant here. From this, it was concluded that the presentation of single mannose residues on a multivalent scaffold might not be a sufficient binding motif, but that oligosaccharides are required. Also, an effect of the enzymatic activities of the related enzymes PNGase F and Endo H could not be observed. For these reasons, the project was not pursued any further. Despite this, it could be demonstrated that the established synthetic pathway is suitable for the preparation of biotinylated glycocalix[4]arenes, which were successfully employed in binding studies with the carbohydrate-binding protein Con A.

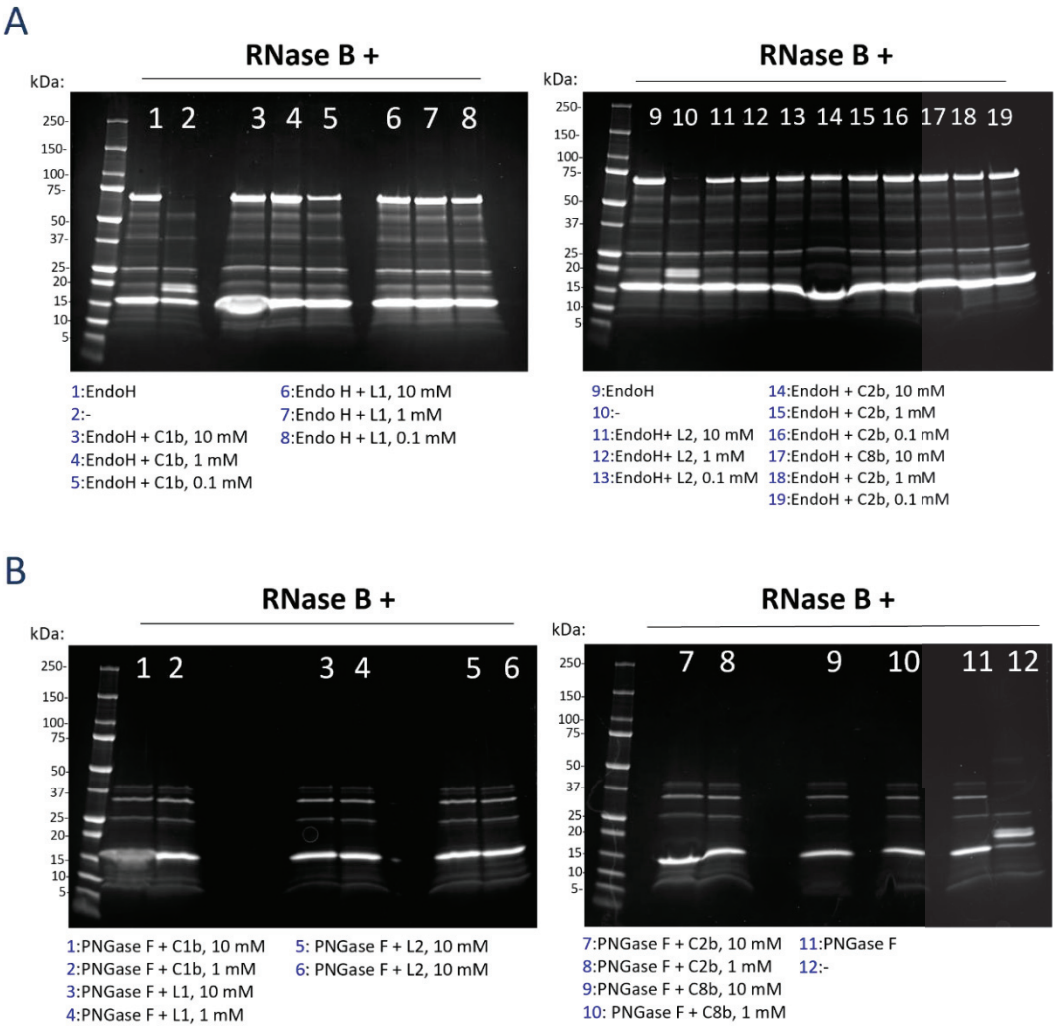

Figure 19: SDS PAGE gel (stained with Coomassie) and loading of the wells. Color and contrast of the gel were adjusted using the ImageJ software.

3.3 Bispecific Glycocalix[4]arene Dimers for Simultaneous Receptor Binding

In the previous chapters, it was successfully demonstrated that the established protocol gives access to a wide range of different glycocalix[4]arene derivatives. Encouraged by these promising results, the next step was to combine two calix[4]arene derivatives to obtain dimeric compounds. This approach allows not only higher molecular weight structures and higher carbohydrate valency, but also the preparation of two-sided heteromultivalent calix[4]arene compounds. In the last decades, the principle of heteromultivalency gained great interest in the field of glycomimetics, as it was shown by numerous working groups that high binding avidities were obtained for different lectins such as FimH from *E. coli* (see also chapter 3.1) or plant lectin Con A due to the so-called hetero glycocluster effect.[219, 250, 251] In contrast to these studies, in this work, the focus lay on the synthesis of two-sided heteromultivalent and bispecific glycocalix[4]arene dimers, which could also be considered as Janus calix[4]arene, for the simultaneous binding to different receptors (e.g., lectins). Recently, interest in biochemical research has been aroused by these kinds of bispecific ligands, as they have been shown to be useful for different applications. For instance, glycoconjugates for the binding to the bacterial lectins LecA and LecB from *Pseudomonas aeruginosa* as potential antiadhesive therapeutics have been reported.[237, 252, 253] Furthermore, another attractive topic of high interest are ligands with the ability to target lectins from different pathogens to give access to multiple (pathogen) detection devices. Beyond applications for pathogen binding, in recent years, bispecific or janus-like (glyco-)ligands have also been intensively studied as mediators for the cellular uptake of different materials.[239] For instance, a current research topic in this field are the so-called lysosome-targeting chimeras (LYTACs), first developed by Banik et al.[254] In contrast to the already established concept of proteolysis-targeting chimeras (PROTACs), this approach enables the targeted protein degradation of extracellular, therapeutic targets, such as growth factors, on the lysosomal pathway.[255] On the molecular level, LYTACs are heterobifunctional compounds that are capable of simultaneously binding lysosome-trafficking membrane receptors on the one side and a protein of interest, which is aimed to be destructed, on the other. For this purpose, different LYTAC designs have been demonstrated to successfully mediate endocytosis following lysosomal degradation of the targeted protein. For instance, some recent studies were able to target the liver-specific asialoglycoprotein receptor (ASPGR) with trivalent GalNAc-LYTACs and proved the successful degradation of several targets.[256-258] Another example of dual specificity ligands has been demonstrated by the group of Garcia Fernandez, investigating glycoligands that are capable of binding both lectins, like the MMR membrane lectin, and glycosidases. This

approach can be interesting for the development of self-deliverable glycosidase regulators.[25, 238, 241, 259]. The examples described show the great utility as well as variety of Janus-like (glyo-)ligands in the field of biochemistry and biotechnology. The development of the established synthetic approach for the straightforward preparation of a diverse range of Janus-calix[4]arene derivatives appeared to be an attractive prospect. Within the scope of this work, the focus lay on the synthesis of hetero- and homomultivalent glycocalix[4]arene dimers and subsequent binding studies to the model plant lectins Con A and PNA as a proof of concept. The synthesis approach, as well as the results from the binding studies, are presented in the following chapters.

3.3.1 Synthesis of Calix[4]arene Dimers Using a Split and Combine Approach.

For the preparation of the calix[4]arene dimers, a straightforward synthesis based on the already established SPPoS was developed. It was reasoned that CuAAC is suitable for the assembly of two calix[4]arene derivatives to dimers, as this click reaction proved to be very efficient in previous studies. To do so, two corresponding glycocalix[4]arene derivatives equipped with an alkyne or azide functionality were envisaged. The reaction scheme of the applied split-split-combine approach is presented in Figure 20. In the first splitting step, α-D-mannose and β-D-galactose were introduced (see Figure 20, I) split). These carbohydrate residues were chosen as they allow the specific binding to Con A and PNA, respectively. The second split allowed the introduction of either an azide or alkyne functionality to the lower rim of the calix[4]arene (see Figure 20, II) split). In chapter 3.1, the synthetic details to prepare alkyne-bearing glyco-calix[4]arenes (**C4** and **C5**, in this chapter referred to as **C9** and **C11**) were already described. In an analogous fashion, the azide functionalized glyco-calix[4]arene **C10** and **C12** were obtained. As an azide component, 4-azido-benzoic acid was used, as it has already been established within the working group for the implementation of an azide functionality to the building block library.[260] Importantly, for small organic azide compounds, a certain ratio of carbon to nitrogen within the molecule must be given to prevent the compound from being explosive. By implementing these two splitting steps, the four anticipated derivatives can be accomplished using the established solid phase synthesis protocol starting from one resin batch. After the successful assembly of the calix[4]arene monomers **C9-C12** and the subsequent cleavage from the solid support the desired products were analyzed using RP-HPLC-MS (see Figure 46, Figure 50, Figure 54, Figure 58, appendix), MALDI-TOF-MS (see Figure 48, Figure 52, Figure 56, Figure 60, appendix) and ^{1}H-NMR spectroscopy (see Figure 45, Figure 49, Figure 53, Figure 57, appendix). Apart from an anion exchange, the crude products were employed without any

further purification. In the following step, the calix[4]arene monomers can be combined in different ways, giving access to the homomultivalent mannose- and galactose dimers (**C13d** and **C15d**) as well as the heteromultivalent dimer **C14d**.

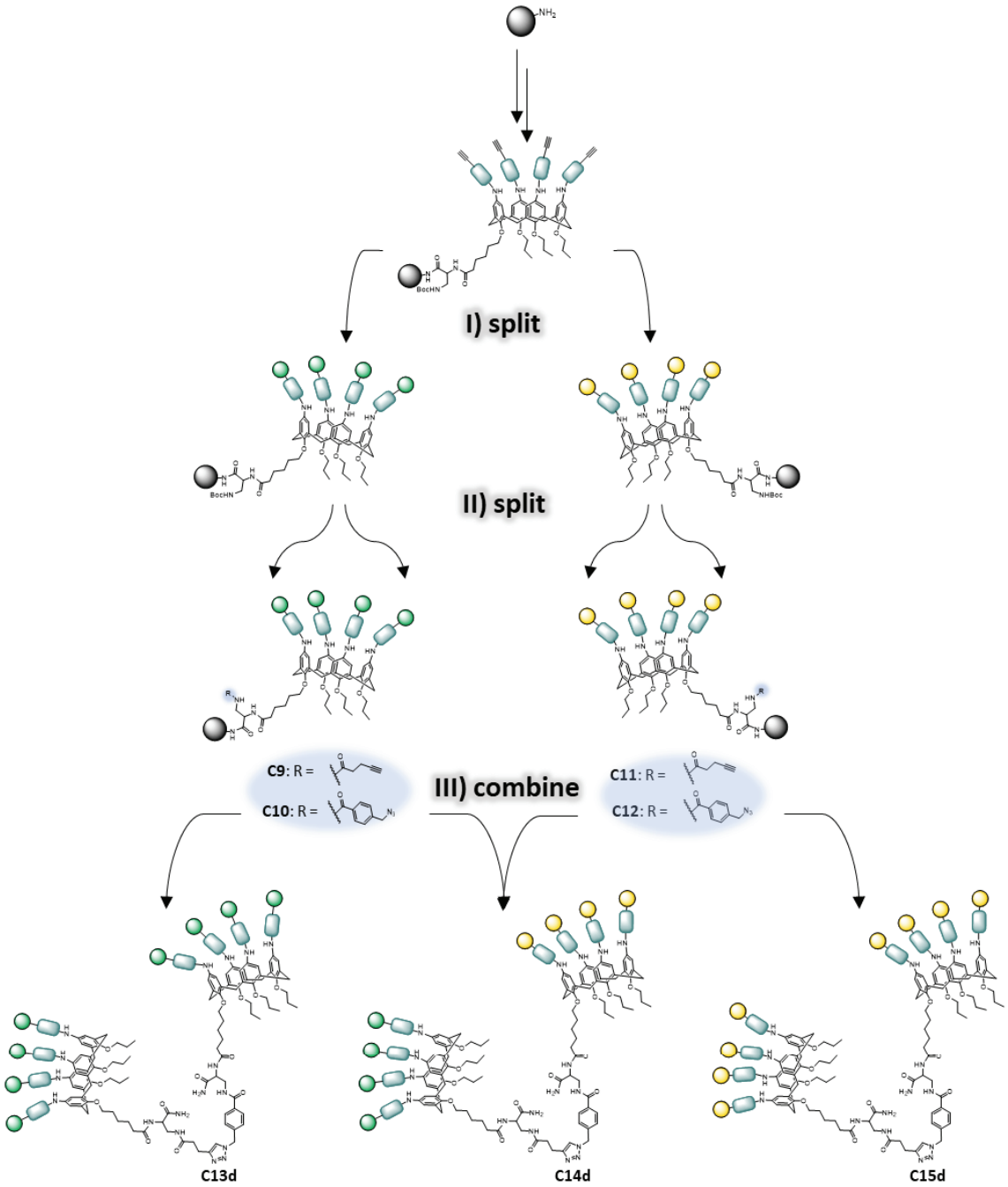

Figure 20: Schematic depiction of a split-split-combine approach towards homo- and heteromultivalent glycocalix[4]arene dimers. The structural definition of the schematically depicted building blocks and carbohydrates, as shown in Figure 12, applies.

The reaction conditions for the final CuAAC reaction (see Figure 20, III combine) were investigated in detail in collaboration with Cleo Macke as part of her bachelor's thesis conducted in the Hartmann working group. Initial studies were performed by means of the

heteromultivalent dimer **C14d**. A synthetic approach adapted from the established click protocol using copper(II) sulfate and sodium ascorbate was tested for use in solution.[222] Since all the reactants are readily water-soluble, water was chosen as the reaction solvent. The corresponding monomers **C9** (14 µmol) and **C12** (14 µmol) were first dissolved in equimolar amounts in water, and the mixture was flushed with nitrogen. Subsequently, sodium ascorbate (50 mol-%, 7 µmol in 0.1 mL MQ water) followed by Cu(II) sulfate (50 mol-%, 7 µmol in 0.1 mL MQ water) were added under nitrogen atmosphere. It was found that the repeated addition of fresh Cu(II) sulfate and sodium ascorbate in three overall portions of 50 mol-% each resulted in higher conversions compared to the addition of a higher equivalent of Cu(II) sulfate and sodium ascorbate directly from the start. This might be due to oxidation processes hampering the formation of the catalytic Cu(I) species. The best results were achieved when the reaction mixture was stirred for 48 h at 35 °C under nitrogen atmosphere. Before HPLC-MS analysis could be performed, excess copper ions had to be removed from the crude product. Initial attempts to remove the excess copper salts by spin filtration or dialysis were not successful. Surprisingly, after chromatographic purification, the copper salts were not completely removed from the product. The occurrence of excess copper salt was tested by the addition of a 23 mM diethyldithiocarbamate solution, as in the presence of copper ions the solution forms a visibly brown complex. Therefore, to remove excess copper, the diethyldithiocarbamate solution prior to preparative purification was added to the crude reaction mixture to form the copper complex, which can be precipitated upon addition of acetonitrile to the mixture, followed by centrifugation. This procedure was repeated until no further brown coloration upon addition of diethyldithiocarbamate was observed.

The subsequent HPLC-MS analysis performed is shown in Figure 21 and confirmed the successful synthesis of the desired heteromultivalent dimer **C14d.** The target product was detected at a t_R of 14.07 min, which was verified by mass spectrometry. Nevertheless, some remaining starting material at a t_R of 13.67 min and 14.34 min was also observed. Following experiments showed that this could not be prevented by longer reaction times or increasing equivalents of copper(II) sulfate and sodium ascorbate.

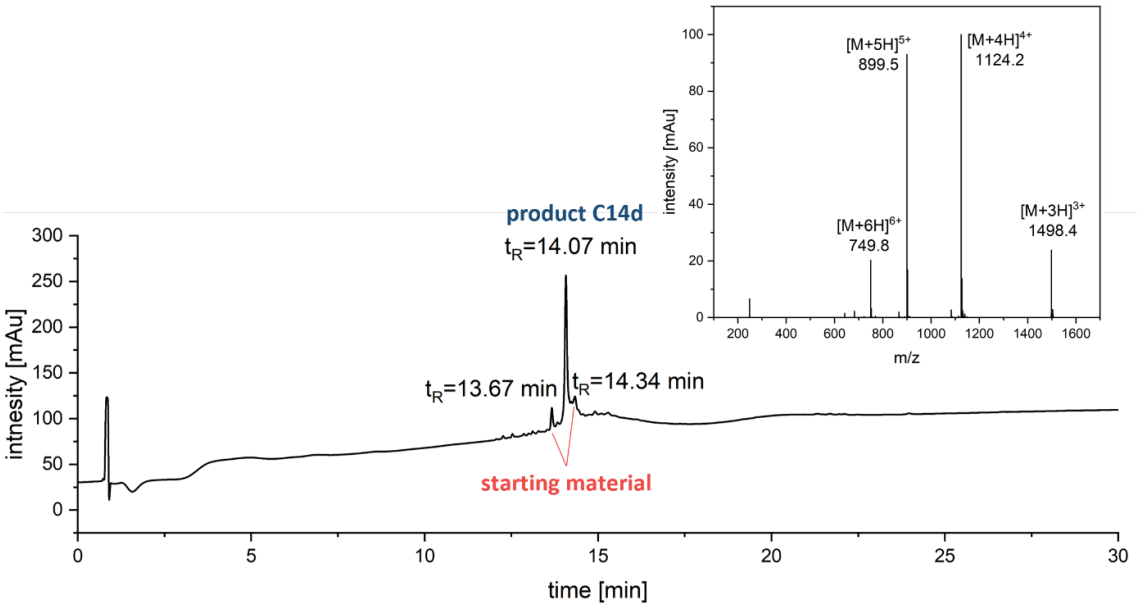

*Figure 21: HPLC chromatogram of compound **C14d** (95/5 to 5/95 vol.-% H_2O/MeCN + 0,1 % formic acid in 30 min) and coupled mass spectra at t_R= 14.07 min.*

As a last step, the copper-free product was purified by preparative HPLC using a linear gradient from 30 to 50 vol.-% acetonitrile (MeCN) to water with 0.1 % formic acid in 15 min. After lyophilization, **C14d** was obtained in a rel. purity of ≥ 95 % as determined by RP-HPLC and in a yield of 20 %. The homomultivalent dimers **C13d** and **C15d** were prepared under analogous reaction pathways. Yield and purity of the homomultivalent dimers were similar compared to **C14d** (see experimental part).

The final compounds were analyzed using ^{1}H-NMR spectroscopy, HPLC-MS, and MALDI-TOF-MS. As an example, the analytical data of **C14d** are discussed in the following. An excerpt of the ^{1}H-NMR analysis of **C14d** in comparison with the educts **C9** and **C12** is shown in Figure 22. The characteristic signals indicating the successful copper-catalyzed click reaction resulting in the dimer **C14d** are highlighted. The signals assigned to the pentynoic acid residues 6, 7, and 8 were found at around 2.45 ppm in the spectra of **C9**. In contrast, for **C14d**, the signals of the ethyl linker protons 6 and 7 were found shifted to the lower field at around 3.0 and 2.5 ppm. The alkyne proton was no longer evident in the product spectra. However, a signal that was assigned to the newly formed triazole proton 8 was found at 7.6 ppm, confirming the successful copper click reaction. Moreover, protons 5 of the 4-azido benzoic acid residues found at around 4.4 ppm in the **C12** spectra were observed significantly shifted to the lower field at 5.4 ppm. Additionally, all expected signals assigned to the aromatic protons 1-4 were identified in the product spectra, further validating the synthesis of the desired dimer product **C14d**. In the MALDI-TOF-MS spectra, a mass to charge ratio (m/z) of 4517.1 was found, which was ascribed to the sodium salt of the

product (see Figure 68, appendix). Additionally, the HPLC chromatogram supported the sufficient purification of the product, as the initial peaks of starting material were not observed any longer. The corresponding ESI-MS showed m/z ratios of 899.5, 1124.2, and 1498.2 at a retention time of 13.75 min (see Figure 67, appendix). These were assigned to $[M+H]^{5+}$, $[M+H]^{4+}$ and $[M+H]^{3+}$ respectively. Also, the analytical data obtained for **C13d** and **C15d** were in agreement and validated the successful synthesis of the homomultivalent dimers (see experimental part and appendix).

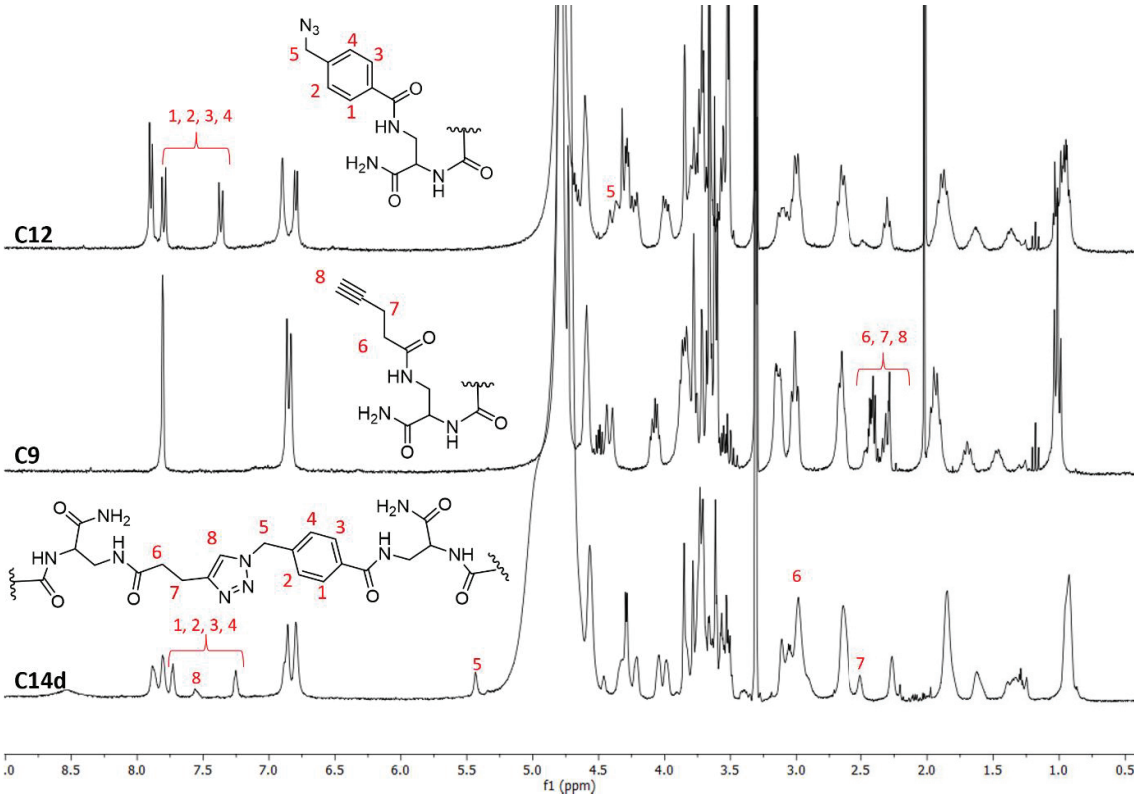

*Figure 22: ^{1}H-NMR (300 and 600 MHz,MeOH-d4 and D_2O) of compound **C9, C12** and **C14d**.*

3.3.2 Binding Studies with the Model Lectins Con A and PNA

After the successful synthesis, it was of particular interest to examine the two-sided heteromultivalent derivative **C14d** for simultaneously binding to two lectins with different binding specificities. For this purpose, the well-known legume lectins Con A and Peanut agglutinin (PNA) were chosen. In a previous binding study described in chapter 3.2, it was already demonstrated that the mannose-functionalized calix[4]arene derivative **C1b** binds to Con A, whereas the analogous galactose-functionalized derivative **C2b** does not show binding at this concentration range. These observations are in good agreement with numerous studies investigating Con A as a model lectin.[10, 13, 234] In contrast, PNA is, in general, known to bind terminal galactosyl residues but has no specificity towards mannose.[234, 261] Crystallographic studies revealed PNA to consist of four identical

monomers with one carbohydrate binding site each.[262] Several studies have assessed the binding affinity and clustering efficiency of galactose-functionalized multivalent ligands with PNA, probing the clustering effect.[263, 264] However, so far, no approach is known that investigates the binding behavior of a bispecific compound to both lectins simultaneously.

Turbidity Assay

To do so, a concentration-dependent turbidity assay as described earlier by Gerke et al. was performed.[224] Upon multimeric interaction of a specific lectin with the synthesized glyo-ligands in solution, clustering can occur, which results in the turbidity of the solution and precipitation of the ligand-lectin complex. By measuring the turbidity of the lectin-ligand solution, the efficiency of the complex formation can be determined. For this purpose, 1 ml of either a Con A or PNA, as well as a solution containing both PNA and Con A in LB buffer, was prepared and transferred to a quartz cuvette. For all solutions, the lectin working concentration was kept constant at 5 µM for Con A and 10 µM for PNA, as initial test suggested these concentrations to be most suitable (data of initial test not shown). Then 2 µL of a ligand stock solution in LB buffer (250 - 500 µM) was titrated to the lectin solution and mixed vigorously. After 20 min, the transmittance at 420 nm was measured. Subsequently, the procedure was repeated as many times as no further decrease in transmittance or a maximum ligand concentration of 10 µM was reached. The curves obtained for the turbidity measurements are shown in Figure 23.

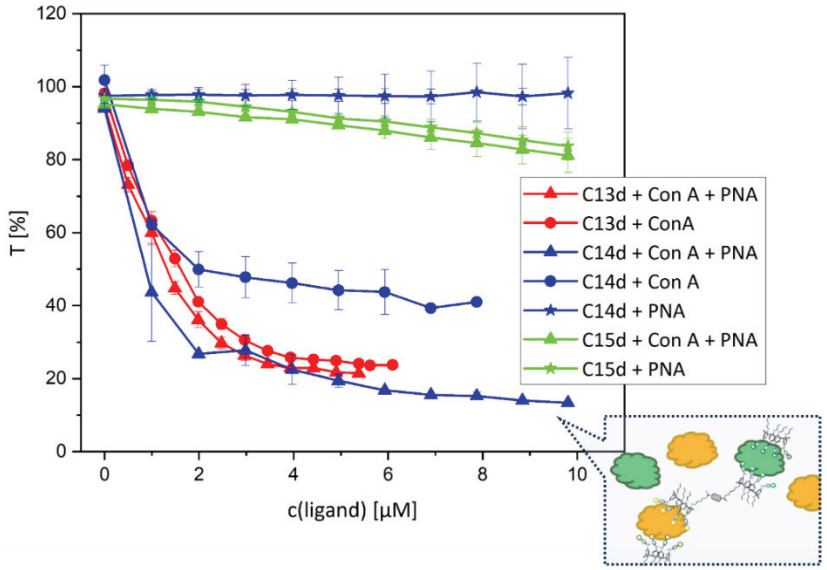

Figure 23: Transmittance values obtained from concentration-dependent turbidity assay titrating C13d/C14d/C15d into Con A (circle), PNA (star), or a mixed (triangle) solution. For negative controls, see appendix Figure 94.

For the heteromultivalent structure **C14d** (blue curves, Figure 23), a significant difference in clustering efficiency was observed when the ligand was added to a mixture of Con A and PNA lectin in comparison to when added to either Con A or PNA in separate solutions. When comparing the obtained transmittance curves, it became evident not only in the reached lower transmittance endpoint, but also in the more rapid transmittance decline that a simultaneous binding of both lectins to **C14d**, as expected for the bispecific ligand, occurred. For the addition of **C14d** to Con A only, an increase in turbidity was also observed, but to a reduced extent, indicating that fewer clusters were formed, since only one side of the bispecific ligand contributes to the lectin binding. In contrast, when the ligand was added to the PNA solution up to 10 µM, no turbidity was observed. This might be accounted for by the lower binding affinity of PNA to β-galactopyranosides compared to the affinity of Con A to α-mannopyranosides. For instance, the binding constant *K* obtained for the binding of monovalent α-methyl-mannopyranoside to Con A determined by Isothermal Titration Calorimetry (ITC) were around 1.5 to 2 times higher compared to binding constants obtained for the binding of a monovalent β-galactopyranoside with a methacrylate aglycon to PNA.[10, 264-267] When **C14b** was titrated in higher concentrations some clustering of PNA was detected from approximately 45 µM (for data see appendix Figure 93). This result is in agreement with a previous turbidity study performed in the Gouin group that found an increase in absorbance at 490 nm at a concentration of 125 µM for different multivalent galactosyl ligands.[263]

For the homomultivalent mannose structure **C13d** (red curves, Figure 23), the results obtained also indicated a two-sided binding of Con A to the ligand, as demonstrated by the significant decrease in transmittance after titration into a solution containing Con A (Con A or Con A+PNA). Compared to the heteromultivalent structure, **C14d** transmittance endpoints in a similar range were reached. Importantly, it was shown by this experiment that the additional presence of non-specific PNA lectin appeared to have no significant effect on the clustering efficiency. Additionally, it should be mentioned that for the homomultivalent compounds, different binding modes are possible. In contrast to the heteromultivalent compound, the homomultivalent compound might also undergo a chelation binding mode in addition to the clustering. However, further investigation of the underlying binding modes is not in the scope of the studies conducted. For the homomultivalent galactosyl compounds **C15d** (green curve, Figure 23) in PNA, a slight turbidity was observed, supporting the assumption that, also for PNA, the clustering efficiency increases for the dimeric compound in contrast to **C14d**.

The negative controls (**C15d** in Con A solution and **C13d** in PNA solution, see appendix Figure 94) didn't show any turbidity. Taking the results together, the turbidity experiment clearly confirmed that the simultaneous binding of Con A and PNA to the two-sided bispecific ligand, as well as a two-sided binding for the homomultivalent ligands.

Precipitation Assay

To further confirm and quantify these results, a precipitation assay adapted from the literature was performed next.[224] According to the common protocol, the lectin-ligand solution was stored overnight at room temperature, and the precipitate formed was removed from the supernatant after centrifugation. Next, after washing with buffer, the pellet was re-dissolved with an appropriate ligand such as methyl α-D-mannopyranoside (for Con A clusters) allowing to determine the protein concentration by UV/Vis absorbance at 280 nm.[24, 224] In this study the stock solutions of the homomultivalent calix[4]arene dimers **C13b** and **C15b** as well as the heteromultivalent dimer **C14b** (500 µM solution in PBS + $CaCl_2$) were prepared and 10 µL were added to either a PNA (10 µM in PBS + $CaCl_2$), Con A (10 µM in PBS + $CaCl_2$) or a solution containing both ligands to give a total volume of 1 ml. To dissolve the obtained Con A clusters, a 0.05 M methyl α-D-mannopyranoside was used. Although mannopyranoside only binds specifically to the binding domains of Con A, the samples containing Con A-PNA clusters were also completely dissolved after treatment with the methyl α-D-mannopyranoside solution. Therefore, the protein solution and the determined protein concentration were a mixture of both proteins. Further, it must be considered that the employed calix[4] arene-based ligands do also absorb at a wavelength of 280 nm due to their aromatic structure. Hence, another method than UV/Vis spectroscopy needed to be applied to determine the protein concentration.

For this purpose, the bicinchoninic acid assay (BCA assay) was used. The detection is based on the reduction of Cu(II) to Cu(I) that binds to the protein and subsequently forms a purple-colored complex with bicinchoninic acid, allowing a colorimetric readout between 540 and 570 nm that is proportional to the protein concentration.[268] The advantage of this method compared to other colorimetric methods, such as Lowry or Bradford protein assay, is that it is less sensitive to interference from other detergents and has a comparable low dependency on the nature of the investigated protein, which is crucial to gain accurate results for protein mixtures. The protein concentration can be determined from the measured OD and further allows the calculation of the protein per ligand ratio.

The data obtained are shown in Table 1. For **C14d** in Con A solution, a protein to ligand ratio of 1.38 ± 0.08 was obtained, indicating that, on average, a mannose-functionalized calix[4]arene binds more than one Con A molecule. This value is in agreement with previous

findings generated in the working group of Prof. Hartmann for glycomacromolecules with similar mannose valency.[224] By adding **C14d** to a Con A + PNA solution, a higher protein/ligand ratio of 1.6 ± 0.04 was obtained, confirming the results of the turbidity measurement. The findings clearly support the conclusion that **C14d** bound to both lectins, Con A and PNA, simultaneously, even though the clustering efficiency to PNA appeared to be lower compared to Con A. For the PNA-containing solution, no precipitation was observed, which is also in accordance with the results found for the turbidity measurements. For the homomultivalent mannose compound **C13b, a** higher protein/ligand ratio of 1.88 ± 0.08 was found, indicating that both calix[4] arene entities contributed to the Con A clustering. This higher protein/ligand ratio for the homomultivalent dimer **C13b** compared to the heteromultivalent compound **C14b** can again be explained by the lower clustering efficiency of PNA compared to Con A. As expected, no significant difference was observed whether the non-specific lectin PNA was present in the mixture or not. For the homomultivalent galactosyl structure **C15d,** no precipitate was formed. In the previous turbidity measurements, a slightly decreased turbidity was detected at this ligand concentration. However, it is likely that the clustering was not sufficient for the formation of a precipitation.

Table 1: Protein concentrations determined by BCA using Con A calibration curve and the resulting protein/ligand ratio. All measurements were performed in triplicate and were blank corrected. For the calibration curve, see appendix Figure 95. Negative controls are highlighted in yellow. N.d. = not determinable.

Ligand (5 µM):	c(protein) [µM]:			c(protein)/c(ligand)		
	Con A (10 µM) **+ PNA** (10 µM)	**Con A** (10 µM)	**PNA** (10 µM)	**Con A** (10 µM) **+ PNA** (10 µM)	**Con A** (10 µM)	**PNA** (10 µM)
C14d	8.0 ± 0.19	6.91 ± 0.39	n.d.	1.6 ± 0.04	1.38 ± 0.08	n.d.
C13d	9.42 ± 0.41	9.45 ± 0.28	n.d.	1.88 ± 0.08	1.89 ± 0.06	n.d.
C15d	n.d.	n.d.	n.d.	n.d	n.d	n.d.

Precipitation Assay II

In a further precipitation assay, it was aimed to assess the ratio of bound Con A to PNA quantitatively. As mentioned earlier, it proved to be difficult to separate the precipitated proteins by the addition of a methyl mannopyranoside solution. Therefore, another attempt using methyl galactopyranoside (0.05 M) was tested to dissolve only the PNA clusters to allow for a quantitative evaluation. However, this again proved to be challenging, and the obtained data did not appear to be reliable (data not shown). Therefore, the precipitation assay design was further enhanced to overcome this limitation. In Figure 24, a schematic procedure of the precipitation assay II is depicted. As the assessment of the protein pellet was not useful, it was reasoned that the amount of ligand-bound Con A and PNA could be determined via the amount of unbound lectin in the supernatant instead. As a first step, the assay was performed as described above, with the precipitation allowed to form overnight at room temperature (step 1, Figure 24). To ensure the protein concentration is high enough to exceed the BCA method detection limit, the concentration of both proteins and ligand was increased to 20 µM each and 10 µM, respectively. Next, the supernatant was removed and submitted to a second precipitation experiment (steps 2 and 4, Figure 24). By the second precipitation, the idea was to precipitate and thus to separate Con A from the remaining solution. Therefore, the two-sided mannose functionalized ligand **C13d** (5µL from 1mM stock in PBS + Ca^{2+}) was added to the supernatant to give a working concentration of around 20 µM. Considering a ratio of 1.88 proteins per ligand for **C13d** calculated in the first precipitation experiment (see Table 1), it can be assumed that all the remaining Con A will be clustered and precipitate overnight. The centrifugation and washing steps were performed according to the protocol described previously (step 5, Figure 24). The Con A pellet was again dissolved in 0.05 M methyl mannopyranoside solution (step 6, Figure 34). This procedure gives access to determining both protein concentrations via BCA method separately and finally allows for calculating the amount of bound Con A and PNA in the initially formed precipitate. Table 2 summarizes the ligand concentrations determined for the supernatant (highlighted with **/***) and the mixed lectin pellet (highlighted with *), as well as the calculated concentrations of Con A and PNA bound by the bispecific ligand **C14d**.

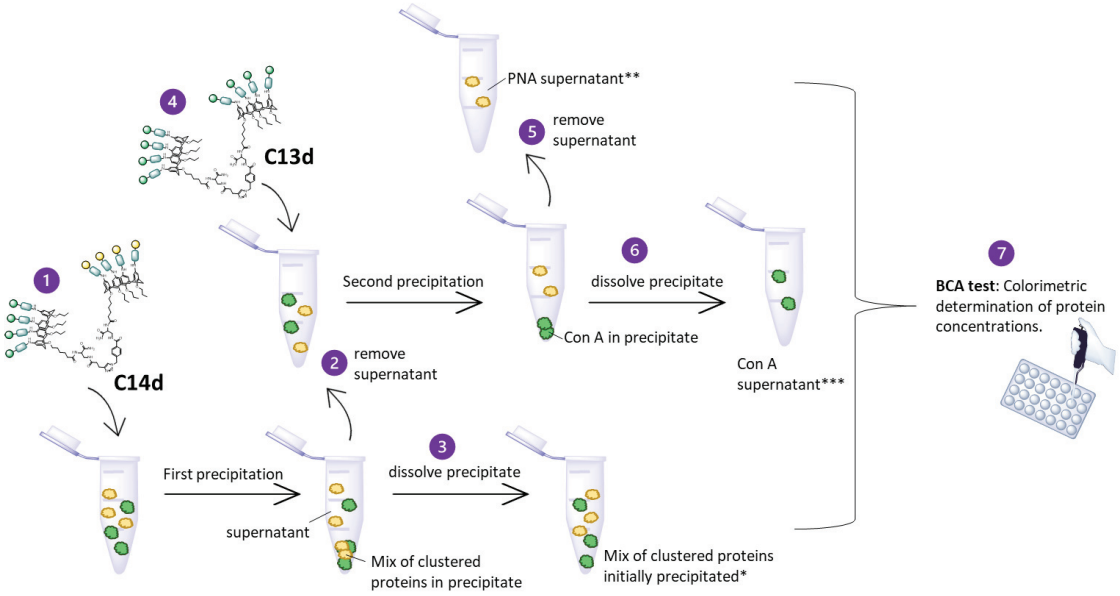

*Figure 24: Schematic depiction of the precipitation assay II procedure for the heteromultivalent dimer **C14b**. **C13b** acts as an affinity tag.*

In the supernatant, a concentration of 6.90 ± 0.2 µM for Con A (***) and 17.50 ± 0.16 µM (**) for PNA was detected. By subtracting these values from the starting concentrations (20 µM each), the concentrations of the initial clustered lectins were determined. As expected, the concentration of clustered Con A (13.10 ± 0.37 µM) was higher than the clustered PNA concentration (2.50 ± 0.02 µM), which is in agreement with the results of the previous precipitation experiment. Further, the concentration of protein was set in relation to the concentration of ligand, giving an average number of 1.31 ± 0.04 Con A proteins and an average number of 0.25 ± 2.2 × 10^{-3} PNA proteins per ligand **C14d**. In summary, this led to a total number of 1.56 ± 0.06 (1.31 ± 0.04 Con A + 0.25 ± 2.2 × 10^{-3} PNA) proteins bound per ligand. In parallel, the mixed protein cluster (*) was assessed via BCA test. For the assessment of the protein mixture, the Con A calibration curve was used. The BCA test for the mixed protein cluster (*) resulted in a total number of 1.43 ± 0.06 bound proteins (Con A + PNA) per ligand **C14d**. This value is slightly lower compared to the calculated value for the total number of bound protein (1.56 ± 0.06). However, considering the systematic error for the concentration determination by BCA method when having a protein mixture, the obtained values are in a similar range, demonstrating the feasibility of the assay. Additionally, when comparing the detected OD of the mixed pellet (OD_{562} = 0.55) and the cumulative OD values of the separately calculated proteins (OD_{562} = 0.54), almost identical values are obtained, supporting the reliability of the assay design (for measured OD values and calculations see Table 7 and

Table 8, experimental part).

To further validate the results, a control experiment using the homomultivalent dimer **C13d** was performed. For the mannosyl dimer a PNA concentration 19.34 ± 0.73 was detected in the supernatant, confirming that nearly no PNA was clustered as expected for this ligand. Additionally, the concentration of clustered Con A calculated from the supernatant (18.89 ± 0.2) agreed with the protein concentration actually detected for the clustered protein pellet (18.35 ± 0.73). These findings clearly validated the accuracy of the precipitation experiment. The quantitative evaluation confirmed the qualitative trends that have already been observed for the previous assays. Taking all results together, it can clearly be concluded that **C14d** is capable of binding the two lectins, Con A and PNA, simultaneously. Further, the experiments showed that the clustering efficiency of PNA is significantly lower compared to Con A for **C14d**.

Table 2: Protein concentration and protein/ligand ratio obtained for the precipitation assay II. All measurements were performed in triplicate and were blank corrected. (*): Mix of proteins in precipitation: Concentration determined via BCA method using Con A calibration curve; (**): PNA in supernatant: Concentration determined using PNA calibration curve; (***): Con A in supernatant: Concentration determined via BCA method using Con A calibration curve. For calibration curves, see appendix Figure 96 and Figure 97. The concentration of clustered Con A and PNA in precipitate (highlighted in orange color) has been calculated by subtracting the protein concentration determined in the supernatant from the total protein concentration (20 µM each).

Ligand [10 µM]		**c(protein) [µM]**			**c(protein)/c(ligand)**
		In total	**In supernatant**	**In precipitate**	
C14d	**Con A**	20	6.90 ± 0.2***	13.10 ± 0.37	1.31 ± 0.04
	PNA	20	17.50 ± 0.16**	2.50 ± 0.02	$0.25 \pm 2.2 \times 10^{-3}$
	Con A + PNA	40	-	14.33 ± 0.64*	1.43 ± 0.06*
C13d	**Con A**	20	1.11 ± 0.01	18.89 ± 0.2	1.89 ± 0.02
	PNA	20	19.34 ± 0.73	0.66 ± 0.02	$0.07 \pm 2.5 \times 10^{-3}$
	Con A + PNA	40	-	18.35 ± 0.73*	1.84 ± 0.07

Initial studies with other lectins

Due to the promising results obtained for the experiment with Con A/PNA, it was envisaged to further expand the concept and to test the bi-specific ligand **C14d** also for other mannose- and galactose-specific lectins. It was intended that the applied lectins ideally have similar clustering efficiency. Therefore, some initial turbidity tests were performed using Lens Culinaris Agglutinin (LCA) or Pisum Sativum Agglutinin (PSA). LCA and PSA are both α-mannose-specific lectins from the legume family with one carbohydrate-recognition domain per monomer. In contrast to Con A, LCA, and PSA consist of dimers at pH 7.4. Additionally, titration calorimetry measurements revealed that the binding affinities of the lectins differ significantly (Con A >> PSA > LCA).[267] This is in good agreement with the observations made. For LCA, even at high concentrations, no visible turbidity was observed. For PSA, turbidity was detected from a ligand concentration of 250 µM **C14d** in a 20 µM PSA solution. The required ligand concentration was significantly higher compared to the ligand concentrations used in previous turbidity and precipitation experiments with Con A. Therefore, it was assumed that the PSA might be a sufficient alternative to Con A with a clustering efficiency similar to PNA. Initial attempts based on visual inspection showed a significant increase in turbidity when the heteromultivalent ligand **C14d** was added to a solution containing PSA and PNA, then when the ligand was given separately to a PSA or PNA solution, implying a simultaneous binding to both lectins. However, these initial tests also illustrated that a high amount of ligand is needed for sufficient PSA/PNA clustering to obtain reasonable results from turbidity or precipitation assays. A more detailed examination was therefore refrained from. Nevertheless, these initial tests indicated that the simultaneous bi-specific binding of **C14d** is also applicable to other lectins. Encouraged by these results, future investigations with varying carbohydrate-recognizing proteins appear promising.

3.4 Calix[5]arene Building Block for the Synthesis of Pentameric Glycomimetics via SPPoS.

This study aimed to extend the methodology described to calix[5]arenes as higher homologues of the calix[4]arenes, with five instead of four phenolic moieties. Calix[5]arenes are not as widely applied as other higher homologs because the synthesis is less readily available compared to the other derivatives.[117] However, in this thesis, the interest lay particularly in the pentameric symmetry provided by the calix[5]arene building block. First, a sufficient synthetic route to prepare an analog calix[5]arene building block for SPPoS was investigated. In the second part of this study, a calix[5]arene derivative was equipped with sialic acid moieties using the established SPPoS protocol. Sialic acid includes a family of acidic nine-carbon carbohydrates that are abundantly expressed at the cell surface and can typically be found as terminal carbohydrate epitopes of various glycoconjugates. They play an important role in many biological processes, e.g., they act as an initial contact point for the adhesion of many virus families, which is the first step of an infectious entry of the viral genome.[17] The counterparts on the virus side are sialic acid recognizing lectins, which are often very specific regarding the structure and linkage of the sialic acid. Haemagglutinin lectin from influenza A virus (HA), capsid protein 1 (VP1) of human polyomavirus BK (BKPyV), or the fiber knob lectin of *Adenoviridae* can be given as examples.[17] As is typically the case for carbohydrate-protein interactions, these also suffer from rather low monovalent binding affinities, which is why multiple receptors of identical binding sites are engaged. Many viral lectins are therefore composed of multiple homomers, and the binding sites are assembled symmetrically.[240]

For the development of antiviral therapeutics, a promising approach is the inhibition of the initial binding of the viral binding protein with the host cell surface. The idea is to engage multiple binding sites with a tailored multivalent ligand via a chelating mechanism. In this way, an increase in binding avidity on a large magnitude is aimed at. To do so, the symmetrical axes of the target protein, as well as the linker length and flexibility, are important features to be considered for rational ligand design. The first group to develop a so-called starfish inhibitor was Kitov et al. for the pentameric Sigha-like toxins.[51] The ligand based on glucose as a scaffold showed to have an inhibitory activity in the subnanomolar range and is the most potent inhibitor reported at that time for the Shiga-like toxins I and II. Furthermore, this concept was applied to viral targets. For instance, Johansson et al. showed that pentameric sialic acid-functionalized ligands, also based on a glucose core, inhibit the infection of HCE cells by coxsackievirus and human adenovirus.[269] In other studies, ligands with matching symmetry to the targeted binding sites based on aromatic scaffolds (such as corannulene) or tertiary amines have been successfully applied to

several viruses.[270-273] Further, sialylated calix[4]arenes have been shown to act as inhibitors for influenza virus A and BK virus, although showing only moderate to no glycocluster effect.[164] Also within the Hartmann group, the binding of multivalent sialylated oligoamido(amines) to different polyomaviruses such as trichodysplasia spinulosa-associated virus (TSPyV), human JC virus (JCPyV), and BKPyV has already been investigated.[260, 274]

In this work, the focus lay on the polyomavirus family (*Polyomaviridae)*, which is less well studied compared to other virus families. In general, polyomaviruses are non-enveloped viruses, which are composed of single capsid proteins (VP1) that form exclusively pentameric multimers (capsomers). The multimers themselves assemble in a stable capsid enclosing the viral genome.[253] It was therefore reasoned that the employment of a pentameric calix[5]arene scaffold for the multivalent presentation of sialic acid residues might be a promising approach for the development of potent polyomavirus inhibitors by chelating several of the binding sites. In the next chapter, first the synthesis of an appropriate calix[5] arene building block **CBB2** is described, and subsequently its application toward the synthesis of sequence-controlled sialylated calix[5]arene ligands on solid support with varying linker length and valency is demonstrated.

3.4.1 Synthesis of the Building Block CBB2.

For the synthesis of a calix[5]arene building block **CBB2,** allowing the application in SPPoS by using the methodology described in the previous chapters, a synthetic pathway in an analogous fashion to the synthesis of the **CBB1** was pursued. As a starting point, the commercially available 4-*tert*-butylcalix[5]arene was chosen. As a first step, four of the five possible phenolic hydroxyl groups were to be alkylated. For calix[4]arenes, the lower rim alkylation has already been intensively studied, and some powerful synthetic procedures to selectively obtain mono-, di-, and tri-alkylated derivatives have been reported. Iwamoto et al. demonstrated that the tri-*n*-propoxy calix[4]arene derivative can selectively be obtained by treatment of *tert*-butyl-calix[4]arene in the cone conformation with an excess of 30 eq. 1-iodopropane upon treatment with barium hydroxide as a base.[275] Furter, for the use of other bases such as sodium hydroxide, cesium carbonate, or potassium carbonate, interesting correlations in terms of the number of substituents and conformation have been shown.[275, 276] However, the procedure was not found to be transferable for the higher homologs. Stewart et al. found in an elaborate investigation on the hydroxyl functionalization of calix[5]arene that product mixtures of partially etherized *tert*-butyl calix[5]arene were obtained for all tested reaction conditions. Best results were obtained

when *tert*-butyl calix[5]arene was refluxed for several hours in acetonitrile with potassium carbonate as a base and adapted equivalents of the alkylation agent, followed by subsequent chromatographic separation.[117]

Therefore, in a first attempt to synthesize the tetra-propoxyl-hydroxyl-calix[5]arene, a similar procedure was tested using 4 eq. of 1-iodopropane as an alkylation agent and potassium carbonate as a base. The reaction mixture was refluxed for several hours in dried acetonitrile. As a reaction control, TLC was applied and indicated the formation of a product mixture. Additionally, MALDI-TOF-MS confirmed the formation of a product mixture of di-, tri-, tetra-, and penta-substituted *n*-propoxyl-calix[5]arene derivatives (see Figure 75, appendix). Longer reaction times or the addition of more equivalents of 1-iodopropane did not give any improvements but yielded a fully alkylated calix[5]arene derivative (see Figure 76, appendix). As the separation via chromatographic methods appeared to be challenging and only small conversions were to be expected, an alternative synthetic pathway using a protecting group strategy, as depicted in Figure 25, was investigated.

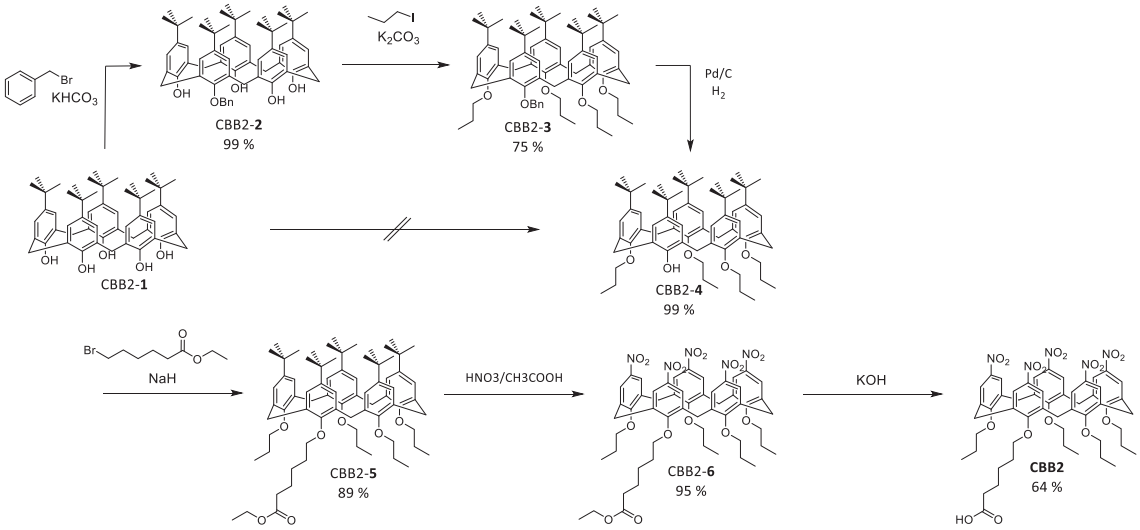

*Figure 25: Synthetic pathway to calix[5]arene building block **CBB2**.*

The use of a benzyl protecting group had already been demonstrated to be efficient for the selective protection of a calix[5]arene derivative. Based on a procedure from the literature, compound CBB2-**2** was synthesized with a yield of 99 %.[117] MALDI-TOF-MS and ^{1}H-NMR analysis confirmed the successful synthesis of compound CBB2-**2** (see Figure 77 and Figure 78, appendix). In the next step, the remaining hydroxyl groups at the lower rim were fully alkylated. To do so, compound CBB2-**2** was refluxed with potassium carbonate, and an excess of 1-iodopropane (35 eq.) was added to the reaction mixture and continued to stir under reflux. The crude product was then recrystallized in a chloroform/methanol mixture

to give the desired product CBB2-**3** in a yield of 80 %. MALDI-TOF-MS confirmed the successful synthesis (see Figure 79, appendix). Interestingly, after full alkylation, the broadening of the signals in ^{1}H-NMR spectra was observed, evidencing the increase of conformational mobility of the macrocycle on the ^{1}H-NMR scale, since hydrogen bonds at the lower rim cannot be formed any longer. This finding is in good agreement with the modeling and NMR studies conducted in the group of Gutsche.[117] In general, the confirmational mobility of calix[n]arenes is an interplay of the ability to form hydrogen bonds and sterical hindrance. For both *tert*-butyl-calix[4]- and -[5]arene, the interconversion of the upper rim through the annulus is hindered. But in contrast to calix[4]arene, the ability of the lower rim to rotate through the annulus increases significantly when the phenolic hydroxyl groups are propylated, as the sterical hindrance is lower with the larger macrocycle. Only very bulky groups, such as benzyl, are able to prevent the mobility of the calix[5]arene macrocycle.[117]

Subsequently, the protecting group was removed by catalyzed hydration to give the desired tetra-*n*-propoxyl-calix[5]arene CBB2-**4**, as confirmed by MALDI-TOF-MS (see Figure 80, appendix), in a yield of 99 %. Also, in ^{1}H-NMR spectra, the disappearance of the benzyl group signals supported this finding. Having compound CBB2-**4** in hand, the attachment of the 6-bromo hexanoate linker was performed analogously to the known protocol for **CBB1,** and compound CBB2-**5** was obtained in a yield of 89 % and characterized by MALDI-TOF-MS (see Figure 81, appendix).[232] Next, the *ipso*-nitration was performed by treatment with fuming nitric acid, giving compound CBB2-**6** in a yield of 95 % (see Figure 82, appendix).[277] In a last step, the desired building block **CBB2** was obtained upon base-catalyzed hydrolysis and acidic work-up according to literature in a yield of 64 %.[232] In total, **CBB2** was successfully synthesized and obtained in an overall yield of around 40 %.

The final product was characterized by using ^{1}H-NMR, ^{13}C-NMR, MALDI-TOF-MS, and HR-ESI. NMR studies were performed at different temperatures in DMSO, as at ambient temperature, the signals are still broad due to conformational mobility. Only at temperatures of 75 °C and higher, coalescence was observed. (In contrast, the calix[4]arene building block CBB1 is fixed in one conformation). At 90 °C, all characteristic signals were found in the ^{1}H-NMR spectra (see Figure 26). At 11.6 pm, a singlet assigned to the carboxylic acid proton was observed. The multiplet found at 8.2 to 8.0 ppm was attributed to the aromatic protons of the phenols. Furthermore, in a range from 4.2 to 3.3 ppm, signals with a total proton intensity of 20 protons were ascribed to the methyl bridges and the protons 6 of the alkyl residues. The triplet, found at 2.2 ppm, was assigned to protons 2. From 1.65 to

1.50 ppm, further protons of the hexyl linker 3 and 4 were identified. Signals with an intensity of 10 occurred from 1.4 to 1.1 ppm and were assigned to protons 5. Finally, protons 7 can be found from 0.85 to 0.4 ppm. Also, in ^{13}C-NMR (see Figure 85, appendix) conducted at 90 °C, all expected signals attributed to **CCB2** were observed. At 173.5 ppm, the carboxylic acid carbon was found. The signals at around 160, 142, 134, and 124 ppm were assigned to carbons of the phenyl units. The resonances at 74.4 and 73.2 ppm confirmed the presence of the propyl- and hexyl-residues (-O-*C*H2-). Further signals that were assigned to the hexyl-linker were found at 28.8, 24.6, and 23.9 ppm. Signals caused by propyl-groups occurred at around 21.9 and 9.0 ppm. Finally, the resonance at 33.2 ppm was accounted for by the carbons of the bridging methyl groups.

Additionally, the successful synthesis was validated by mass spectrometry. In MALDI-TOF-MS (see Figure 27), a m/z ratio of 1060.43, which is in agreement with the calculated m/z value of the sodium salt, was detected. Further, HR-ESI-MS (see Figure 27) was performed, and a m/z value of 1055.42 corresponding to the ammonia salt was found.

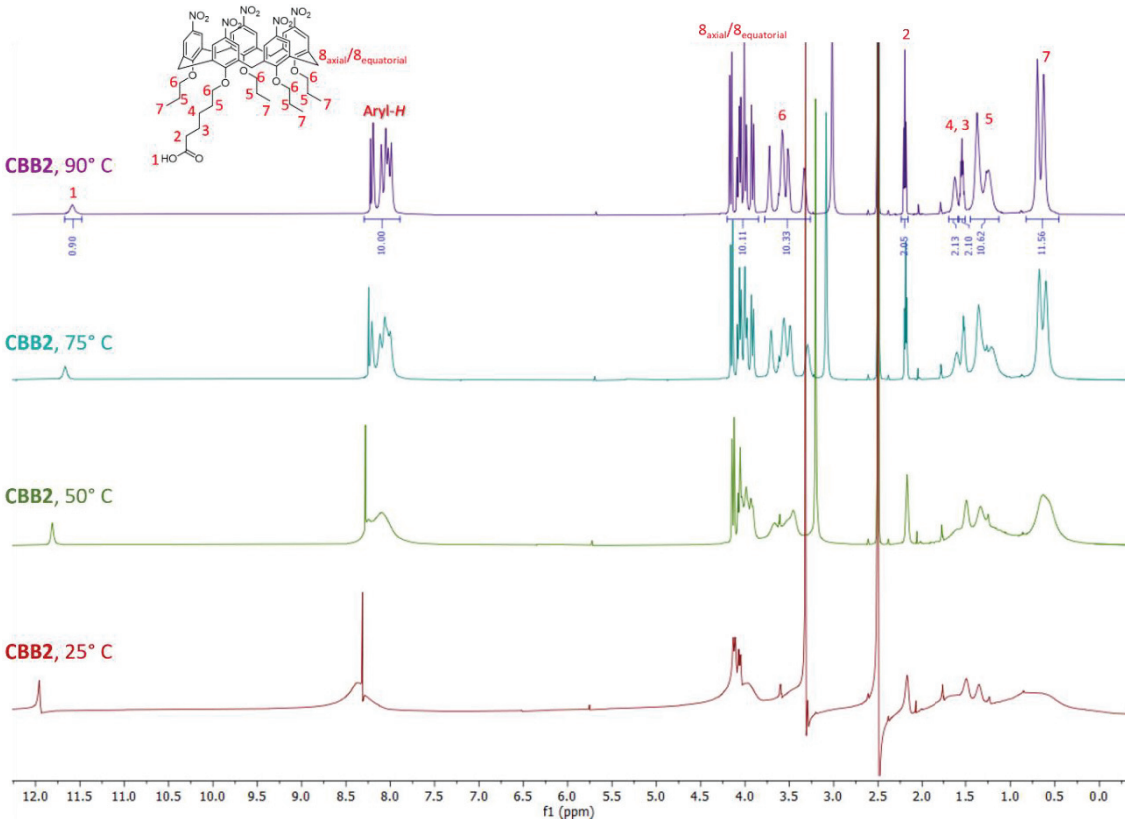

*Figure 26: ^{1}H-NMR (600 MHz, MeOH-d4 and D_2O) of **CBB2** at 25 °C (red), 50 °C (green), 75 °C (turquoise), and 90 °C (lilac).*

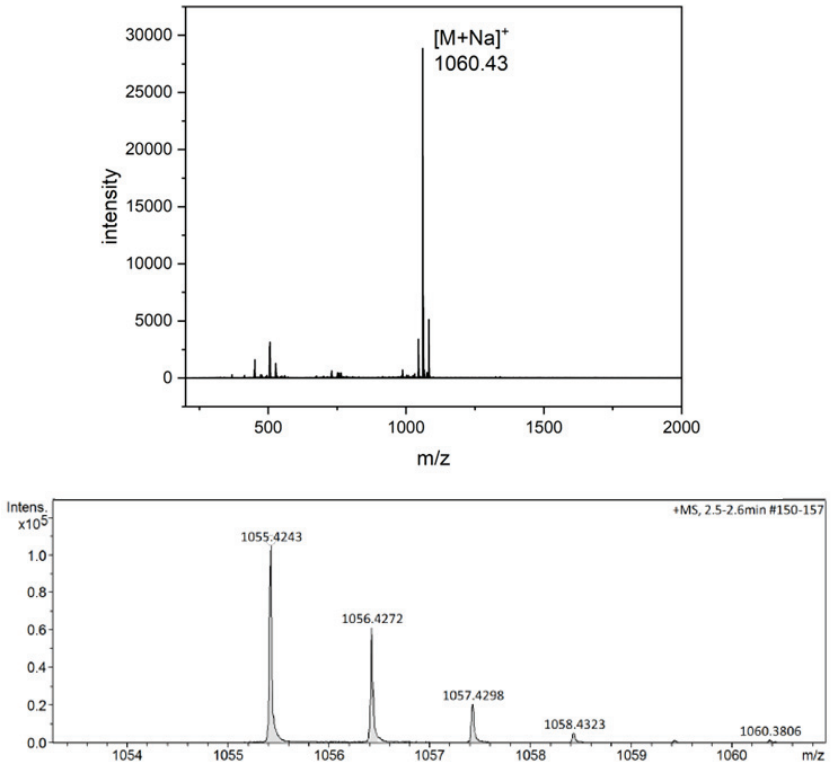

*Figure 27: MS spectra of **CBB2**; top: MALDI-TOF-MS and bottom: HR-ESI MS (positive mode).*

3.4.2. Synthesis of Sialic Acid Functionalized Calix[5]arene via SPPoS.

In the next step, the compatibility of **CBB2** with the established SPPoS approach was tested. A TentaGel S RAM® resin was used again in this study as solid support. In an initial small-scale experiment, **CBB2** was coupled to a spacer unit consisting of two EDS building blocks using PyBOP and DIPEA as coupling reagents. 3 equivalents of **CBB2** in DMF were employed, and the mixture was shaken overnight. For reaction control, HPLC-MS, MALDI-TOF-MS, and HR-ESI were used to confirm the sufficient coupling of **CBB2**. An exemplary HPLC chromatogram with corresponding ESI-MS spectra is shown in Figure 28. In the chromatogram, the main peak was found at t_R of 15.25 min with corresponding m/z ratios of 1499.5 and 749.4 that correspond to the targeted compound. After the successful implementation of **CBB2** with solid support, the synthesis was reproduced in a larger batch size. Further, analog reaction conditions (excess of tin chloride in NMP, for more details see chapter 3.1) that were used for the reduction of **CBB1** were sufficient to obtain full conversion as verified by HPLC-MS and MALDI-TOF-MS (see Figure 86, and Figure 87, appendix).

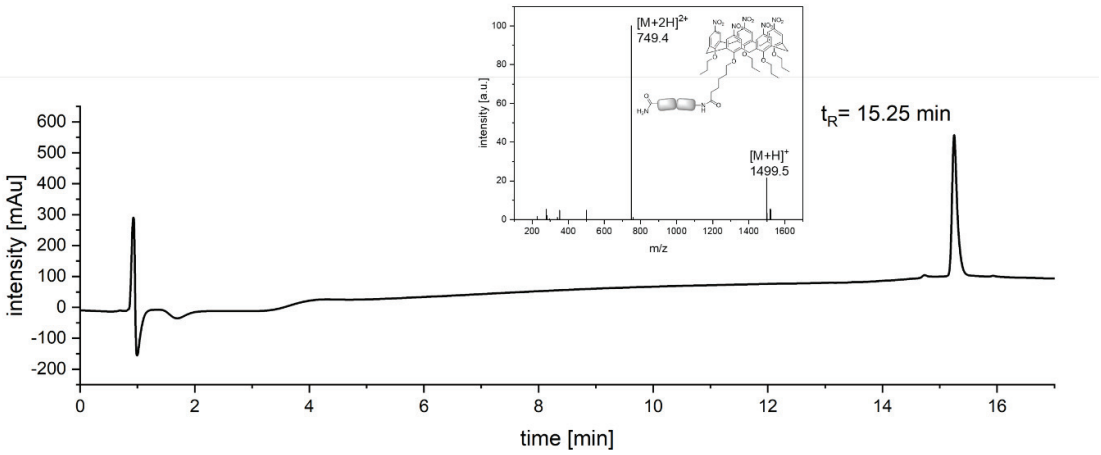

Figure 28: RP-HPLC chromatogram of an initial test intermediate compound $(EDS)_2$-CBB2 (95/5 to 5/95 vol.-% H_2O/MeCN + 0,1 % formic acid in 17 min) and coupled mass spectra at t_R= 15.25 min.

It was reported previously that not only the choice of scaffold and carbohydrate epitope, but also the nature and length of the linker are of high importance to obtain the perfectly matching ligand. It can be assumed that if the employed linker is too short, the ligand is not capable of bridging several binding sites, and some steric clashes will occur. On the other hand, if the linker is long, an entropic penalty can result.[26, 47] Therefore, in the next step, the batch was aliquoted and sequences varying in length, as schematically depicted in Figure 29, were pursued. Additionally, the carbohydrate valency can be altered in this way, allowing the synthesis of pentamers and decamers. Another interesting feature of the calix[5]arene is the mobility of the scaffold. For instance, André et al. proved the flexible galactosyl- and lactosyl-functionalized calix[6]arenes and calix[8]arenes to be the stronger inhibitors for an AB-toxin compared to the fixed calix[4]arene derivatives.[68] It can be reasoned that the possibility of an induced fit to the target protein might be beneficial to reach several binding sites. To probe this feature for the viral lectin, in addition to the flexible calix[5]arene ligands, a conformationally fixed calix[4]arene ligand **C16** was synthesized to act as a reference structure.

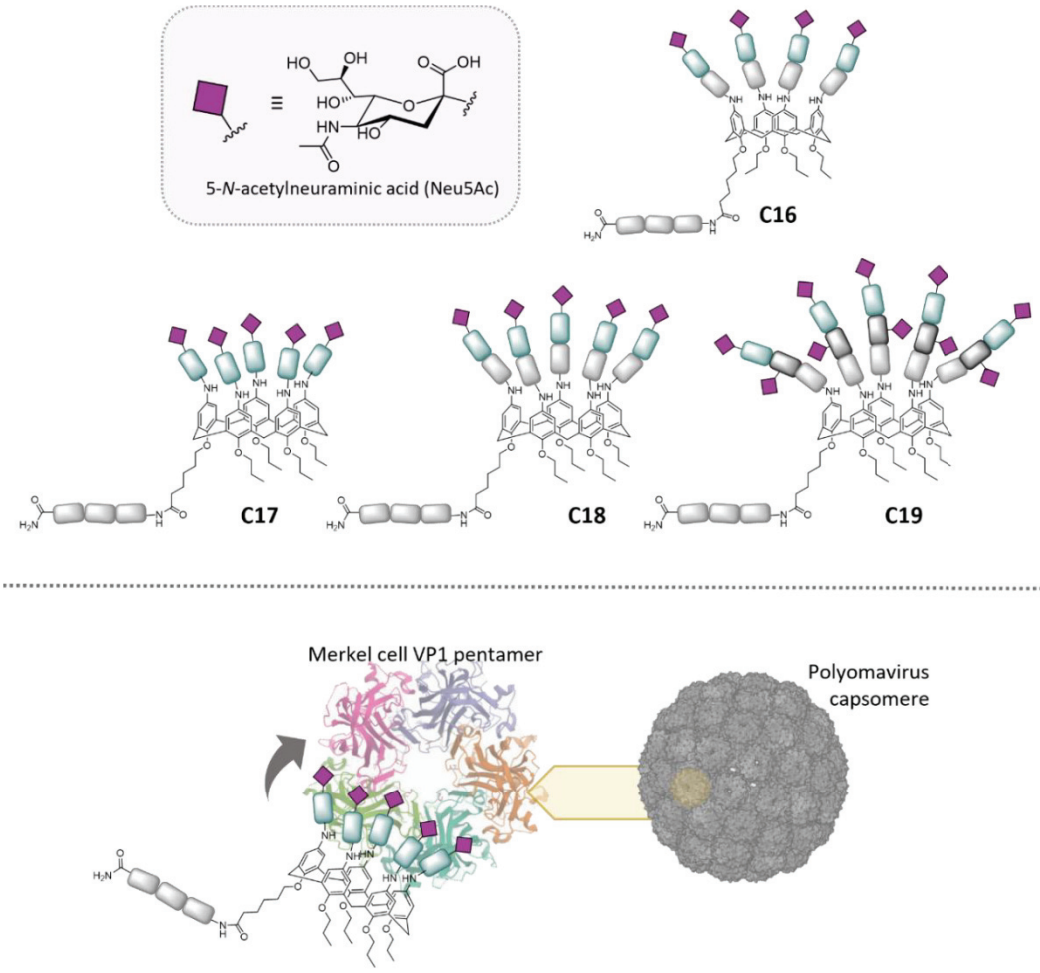

Figure 29: top: Schematic representation of sialic acid functionalized ligands ***C16-C19****. The structural definition of the schematically depicted building blocks applies as shown in Figure 12. Bottom: depiction of polyomavirus capsomer (PDB ID: 6ZLZ) and VP1 pentamer of Merkel cell virus (PDB ID: 4FMG).*

The couplings of all building blocks to the upper rim were performed according to the established protocol using 5 eq. PyBOP and 10 eq. *N*-methyl morpholine per amine together with 5eq. building block per amine in DMF for one hour. After all coupling steps, microcleavages were performed, and the reaction performance was controlled using HPLC-MS and MALDI-TOF-MS. However, it turned out that for some of the intermediate structures, the established HPLC methods using water and acetonitrile as eluent system and a C18-RP column were not suitable due to polarity. However, ESI-MS and MALDI-TOF-MS (data not shown) could be used to verify reaction success. A detailed examination of the MS spectra implies that smaller compounds like pentynoic acid, as well as building blocks like EDS, can be successfully coupled onto the calix[5]arene scaffold. The main occurring side-products resulted from incomplete couplings, as already experienced for the calix[4]arene derivative. However, no indication of poorer coupling efficiency in comparison to the calx[4]arene derivatives became evident.

After the successful assembly of the desired sequence, the sialic acid epitopes were conjugated. More in detail, 5-*N*-acetylneuraminic acid (Neu5Ac, see Figure 29), one of the most common naturally occurring sialic acid derivatives, was chosen. The VP1 proteins of polyomaviruses (such as MCPyV, BKPyV, and TSPyV) specifically recognize terminally α-bound Neu5Ac. The synthesis of the methyl 2-azido-tetra-*O*-acetyl-*N*-acetyl-α-neuraminate was performed within the Hartmann group by Lennart Hofer according to the literature.[278] The azide functionality allows for effective conjugation via CuAAC, as already demonstrated for mannosyl and galactosyl residues. However, for Neu5Ac, the conjugation is somewhat challenging as some side reactions can occur, especially after the removal of the methyl protecting group to give the carboxylic acid at the C1 position. Therefore, the synthetic procedure has been adopted to ensure that the critical deprotection of the carboxylic acid was performed as the last step. To do so, the fully protected product was cleaved from the solid support according to the established protocol. Subsequently, an Anion exchange using an AG® 1-X8 resin was performed. Afterwards, both the methyl and the acetyl groups were deprotected by treatment with a 0.1 M solution of lithium hydroxide monohydrate following the addition of an Amberlite® IR 120H$^+$ ion exchange resin until a pH of 4-5 was reached. Subsequently, the deprotected products were freeze-dried to remove the solvent. During the entire process, it was crucial to avoid temperatures above ambient temperature to prevent side reactions. The final products were analyzed via HPLC-MS, ESI-MS, and ^{1}H-NMR. It should be mentioned that conformational flexibility of the calix[5]arene scaffold alongside the temperature sensitivity of the sialic acid residues and additional high charge of the final compounds made the accurate characterization challenging. However, the results clearly supported the successful synthesis of all three calix[5]arene structures. Figure 30 shows the HPLC chromatogram and ESI MS spectra of the compounds **C17-C19**. The retention times of **C17** and **C18** were nearly identical at 11.1 min and 11.2 min, respectively. For **C19,** the retention time shifted to 9.5 min due to the higher hydrophilicity of the higher carbohydrate-functionalized compound. In general, the peaks were rather broad, which can be explained by the negative charge of the carboxylic acid groups present in the structure. Additionally, some by-products of similar retention times were observed for all compounds. The examination of the mass spectra showed that the main by-products were caused by the hydrolysis of one or more Neu5Ac residues, as highlighted in Figure 30. Neu5Ac residues are more sensitive towards glycosidic bond cleavage due to the carboxylic acid at the anomeric position.[279, 280] It is not yet fully clear whether the found by-products were present in the probe or were formed during the HPLC-MS analysis. Variation of the

analysis conditions, such as mobile phase (no acid), temperature, or the reduction of energy level of the ionization source, did not show clear improvements.

In ^{1}H-NMR spectra, the broadening and shifting of the calix[5]arene backbone signals again showed the conformational flexibility of the structures, as already described for **CBB2**. Here, the calix[4]arene analog was used as reference structure (see Figure 78, appendix). Comparing the spectra, the expected characteristic resonances were observed, indicating the synthesis of the target structures. Interestingly, for the shortest compound **C17,** the largest increase in signal broadening and shifting was observed. In contrast, for the larger compounds **C18** and **C19**, signals ascribed to the linker with an increased spatial distance to the flexible calix[5]arene backbone appeared sharper. However, the signals assigned to the protons of the calix[5]arene scaffold remained significantly broadened when compared to the calix[4]arene derivative **C17**. Therefore, a detailed assessment of the proton intensities was not feasible for these flexible structures. Additionally, measurements above the coalescence temperatures, as successfully performed for **CBB2,** were not applicable due to the sensitivity of the sialic acid residues. Nevertheless, taking all analytical data into consideration, compounds **C18-C19** were successfully synthesized.

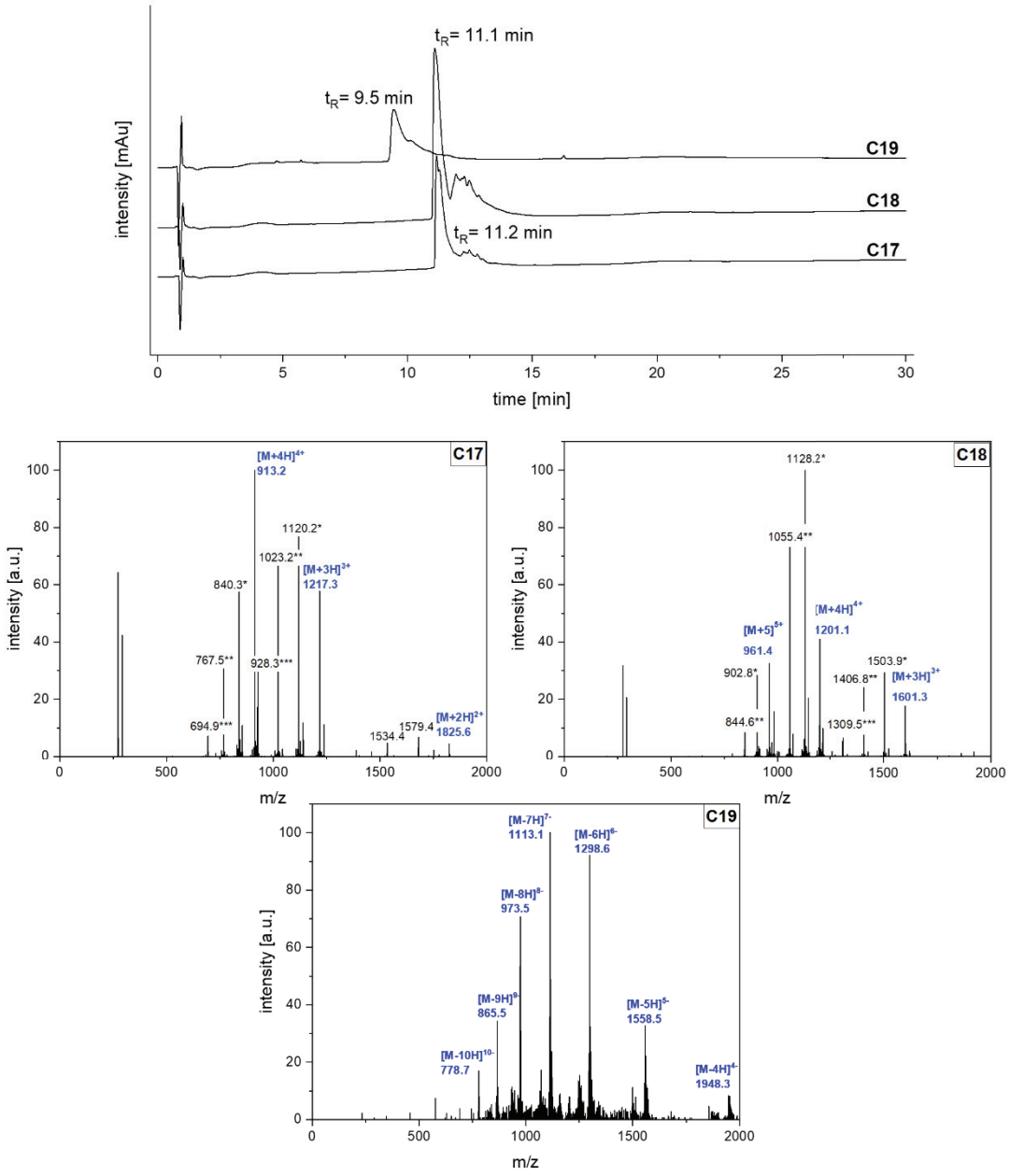

*Figure 30: RP-HPLC chromatogram of **C17**-**C19** (95/5 to 5/95 vol.-% H_2O/MeCN + 0,1 % formic acid in 17 min) and coupled mass spectra (ESI, positive mode) at t_R= 11.2 min for **C17** and t_R= 11.1 min for **C18**. ESI-MS (negative mode, lower energy) for **C19**. m/z of main products are highlighted in blue color. m/z assigned to by-products due to Neu5Ac cleavage are marked with * (-1 Neu5Nac), ** (-2 Neu5Ac) or *** (-3 Neu5Ac).*

First diffraction experiments were conducted by the Stehle group at CERN (Geneva, Switzerland) but did not show an occupation of the protein binding sites by Neu5Ac residues. It can be assumed that the complexation of Merkel cell VP1 protein with the large and flexible calix[5]arene ligands failed. Further measurements using other more suitable methods, e.g., saturation transfer difference (STD) NMR experiments, must be applied in future studies to investigate the binding behavior of the presented compounds.

4. Conclusion and Outlook.

The objective of this thesis was the incorporation of a calix[n]arene motif into the established SPPoS approach developed by Hartmann, enabling the synthesis of sequence-defined and tailor-made glycocalix[4]arene conjugates. Glycocalix[n]arenes represent a promising class of compounds that have already been successfully employed as glycomimetic structures to study carbohydrate-protein interactions that play key roles in numerous biological processes.[53, 68, 155, 162] The initial part of this work was the establishment of a suitable and robust synthetic procedure towards glycocalix[n]arenes. Preliminary studies demonstrated that calix[4]arene derivatives with a carboxylic acid group at the lower rim and nitrogen groups at the upper rim could serve as a building block in solid-phase synthesis. The synthesis of the key building block, **CBB1**, was performed following previously published protocols.[232] Subsequently, the ideal reaction conditions in solid-phase synthesis were investigated in detail. It was found that **CBB1** can be attached to a TentaGel S RAM® resin using the standard coupling protocol as established in the Hartmann group.[225] An especially critical step of this work was the optimization of the synthetic protocol to convert the nitrogen groups to amines. The full conversion was achieved by treatment with an excess of tin chloride dihydrate in NMP at 30 °C. Notably, it was found that the temperature is an essential reaction parameter for this step. Afterwards, the coupling of further building blocks onto the calix[4]arene scaffold and the conjugation of carbohydrate azides via CuAAC was successfully implemented. The successful synthesis of glycocalix[4]arenes was demonstrated by the preparation of a first set of sequence-defined multivalent glycocalix[4]arenes, each bearing eight carbohydrate moieties in total. In detail, two homomultivalent structures with mannosyl (**C1**) or galactosyl residues (**C2**) and a heteromultivalent structure carrying four residues of each glycosyl type (**C3**) were prepared. Subsequently, the mannose-functionalized glycocalix[4]arene ligands (**C1**, **C3**) were evaluated as bacterial inhibitors, performing an established adhesion-inhibition assay with GFP-tagged *E.coli* bacteria. This allowed comparison with other ligands that have already been tested previously within the group. The results showed effective bacterial inhibition, with IC_{50} values in a micromolar range, representing an approximately 100-fold improvement compared to the single MeMan interaction. Moreover, a more than 3 times higher RIP value per sugar was observed for the calix[4] arene-based ligand **C1** compared to previously studied linear PAA-based ligands with additional aromatic motifs in the backbone, indicating the beneficial effect of the cluster-like ligand presentation on the

calix[4]arene scaffold.[281] Additionally, when considering the valency corrected RIP values, a heteromultivalent effect for ligand **C3** was observed.

Next, the synthesis of a second set of functional glycocalix[4]arenes, which were further covalently attached to gold nanoparticles, was presented. Although a decrease in the IC_{50} values was observed for **C1** and **C3**, it is likely that this is primarily due to statistical rebinding rather than clustering of bacterial lectin receptors. It was reasoned that the presentation on a larger scaffold could result in even improved bacterial inhibition as an increased binding avidity to lectins, leveraging the concept of multivalency by binding to multiple bacterial receptors simultaneously. Therefore, the synthetic procedure was adapted toward the additional introduction of functional groups and/or glycosyl moieties at the lower rim of the calix[4]arene. The specific goal was to obtain the alkyne-functionalized glycocalix[4]arenes for CuAAC-mediated conjugation to ultrasmall gold nanoparticles in a single or multiple fashion (performed by Kai Klein from the Epple group at University Duisburg-Essen). To achieve this, the glycocalix[4]arenes were equipped with either a single alkyne at the lower rim for one click reaction (**C6**, **C7**) or four alkyne moieties at the upper rim (**C4**, **C5**) four multiple click reactions demonstrating a new concept to fine-tune the amount and density of carbohydrate residues and to avoid ligand overcrowding on the particle surface. The successful modification was validated using a suitable sulfuric acid-phenol method, a well-known colorimetric method for determining the total carbohydrate concentration in a sample. This highlights the modularity of the approach to make a broad range of multifunctional calix[n] arene derivatives feasible for diverse applications. Further, the glycocalix[4]arene-nanoparticle conjugates have been tested as bacterial inhibitors. However, the adhesion-inhibition assay did not deliver reliable results for the nanoparticle conjugates, which likely can be accounted for by bacteria clustering. Additionally, the performed fluorescence microscopy imaging does support this hypothesis. Although the results indicated that bacteria clustering occurred, further experiments are required to confirm this finding and to gain a deeper understanding of the underlying binding events. For subsequent work, it appears promising to focus on studies making use of the agglomeration behavior. For instance, a fluorescence competition assay has been previously demonstrated for carbohydrate-functionalized GNPs.[282]

In the second chapter of this thesis, the focus of potential protein targets for the presented class of sequence-defined glycocalix[4]arene conjugates was shifted from lectins to carbohydrate-processing enzymes. They are therapeutic targets for the treatment of many severe diseases. However, so far multivalent binders or inhibitors have not been considered

on a broad scale as is known for lectins. Specifically, the carbohydrate-binding domain of NGLY1 (PAW domain), a de-glycosylating enzyme that is known to play an important role in the ERAD of human species, was targeted in this thesis. As NGLY1 is known to bind to high-mannose glycans, it was hypothesized that the branched mannosyl-functionalized calix[4]arene derivative **C1** might be a sufficient synthetic ligand for the PAW domain of NGLY1, which could also affect the enzymatic activity. To have an enhanced array of investigation methods **C1b**, a derivative of **C1**, additionally equipped with a biotin tag, was synthesized according to the established SPPoS protocol. Moreover, linear reference structures (**L1**, **L2**) and negative controls (**C2b**, **C8b**) carrying biotin tags were prepared. For an initial experiment, a qualitative pull-down assay using a streptavidin agarose resin was conducted. The results indicated a noteworthy binding of NGLY1 to **C1b**. However, also for some of the negative controls, binding was observed. Consequently, no conclusion could be drawn from the results obtained. To gain a deeper understanding, an additional assay with a quantitative outcome was needed. To do so, an ELISA-inspired adhesion assay using a streptavidin-tagged horse radish peroxidase was developed. For the development phase of the assay, Con A was used, as just limited amounts of NGLY1 were available. Although the assay was successfully established for Con A, for NGLY1, no reliable results could be obtained. Due to the limited amount of available protein, further assay development was not in the scope of this project. Despite the inconclusive results regarding the binding of C1b to the PAW domain, another study investigating a potential effect on the enzyme efficiency was conducted. As a result of the limited amount of active NGYL1 it was decided to continue with PNGase F, which is like NGYLY1, an Amidase cleaving the glycosidic bond between the innermost GlcNAc and the asparagine side chain. For PNGase F and for Endo H, another high-mannose binding enzyme, no effect on the enzyme activity was observed when preincubated with **C1b** or any of the other derivatives. Therefore, it was concluded that the binding that was observed in the initial pull-down assay was likely a result of unspecific binding of the calix[4]arene scaffold with the protein and not due to specific carbohydrate-protein interactions. It can be assumed that the mannose motif would have to be exchanged towards larger oligomannosidic structures.

In the third part of the thesis, a straightforward split-and-combine approach was applied to synthesize two-sided homo- and heteromultivalent glycocalix[4]arene dimers. Following the established SPPoS protocol, four mannosyl- or galactosyl-functionalized glycocalix[4]arenes with either an alkyne or azide functionality were obtained **(C9**, **C10**, **C11**, **C12**) starting from one single batch. After cleavage from the solid support, the monomers can be mixed and matched to give the desired dimers. This work particularly

focused on the two-sided bispecific dimer (**C14d**) and its ability to bind two distinct targets simultaneously. As a proof of concept, the model legume lectins Con A, specific for mannosyl ligands, and PNA, specific for galactosyl ligands, were selected. In a first qualitative turbidity experiment, the bispecific ligand (**C14d**) exhibited a higher clustering efficiency when added to a mixed Con A/PNA solution compared to the homomultivalent ligands (**C13d**, **C15d**), indicating the simultaneous binding to both present ligands in solution. To validate and to quantify this finding, a precipitation assay was performed. The ligand was added to the protein mixture, and the precipitate was formed overnight. Initial attempts to separate the mixed pallet failed, prompting the design of a "double precipitation assay". The rationale behind this assay was to separate the unbound protein in the supernatant after the first precipitation. Using an affinity tag (the mannose-functionalized ligand **C13d**), the remaining Con A was isolated, allowing the separate quantification of unbound Con A and PNA. The results obtained demonstrated that both proteins, Con A and PNA, bind to **C14d,** with Con A exhibiting approximately five times greater clustering efficiency than PNA. These proof-of-concept experiments confirmed the potential of bispecific ligands like **C14d** for simultaneous targeting of multiple proteins. Future studies could involve the screening of diverse lectin pairs, particularly those with similar clustering efficiencies, to further evaluate the general applicability of this approach. For instance, initial experiments using mannosyl-specific lectins, LCA and PSA, that exhibit a reduced clustering efficiency compared to Con A (due to their dimeric structure) have already been conducted. However, due to the reduced affinity, studies had to be performed at higher concentrations, and for a detailed study, large amounts of the samples would have been required. Consequently, the experiments using LCA or PSA were not further pursued. In contrast, RCA, as a galactosyl-specific lectin with a large number of binding sites, emerges as a promising candidate for further studies. Another interesting perspective might be the investigation of the two-sided ligands on the surface, with the aim of mimicking cell surface attachment. This investigation could be relevant for potential therapeutic applications targeting cell surface receptors. First attempts on PNA-coated glass surfaces have been performed and indicated the successful binding to the surface on one side and interaction with Con A in solution on the other. However, further improvements to the assay design are required. Furthermore, the established SPPoS protocol allows for easy adjustment of the ligands in regard to carbohydrate valency and sequence to optimize binding affinity. Beyond carbohydrate ligands, the presentation of various supramolecular binding motifs on Janus-like platforms has the potential to further expand the scope of applications.

In the last part of the thesis, it was demonstrated that the synthetic methodology can also be applied to calix[5]arenes, the higher homologs of calix[4]arenes. An interesting feature of the higher homologs in comparison to **CBB1** is the conformational mobility due to the larger macrocycle, which might allow the final ligand to better adapt to the structural environment of the protein, leading to a so-called induced fit of the ligand. Additionally, the calix[5]arene scaffold is particularly interesting for the application as viral anti-adhesive treatments. Many viral binding proteins that mediate the first attachment to the cell have symmetric, in some cases pentameric, architecture. For instance, this is true for polyomaviruses, which can cause severe asymptomatic infections in various species, and which were focused on in this study. The goal was to achieve a pentameric multivalent ligand that is ideally capable of engaging all five carbohydrate-binding sites simultaneously. The chelate binding mode would yield a significant increase in binding avidity. First, the synthesis of an analog calix[5]arene building block, **CBB2,** was developed. An adapted synthetic route using a protection group strategy was required to obtain the desired building block. Further, it was demonstrated that **CBB2** is applicable at the solid phase using the established protocol for **CBB1**, again proving the modularity of the developed SPPOs approach. This approach enabled the synthesis of a series of sequence-defined sialic acid functionalized calix[5]arene derivatives with varying linker length and valency. Previous studies had already shown that especially the linker length and flexibility can impact the binding avidity. The successful synthesis was confirmed via HPLC-MS and ^{1}H-NMR analysis. For initial investigation, the ligands were submitted to a crystallographic experiment that was performed by Jasmin Freitag and co-workers (University of Tübingen) at CERN but did not result in detectable electron density at the binding sites. It can be assumed that the co-crystallization of the large ligands has failed. Other binding studies (in solution) might be more appropriate for this system. For instance, saturation transfer difference (STD) NMR spectroscopy, SPR, or cell binding and/or cell infection have been reported for the investigation of viral binding studies. However, the project demonstrates the wide range of different glycocalix[n]aren ligands that are feasible with the presented synthetic approach. In further studies, this could also be extended to other calix[n]arene homologs, such as calix[6]arenes, to create a range of symmetrical ligands as potential anti-viral therapeutics.

Overall, this work established a modular and robust method for synthesizing sequence-defined glycocalix[n]arenes conjugates. The approach presented here enables not only the precise tailoring of carbohydrate valency and sequence but also the incorporation of additional functionalities, allowing a straightforward ligand modification on solid support, as demonstrated across multiple projects. In this way, a versatile platform for glycomimetic

compounds was achieved, and promising results in areas such as antibacterial therapy have already been shown, emphasizing its potential in biomedicine. Furthermore, initial explorations into new applications underscore the versatility of glycocalix[n]arenes, laying a strong foundation for future studies in this field

5. Experimental Part

5.1 Materials

The following chemicals were used without further purification: Dimethylformamide was purchased from Biosolve Chemicals. Azido-PEG2-alcohol was purchased from Biosynth. 4-*tert*-butylcalix[4]arene, 4-*tert*-butylcalix[5]arene, benzotriazole-1-yloxytripyrrolidinophosphonium hexafluorophosphate were purchased from Carbosynth. Dichloromethane, potassium carbonate, 2-(4-(2-Hydroxyethyl)piperazin-1-yl)ethane-1-sulfonic acid (HEPES), manganese(II) chloride tetrahydrate, calcium chloride, sodium hydroxide (1M) and phenol were purchased from Fisher Scientific. Chloroform and hydrochloric acid were purchased from Fisher Chemical. Tetrahydrofuran, 1,4-dioxane, 4-pentynoic acid, triisopropyl silane, sodium methoxide, barium hydroxide octahydrate, 1-iodopropane, sodium hydride, nitric acid, acetic acid, potassium hydroxide, tris(3-hydroxypropyl-triazoylmethyl) amine, Amberlite IR 120, celite 545, methyl α-D-mannopyranoside and mannan from *Saccharomyces cerevisiae* were purchased from Sigma Aldrich. Methanol, ethyl acetate and *n*-hexane were purchased from VWR Chemicals. Acetonitrile and diethyl ether were purchased from Honeywell. Dimethyl sulfoxide, *N*,*N*-diisopropylethylamine, tin(II) chloride dihydrate, sodium chloride, Tween® 20 (polyoxyethylen-20-sorbitanmonolaurat) and sodium ascorbate were purchased from Carl Roth. Nβ-boc-Nα-Fmoc-L-2,3-diaminopropionic acid, and Biotin were purchased from TCI Chemicals. Nβ-boc-Nα-Fmoc-L-lysine was purchased from Iris Biotech. *N*-methyl-2-pyrrolidone, piperidine, trifluoroacetic acid, magnesium sulfate and copper(II) sulfate were purchased from Acros Organics. Sodium diethyldithiocarbamate trihydrate, palladium (10%) on carbon and aminoguanidine hydrogen carbonate were purchased from Alfa Aesar. Barium oxide was purchased from abcr. Ethyl 6-bromohexanoate was purchased from Fluorochem. Benzyl bromide was purchased from Merck. TentaGel S RAM was purchased from Rapp Polymere. AG® 1-X8 resin, Precision Plus Protein™ Dual Xtra Standard, 4 x Laemmli sample buffer, 10x Tris/Glycine/SDS and Bio-Safe Coomassie G-250 Stain were purchased from Bio-Rad Laboratories. Bovine Serum Albumin was purchased from Sigma Life Science. High-Capacity Streptavidin Agarose Resin and HRP-conjugated Streptavidin were purchased from Thermo Scientific. PNGase F and Endo H were purchased from New England Biolabs. RNase B was purchased from Abnova. Silica was purchased from Macherey-Nagel. Lens culinaris agglutinin (LCA) and pisum sativum lectin (PSA) and peanut agglutinin (PNA) were purchased from Medicago. Concanavalin A (Con A) was purchased from MP Biomedicals.

Buffer: PBS was prepared using PBS buffer tablets from Carl Roth for 100 ml. For PBST 0.05 vol.-% Tween® 20 was added to PBS buffer (pH = 7.4). Lectin Binding Buffer (LB buffer) was prepared by adding 50 mM sodium chloride, 1 mM manganese(II) chloride tetrahydrate, 1 mM calcium chloride to 10 mM HEPES buffer (pH = 7.4). The pH value was adjusted with 1 M sodium hydroxide using a pH-electrode by Mettler Toledo.

Milli-Q water was gained by a MicroPure water purification system from Thermo Scientific.

5.2 Instrumentation and Analytical Methods

Reversed Phase – High Pressure Liquid Chromatography (RP-HPLC-MS): Chromatography measurements were performed on an Agilent 1260 Infinity instrument coupled to a variable wavelength detector at an absorption wavelength of 214 nm and an Agilent Quadrupole mass spectrometer with an electrospray ionization (ESI) source (m/z range from 200-2000). A MZ-Aqua Perfect C18 column (3.0 x 50 nm, 3 µm) was used at 25°C. As mobile phase, linear gradients of an eluent system A and B were used: A) H_2O/MeCN (95/5 vol.-%) + 0.1 vol.-% formic acid; B) H_2O/MeCN (5/95 vol.%) + 0.1 vol.-% formic acid. Only for compound C8b: AII) H_2O/MeCN (95/5 vol.-%); BII) H_2O/MeCN (5/95 vol.-%)). The flow rate was 0.4 ml/min. All relative purities were determined via integration using the OpenLab ChemStation software from Agilent Technologies.

Preparative RP-HPLC: Chromatographic purifications were done on an Agilent 1200 Series instrument with a variable wavelength detector at 214 nm and an automatic fraction collector was used. A UG80 C18 RP column (20 x 250 nm, 5 µM) from Shiseido was used at 25 °C. A flow rate of 10 ml/min was applied. For all samples, an eluent system A and B was used in linear gradients: A) H_2O + 0.1 vol.-% formic acid; B) MeCN + 0.1 vol.-% formic acid.

Thin layer chromatography (TLC): Reactions in solution were monitored using TLC. Aluminum sheets with silica gel layer from Macherey-Nagel were used for this purpose. The substances were visualized with UV light at 254 nm.

Matrix Assisted Laser Desorption Ionization – Time of Flight – Mass Spectrometry (MALDI-TOF-MS): The MALDI-TOF mass spectra were measured on a Bruker UltrafleXtreme instrument from Bruker Daltonics. The measurements were performed using 2,5-dihydroxybenzoic acid (DHB) or dithranol (DIT) in combination with sodium trifluoroacetate as a matrix in linear or reflector mode.

^{1}H-Nuclear Magnetic Resonance (^{1}H-NMR): ^{1}H-NMR spectra were either recorded on a Bruker Avance III-300 (300 MHz) or 600 (600 MHz). All measurements were recorded at 25 °C unless stated otherwise. The chemical shifts are reported in delta (δ) expressed in parts per million (ppm). The residual, non-deuterated solvents (δ 3.31 ppm for CD_3OD, δ 2.50 ppm for DMSO-*d6* or 7.26 ppm for $CDCl_3$) were used as an internal reference. The multiplicities are abbreviated as follows: s = singlet, d = doublet, t = triplet, q = quartet, quin = quintet, and m = multiplet. The spectra are analyzed using MestreNova software.

UV/Vis Spectroscopy: UV/Vis spectroscopy was performed with a dual-trace spectrometer Specord® 210 Plus from Analytik Jena AG. The measurements were performed in quartz glass cuvettes (Starna GmbH, d = 1 cm) at 20 °C. The instrument was operated with Win ASPECT PLUS software.

UV/Vis Plate Reader: UV/Vis studies performed on clear polystyrene 96-well microtiter plates from Greiner and were analyzed using a CLARIOstar® reader from BMG LABTECH or a Multiskan Go reader from Thermo Scientific. The measurements were performed at 20 °C.

Freeze-dryer: The final products were freeze-dried with an Alpha 1-4 LD plus instrument from Martin Christ set to -50 °C at 0.1 mbar.

Sodium Dodecyl Sulfate Polyacrylamide Gel Electrophoresis (SDS-PAGE): All SDS-PAGE analyses were performed using a Mini-PROTEAN® Tetra Vertical Electrophoresis Chamber and 4-20% Mini-PROTEAN® TGX™ stain-free Gels (both purchased from BioRad). 4x Laemmli sample buffer from BioRad was used and prepared according to the supplier's instruction manual. As a running buffer, 10x Tris/Glycine/SDS electrophoresis buffer and as a protein ladder Precision Plus Protein™ Dual Xtra Standard (5 µL) was used. The electrophoresis was run at 200 V and 180 A for 32 min. The gels were stained using Bio-Safe™ Coomassie staining solution. The gels were scanned and edited using the Image Lab 6.1 software from BioRad.

BCA Method: For the determination of the Con A and PNA concentration, a Pierce™ BCA Protein Assay Kit from Thermo Scientific was used according to the user manual provided by the supplier. The measurements were performed in triplicate using clear polystyrene 96-well microtiter plates from Greiner. As HEPES (LB buffer) proved to interfere with the BCA test, PBS buffer + $CaCl_2$ was used for all precipitation measurements. Calibration curves were measured for both proteins in triplicates (see Figure 95, Figure 96, and Figure 97, appendix).

5.3 General SPPoS Conditions

Standard Fmoc-protocol: All solid phase reactions were performed on TentaGel S RAM resin in batch sizes between 0.05 mM to 0.15 mM in polypropylene syringes with integrated frits. Prior to use, the resin was swollen in DCM for 30 minutes, followed by washing with DMF five times. The reaction conditions for the coupling of all used building blocks are given in the table below (Table 3) and differ prior to and subsequent to the introduction of CBB1/CBB2. The coupling steps at the lower rim of CBB1/CBB2 were performed according to a protocol previously established in the Hartmann group using 5 eq. PyBOP and 10 eq. DIPEA as coupling reagent.[225] For the couplings to the upper rim of CBB1/CBB2, reaction conditions were slightly altered, and *N*-methyl morpholine is standardly used as a base. After each coupling, the resin was washed 10 times with DMF and DCM. Fmoc removal for all deprotection steps was performed using 25 vol.-% piperidine in DMF for 30 min (fresh solution added after 20 min). The resin was washed 10 times with DMF before the next coupling step.

Table 3: Overview of coupling conditions.

Coupling at:	Building block eq.	Coupling agents	Reaction time	Solvent
Lower rim CBB1/ CBB2	5 eq. Fmoc-Dap(Boc)-OH	5 eq. PyBOP + 10 eq. DIPEA	1h	DMF
	5 eq. EDS			
-	3 eq. CBB1/CBB2	5 eq. PyBOP + 10 eq. DIPEA	5h	DMF
Upper rim CBB1/ CBB2	5 eq./amine EDS	5 eq./amine PyBOP + 10 eq./amine *N*-methyl morpholine	1h	DMF
	5 eq./amine TDS			
	5 eq./amine pentynoic acid			

Boc group removal: The Boc group as a temporary protecting group of *N*β-dap and *N*β-lysin, was removed using 4M HCl in dioxan solution. The resin was first washed five times with dioxan before the HCl solution was added to the syringe and shaken vigorously for 10 min.

The resin was then washed three times with dioxan, and the procedure was repeated for a further 20 min. For neutralization, the resin was shaken (2x10 min) in 10 vol.-% DIPEA in DCM. The resin was then washed three times with approximately 2 ml dioxan and DCM and finally ten times with 2 ml DMF. The deprotection was followed by a coupling step to the side chain. Pentynoic acid (5 eq.), 4-azidobenzoic acid (5 eq.), and biotin (2 eq.) were coupled with PyBOP and DIEPA according to the established protocol described above.

Reduction of Aryl-nitro groups: The nitro groups at the upper rim of CBB1 were reduced to amines by treating the resin with 25 eq. Tin(II) chloride dihydrate in NMP (3 ml) for 24 hours at 30 °C. To remove excess tin salt, the resin was washed thoroughly ten times with NMP, methanol, DCM and DMF.

Copper(I)-catalyzed azide-alkyne cycloaddition (CuAAC): For the cycloaddition, 2 eq. of the azide component was dissolved in 1 ml DMF. In addition, 20 mol-% relative to the azide component of sodium ascorbate, as well as copper(II) sulfate, were dissolved separately in 0.1 mL of MQ water each. The solutions were then added to the syringe in the mentioned order and shaken overnight in the dark. By washing the resin alternately with a 0.23 M solution of sodium diethyldithiocarbamate in DMF/water and DMF the excess copper is removed, which can be monitored by color change.

Deprotection of carbohydrate residues: The Deacetylation of the mannosyl and galactosyl carbohydrates was performed on-resin. To do so, approximately 2 ml of a 0.2 M sodium methanolate solution in methanol was added to the syringe and shaken vigorously for 30 minutes. Subsequently, the resin was washed ten times with methanol and DMF.

In contrast, the sialic acid functionalized compounds were deprotected in solution after TFA anion exchange. To the lyophilized compounds, 3 ml of a 1 M lithium hydroxide monohydrate solution in methanol/water (50/50 vol.-%) was added and stirred for 3h at room temperature. Subsequently, Amberlite® IR 120 H^+ resin was added until a pH of 5 was reached. After the removal of the resin via filtration, the deprotected product was again lyophilized.

Cleavage from the solid support: A solution of TFA/TIPS/DCM (95/2.5/2.5 vol.%) was used to cleave the final glycocalix[4]arene from the solid support. The resin was treated with the cleavage solution for 1h, and subsequently, the product was precipitated in ice-cold diethyl ether. After centrifugation at 4000 rpm, the supernatant was decanted, and the remaining

precipitate was dissolved in water or water/DMSO (for water-insoluble derivative C4 and C5) and finally lyophilized.

Microcleavage: To monitor the SPPS reactions, small amounts of the resin were separated and treated according to the cleavage conditions described above (referred to as micro cleavage). The obtained precipitate was then analyzed via RP-HPLC-MS.

TFA anion exchange: For the anion exchange, an AG® 1-X8 resin was used. The resin was first washed three times with 1,6 M aqueous acetic acid, followed by three times with 0.16 M acetic acid before use. The exchange was performed for two hours.

5.4 Solution-phase Synthesis

Building Blocks:

The building blocks TDS ((triple-bond diethylenetriamine-succinic acid, 1-(fluorenyl)-3,11-dioxo-7- (pent-4-ynoyl)-2-oxa-4,7,10-triazatetra-decan-14-oic acid) and EDS (ethylene glycol diamine-succinic acid 1-(9H-fluoren-9-yl)-3,14-dioxo-2,7,10-trioxa-4,13-diazaheptadecan-17-oic acid) were synthesized as previously reported.[170, 225]

The Syntheses of the carbohydrate derivatives 2-azidoethyl 2,3,4,-tetra-*O*-acetyl-α-D-mannopyranoside and 2-azidoethyl 2,3,4,-tetra-*O*-acetyl-β-D-galactopyranoside were synthesized according to the literature.[170, 283]

4-Azidobenzoic acid and methyl 2-azido-4,7,8,9-tetra-*O*-acetyl-*N*-acetyl-α-D-neuraminate were synthesized and provided by Lennart Hofer (Hartmann lab, HHU).[260, 278]

Compound CBB1:

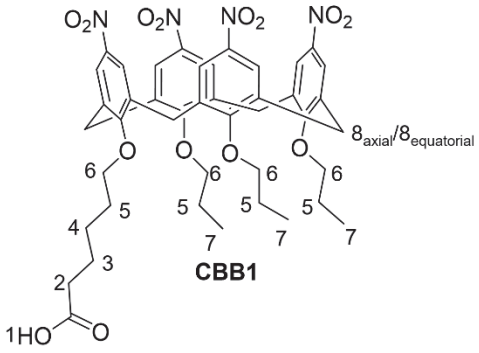

CBB1

The building block was prepared as previously reported and obtained as an off-white solid in an overall yield of 30 %.[232]

^{1}H-NMR (300 MHz, DMSO-d_6): δ 12.04 (s, 1H, 1), 7.65 (s, 8H, Aryl-H), 4.37 (d, ^{2}J= 12.1 Hz, 4H, 8_{axial}), 3.95 (m, 8H, 6), 3.69 (d, ^{2}J=12.1 Hz, 4H, $8_{equatorial}$), 2.24 (t, ^{3}J = 7.2, 2H, 2), 1.85 (m, 8H, 5), 1.58 (p, ^{3}J=7.1 Hz, 2H, 3), 1.41 (m, 2H, 4), 1.05-0.90 (m, 9H, 7) ppm.

MALDI-TOF-MS: m/z calculated for $C_{43}H_{48}N_4O_{14}$: 867.32 $[M+Na]^+$, found: 867.36 $[M+Na]^+$.

Compound CBB2*:*

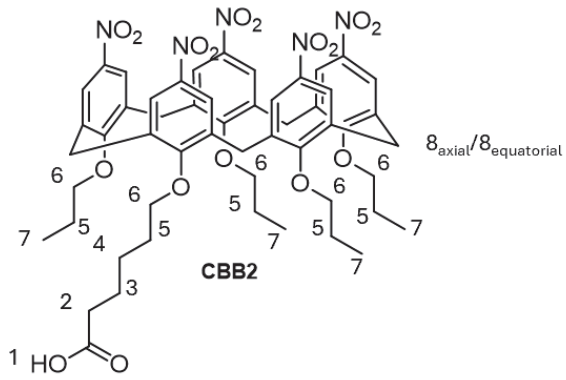

The compound CBB2 was prepared in a six-step synthesis starting from the commercially available 4-*tert*-butyl calix[5]arene, which is referred to as CBB2-1. The further intermediates are CBB2-2, CBB2-3, CBB2-4, CBB2-5 and CBB2-6. For the structures of these, see chapter 3.4.

*CBB2-**2:*** CBB2-2 was synthesized according to the literature with a few alterations.[117] CBB2-1 (8 g, 9.9 mmol, 1eq.) and $KHCO_3$ (2 g, 20 mmol) were dissolved and refluxed in 400 mL dry acetonitrile in nitrogen atmosphere. After 1 h, benzyl bromide (0.39 ml, 3.3 mmol) in 40 mL of acetonitrile was added dropwise and the reaction mixture continued to reflux for 21 h. Afterwards, the solvent was removed under reduced pressure, and subsequently the residue was partitioned between 200 mL of chloroform and 150 mL of 1 M HCl. The organic phase was washed twice with H_2O, dried over $MgSO_4$ and finally the solvent was removed under reduced pressure. The crude product was purified by column chromatography (SiO_2, toluene/hexane 1:1 v/v) to give 3 g (3.3 mmol, quantitative yield) CBB2-2. Additionally, starting material CBB1-1 was also recovered.

^{1}H-NMR (300 MHz, $CDCl_3$): δ 7.95-7.68 (m, 6H, Aryl-H), 7.62-7.45 (m, 3H, Aryl-H), 7.37-7.12 (m, 17H, Aryl-H, overlap with solvent peak), 5.22 (s, 2H, -O-C*H*$_2$-Aryl), 4.48 (d, 2H, ^{2}J = 13.8 Hz, Aryl-C*H*$_2$-Aryl), 4.17 (d, 2H, ^{2}J =14.0 Hz, Aryl-C*H*$_2$-Aryl), 4.13 (d, 1H, ^{2}J =14.2 Hz, Aryl-C*H*$_2$-Aryl), 3.62-3.42 (m, 5H, Aryl-C*H*$_2$-Aryl), 1.35 (s, 18H, -C$(CH_3)_3$), 1.30 (s, 18H, -C$(CH_3)_3$), 1.16 (s, 9H, -C$(CH_3)_3$) ppm.

MALDI-TOF-MS: m/z calculated for $C_{62}H_{76}O_5$: 923.57 $[M+Na]^+$; found: 923.66 $[M+Na]^+$.

*CBB2-**3**:* CBB2-2 (3 g, 3.3 mmol) was heated to reflux in 300 mL dry acetonitrile, and subsequently K_2CO_3 (6 g, 43 mmol) was added. After 45 min, 1-iodopropane (12 ml, 115 mmol) was transferred to the reaction vessel via a syringe, and the mixture was refluxed for another 12 h. After cooling to room temperature, the solvent was removed under reduced pressure, and the residue was partitioned between 200 mL of chloroform and 150 mL of 1 M HCl. The organic phase was washed twice with water, dried over $MgSO_4$ and finally the solvent was removed under reduced pressure. The crude product was recrystallized from chloroform/methanol, dried in vacuo to give 2.9 g (2.7 mmol, 80%) of CBB2-**3**.

MALDI-TOF-MS: m/z calculated for $C_{74}H_{100}O_5$: 1091.76 $[M+Na]^+$, 1107.76 $[M+K]^+$; found: 1091.92 $[M+Na]^+$, 1107.90 $[M+K]^+$.

*CBB2-**4**:* The reaction was performed with some alteration according to the literature.[284] CBB2-3 (2.9 g, 2.7 mmol) was suspended in 300 mL of ethyl acetate. In nitrogen atmosphere, four spatula tips of Pd/C were added. The reaction vessel was flushed with hydrogen (H_2), and the reaction was stirred at 30 °C in H_2 atmosphere for 21 h. The reaction mixture was filtered over Celite, and the solvent was removed under reduced pressure. The crude obtained (2.6 g, 2.7 mmol, quantitative yield) was used without any further purification.

MALDI-TOF-MS: m/z calculated for $C_{67}H_{94}O_5$: 1001.71 $[M+Na]^+$; found: 1001.70 $[M+Na]^+$.

*CBB2-**5**:* CBB2-5 was synthesized in an analogous way to the calix[4]arene derivative based on a literature-known protocol by Shuker.[232] CBB2-**4** (2.6 g, 2.7 mmol) was dissolved in dry DMF, and nitrogen-flushed for 30 min. Subsequently, NaH (130 mg, 5.3 mmol) was added portion-wise, and the mixture was stirred under reflux. After 30 min, 6-bromo hexanoate was transferred (0.9 ml, 4.9 mmol) via a syringe, and the mixture was refluxed for another 50 min. Subsequently, after cooling to room temperature, the reaction was quenched by the addition of 250 mL of 1 M HCl and continued to stir for 30 min at room temperature. The organic phase was extracted three times with 200 mL of chloroform. Afterwards, the organic phase was washed twice with water (150 mL) and brine (200 mL), dried over $MgSO_4$, filtered and finally the solvent was removed under reduced pressure. The crude product was purified by column chromatography (SiO_2, Hexane/Ethyl acetate 98:2 v/v) to yield 2.7 g of CBB2-5 (2.4 mmol, 89%).

MALDI-TOF-MS: m/z calculated for $C_{75}H_{108}O_7$: 1143.81 $[M+Na]^+$, 1159.81 $[M+K]^+$; found: 1143.78 $[M+Na]^+$, 1159.81 $[M+K]^+$.

CBB2-**6***:* The *ipso*-nitration was performed following the procedure described for a calix[4]arene derivative.[277] CBB2-5 (2.6 g, 2.3 mmol) was dissolved in 150 mL dry DCM. A mixture of concentrated acetic acid and fuming nitric acid (14 ml/10 ml) was prepared and dropped slowly into the ice bath-cooled reaction vessel. Afterwards, the cooling bath was removed, and the reaction continued to stir at room temperature for 5 h. During this time, a color change of the reaction mixture from black to orange could be observed. The reaction was quenched by the addition of 200 mL of water and was stirred for around another 10 min, before the organic phase was extracted three times with chloroform (100 mL). The organic phase was then washed twice with water (200 ml) and brine (200 ml). After drying over $MgSO_4$, the solvent was removed under reduced pressure. After drying in vacuo, CBB2-6 was obtained in a yield of 2.35 g (2.2 mmol, 92%). The product was used in the final reaction step without further purification.

MALDI-TOF-MS: m/z calculated for $C_{55}H_{63}N_5O_{17}$: 1088.42 $[M+Na]^+$; found: 1088.52 $[M+Na]^+$.

The hydrolysis in the final step to obtain **CBB2** was performed following the CBB1 synthesis. CBB2-6 (2.35 g, 2.2 mmol) was dissolved in 150 mL of THF/MeOH/H_2O (10:1:1 v/v/v) mixture. Next, KOH (4 g, 70 mmol) was added, and the mixture was stirred overnight at 45 °C. After cooling, the reaction was quenched by the addition of 150 mL 1 M HCl. The mixture continued to stir for another 1.5 h at room temperature. Afterwards, the organic phase was extracted three times with chloroform (150 mL). The organic phase was washed twice with water (200 mL) and once with brine (200 mL). After drying over $MgSO_4$, the solvent was removed under reduced pressure to give a red-brownish solid. The solid was washed with chloroform (50 mL) and filtered off to yield an off-white product. After drying in vacuo, 1.45 g (1.4 mmol, 64%) **CBB2** was obtained. The yield over all steps is 42 %.

^{1}H-NMR (600 MHz, DMSO, 90° C): δ 11.59 (s, 1H, 1), 8.44-7.74 (m, 10H, Aryl-H), 4.22-3.86 (m, 10H, 8_{axial}, $8_{equatorial}$), 3.78-3.24 (m, 10H, 6), 2.20 (t, ^3J = 7.4 Hz, 2H, 2), 1.68-1.58 (m, 2H, 4), 1.54 (quin, ^3J = 7.6 Hz, 2H, 3), 1.46-1.10 (m, 10H, 5), 0.87-0.39 (m, 12H, 7) ppm.

^{13}C-NMR (150 MHz, DMSO, 90° C): 173.45 (*C*(O)OH), 160.64 (Aryl-*C*), 160.52 (Aryl-*C*), 142.38 (Aryl-*C*), 142.33 (Aryl-*C*), 134.27 (Aryl-*C*), 134.20 (Aryl-*C*), 132.11 (Aryl-C), 134.09 (Aryl-*C*), 124.5 (Aryl-*C*), 74.36 (-O-*CH$_2$*), 73.19 (-O-*CH$_2$*), 33.16 (Aryl-*CH$_2$*-Aryl), 28.78 (*CH$_2$*), 24.56 (*CH$_2$*), 23.92 (*CH$_2$*), 21.93 (*CH$_2$*), 9.03 (*CH$_3$*), 8.89 (*CH$_3$*) ppm.

MALDI-TOF-MS: m/z calculated for $C_{53}H_{59}N_5O_{17}$: 1060.39 $[M+Na]^+$; found: 1060.43 $[M+Na]^+$.

Dimer synthesis (C13d-C15d), CuAAC:

For the synthesis of the dimeric calix[4]arene compounds C13d/C14d/C15d, a CuAAC protocol was employed. The glycocalix[4]arene monomers C9-C12 were used without prior purification. Equimolar amounts (0.014 mmol) of the azide and alkyne monomer were placed in a 5 mL round-bottom flask and dissolved in 3 mL of MQ water. The solution was flushed with nitrogen for 30 minutes. 50 mol-% (7 µmol) of sodium ascorbate and copper(II) sulfate were dissolved in 1 mL of MQ water each and subsequently added to the reaction mixture in the mentioned order. The reaction mixture was stirred under nitrogen atmosphere at 35° C. After seven hours, further 7 µmol of sodium ascorbate and copper(II) sulfate were added, and the mixture continued to stir. After 24h in total, the reaction was stopped by adding 3 mL of a 23 mM aqueous sodium diethyldithiocarbamate solution until a rich brown coloring was observed. Then, acetonitrile was added to the mixture to obtain 1:1 vol.-% water to acetonitrile. The formed brown precipitate was removed after thorough centrifugation (4000 rpm, until the centrifugate is clear). Subsequently, acetonitrile and water were removed under reduced pressure, and the crude product was re-dissolved in MQ water and lyophilized. The lyophilizate was then purified using preparative RP-HPLC. For analytical data of C13d/C14d/C15d, see chapter 5.6.

5.5 Assays and Binding studies

Pull-down Assay: 10 mM ligand stock solutions in water have been prepared. A stock of NGLY-1 (0.91 mg/mL) has been provided by Grace Science LLC. 20 µL of the NGLY1 stock was incubated with 2.5 µL of ligand stock for 1h at 37° C. Additionally, a zero-sample has been prepared analogously. Next, 80 µL of streptavidin agarose resin was added to each sample, and they were shaken overnight at 37° C. The supernatant was removed via centrifugation at 3000 rpm using a spin column. The resin was washed three times with PBS. Subsequently, the resin as well as the supernatant were analyzed via SDS-PAGE. Prior to this, the resin samples were prepared by adding 15 µL PBS, 5µL of a saturated biotin solution, and 7 µL Laemmli buffer. For the supernatant sample, 7 µL of Laemmli buffer was added to 20 µL of supernatant solution. The samples were then boiled at 95° C for 100 min.

Gel-Shift Assay with PNGase F and Endo H: Two individual experiments for PNGase F and Endo H were performed using Gel Shift Assay kits from New England Biolabs.

RNase B was used as a glycoprotein substrate. RNase B was dissolved in PBS to yield a 10 mg/mL stock solution. For each experiment, 2 µL of the stock solution was mixed with 1 µL denaturation buffer and 7 µL of water. This mixture was then boiled at 95° C for 15 min to obtain denatured glycoprotein.

In parallel, the enzymes (Endo H / PNGase F) were preincubated with the inhibitors to be tested for 30 min at 37° C according to Tables 4 and 5.

Table 4: Composition of all samples tested in the Gel-Shift Assay using the enzyme PNGase F.

Sample #	Inhibitor		PNGase F [µL]	Buffer* [µL]	NP-40 [µL]	H_20 [µL]
	Conc. [mM]	Vol. [µL]				
	C1b					
1	10	5	1	1	1	1
2	1	5				
	L1					
3	10	5	1	1	1	1
4	1	5				
	L2					
5	10	5	1	1	1	1
6	1	5				
	C2b					
8	10	5	1	1	1	1
	1	5				
	C8b					
10	10	5	1	1	1	1
	1	5				
	zero-sample control					
11	-		1	1	1	6
12	-		-	1	1	7

* GlycoBuffer 2 New England Biolabs

Table 5: Composition of all samples tested in the Gel-Shift Assay using the enzyme Endo H.

Sample #	Inhibitor		Endo H [µL]	Buffer* [µL]	H_20 [µL]
	Conc. [µM]	Vol. [µL]			
	C1b				
1	10	5	1	1	2
2	1	5			
3	0.1	5			
	L1				
4	10	5	1	1	2
5	1	5			
6	0.1	5			
	L2				
7	10	5	1	1	2
8	1	5			
9	0.1	5			
	C2b				
10	10	5	1	1	2
11	1	5			
12	0.1	5			
	C8b				
13	10	5	1	1	2
14	1	5			
15	0.1	5			
	zero-sample control				
16	-		1	1	7
17	-		-	1	8

* GlyoBuffer 2 New England Biolabs

Next, the preincubated enzyme is added to the denatured glycoprotein (RNase B), and 1 µL of GlyoBuffer is added to give a total volume of 20 µL, and the mixture is incubated under agitation for 1 h at 37 °C. Afterwards, the samples were analyzed by SDS-PAGE. For sample

preparation, 7 µL Laemmli buffer was added to each sample prior to denaturing at 95° C for 10 minutes, followed by application to the precast gels.

HRP-streptavidin Adhesion Assay: For the microplate Con A coating, each well was filled with 100 µL Con A solution (1 mg/mL in LBB) and the plate was shaken overnight at 37 °C. Subsequently, the plate was washed 4 times with PBST (150 µL/well). Next, the plate was incubated with a blocking solution (1% BSA + 0.1% galactose) for 2h at 37 °C, followed by 4 washing steps with PBST (150 µL). For NGLY1 coating, the plate was filled with 60 µL/well NGLY1 stock solution (0.91 mg/mL) overnight at 37 °C. The following washing and blocking steps are performed according to the protocol described for Con A coating.

10 mM stock solutions of the ligands are prepared, added in serial dilution to the plate (highest concentration: 1mM, 50 µL/well), and incubated for 1h at room temperature. Afterwards, the plate is washed 4 times with 150 µL PBS.

The streptavidin-HRP conjugate was diluted in PBS according to the supplier's recommended dilution range (1:10,000) and mixed vigorously before use. 100 µL were added to each well and again incubated for 1h at room temperature, followed by 4 washing steps using 150 µL PBS. Next, 50 µL substrate solution (1-Step™ Ultra TMB-ELISA) was added to the plate. After an incubation time of 15 minutes at room temperature, 50 µL of 2 M sulfuric acid was added to each well to stop the reaction. Subsequently, the absorbance at 450 nm was measured.

Turbidity Assay: For the turbidity assay, an adapted protocol from previous work was employed.[224] For each experiment, 1 mL of a lectin solution in LBB was prepared and placed in a quartz cuvette. For all solutions, the lectin concentration was kept constant at 5 µM Con A and 10 µM PNA. The transmittance at 420 nm was measured for the clear lectin solutions and corresponds to 100 % intensity. Ligand stock solutions in LB buffer (250 -500 µM) were prepared and titrated to the lectin solutions in portions of 2 µL. The mixture was vigorously mixed, and after 20 min, the transmittance at 420 nm was measured. Subsequently, the procedure was repeated as many times as no further decrease in transmittance or a maximum ligand solution of 10 µM was reached. The measurement was repeated each time for each ligand and lectin solution.

Precipitation Assay I: The precipitation assay was performed according to an adapted literature-known protocol.[224] Stock solutions of the ligands were prepared (500 µM in PBS+$CaCl_2$) and 10 µL were added to either a PNA (10 µM in PBS+$CaCl_2$), Con A (10 µM in PBS+$CaCl_2$), or a mixture of both ligands (10 µM of each lectin) to give a total volume of 1

mL. The clusters were allowed to form overnight at room temperature in 2 mL Eppendorf tubes. In the next step, the clusters were centrifuged at 13500 rpm for 10 min. The supernatant was removed, and the pellet was washed with 1 ml of cold buffer. Subsequently, the clusters were again centrifuged, and the washing solution was removed. To the pellet, 1 mL of a 0.05 M methyl mannose solution was added and mixed vigorously for 1 min, yielding a clear solution for all samples. The solution was then analyzed using a BCA test kit. The measurement was repeated for each ligand and lectin solution. Additionally, negative controls and a zero-sample control were performed and did not result in the formation of any clusters. The obtained OD_{540} is shown in Table 6.

Table 6: OD_{540} values were blank corrected, and the given errors equal the standard deviation obtained from triple determination.

Ligand	**OD_{540}**		
	Con A + PNA	**Con A**	**PNA**
C14d	0.31 ± 0.01	0.27 ± 0.02	n.d.
C13d	0.37 ± 0.01	0.37 ± 0.02	n.d.
C15d	n.d.	n.d.	n.d.

Precipitation Assay II: The precipitation protocol is further adapted to enable the separate quantitative determination of the bound lectins. The assay was performed as described above, and the cluster protein concentration was determined via BCA method. However, the supernatant was not disposed of but transferred to another Eppendorf tube. An affinity tag (C13d, 5µL from 1mM stock in PBS+Ca^2) was added to the supernatant, and the precipitate was formed overnight at room temperature. Next, the precipitate was centrifuged at 13500 rpm for 10 minutes, followed by a washing step that was performed as described previously. The supernatant was again not disposed of but transferred to another Eppendorf tube. The pellet was dissolved using 1 mL of a 0.05 M methyl mannose solution as described above. The concentration of the supernatant (PNA concentration) as well as the cluster protein concentration (Con A concentration) was determined separately using the BCA method.

Table 7: OD_{562} values were blank corrected, and the given errors equal the standard deviation obtained from triple determination.

Ligand	**OD_{562}**		
	Con A+ PNA precipitate	**Con A** supernatant	**PNA** supernatant
C14d	0.55 ± 0.02	0.27 ± 0.01	0.59 ± 0.01
C13d	0.71 ± 0.03	0.04 ± 4.5 x10-4	0.65 ± 0.02

Table 8: Summary calculations made for precipitation assay II of C14b. For the wash solution, an OD_{562} of 0.04 was detected.

	Con A	**PNA**	**Sum:**
c [µM] supernatant	6.90 ± 0.2	17.50 ± 0.16	-
c[µM] stock solution	20	20	-
Difference: **c [µM]** precipitate	13.10 ± 0.37	2.50 ± 0.02	-
c(protein)/c(ligand)	1.31 ± 0.04	0.25 ± 2.2 x 10^{-3}	1.56 ± 0.04
OD_{562}	0.5	0.08	0.58 0.54 (minus wash)

5.6 Analytical Data Oligomers

Compound C1b:

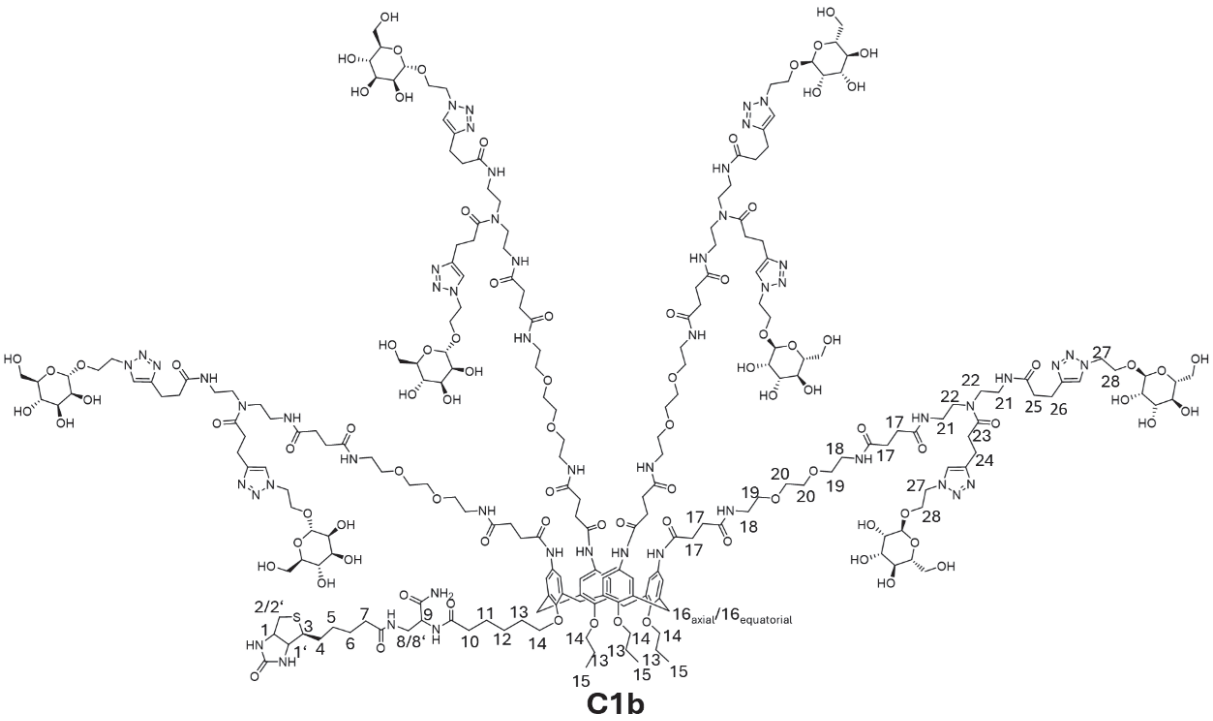

RP-HPLC: 100 % A to 0 % A in 30 min at 25 °C: t_R = 11.4 min, rel. purity: 66 %.

ESI-MS: calculated for $C_{232}H_{361}N_{53}O_{88}S$: 1777.5 $[M+3H]^{3+}$, 1333.4 $[M+4H]^{4+}$, 1066.9 $[M+5H]^{5+}$, 889.3 $[M+6H]^{6+}$; found: 1778.2 $[M+3H]^{3+}$, 1333.8 $[M+4H]^{4+}$, 1067.4 $[M+5H]^{5+}$, 889.5 $[M+6H]^{6+}$.

MALDI-TOF-MS: calculated for $C_{232}H_{361}N_{53}O_{88}S$: 5352.5 $[M+Na]^+$; found: 5355.7 $[M+Na]^+$.

^{1}H-NMR (600 MHz, MeOH-*d4*/D_2O): δ 7.88-7.71 (m, 8H, Triazole-H), 7.0-6.7 (m, 8H, Aryl-H), 4.73 (s, 8H, $CH_{mannose}$), 4.61-4.54 (m, 17H, 27, overlap with solvent peak), 4.52 (dd, ^3J = 8.4, 4.6 Hz, 2H, 1, overlap with other peaks), 4.48 (dd, ^3J = 7.9, 4.9 Hz, 1H, 9), 4.41 (d, ^2J = 13.0 Hz, 4H, 16_{axial}), 4.29 (dd, ^3J = 8.1, 4.3 Hz, 1H, 1'), 4.12-4.04 (m, 8H, $CH_{mannose}$), 3.90-3.31 (m, 146H, 8, 8', 14, 18, 19, 20, 21, 22, $CH_{mannose}$, overlap with solvent peak, PEG impurities), 3.18-3.07 (m, 13H, 3, $16_{equatorial}$, $CH_{mannose}$), 3.01-2.93 (m, 16H, 26, 24), 2.88 (dd, ^2J = 12.9 Hz, ^3J = 5.0 Hz, 1H, 2), 2.82-2.74 (m, 8H, 23), 2.69 (d, ^2J = 12.9 Hz, 2H, 2', overlap with impurity), 2.65-2.42 (m, 40H, 17, 25), 2.31 (t, ^3J = 7.8 Hz, 2H, 10), 2.25-2.15 (m, 2H, 7), 2.0-1.85 (m,10H, 13, overlap with impurities), 1.77-1.34 (m, 13H, 4, 5, 6, 11, 12, overlap with impurities), 1.06-0.94 (m, 9H, 15) ppm.

Yield: 65 %

Compound C2b:

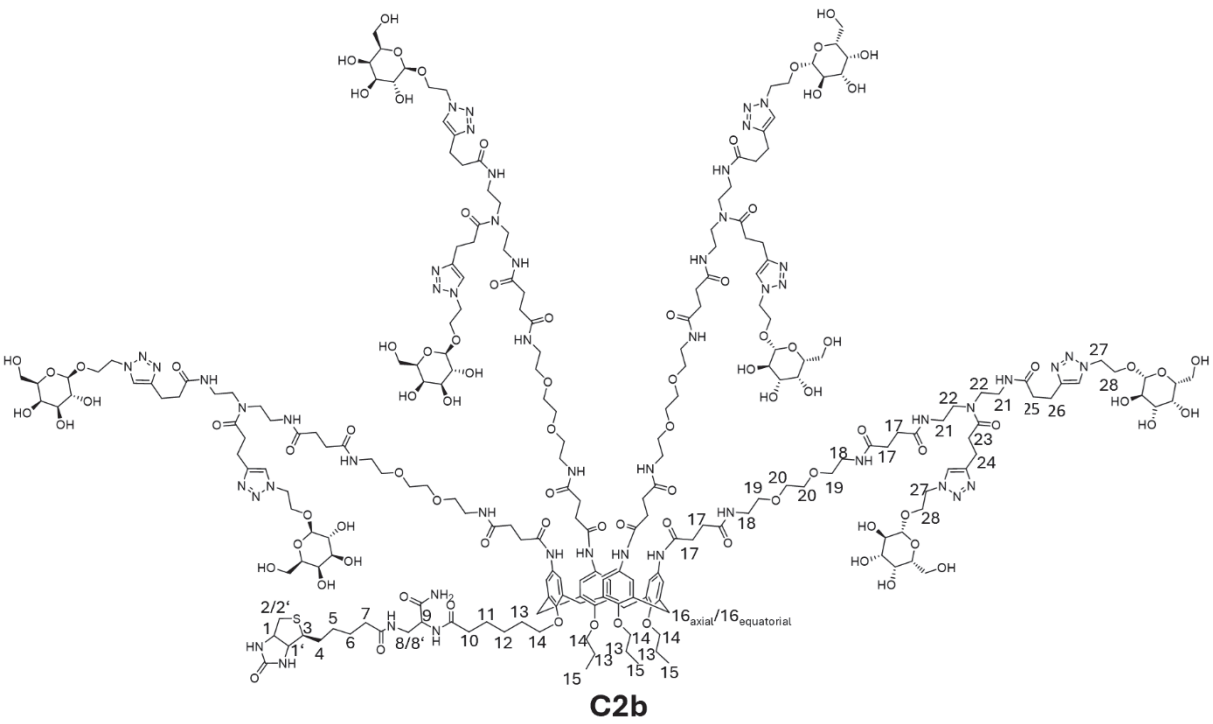

RP-HPLC: 100 % A to 0 % A in 30 min at 25 °C: t_R = 11.3 min, rel. purity: 53 %.

ESI-MS: calculated for $C_{232}H_{361}N_{53}O_{88}S$: 1333. $[M+4H]^{4+}$, 1066.9 $[M+5H]^{5+}$, 889.3 $[M+6H]^{6+}$ 762.4 $[M+7H]^{7+}$; found: 1334.2 $[M+4H]^{4+}$, 1067.6 $[M+5H]^{5+}$, 889.6 $[M+6H]^{6+}$, 762.8 $[M+7H]^{7+}$.

MALDI-TOF-MS: calculated for $C_{232}H_{361}N_{53}O_{88}S$: 5352.5 $[M+Na]^+$; found: 5355.7 $[M+Na]^+$.

^{1}H-NMR (600 MHz, MeOH-*d4*/D_2O): δ 8.24-7.84 (m, 7H, Triazole-H), 7.03-6.75 (m, 8H, Aryl-H), 4.73 (s, 8H, $CH_{mannose}$), 4.64-4.58 (m, 17H, 27, overlap with solvent peak), 4.55-4.48 (m, 5H, 1, 9, overlap with other peaks and solvent peak), 4.43 (m, 5H, 16_{axial}, overlap with other peaks and solvent peak), 4.34-4.28 (m, 8H, 1', $CH_{galactose}$), 4.27-4.21 (m, 6H, $CH_{galactose}$), 4.07-3.95 (m, 7H, $CH_{galactose}$), 3.94-3.35 (m, 138H, 8, 8', 14, 18, 19, 20, 21, 22, $CH_{galactose}$, overlap with solvent peak), 3.20-3.08 (m, 5H, 3, $16_{equatorial}$), 3.04-2.93 (m, 12H, 26, 24), 2.90 (dd, ^2J = 13.0 Hz, ^3J = 4.9 Hz, 1H, 2), 2.83-2.74 (m, 6H, 23), 2.71 (d, ^2J = 13.0 Hz, 1H, 2'), 2.63-2.44 (m, 42H, 17, 25, overlap with impurities), 2.35-2.3 (m, 3H, 10, overlap with impurities), 2.27-2.16 (m, 2H, 7), 2.0-1.9 (m, 9H, 13), 1.77-1.36 (m, 13H, 4, 5, 6, 11, 12, impurities), 1.07-0.97 (m, 10H, 15) ppm.

At 2.04 ppm, signals of acetate counter ions can be found. Phase and baseline correction have been performed using the MestreNova software.

Yield: 50 %

Compound C8b:

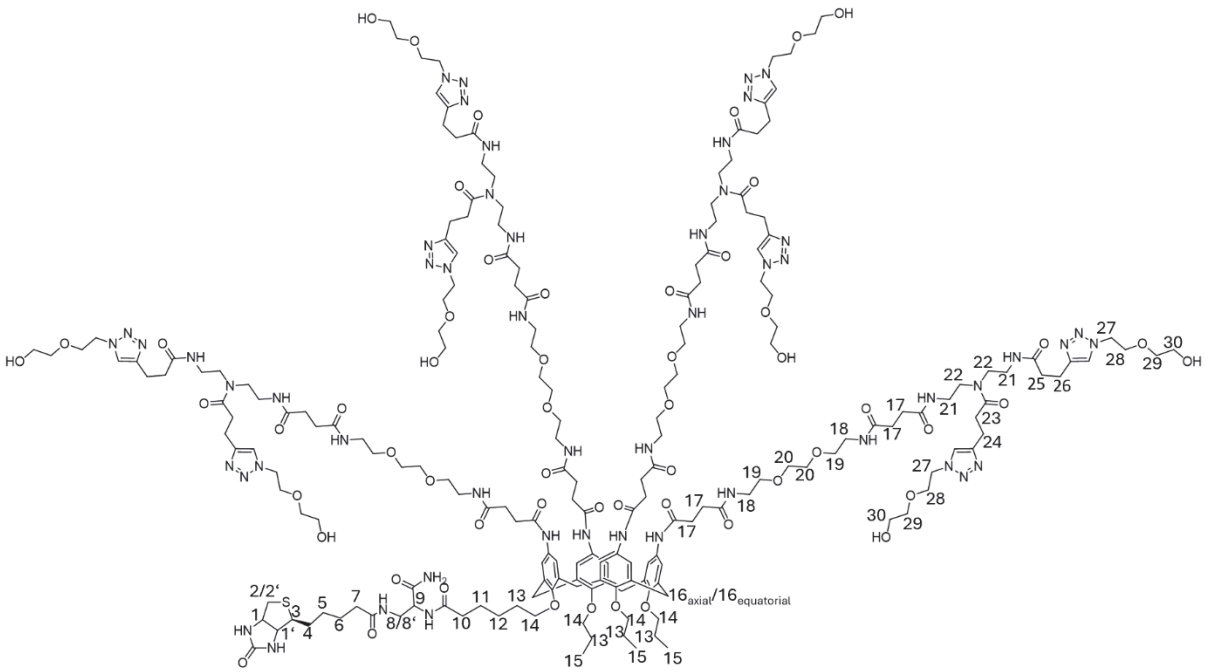

C8b

RP-HPLC: 100 % A to 0 % A in 17 min at 25 °C: t_R = 8.4 min, rel. purity: 60 %.

ESI-MS: calculated for $C_{200}H_{313}N_{53}O_{56}S$: 1462.8 $[M+3H]^{3+}$, 1097.3 $[M+4H]^{4+}$; found: 1463.3 $[M+3H]^{3+}$, 1097.8 $[M+4H]^{4+}$.

MALDI-TOF-MS: calculated for $C_{200}H_{313}N_{53}O_{56}S$: 4408.3 $[M+Na]^{+}$; found: 4411.4 $[M+Na]^{+}$.

^{1}H-NMR (600 MHz, MeOH-*d4*/D_2O): δ 7.88-7.76 (m, 8H, Triazole-H), 7.0-6.7 (m, 8H, Aryl-H), 4.73 (s, 8H, $CH_{mannose}$), 4.56-4.50 (m, 18H, 27, 1, overlap with solvent peak), 4.48 (dd, ^3J = 7.9, 4.8 Hz, 1H, 9), 4.41 (d, ^2J = 11.5 Hz, 4H, 16_{axial}), 4.29 (dd, ^3J = 8.0, 4.4 Hz, 1H, 1'), 4.12-4.04 (m, 8H, $CH_{mannose}$), 4.0-3.34 (m, 138H, 8, 8', 14, 18, 19, 20, 21, 22, 28, 29, 30, overlap with solvent peak), 3.16 (dt, ^3J = 9.4, 5.1 Hz,1H ,3), 3.13.-3.05 (m, 4H, $16_{equatorial}$), 3.01-2.91 (m, 16H, 26, 24), 2.88 (dd, ^2J = 12.8 Hz, ^3J = 4.9 Hz, 1H, 2), 2.8-2.73 (m, 8H, 23), 2.69 (d, ^2J = 12.8 Hz, 2H, 2', overlap with impurity), 2.62-2.41 (m, 43H, 17, 25), 2.31 (t, ^3J = 7.6 Hz, 2H, 10), 2.25-2.15 (m, 2H, 7), 2.0-1.86 (m,9H, 13), 1.75-1.35 (m, 12H, 4, 5, 6, 11, 12, overlap with impurities), 1.05-0.95 (m, 9H, 15) ppm.

Yield: 65 %

Compound L1:

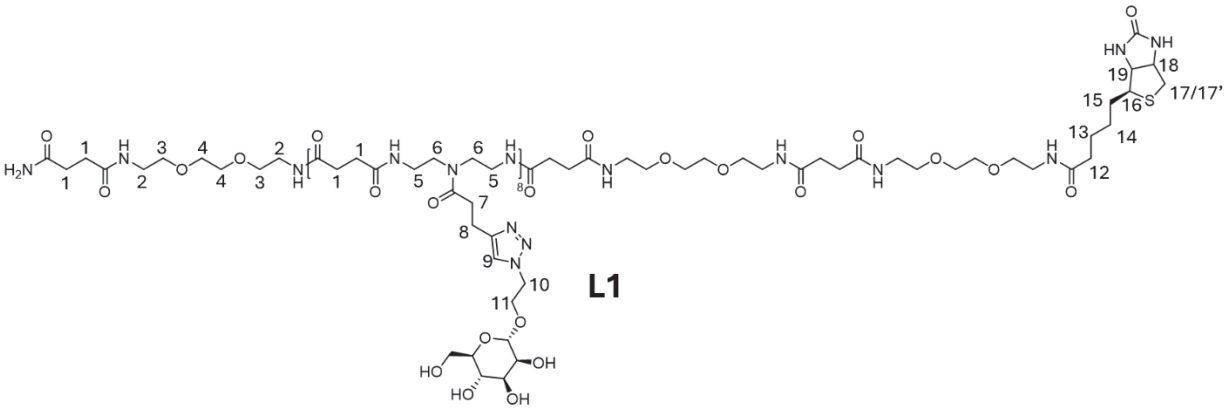

RP-HPLC: 100 % A to 0 % A in 30 min at 25 °C: t_R = 6.7 min, rel. purity: 90 %.

ESI-MS: calculated for $C_{208}H_{343}N_{57}O_{86}S$: 1683.5 $[M+3H]^{3+}$, 1262.8 $[M+4H]^{4+}$, 1010.5 $[M+5H]^{5+}$ 842.2 $[M+6H]^{6+}$ 722.1 $[M+7H]^{7+}$; found: 1684.3 $[M+3H]^{3+}$, 1263.3 $[M+4H]^{4+}$, 1010.9 $[M+5H]^{5+}$ 842.6 $[M+6H]^{6+}$ 722.3 $[M+7H]^{7+}$.

MALDI-TOF-MS: calculated for $C_{200}H_{313}N_{53}O_{56}S$: 5070.4 $[M+Na]^+$; found: 5073.5 $[M+Na]^{+\cdot}$

^{1}H-NMR (600 MHz, MeOH-*d4*/D_2O): δ 7.84 (s, 8H, 9), 4.73 (m, $CH_{mannose}$, overlap with solvent peak), 4.65-4.56 (m, 10, overlap with solvent peak), 4.53 (dd, ^3J = 7.9, 4.3 Hz, 1H,18), 4.34 (dd, ^3J = 7.9, 4.5 Hz, 1H, 19), 4.14-4.05 (m, 8H, $CH_{mannose}$), 3.90-3.84 (m, 8H, $CH_{mannose}$), 3.79-3.32 (m, 142H, 2, 3, 4, 5, 6, 11, $CH_{mannose}$, overlap with solvent peak), 3.23 (dt, ^3J = 9.5, 5.3 Hz,1H ,16), 3.15-3.08 (m, 8H, $CH_{mannose}$), 3.04-2.96 (m, 16H, 8), 2.94 (dd, ^2J = 12.9 Hz, ^3J = 5.0 Hz, 1H, 17), 2.85-2.76 (m, 16H, 7), 2.72 (d, ^2J = 12.6 Hz, 1H, 17'), 2.57-2.37 (m, 44H, 1), 2.24 (t, ^3J = 7.4 Hz, 2H, 12), 1.79-1.52 (m, 4H, 13, 15), 1.47-1.39 (m, 2H, 14) ppm.

Yield: 70 %

Compound L2:

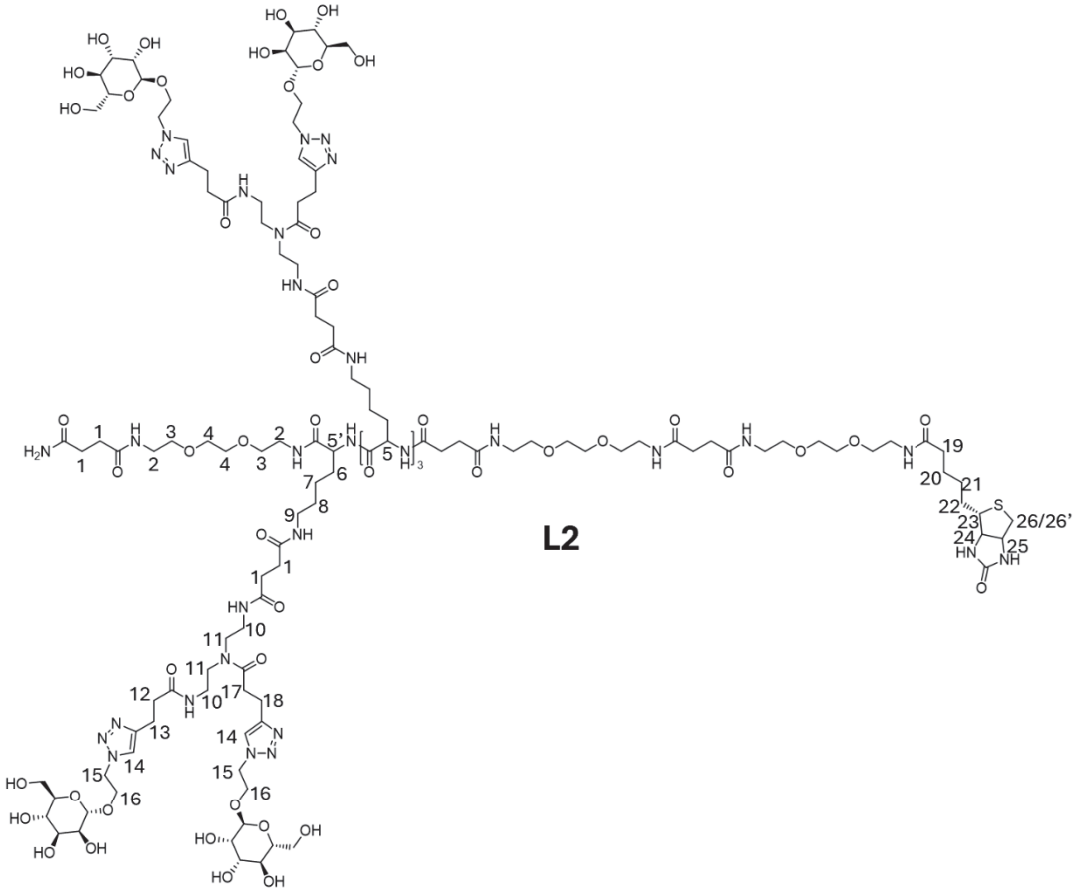

RP-HPLC: 100 % A to 0% A in 30 min at 25 °C: t_R = 6.7 min, rel. purity: 85 %.

ESI-MS: calculated for $C_{200}H_{331}N_{53}O_{82}S$: 1607.4 $[M+3H]^{3+}$, 1205.8 $[M+4H]^{4+}$, 964.9 $[M+5H]^{5+}$ 804.2 $[M+6H]^{6+}$; found: 1608.2 $[M+3H]^{3+}$, 1206.2 $[M+4H]^{4+}$, 965.2 $[M+5H]^{5+}$ 804.7 $[M+6H]^{6+}$.

MALDI-TOF-MS: calculated for $C_{200}H_{331}N_{53}O_{82}S$: 4842.1 $[M+Na]^+$; found: 4845.8 $[M+Na]^+$.

^{1}H-NMR (600 MHz, MeOH-*d4*/D_2O): δ 7.87-7-71 (m, 8H, 14), 4.73 (m, $CH_{mannose}$, overlap with solvent peak), 4.61-4.57 m, 15, overlap with solvent peal), 4.53 (dd, ^3J = 8.1, 4.7 Hz, 2H, 25, overlap with solvent peak), 4.34 (dd, ^3J = 7.9, 4.5 Hz, 1H, 24), 4.29-4.20 (m, 3H, 5), 4.19-4.14 (m, 1H, 5'), 4.14-4.04 (m, 8H, $CH_{mannose}$), 3.91-3.82 (m, 8H, $CH_{mannose}$), 3.8-3.33 (m, 110H, 2,3,4,10,11,16,$CH_{mannose}$, overlap with solvent peak), 3.23 (dt, ^3J = 9.5, 5.2 Hz,1H ,23), 3.18-3.10 (m, 16H, 9, $CH_{mannose}$), 3.03-2.9 (m, 17H, 13, 18, 26), 2.82-2.7 (m, 9H, 17, 26', overlap with impurity peaks), 2.66-2.42 (m, 36H, 1, 12), 2.24 (t, ^3J = 7.4 Hz, 2H, 19), 1.89-1.28 (m, 31H, 6, 7, 8, 20, 21, 22) ppm.

Yield: 70 %

Compound C9:

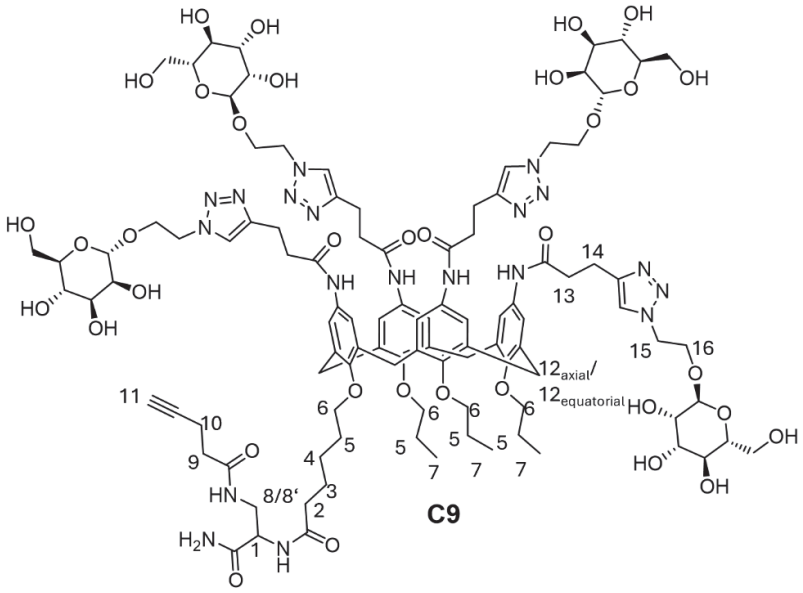

RP-HPLC: 100 % A to 0 % A in 30 min at 25° C: t_R = 14.5 min, rel. purity: 94 %.

ESI-MS: calculated for $C_{103}H_{142}N_{19}O_{35}$: 1103.5 $[M+2H]^{2+}$, 736.0 $[M+3H]^{3+}$, 552.3 $[M+4H]^{4+}$; found: 1104.4 $[M+2H]^{2+}$, 736.6 $[M+3H]^{3+}$, 552.7 $[M+4H]^{4+}$.

MALDI-TOF-MS: calculated for $C_{103}H_{142}N_{19}O_{35}$: 2231.0 $[M+Na]^+$; found: 2229.2 $[M+Na]^+$.

^{1}H-NMR (600 MHz, MeOH-*d4*/D_2O): δ 7.90-7.8 (m, 4H, Triazol-H), 7.12-6.81 (m, 8H, Aryl-H), 4.73 (m, $CH_{mannose}$, overlap with solvent peak), 4.64-4.55 (m, 10H, 15, overlap with solvent peak), 4.50 (dd, ^3J = 8.2, 4.8 Hz, 1H, 1), 4.46-4.39 (m, 4H, 12_{axial}), 4.12-4.04 (m, 4H, $CH_{mannose}$), 3.93-3.46 (m, 43H, 8, 8', 6, 16, $CH_{mannose}$, PEG impurities), 3.19-3.09 (m, 8H, $12_{equatorial}$, $CH_{mannose}$), 3.06-3.0 (m, 8H, 14), 2.74-2.60 (m, 8H, 13), 2.47-37 (m, 4H, 9, 10), 2.31 (t, ^3J = 7.6 Hz, 2H, 2), 2.28 (t, ^3J = 2.5 Hz, 1H, 11), 2.0-1.89 (m, 8H, 5), 1.70 (p, ^3J = 7.6 Hz, 2H, 3), 1.51-1.42 (m, 2H, 4), 1.01 (t, ^3J = 7.4 Hz, 9H, 7) ppm.

Yield: 50 %

Compound C10:

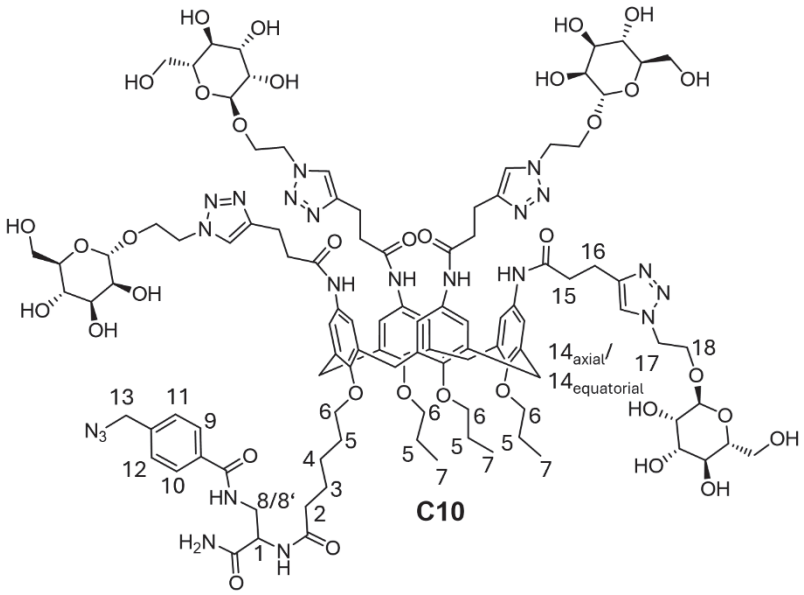

RP-HPLC: 100 % A to 0 % A in 30 min at 25 °C: t_R = 15.1 min, rel. purity: 89 %.

ESI-MS: calculated for $C_{106}H_{144}N_{22}O_{34}$: 1143.5 $[M+2H]^{2+}$, 762.6 $[M+3H]^{3+}$, 572.3 $[M+4H]^{4+}$; found: 1143.6 $[M+2H]^{2+}$, 763.0 $[M+3H]^{3+}$, 572.4 $[M+4H]^{4+}$.

MALDI-TOF-MS: calculated for $C_{106}H_{144}N_{22}O_{34}$: 2308.0 $[M+Na]^+$; found: 2308.4 $[M+Na]^+$.

^{1}H-NMR (300 MHz, MeOH-*d4*/D_2O): δ 7.89-7.77 (m, 6H, Triazol-H, 9, 10), 7.37 (d, 2H, ^3J = 8.3 Hz, 11, 12), 7.04-6.76 (m, 8H, Aryl-H), 4.73 (m, $CH_{mannose}$, overlap with solvent peak), 4.63-4.48 (m, 10H, 17, overlap with solvent peak), 4.44-4.29 (m, 6H, 13, 14_{axial}), 4.14-4.01 (m, 4H, $CH_{mannose}$), 3.91-3.54 (m, 45H, 8, 8', 6, 18, $CH_{mannose}$, PEG impurities), 3.21-2.95 (m, 16H, $14_{equatorial}$, 16, $CH_{mannose}$), 2.76-2.57 (m, 8H, 15), 2.31 (t, ^3J= 7.3 Hz, 2H, 2), 1.96-1.78 (m, 8H, 5), 1.72-1.55 (m, 2H, 3), 1.44-1.28 (m, 2H, 4), 1.04-0.84 (m, 10H, 7) ppm.

It is assumed that the signal of proton 1 overlaps with the solvent peak at around 5.1 - 4.5 ppm.

Yield: 65 %

Compound C11:

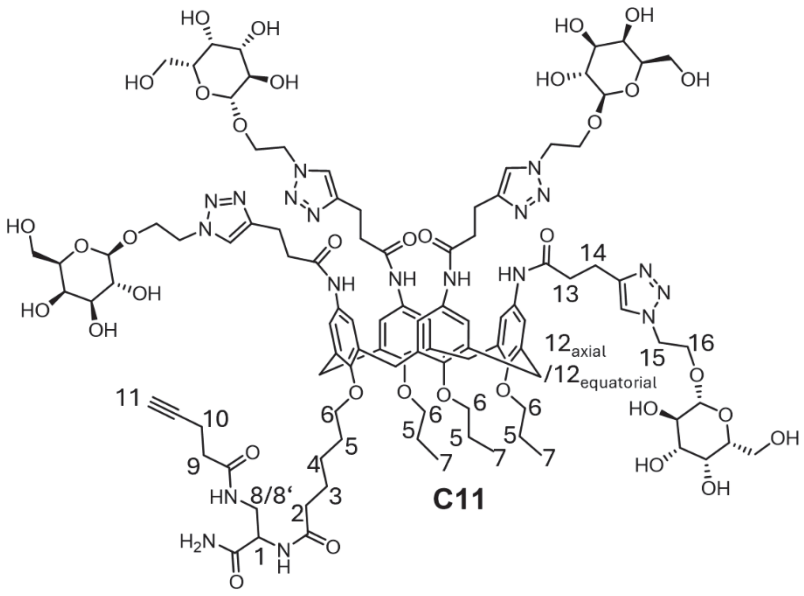

RP-HPLC: 100 % A to 0 % A in 30 min at 25 °C: t_R = 14.0 min, rel. purity: 87 %.

ESI-MS: calculated for $C_{103}H_{142}N_{19}O_{35}$: 1103.5 $[M+2H]^{2+}$, 736.0 $[M+3H]^{3+}$, 552.3 $[M+4H]^{4+}$; found: 1104.4 $[M+2H]^{2+}$, 736.6 $[M+3H]^{3+}$, 552.8 $[M+4H]^{4+}$.

MALDI-TOF-MS: calculated for $C_{103}H_{142}N_{19}O_{35}$: 2231.0 $[M+Na]^+$; found: 2230.3 $[M+Na]^+$.

^{1}H-NMR (300 MHz, MeOH-*d*/D_2O): δ 8.06-7.81(m, 4H, Triazol-H), 7.03-6.76 (m, 8H, Aryl-H), 4.63-4.56 (m, 11H, 15, overlap with solvent peak), 4.50 (dd, 2H, ^{3}J=7.9, 4.9 Hz, 1, overlap with other signals), 4.42 (d, 4H, ^{2}J = 13.4 Hz, 12_{axial}), 4.34-4.16 (m, 8H, $CH_{galactose}$), 4.07-3.43 (m, 48H, 8, 8', 6, 16, $CH_{galactose}$, PEG impurities), 3.14 (d, 4H, ^{2}J = 12.5 Hz, $12_{equatorial}$), 3.07-2.90 (m, 8H, 14), 2.75-2.54 (m, 8H, 13), 2.45-2.25 (m, 7H, 9, 10, 11, 2), 2.06-1.81 (m, 8H, 5, overlap with acetate), 1.77-1.61 (m, 2H, 3), 1.55-1.36 (m, 2H, 4), 1.02 (t, ^{3}J = 7.5 Hz, 9H, 7) ppm.

Yield: 50 %

Compound C12

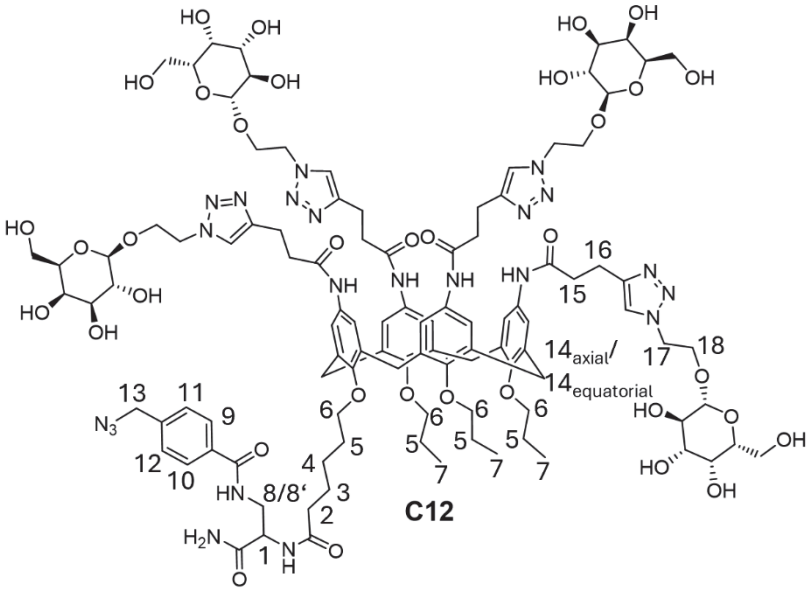

RP-HPLC: 100 % A to 0 % A in 30 min at 25 °C: t_R = 15.2 min, rel. purity: 86 %.

ESI-MS: calculated for $C_{106}H_{144}N_{22}O_{34}$: 1143.5 $[M+2H]^{2+}$, 762.7 $[M+3H]^{3+}$, 572.3 $[M+4H]^{4+}$; found: 1143.8 $[M+2H]^{2+}$, 763.0 $[M+3H]^{3+}$, 572.5 $[M+4H]^{4+}$.

MALDI-TOF-MS: calculated for $C_{106}H_{144}N_{22}O_{34}$: 2308.0 $[M+Na]^+$; found: 2308.2 $[M+Na]^+$.

^{1}H-NMR (600 MHz, MeOH-*d4*/D_2O): δ 7.94-7.86 (m, 4H, Triazol-H), 7.80 (d, 2H, ^3J= 8.3 Hz, 9, 10), 7.37 (d, 2H, ^3J = 8.3 Hz, 11, 12), 6.99-6.74 (m, 8H, Aryl-H), 4.63-4.53 (m, 8H, 17, overlap with solvent peak), 4.44-4.34 (m, 2H, 13), 4.37-4.32 (m, 4H, 14_{axial}), 4.31-4.26 (m, 4H, $CH_{galactose}$), 4.25-4.17 (m, 4H, $CH_{galactose}$), 4.04-3.94 (m, 4H, $CH_{galactose}$) 3.88-3.49 (m, 41H, 8, 8', 6, 18, $CH_{galactose}$, PEG impurities), 3.18-3.06 (m, 4H, $14_{equatorial}$) 3.05-2.91 (m, 8H, 16), 2.73-2.52 (m, 8H, 15), 2.30 (t, ^3J= 7.5 Hz, 2H, 2), 1.95-1.8 (m, 8H, 5), 1.69-1.58 (m, 2H, 3), 1.41-1.33 (m, 2H, 4), 1.03-0.9 (m, 10H, 7) ppm.

It is assumed that the signal of proton 1 overlaps with the solvent peak at around 5.1 - 4.6 ppm.

Yield: 65 %

Compound C13d:

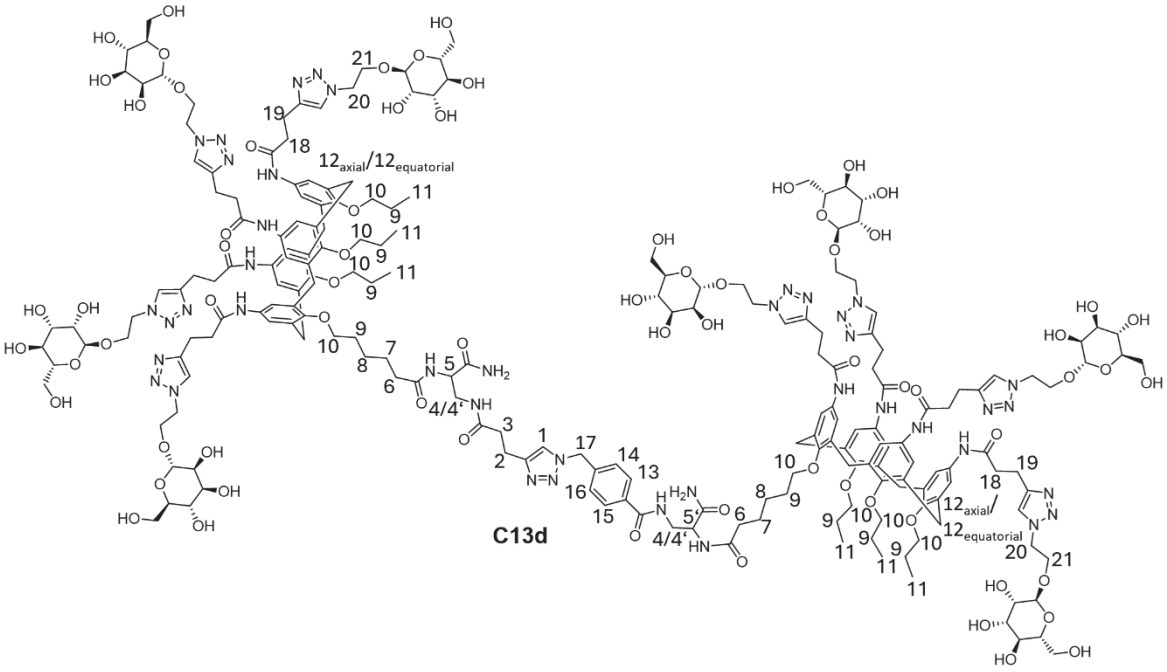

RP-HPLC: 100 % A to 0 % A in 30 min at 25 °C: t_R = 14.2 min, rel. purity: ≥ 95%.

Preparative Purification: 70% A to 50% A in 15 min at 25° C.

ESI-MS: calculated for $C_{209}H_{287}N_{41}O_{70}$: 1498.0 $[M+3H]^{3+}$, 1123.8 $[M+4H]^{4+}$, 899.2 $[M+5H]^{5+}$; found: 1498.6 $[M+3H]^{3+}$, 1124.2 $[M+4H]^{4+}$, 899.6 $[M+5H]^{5+}$.

MALDI-TOF-MS: calculated for $C_{209}H_{287}N_{41}O_{70}$: 4514.0 $[M+Na]^+$; found: 4517.1 $[M+Na]^+$.

^{1}H-NMR (300 MHz, MeOH-*d4*/D_2O): δ 8.24-6.6 (m, 29H, Aryl-H, Triazol-H, 1, 13, 14, 15, 16), 5.47 (s, 3H, 17, overlap with solvent peak), 4.61-4.23 (m, 5, 5', 12_{axial}, 20, $CH_{mannose}$, overlap with solvent peak), 4.17-3.99 (8H, $CH_{mannose}$), 4.0-3.44 (m, 73H, 4, 4', 10, 21, $CH_{mannose}$, PEG impurities), 3.22-2.41 (m, 52H, 2, 3, $12_{equatorial}$, 18, 19, $CH_{mannose}$), 2.34-2.21 (m, 4H, 6), 1.98-1.77 (m, 16H, 9), 1.73-1.54 (m, 4H, 7), 1.48-1.23 (m, 5H, 8, impurities), 1.03-0.85 (m, 20H, 11, impurities) ppm.

Yield: 20 %

Compound C14d:

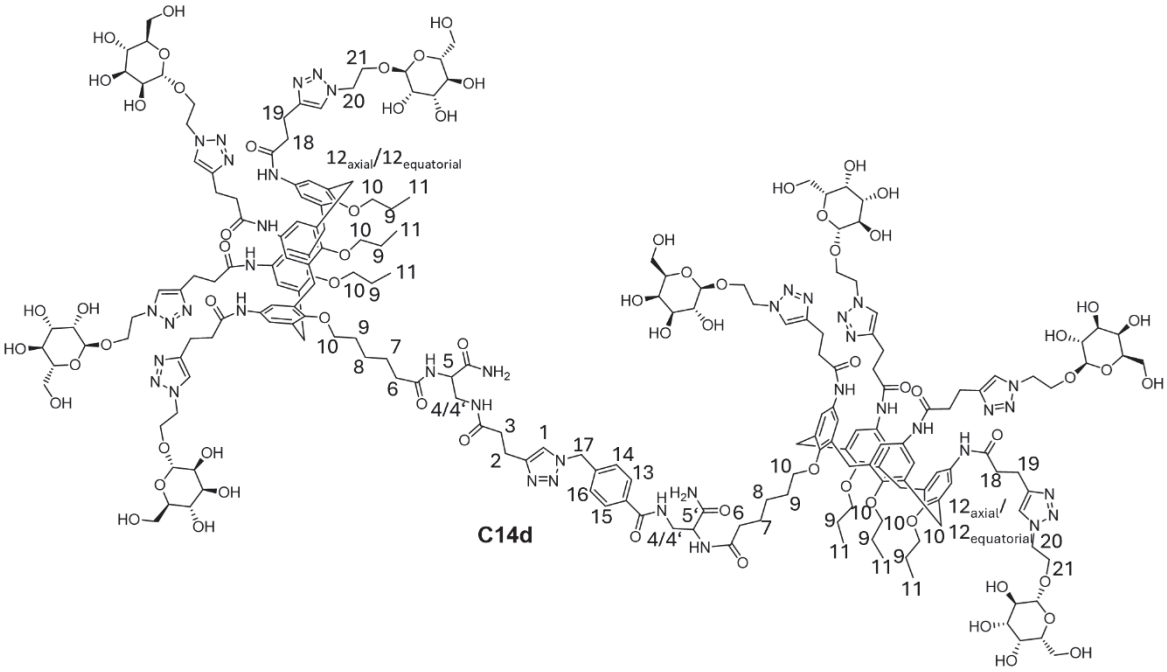

RP-HPLC: 100 % A to 0 % A in 30 min at 25 °C: t_R = 14.09 min, rel. purity: ≥ 95 %.

Preparative Purification: 70 % A to 50 % A in 15 min at 25 °C.

ESI-MS: calculated for $C_{209}H_{287}N_{41}O_{70}$: 1498.0 $[M+3H]^{3+}$, 1123.8 $[M+4H]^{4+}$, 899.2 $[M+5H]^{5+}$, 749.5 $[M+6H]^{6+}$; found: 1498.6 $[M+3H]^{3+}$, 1124.2 $[M+4H]^{4+}$, 899.6 $[M+5H]^{5+}$.

MALDI-TOF-MS: calculated for $C_{209}H_{287}N_{41}O_{70}$: 4514.0 $[M+Na]^+$; found: 4517.1 $[M+Na]^+$.

^{1}H-NMR (600 MHz, MeOH-*d4*/D_2O): δ 8.53 (bs, 4H, formic acid), 7.95-7.89 (m, 4H, Triazole-H), 7.84-7.78 (m, 4H, Triazole-H), 7.85 (d, ^{3}J = 8.5 Hz, 2H, 13, 15), 7.62 (s, 1H, 1), 7.28 (d, ^{3}J=8.5 Hz, 2H, 14, 16), 7.00-6.76 (m, 16H, Aryl-H), 5.46 (s, 2H, 17), 4.74-4.72 (m, 6H, $CH_{mannose,}$ overlap with solvent peak), 4.62-4.52 (m, 16H, 20, overlap with solvent peak), 4.47 (dd, ^{3}J=7.7, 7.4 Hz, 1H, 5), 4.43-4.25 (m, 12H, 12_{axial}, $CH_{galactose}$) 4.24-4.17 (m, 4H, $CH_{galactose}$), 4.10-4.02 (m, 4H, $CH_{mannose}$), 4.01-3.94 (m, 4H, $CH_{galactose}$), 3.88-3.49 (m, 73H, 4, 4', 21, 10, $CH_{galactose}$, $CH_{mannose}$, impurities), 3.16-2.88 (m, 31H, 3, $12_{equatoial}$, 19, $CH_{mannose}$), 2.71-2.57 (m, 16H, 18), 2.51 (t, ^{3}J=7.7 Hz, 2H, 2), 2.31-2.24 (m, 4H, 6), 1.94-1.8 (m, 17H, 9), 1.7-1.6 (m, 6H, 7), 1.45-1.33 (m, 4H, 8), 1.00-0.90 (m, 19H, 11) ppm.

It is assumed that the signal of proton 5' overlaps with the solvent peak at around 5.1 -4.60 ppm.

Unidentified impurities can be found in the aliphatic field from 2.25 to 0.85 ppm. These might be due to remaining diethyldithiocarbamate. An additional dialysis purification is advisable.

Yield: 20 %

Compound C15d:

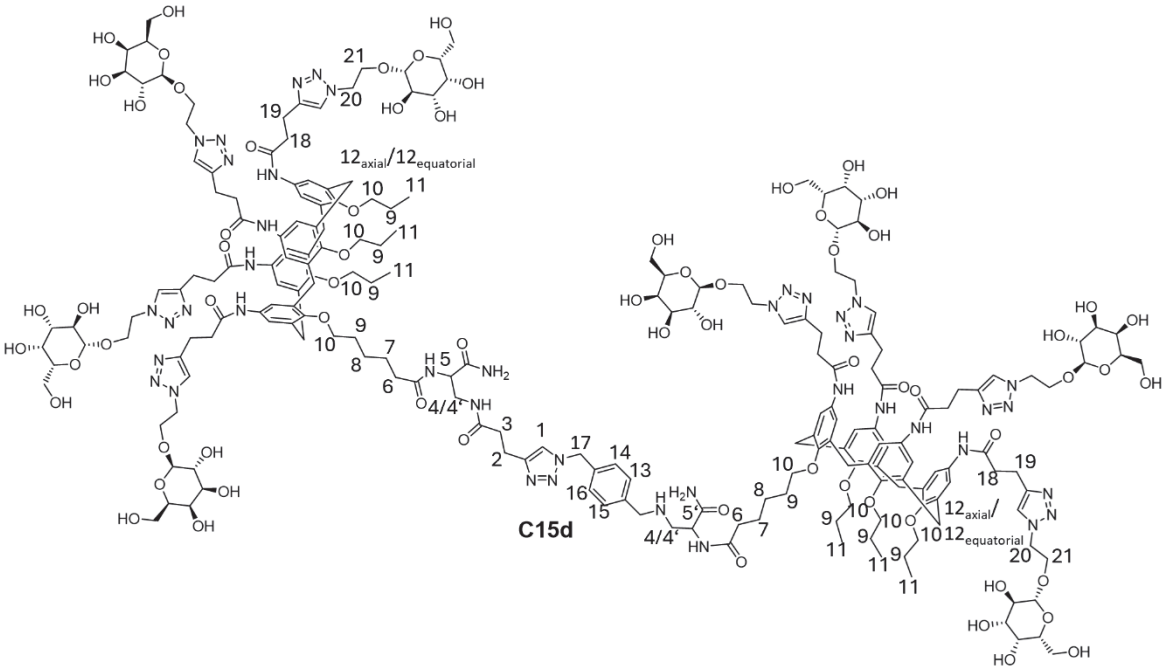

RP-HPLC: 100 % A to 0% A in 30 min at 25 °C: t_R = 14.0 min, rel. purity: ≥ 95 %.

Preparative Purification: 70 % A to 50 % A in 15 min at 25 °C.

calculated for $C_{209}H_{287}N_{41}O_{70}$: 1498.0 $[M+3H]^{3+}$, 1123.8 $[M+4H]^{4+}$, 899.2 $[M+5H]^{5+}$, 749.5 $[M+6H]^{6+}$; found: 1498.7 $[M+3H]^{3+}$, 1124.4 $[M+4H]^{4+}$, 899.6 $[M+5H]^{5+}$, 749.8 $[M+6H]^{6+}$.

MALDI-TOF-MS: calculated for $C_{209}H_{287}N_{41}O_{70}$: 4514.0 $[M+Na]^+$; found: 4517.1 $[M+Na]^+$.

^{1}H-NMR (300 MHz, MeOH-*d4*/D_2O): δ 8.09-6-64 (m, 29H, Aryl-H, Triazole-H, 1, 13, 14, 15, 16), 5.44 (s, 2H, 17, overlap with solvent peak), 4.63-4.51 (m, 16H, 20, overlap with solvent peak), 4.41-4.14 (m, 24H, 12_{axial}, $CH_{galactose}$) 4.05-3.64 (m, 77, 4, 4', 10, 21, $CH_{galactose}$), 3.20-2.82 (m, 26H, $12_{equatorial}$, 19, 2), 2.71-2.42 (m, 18H, 18, 3), 2.34-2.21 (m, 4H, 6), 1.98-1.74 (m, 16H, 9), 1.72-1.52 (m, 5H, 7), 1.46-1.2 (m, 8H, 8, impurities), 1.07-0.77 (m, 18H, 11) ppm.
It is assumed that the signals of proton 5 and 5' overlap with the solvent peak.

Yield: 25 %

Compound C16:

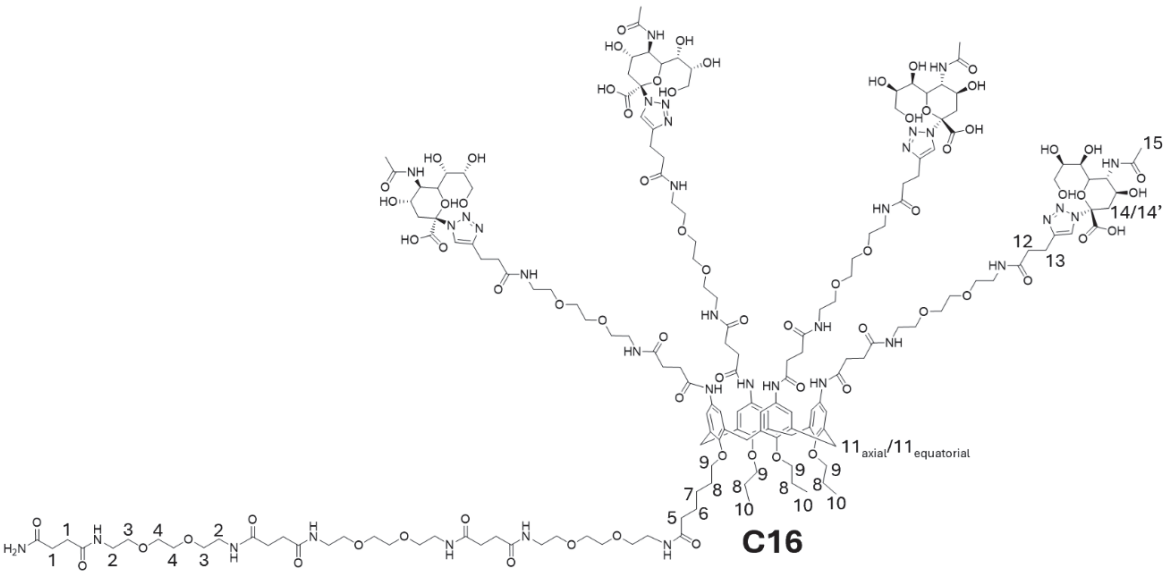

RP-HPLC: 100 % A to 0 % A in 30 min at 25 °C: t_R = min, rel. purity: 55 % (It cannot be fully clarified whether the cleavage of Sia ligands occurs exclusively or partially during HPLC analysis).

ESI-MS: calculated for $C_{177}H_{271}N_{35}O_{69}$: 1996.4 $[M+2H]^{2+}$, 1331.3 $[M+3H]^{3+}$, 998.7 $[M+4H]^{4+}$, found: 1997.9 $[M+2H]^{2+}$, 1331.9 $[M+3H]^{3+}$, 999.4 $[M+4H]^{4+}$.

^{1}H-NMR (300 MHz, MeOH-*d4*/D_2O): 8.03 (bs, 4H, Triazole-H), 6.93 (bs, 7H, Aryl-H), 4.49 (d, ^2J = 13.0 Hz, 4H, 11_{axial}), 4.17-3.43 (m, 125H, 2, 3, 4, 9, CH_{Sia}, overlap with solvent peak), 3.2 (d, ^2J = 13.8 Hz, 5H, $11_{equatorial}$, overlap with other peaks), 3.13-3.0 (m, 8H, 13), 2.76-2.52 (m, 37H, 1, 12), 2.39-2.22 (m, 8H, 14, 14'), 2.17-1.9 (m, 23H, 5, 8, 15), 1.83-1.73 (m, 2H, 6), 1.72-1.61(m, 2H, 7), 1.15-1.02 (m, 9H, 10) ppm.
Non-identified impurities can be found from 1.6 to 0.9 ppm.

Yield: 12 %

Compound C17:

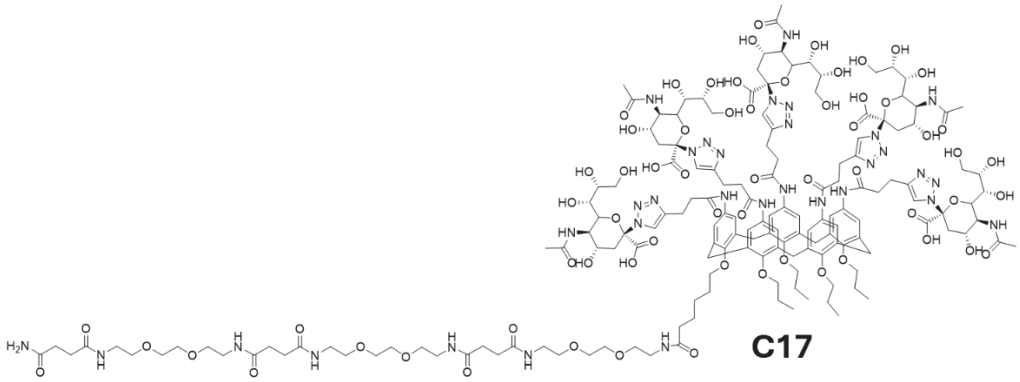

RP-HPLC: 100 % A to 0 % A in 30 min at 25 ° C: t_R = 11.2 min, rel. purity: 85 % (It cannot be fully clarified whether the cleavage of Sia ligands occurs exclusively or partially during HPLC analysis).

ESI-MS: calculated for $C_{163}H_{234}N_{32}O_{63}$: 1824.8 $[M+2H]^{2+}$, 1216. $[M+3H]^{3+}$, 912.90 $[M+4H]^{4+}$, found: 1825.6 $[M+2H]^{2+}$, 1217.3 $[M+3H]^{3+}$, 913.2 $[M+4H]^{4+}$.

^{1}H-NMR: Due to signal broadening the ^{1}H-NMR was analyzed qualitatively (see Figure 92, appendix).

Yield: 20 %

Compound C18:

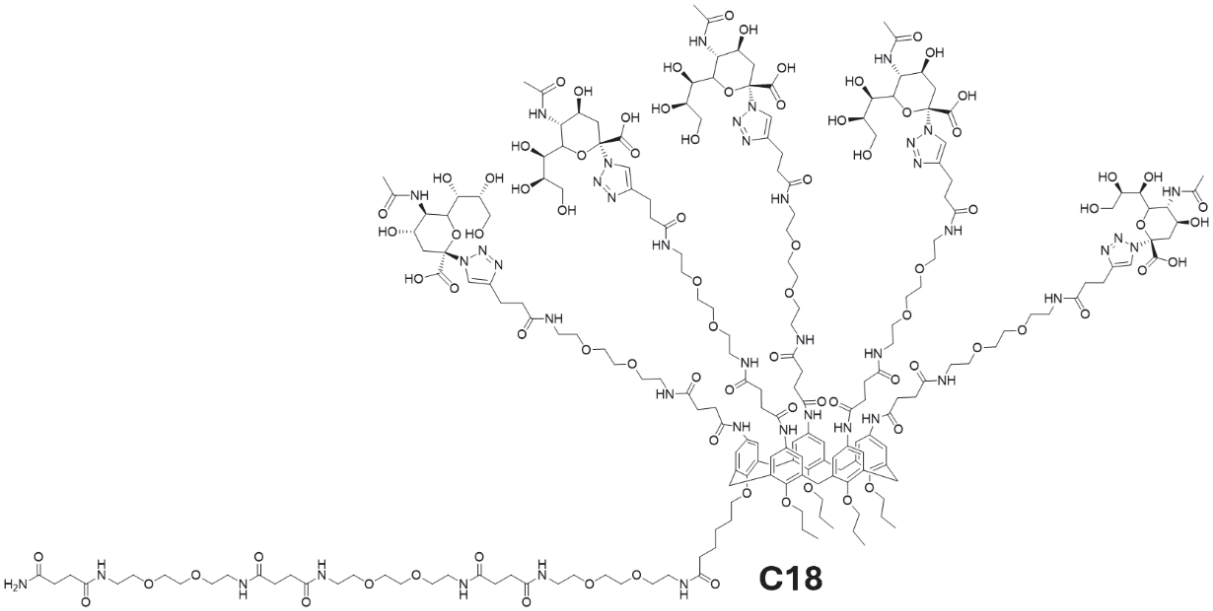

RP-HPLC: 100 % A to 0 % A in 30 min at 25 °C: t_R = 11.1 min, rel. purity: 65 % (It cannot be fully clarified whether the cleavage of Sia ligands occurs exclusively or partially during HPLC analysis).

ESI-MS: calculated for $C_{213}H_{324}N_{42}O_{83}$: 1600.4 $[M+3H]^{3+}$, 1200.6 $[M+4H]^{4+}$, 960.7 $[M+5H]^{5+}$, found: 1601.3 $[M+3H]^{3+}$, 1201.1 $[M+4H]^{4+}$, 961.4 $[M+5H]^{5+}$.

^{1}H-NMR: Due to signal broadening the ^{1}H-NMR was analyzed qualitatively (see Figure 92, appendix).

Yield: 15 %

Compound C19:

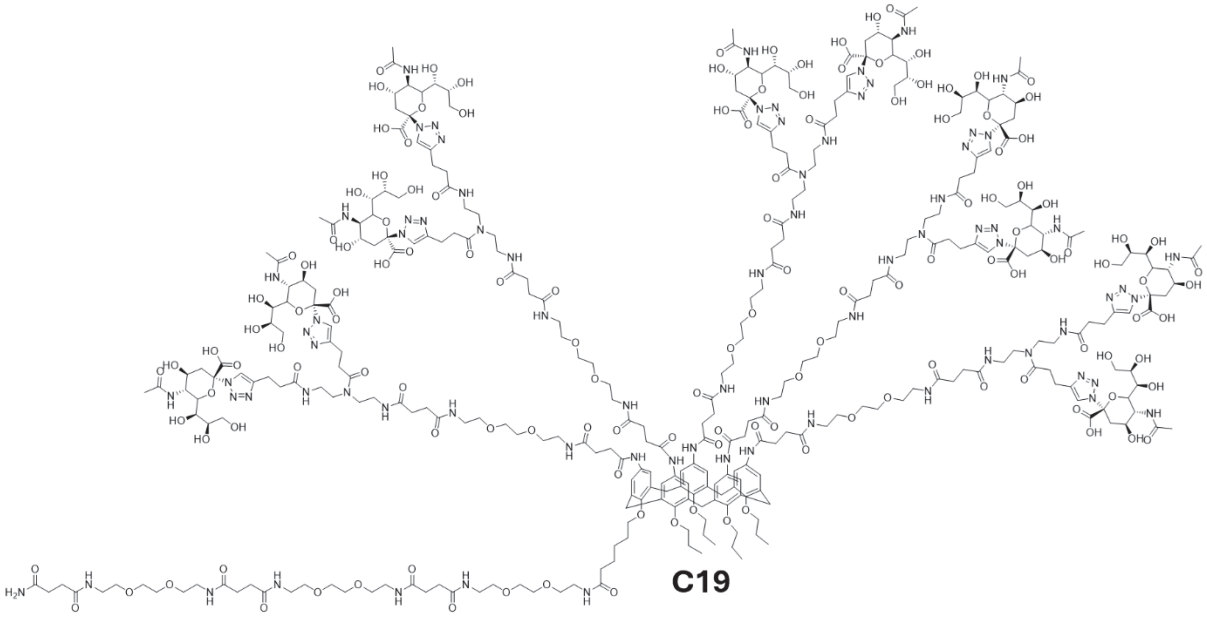

RP-HPLC: 100 % A to 0 % A in 30 min at 25 °C: t_R = 9.5 min, rel. purity: not applicable due to broad overlapping peaks.

ESI-MS: calculated for $C_{333}H_{509}N_{77}O_{138}$: 1559.9 $[M+5H]^{5+}$, 1300.1 $[M+6H]^{6+}$ found: 1560.5 $[M+5H]^{5+}$, 1300.6 $[M+6H]^{6+}$.

ESI-MS (negative mode): calculated for $C_{333}H_{509}N_{77}O_{138}$: 1947.6 $[M-4H]^{4-}$, 1557.9 $[M-5H]^{5-}$, 1298.1 $[M-6H]^{6-}$, 1112.5 $[M-7H]^{7-}$, 973.3 $[M-8H]^{8-}$, 865.1 $[M-9H]^{9-}$, 778.5 $[M-10H]^{10}$; found: 1948.3 $[M-4H]^{4}$, 1558.5 $[M-5H]^{5-}$, 1298.6 $[M-6H]^{6-}$, 1113.1 $[M-7H]^{7-}$, 973.5 $[M-8H]^{8-}$, 865.5 $[M-9H]^{9-}$, 778.7 $[M-10H]^{10-}$.

^{1}H-NMR: Due to signal broadening the ^{1}H-NMR was analyzed qualitatively (see Figure 92, appendix).

Yield: 10 %

6. Appendix

6.1 List of Abbreviations

General Abbreviations:

GNP	gold nanoparticle
e.g.	exempli gratia
ER	endoplasmic reticulum
et al.	et alii
rel.	relative

Chemicals:

Alloc	allyloxycarbonyl
Au	gold
Boc	*tert*-butyloxycarbonyl
BOP	benzotriazol-1-yloxytris(dimethylamino)phosphonium hexafluorophosphate
Ca^{2+}	calcium (II)
$CaCl_2$	calcium chloride
Cu	copper
$CuSO_4$	copper sulfate
D_2O	deuterium oxide
DCM	dichloromethane
DCC	*N*,*N'*-dicyclohexylcarbodiimide
DIPEA	*N*,*N*-diisopropylethylamine
DMF	dimethylformamide
DMSO	dimethyl sulfoxide
EDS	ethylene glycol diamine succinic acid
Fmoc	9-fluorenylmethoxycarbonyl
HATU	*O*-(7-azabenzotriazol-1-yl)-*N*,*N*,*N*',*N*'-tetramethyluronium hexafluorophosphate
HCl	hydrochloric acid
HEPES	4-(2-hydroxyethyl)-1-piperazineethanesulfonic acid
HNO_3	nitric acid
H_2O	water

HOBt	1-hydorxybenzotriazole
LBB	lectin binding buffer
LiCl	lithium chloride
K_2CO_3	potassium carbonate
KOH	potassium hydroxide
MeCN	acetonitrile
MeOH	methanol
$MgSO_4$	magnesium sulfate
Mn^{2+}	manganese (II)
MnCl	manganese chloride
NaH	sodium hydride
NMP	*N*-methyl-2-pyrrolidon
PBS	phosphate buffered saline
PEG	polyethylene glycol
PyBOP	benzotriazol-1-yloxytris(pyrrolidino)phosphonium hexafluorophosphate
$SnCl_2$	tin chloride
TIPS	triisopropylsilane
TDS	triple-bond diethylenetriamine succinic acid
TMB	3,3’-5,5’-tetramethylbenzidine

Proteins:

BSA	Bovine serum albumin
Con A	Concanavalin A
Endo H	Endoglycosidase H
LCA	Lens culinaris agglutinin
NGYL1	*N*-glycanase 1
PNA	Peanut agglutinin
PNGase F	Peptide-*N*-glycosidase F
PSA	Pisum sativum agglutinin
HRP	horse radish peroxidase
RNase B	Ribonuclease B
RCA	Ricinus communis agglutinin

Monosaccharides:

Man	D-mannose
MeMan	methyl-α-D-mannose
Fuc	L-fucose
Gal	D-galactose
GalNAc	D-*N*-acetylgalactosamine
Glc	D-glucose
GlcNAc	D-*N*-acetylglucosamine
Lac	D-lactose
Neu5NAc	*N*-acetylneuraminic acid

Amino Acids:

Asn	L-asparagine
Asp	L-aspartic acid
Thr	L-threonine
Tyr	L-tyrosine
Ser	L-serine
Pro	L-proline

Methods and Instruments:

BCA	bicinchoninic acid assay
CuAAC	copper-catalyzed alkyne-azide cycloaddition
DCS	differentia centrifugal sedimentation
ELISA	enzyme-linked immunosorbent assay
ESI-MS	electrospray ionization mass spectrometry
ITC	isothermal titration calorimetry
MALDI-TOF-MS	matrix-assisted laser desorption ionization – time of flight mass spectrometry
NMR	nuclear magnetic resonance spectroscopy
RP-HPLC	reverse phase-high pressure liquid chromatography
SDS-PAGE	sodium dodecyl sulfate polyacrylamide gel electrophoreses
SPS	solid-phase synthesis
SPPS	solid-phase peptide synthesis

SPPoS	solid-phase polymer synthesis
TEC	thiol-ene click
UV/Vis	ultraviolet/visible

Units and Symbols:

%	percent
°C	degree Celsius
δ	chemical shift
µL	microliter
µM	micromolar
µm	micrometer
cm	centimeter
Da	dalton
eq.	equivalents
g	gram
h	hour
Hz	hertz
IC_{50}	half maximum inhibitory concentration
J	coupling constant
K_A	binding constant
M	moles per liter
m	meter
mAu	milliabsorption units
mg	milligram
MHz	Megahertz
min	minutes
mL	milliliter
mM	millimolar
mmol	millimole
m/z	mass-to-charge ratio
nm	nanometer
pH	potential hydrogenii
ppm	parts per million
RIP	relative inhibitory potency
RIP_{VC}	valency corrected relative inhibitory potency

rpm	rounds per minute
t_R	retention time

6.2 List of Figures

6.3 List of Tables

6.4 Analytics

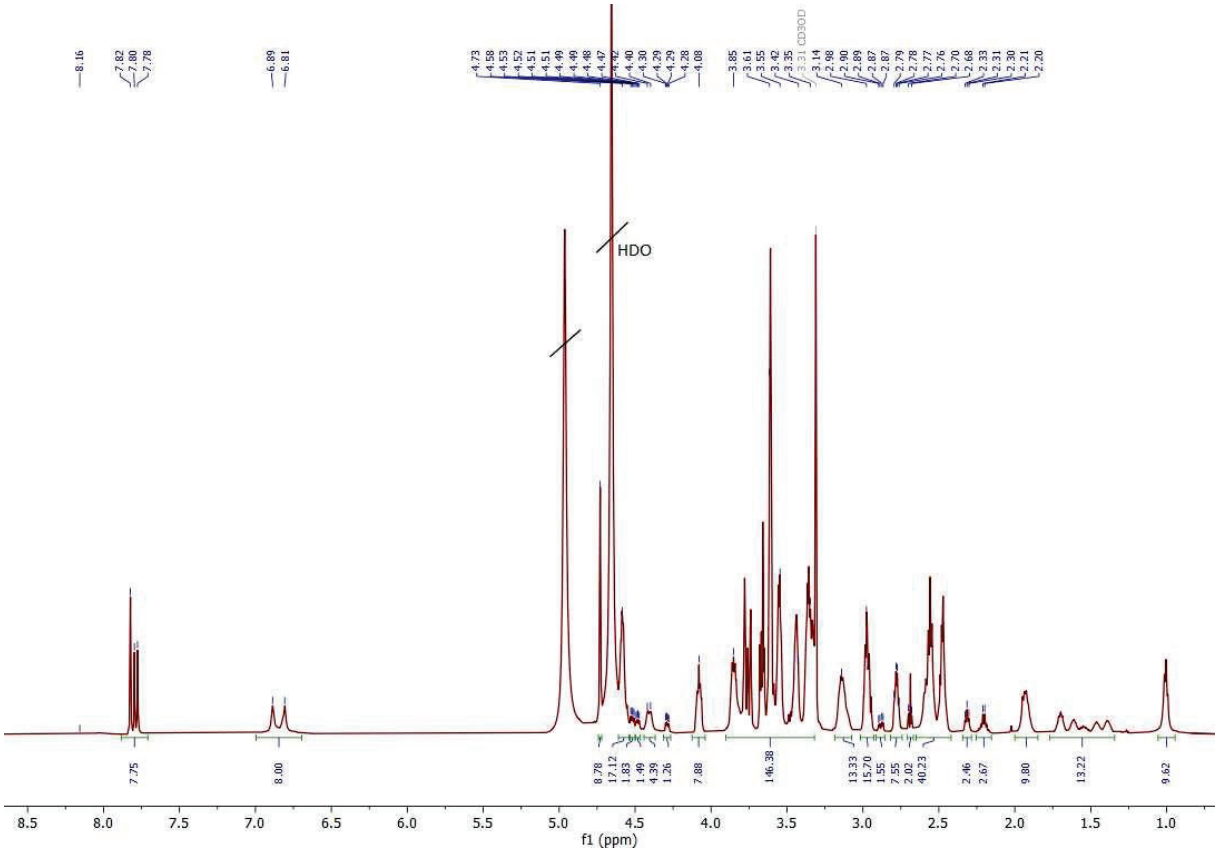

Figure 31: ^{1}H-NMR spectrum (600 MHz) of compound C1b in MeOH-d4/D_2O.

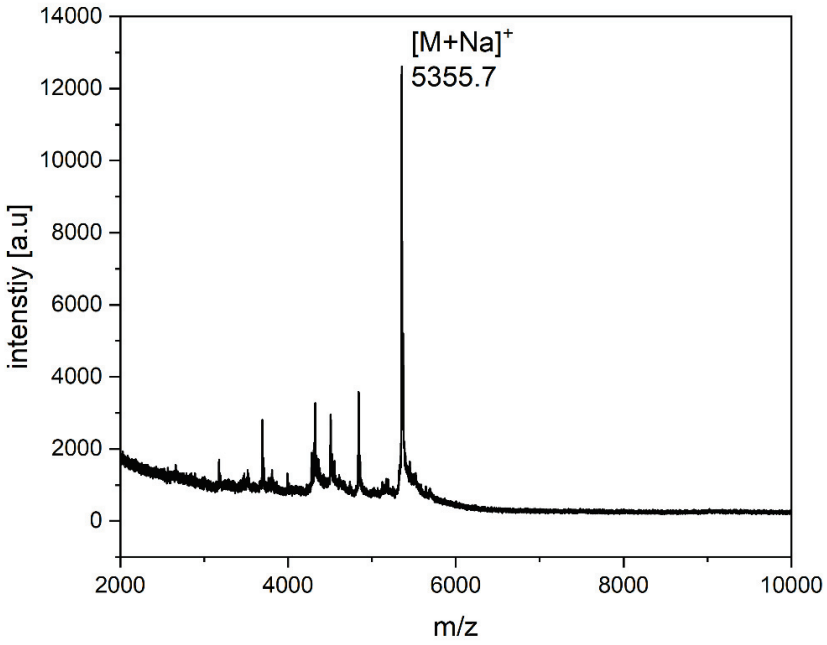

Figure 32: MALD-TOF-MS spectrum of compound C1b.

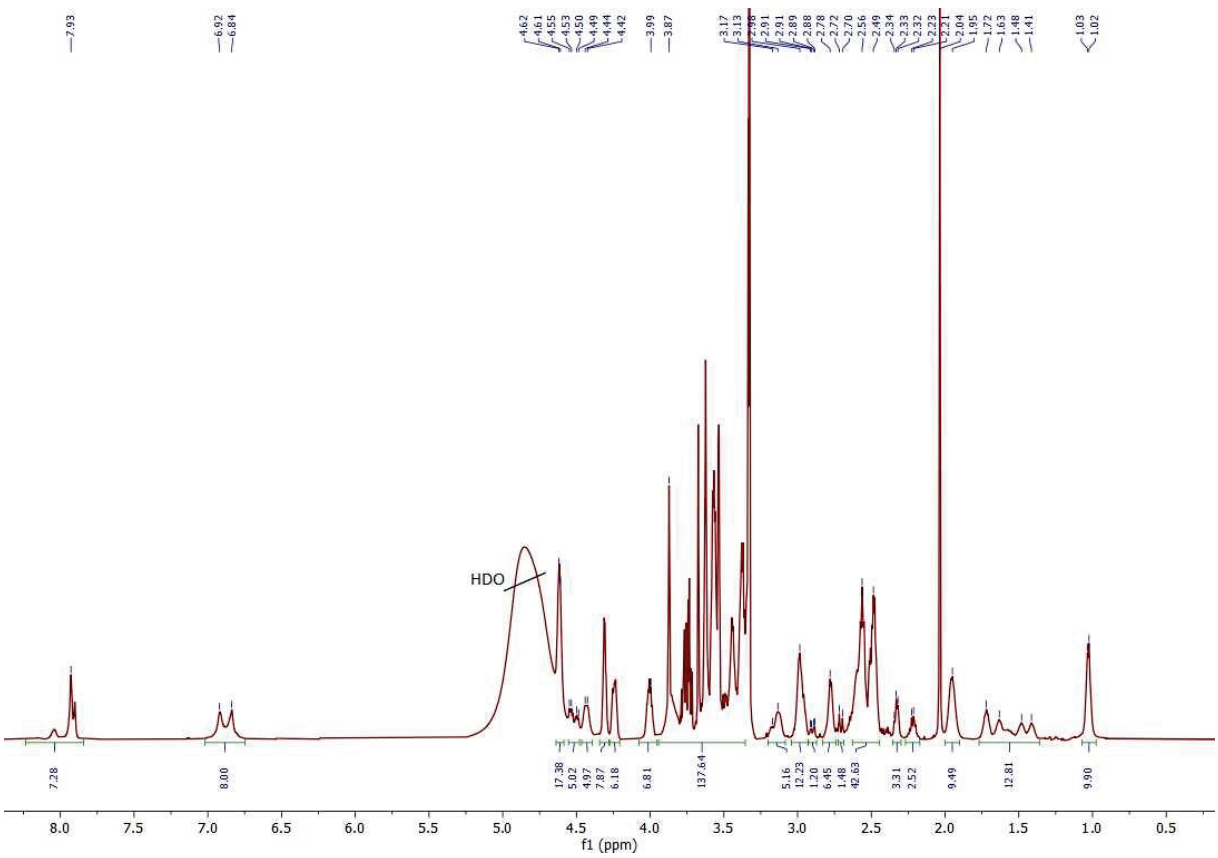

Figure 33: ^{1}H-NMR spectrum (600 MHz) of compound C2b in MeOH-d4/D_2O.

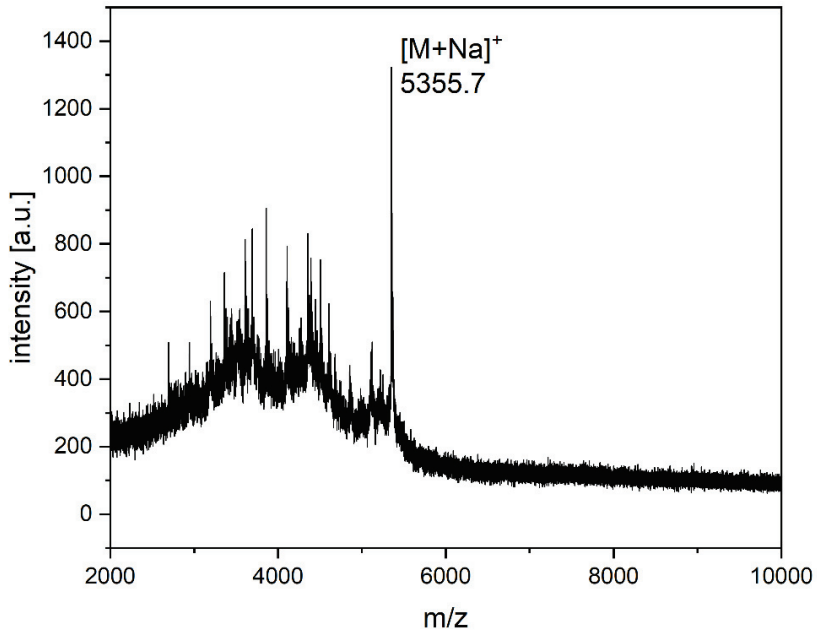

Figure 34: MALD-TOF-MS spectrum of compound C2b.

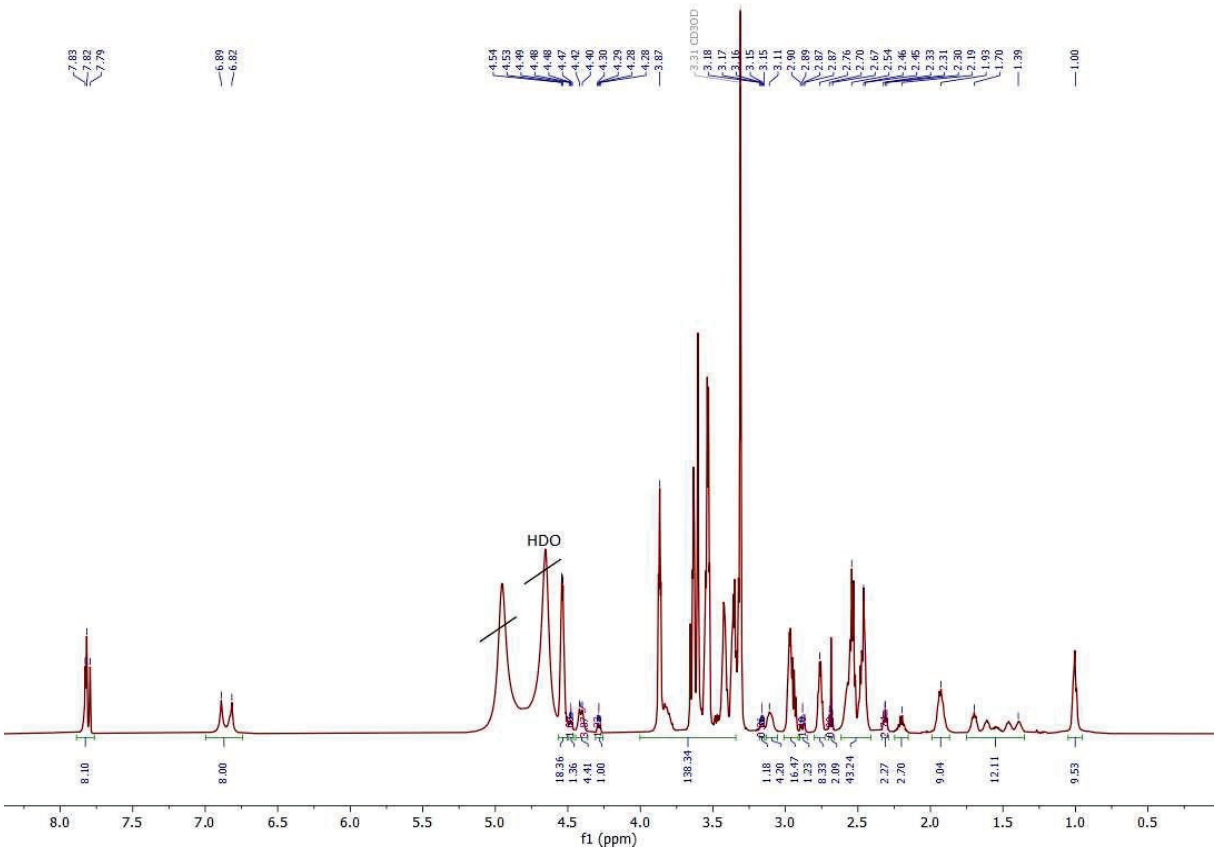

Figure 35: ^{1}H-NMR spectrum (600 MHz) of compound C8b in MeOH-d4/D_2O.

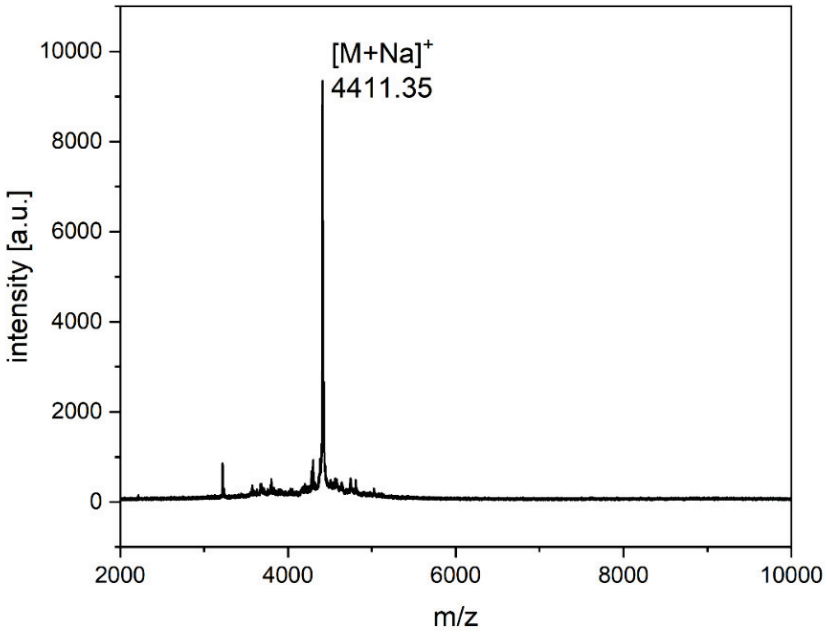

Figure 36: MALD-TOF-MS spectrum of compound C8b.

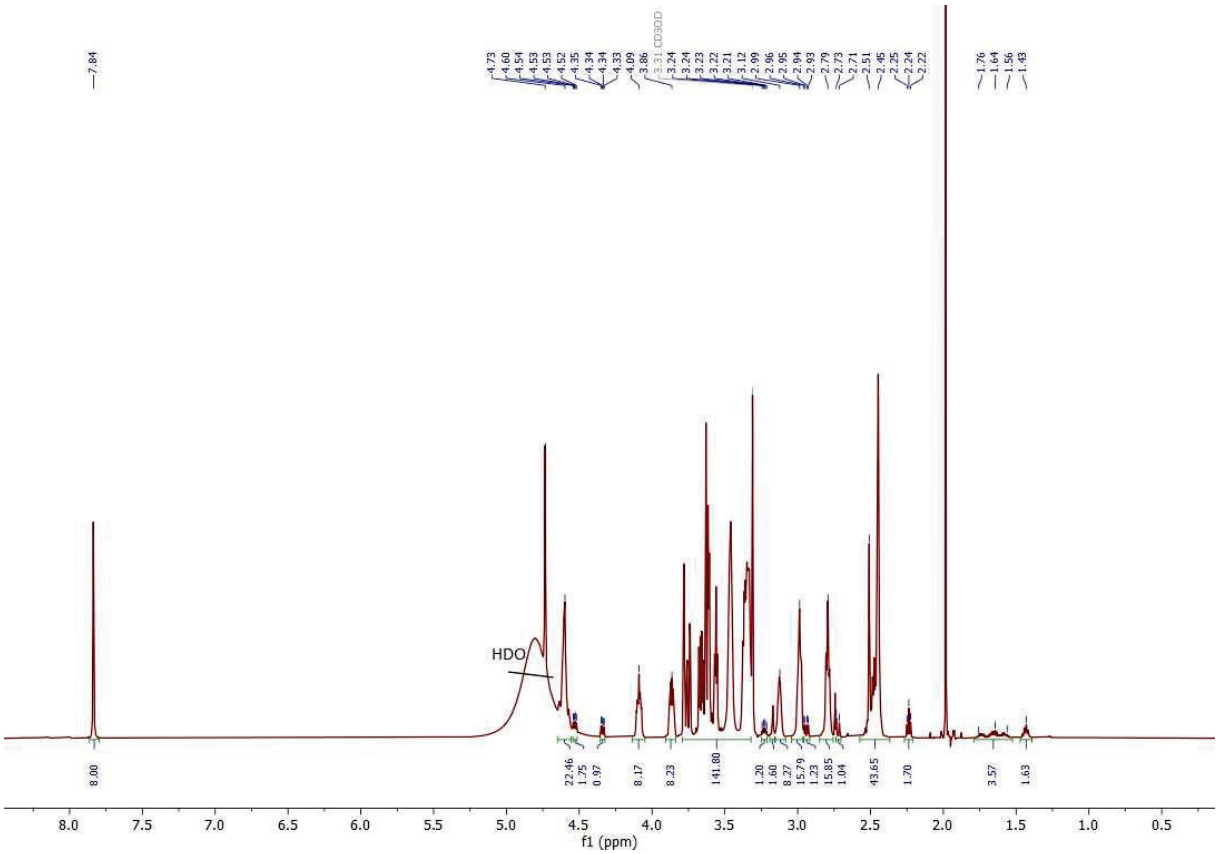

Figure 37: ^{1}H-NMR spectrum (600 MHz) of compound L1 in MeOH-d4/D_2O.

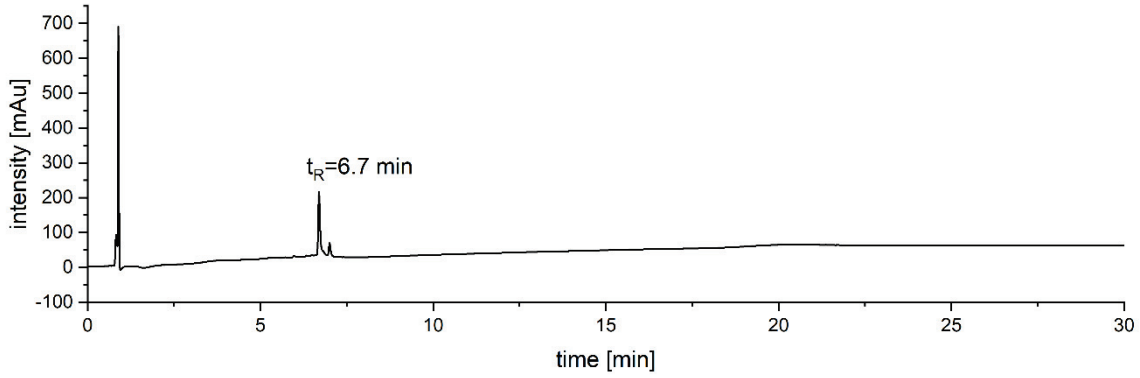

Figure 38: RP-HPLC chromatogram (100 % A to 0 % A in 30 min at 25 °C) of compound L1.

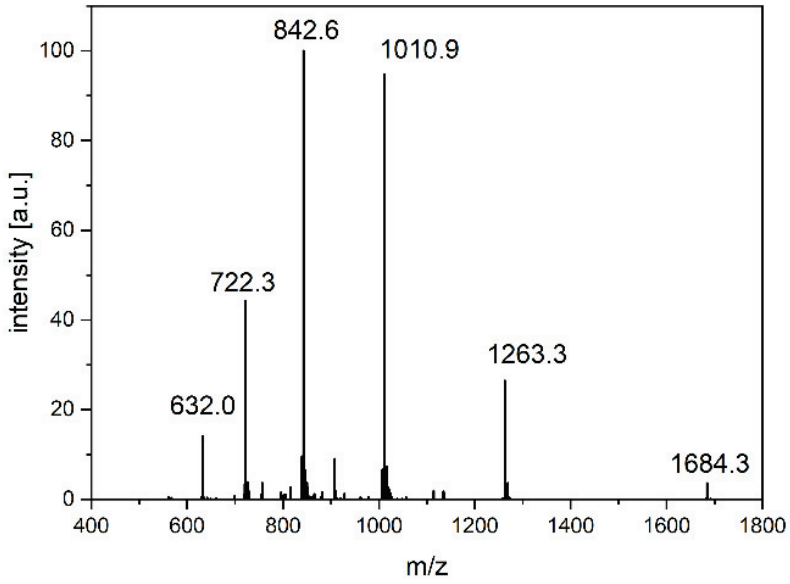

Figure 39: ESI-MS spectrum at t_R = 6.7 min (100 % A to 0 % A in 30 min at 25 °C) of compound L1.

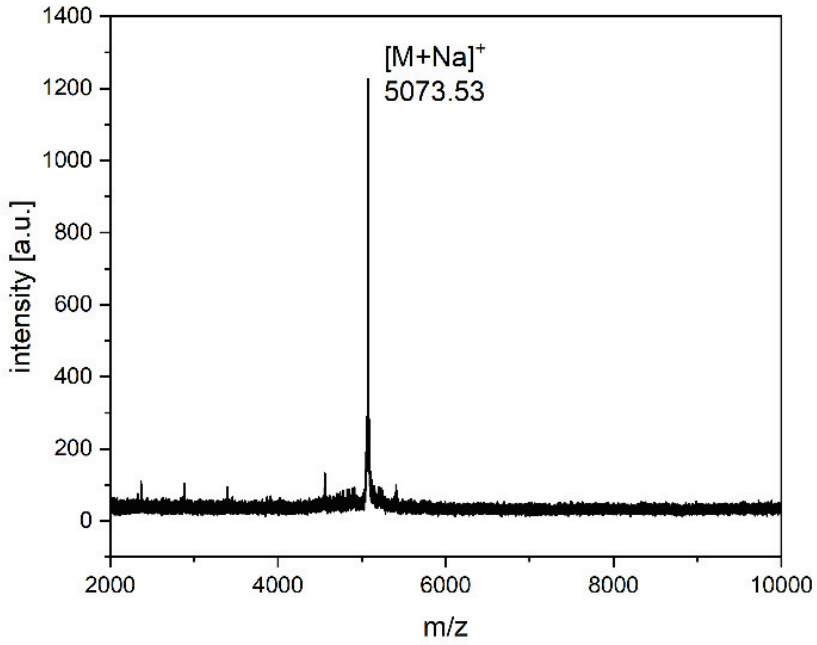

Figure 40: MALD-TOF-MS spectrum of compound L1.

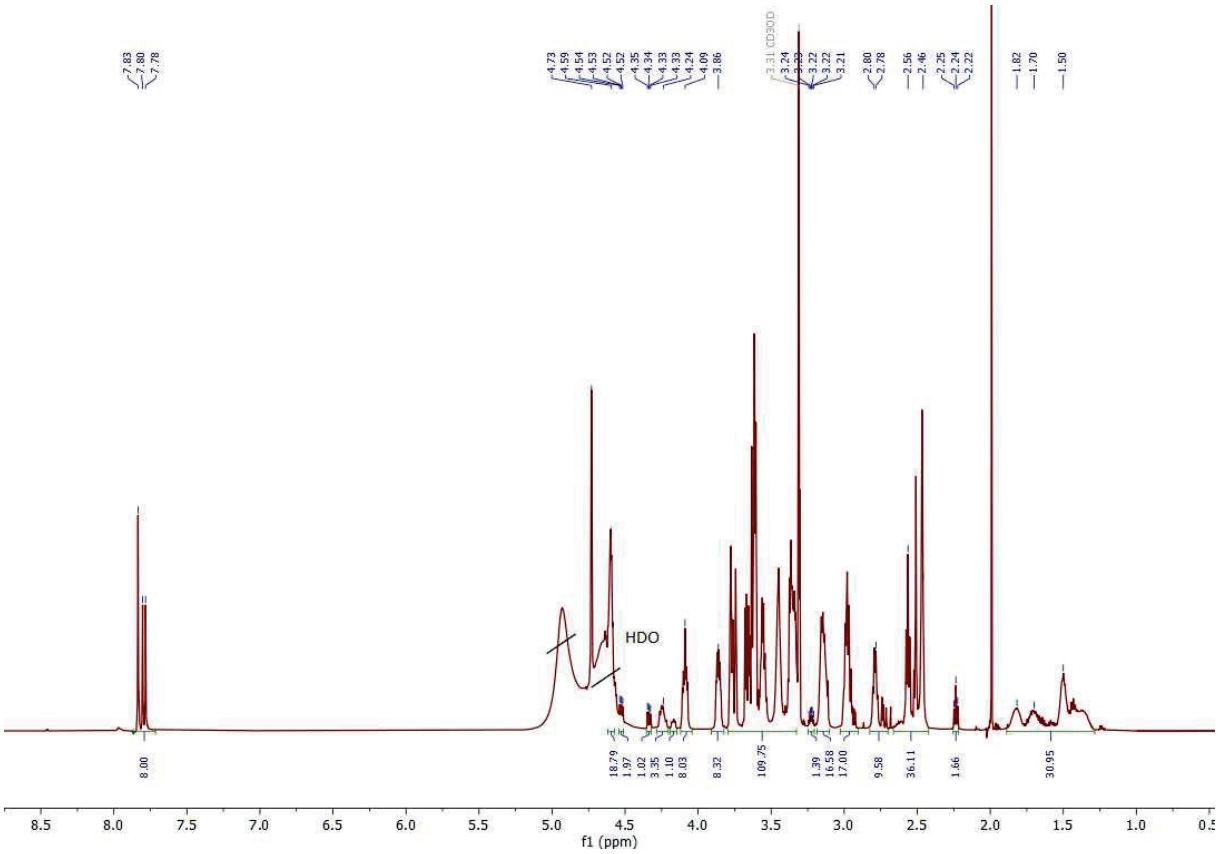

Figure 41: ^{1}H-NMR spectrum (600 MHz) of compound L2 in MeOH-d4/D_2O.

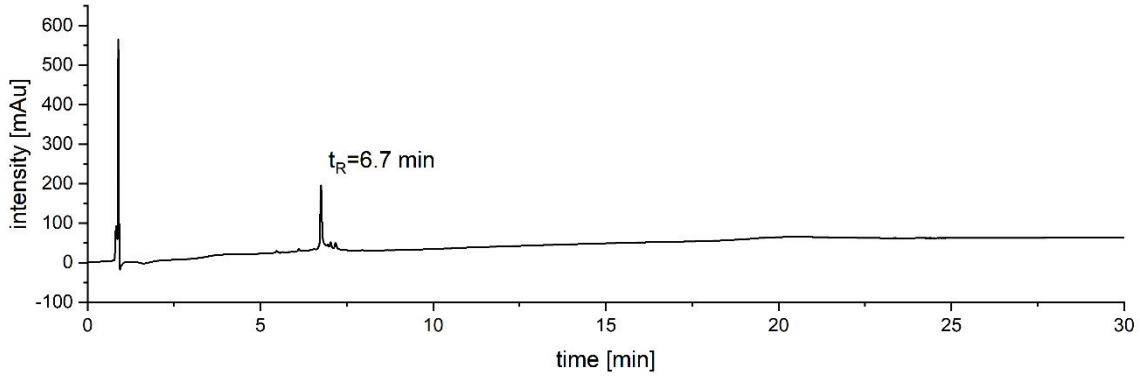

Figure 42: RP-HPLC chromatogram (100 % A to 50 % A in 30 min at 25 °C) of compound L2.

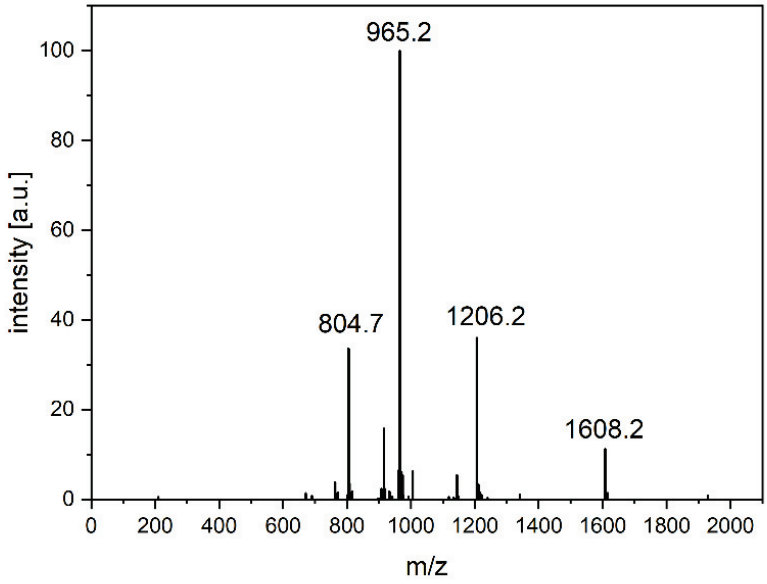

Figure 43: ESI-MS spectrum at t_R = 6.7 min (100 % A to 50 % A in 30 min at 25 °C) of compound L2.

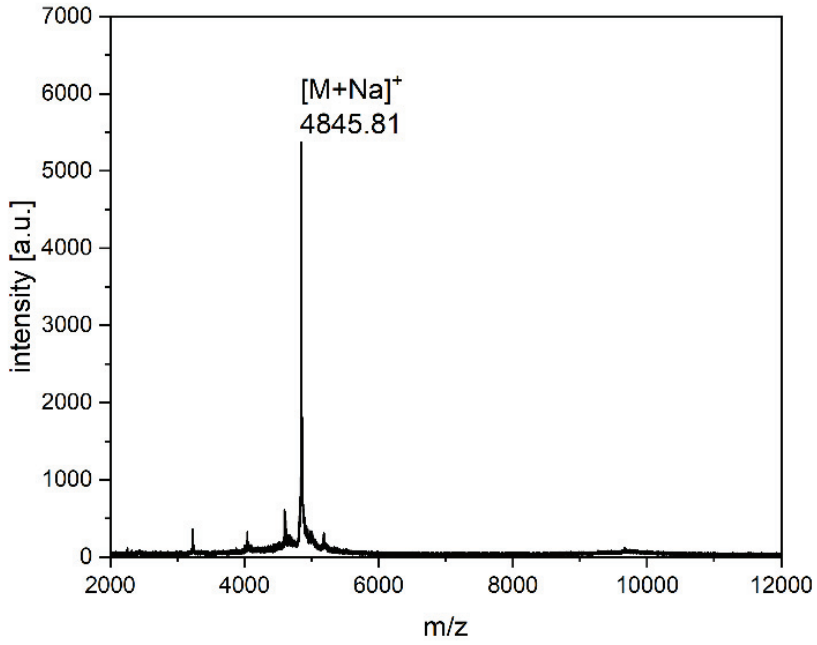

Figure 44: MALD-TOF-MS spectrum of compound L2.

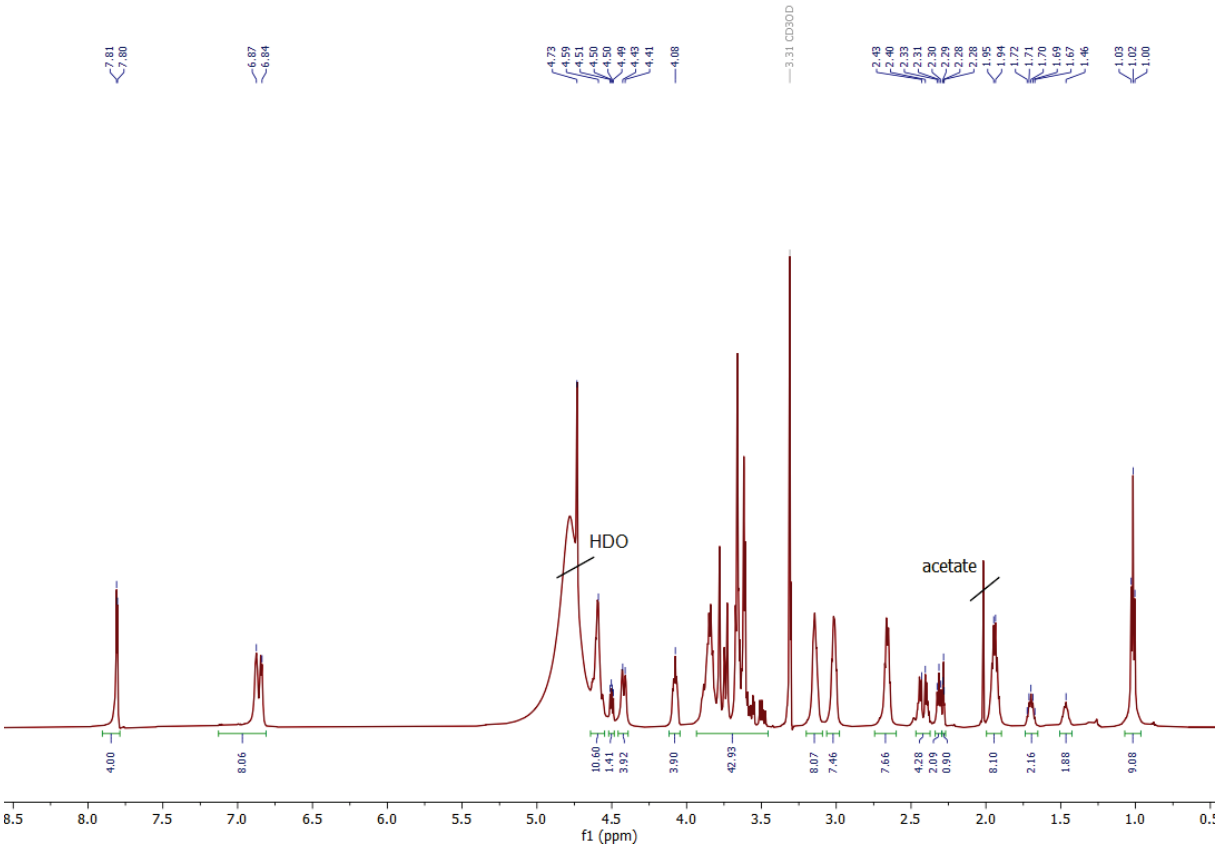

Figure 45: ^{1}H-NMR spectrum (600 MHz) of compound C9 in MeOH-d4/D_2O.

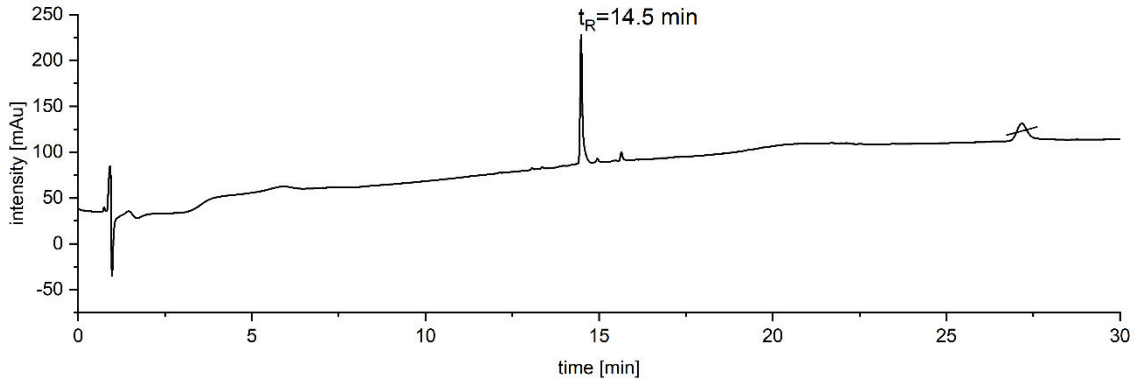

Figure 46: RP-HPLC chromatogram (100 % A to 50 % A in 30 min at 25 °C) of compound C9.

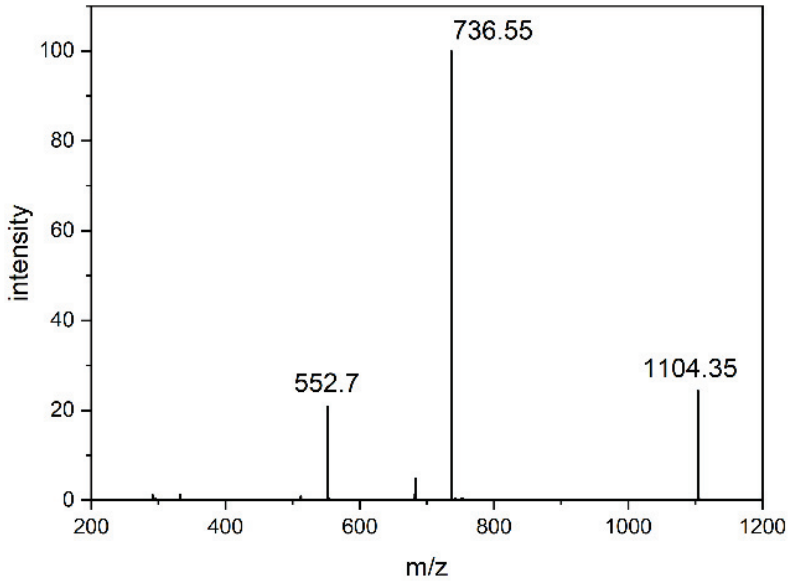

Figure 47: ESI-MS spectrum at t_R = 14.5 min (100 % A to 0 % A in 30 min at 25 °C) of compound C9.

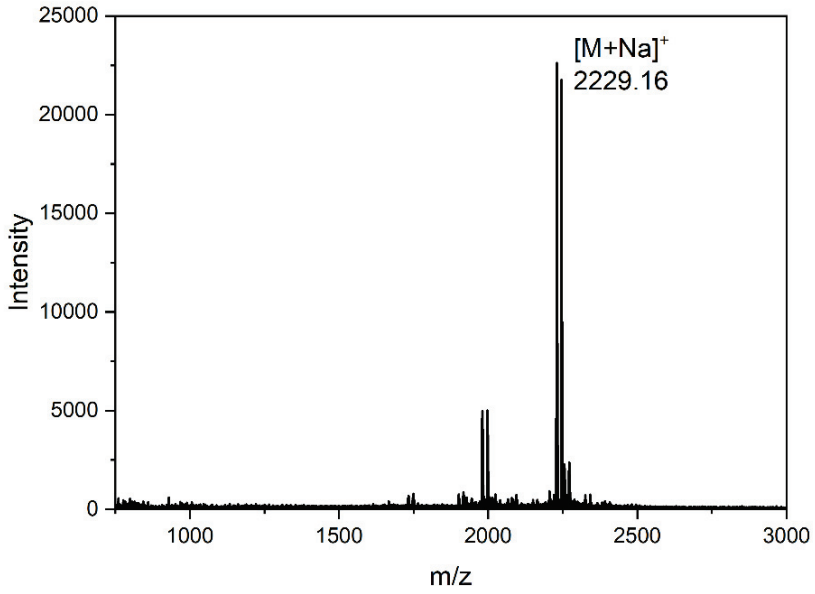

Figure 48: MALD-TOF-MS spectrum of compound C9.

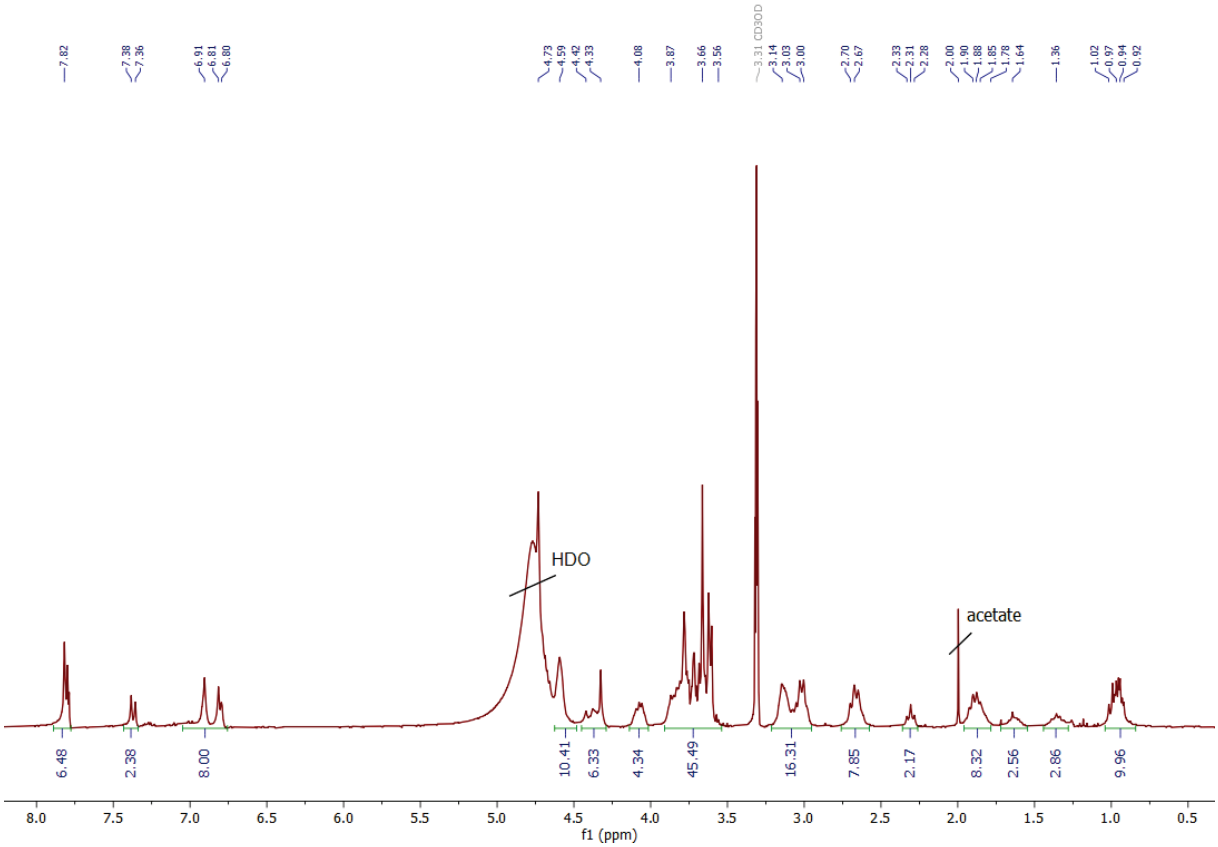

Figure 49: ^{1}H-NMR spectrum (300 MHz) of compound C10 in MeOH-d4/D_2O.

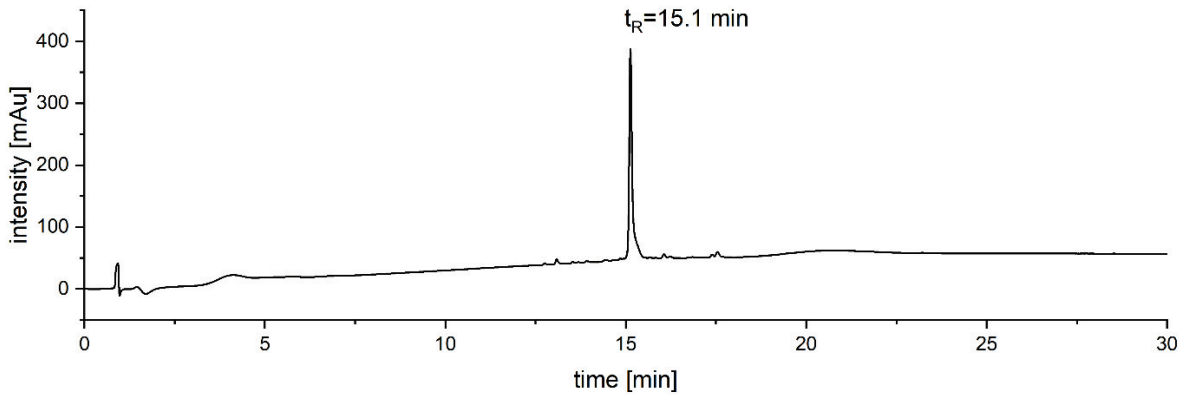

Figure 50: RP-HPLC chromatogram (100 % A to 50 % A in 30 min at 25 °C) of compound C10.

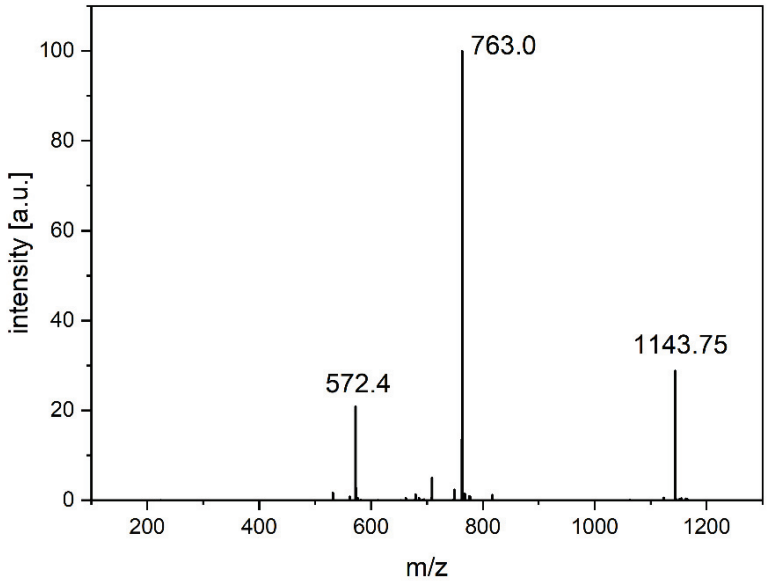

Figure 51: ESI-MS spectrum at t_R = 15.1 min (100 % A to 0 % A in 30 min at 25 °C) of compound C10.

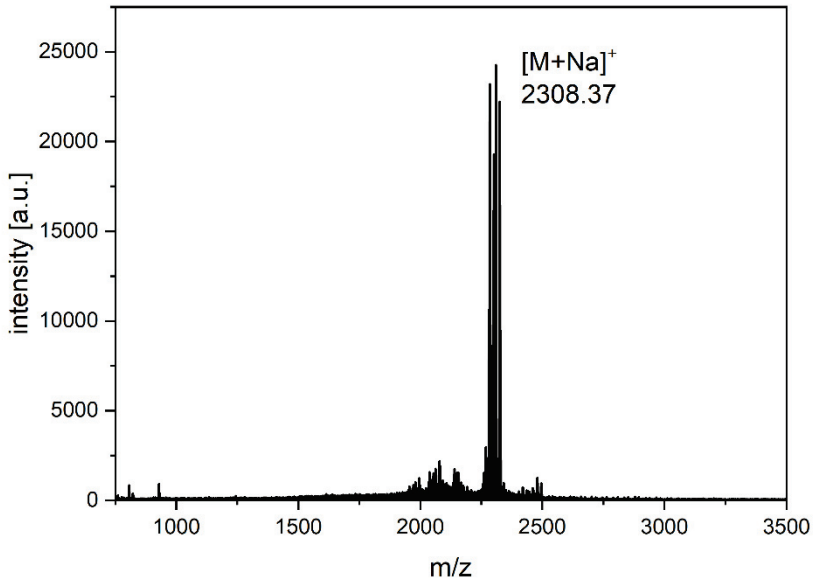

Figure 52: MALD-TOF-MS spectrum of compound C10.

Figure 53: ^{1}H-NMR spectrum (300 MHz) of compound C11 in MeOH-d4/D_2O.

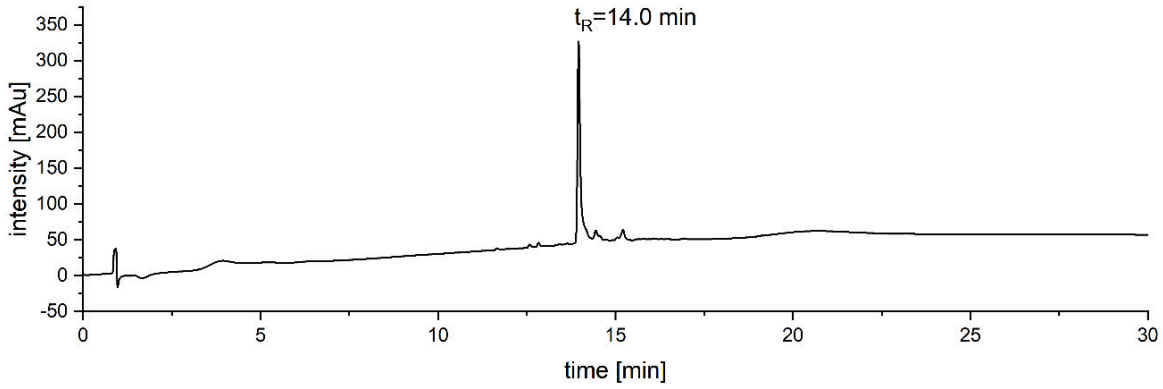

Figure 54: RP-HPLC chromatogram (100 % A to 50 % A in 30 min at 25 °C) of compound C11.

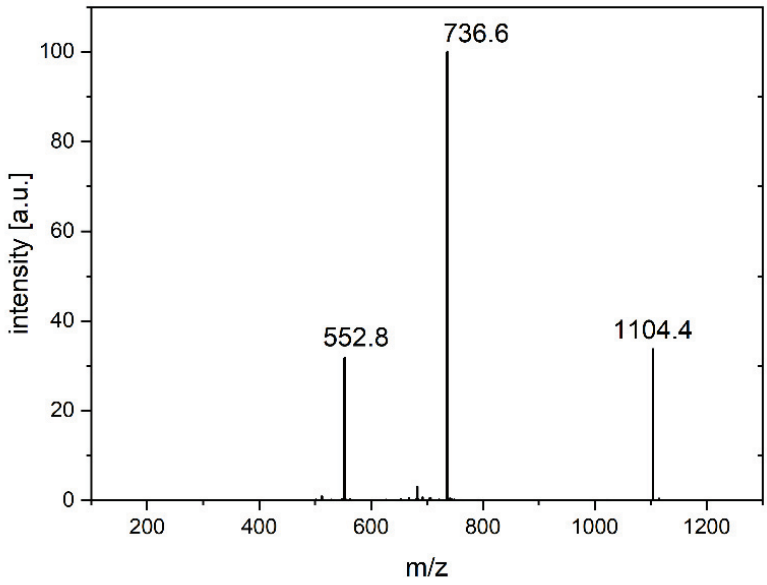

Figure 55: ESI-MS spectrum at t_R = 14.0 min (100 % A to 0 % A in 30 min at 25 °C) of compound C11.

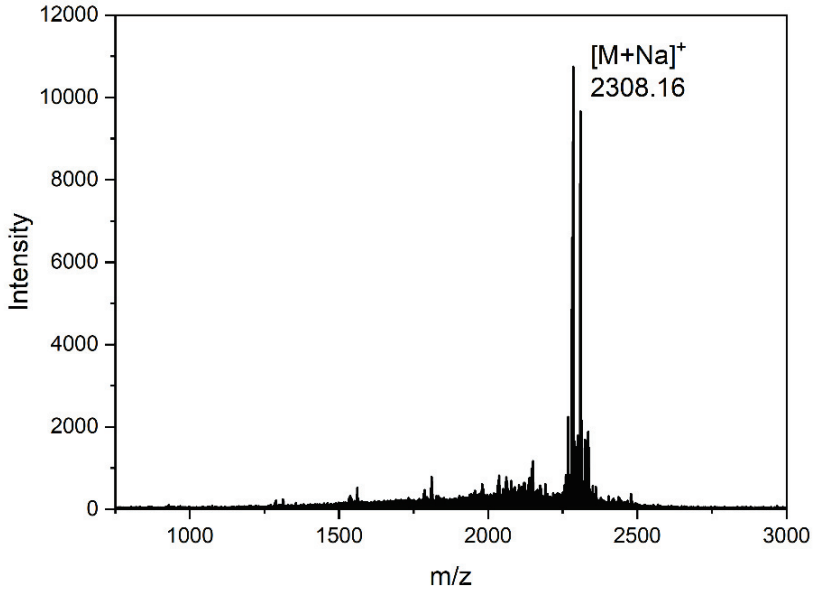

Figure 56: MALD-TOF-MS spectrum of compound C11.

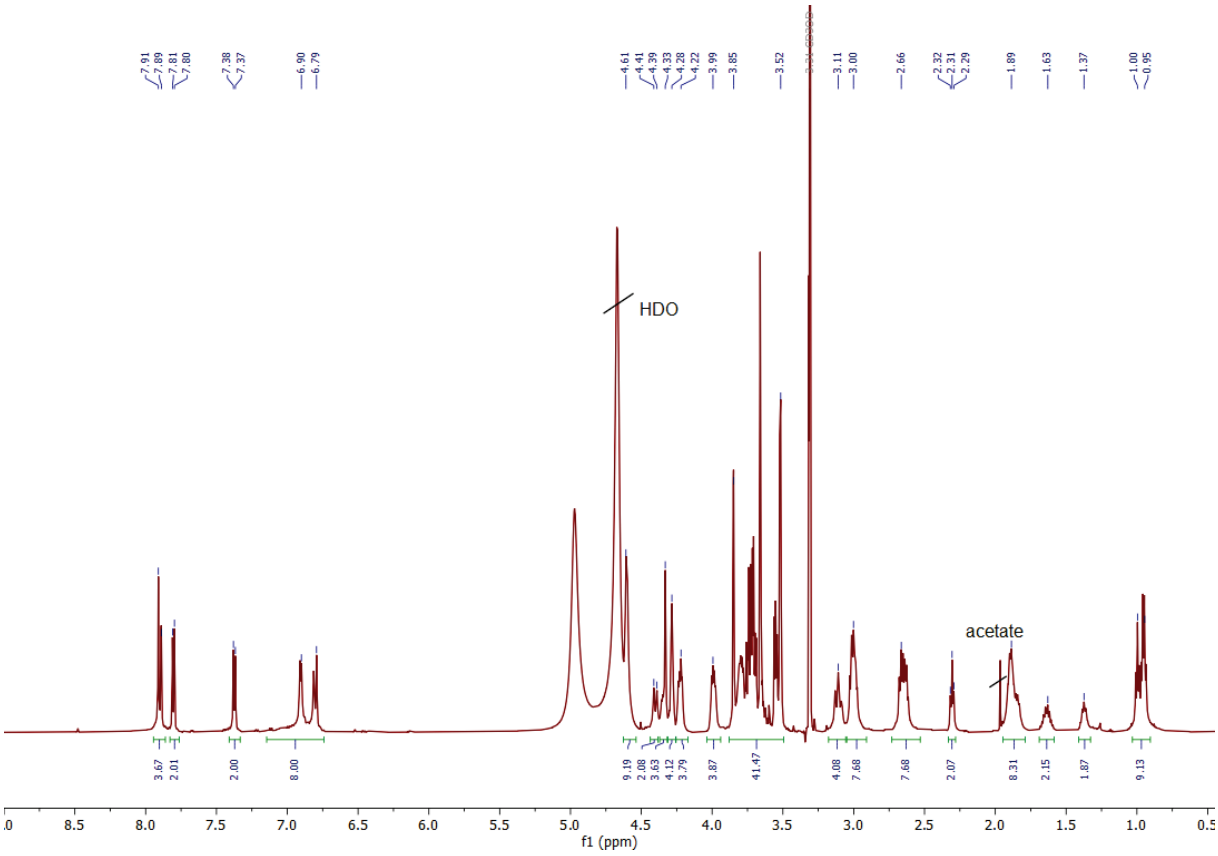

Figure 57: ^{1}H-NMR spectrum (600 MHz) of compound C12 in MeOH-d4/D_2O.

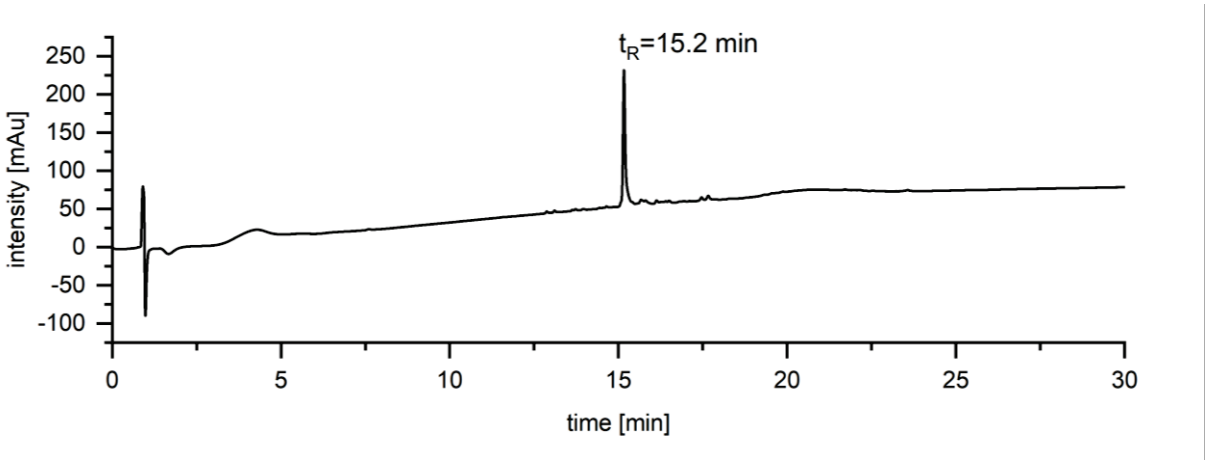

Figure 58: RP-HPLC chromatogram (100 % A to 50 % A in 30 min at 25 °C) of compound C12.

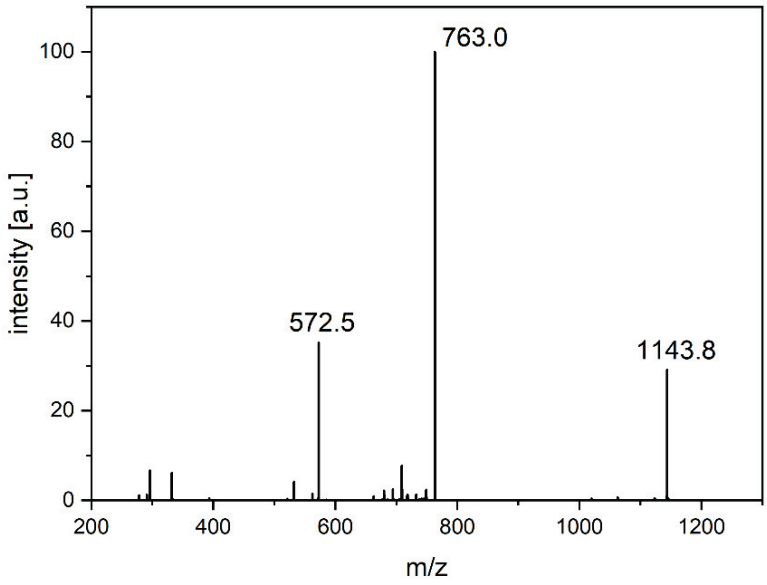

Figure 59: ESI-MS spectrum at t_R = 15.0 min (100 % A to 0 % A in 30 min at 25 °C) of compound C12.

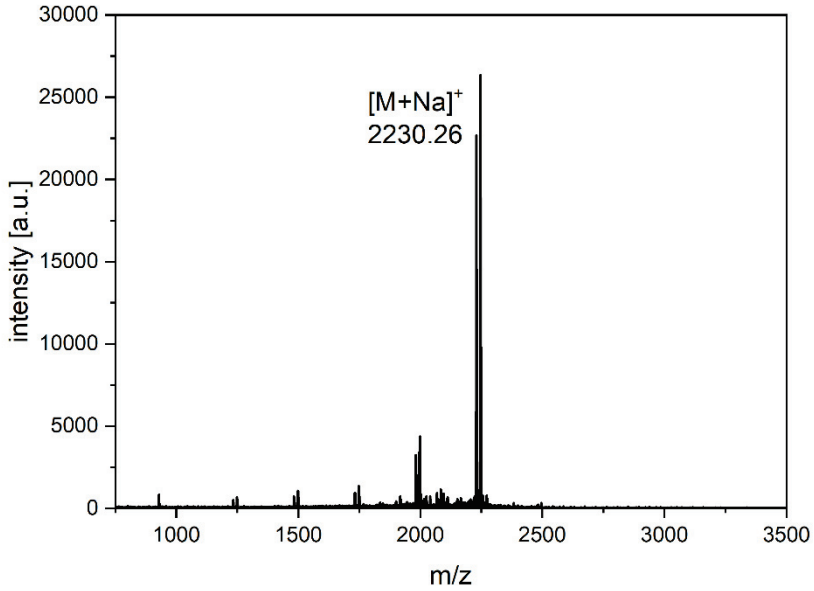

Figure 60: MALD-TOF-MS spectrum of compound C12.

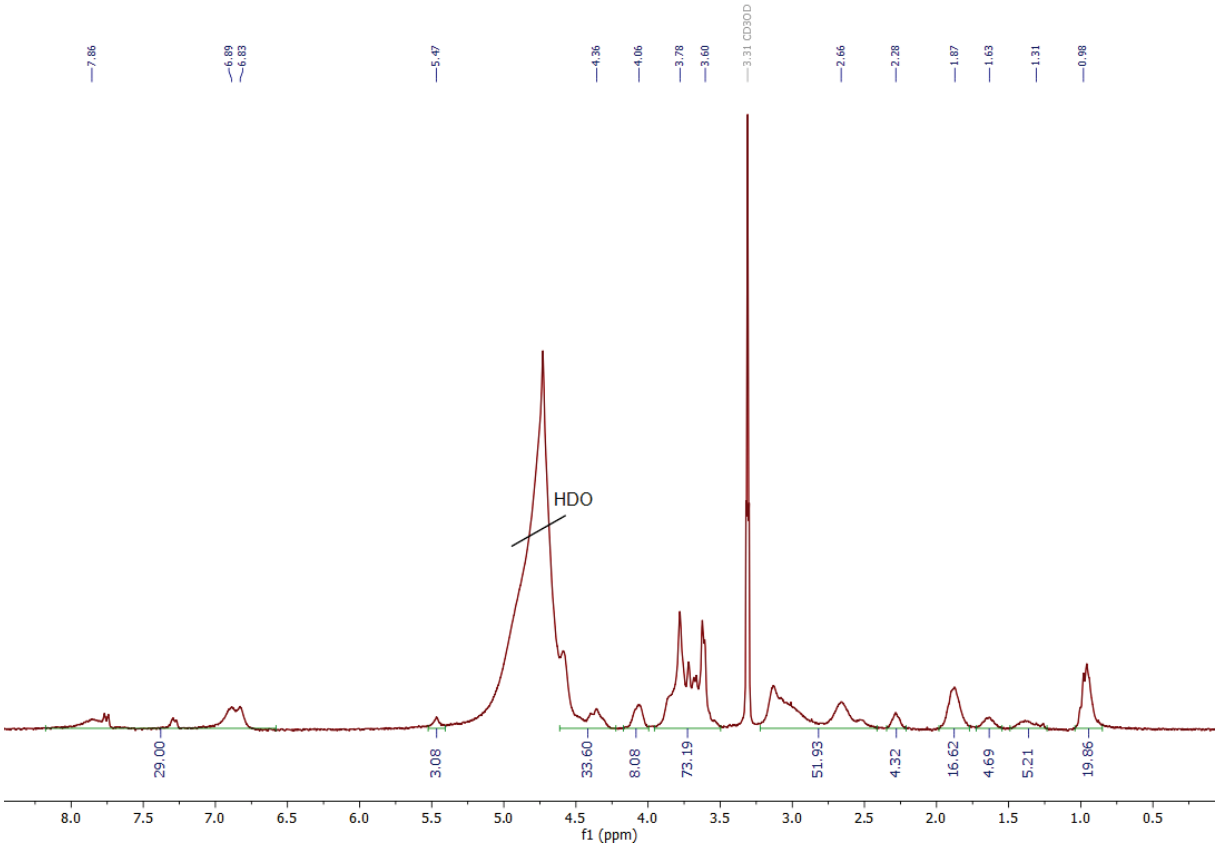

Figure 61: ^{1}H-NMR spectrum (600 MHz) of compound C13d in MeOH-d4/D_2O.

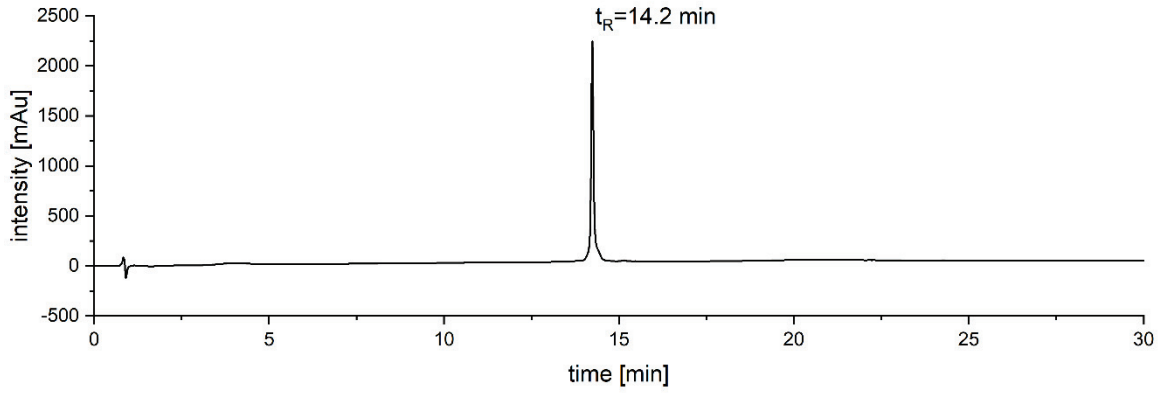

Figure 62: RP-HPLC chromatogram (100 % A to 0 % A in 30 min at 25 °C) of compound C13d.

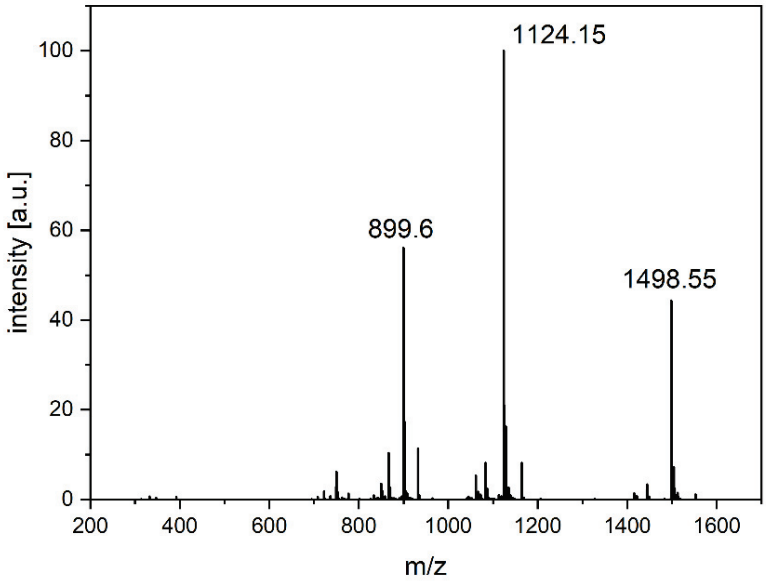

Figure 63: ESI-MS spectrum at t_R = 14.1 min (100 % A to 0 % A in 30 min at 25 °C) of compound C13d.

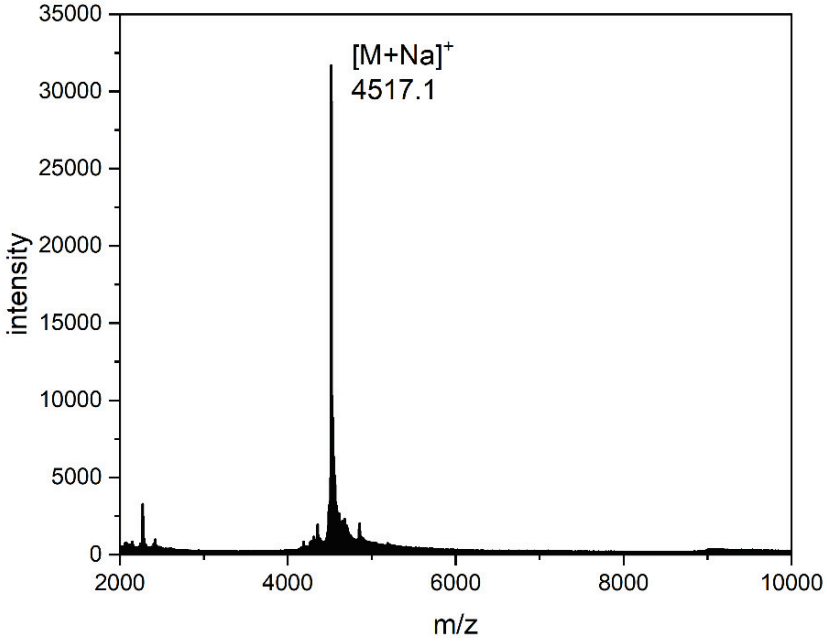

Figure 64: MALD-TOF-MS spectrum of compound C13d.

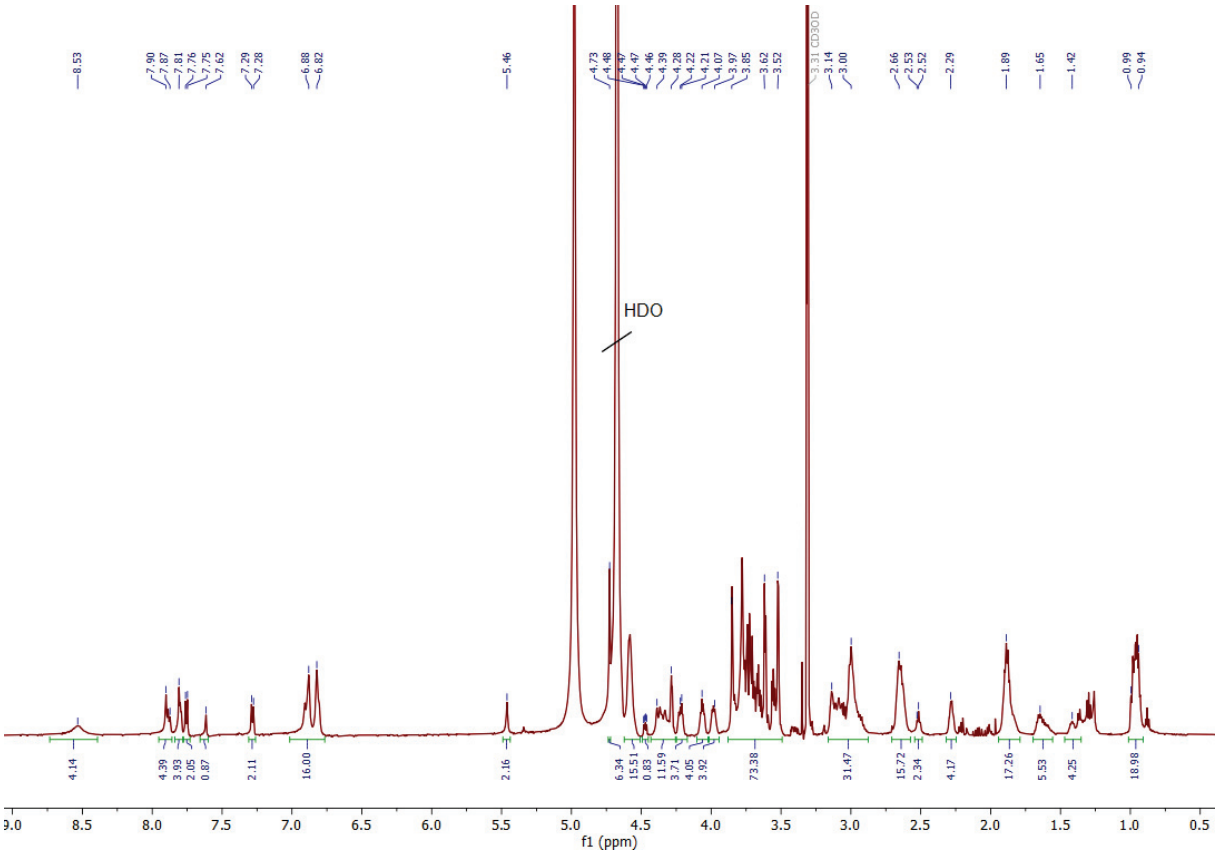

Figure 65: ^{1}H-NMR spectrum (300 MHz) of compound C14d in MeOH-d4/D_2O

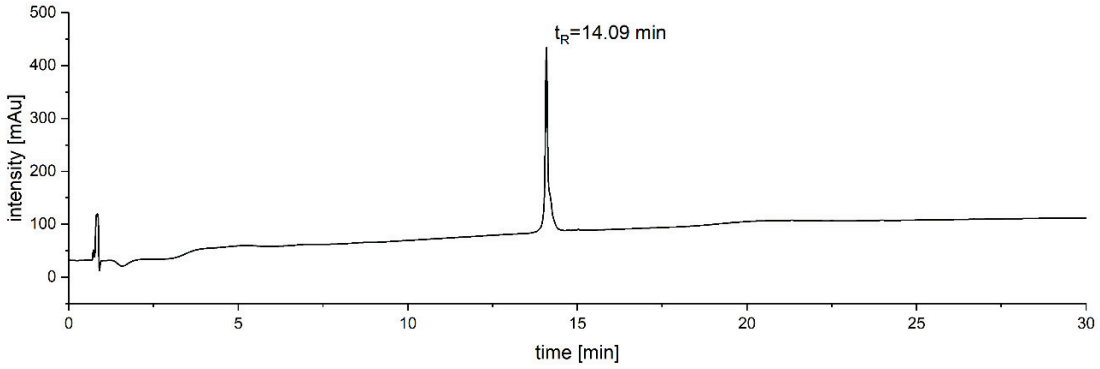

Figure 66: RP-HPLC chromatogram (100 % A to 0 % A in 30 min at 25 °C) of compound C14d.

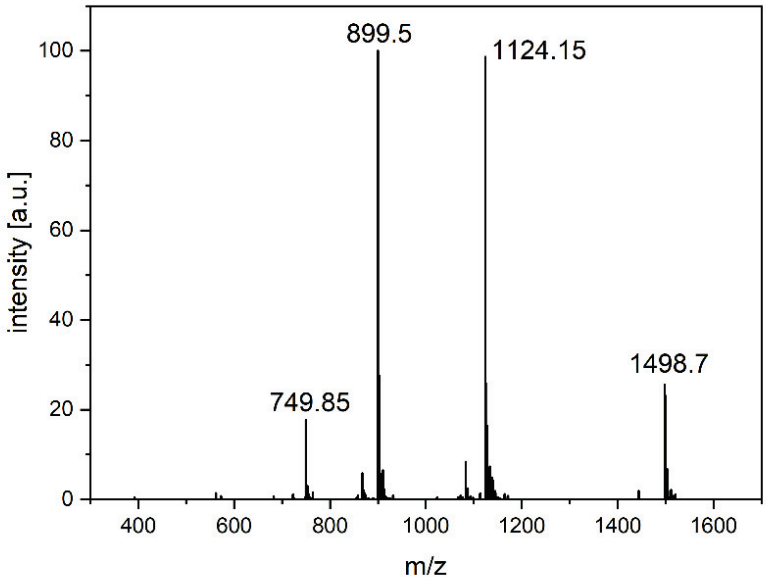

Figure 67: ESI-MS spectrum at t_R = 14.2 min (100 % A to 0 % A in 30 min at 25 °C) of compound C14d.

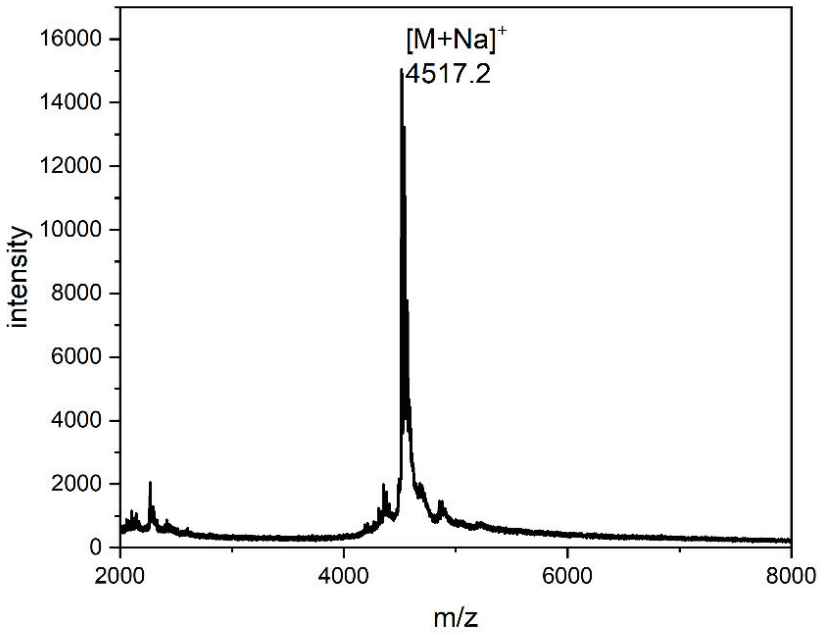

Figure 68: MALD-TOF-MS spectrum of compound C14d.

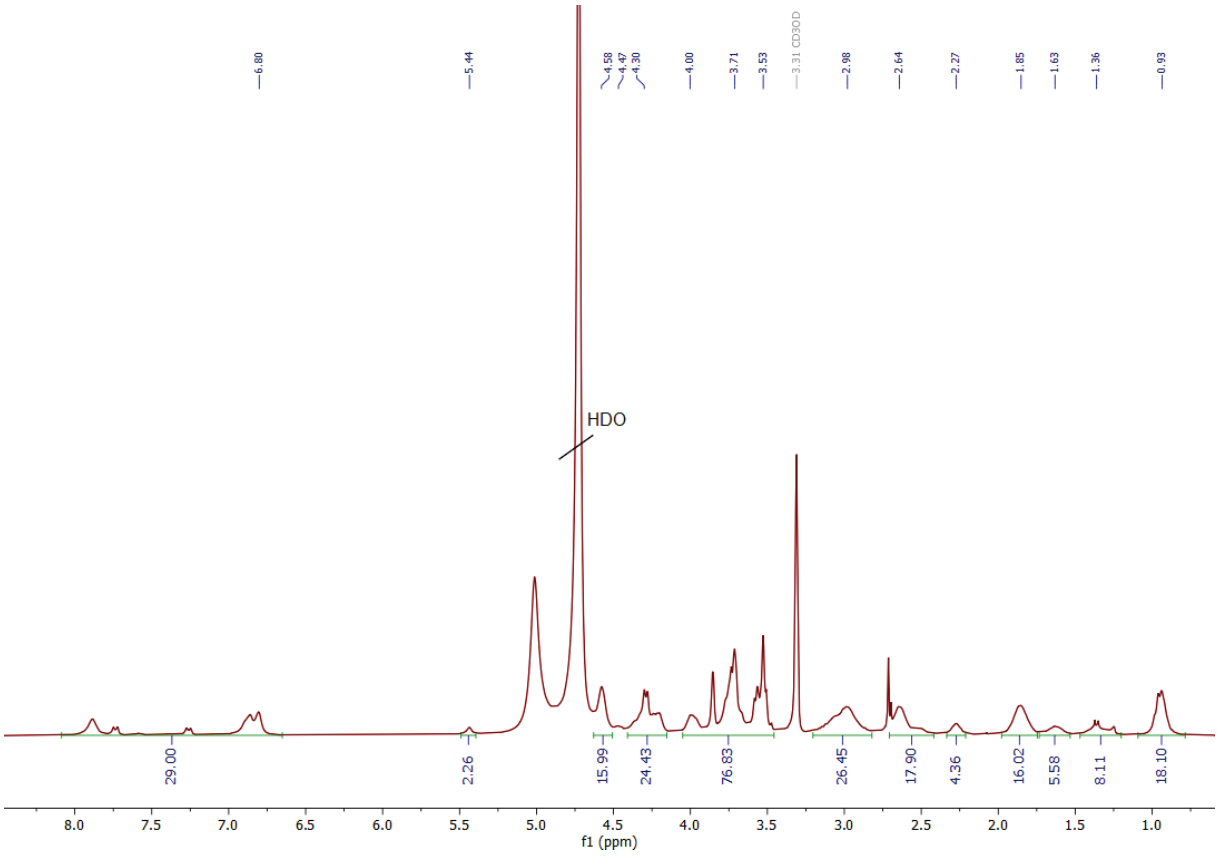

Figure 69: ^{1}H-NMR spectrum (300 MHz) of compound C15d in MeOH-d4/D_2O.

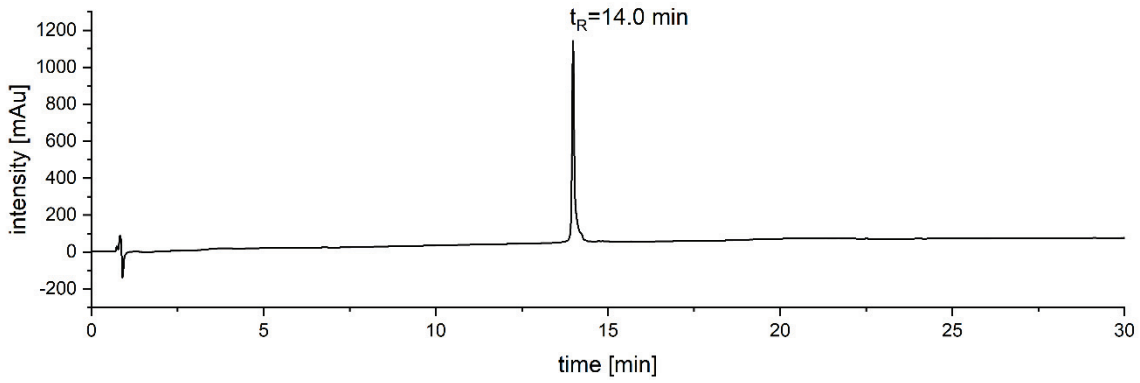

Figure 70: RP-HPLC chromatogram (100 % A to 0 % A in 30 min at 25 °C) of compound C15d.

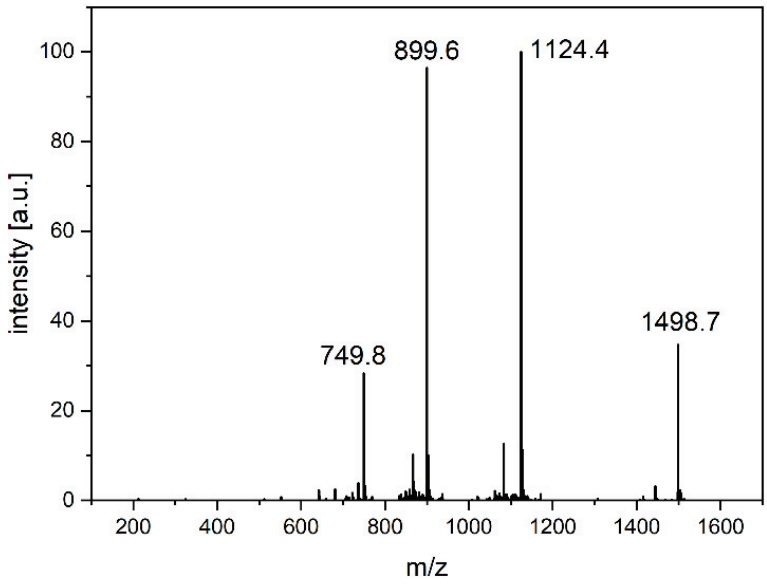

Figure 71: ESI-MS spectrum at t_R = 14.0 min (100 % A to 0 % A in 30 min at 25 °C) of compound C15d.

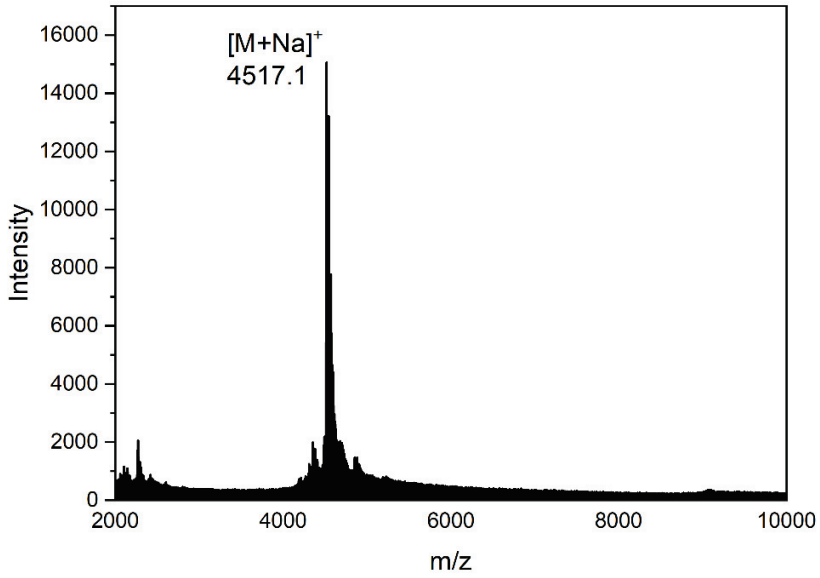

Figure 72: MALD-TOF-MS spectrum of compound C15d.

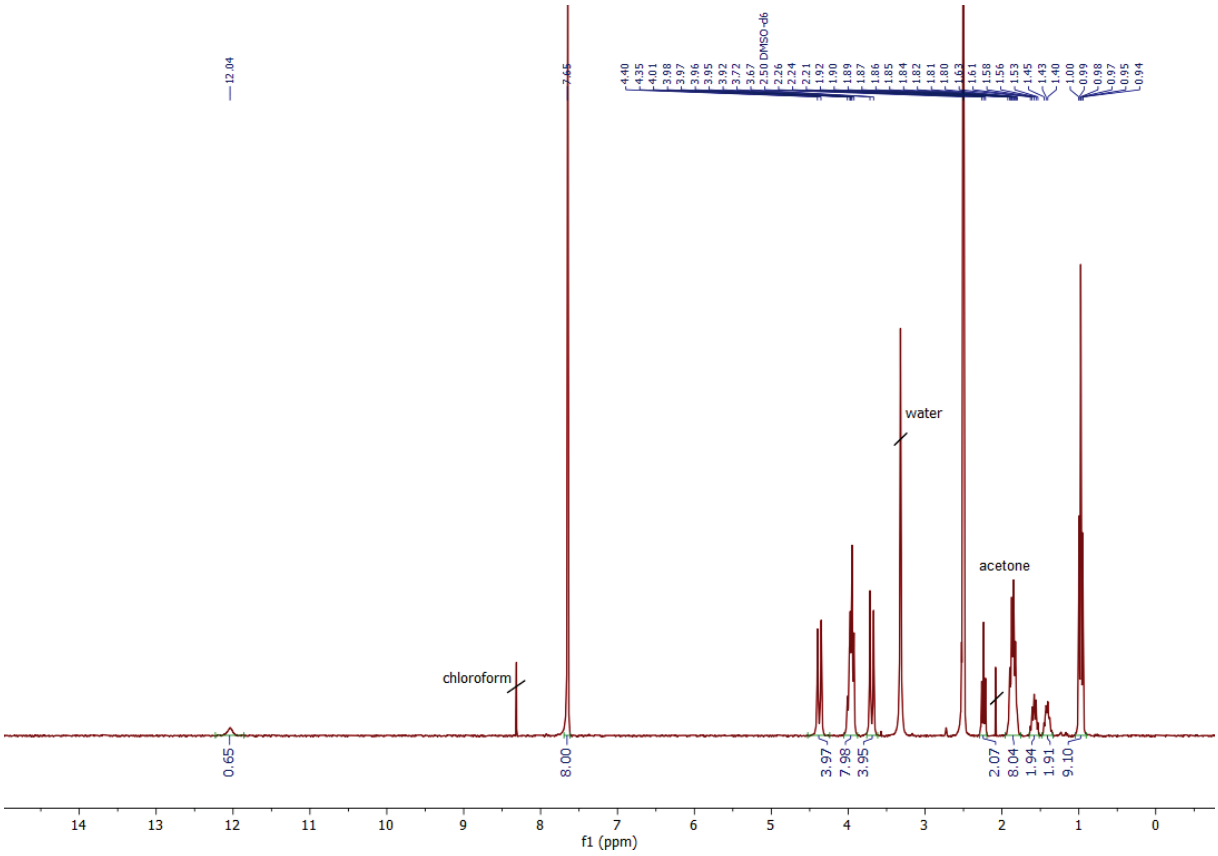

Figure 73: ^{1}H-NMR spectrum (300 MHz) of CBB1 in DMSO.

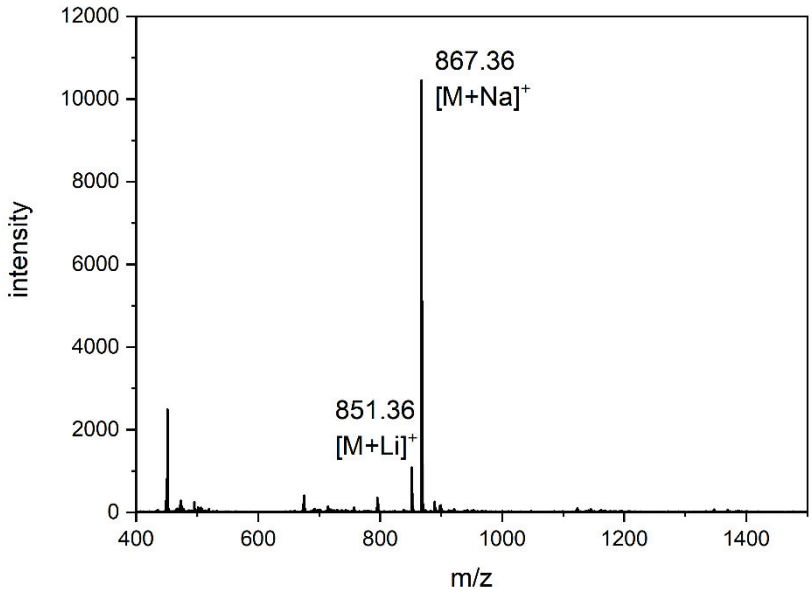

Figure 74: MALDI-TOF-MS of CBB1.

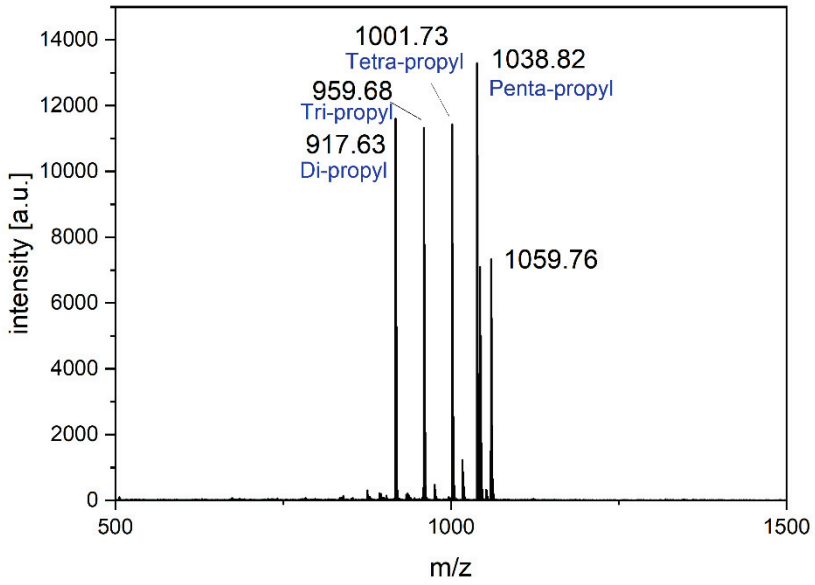

Figure 75: MALDI-TOF-MS of product mixture obtained from alkylation of CBB2-1 with1-iodopropane.

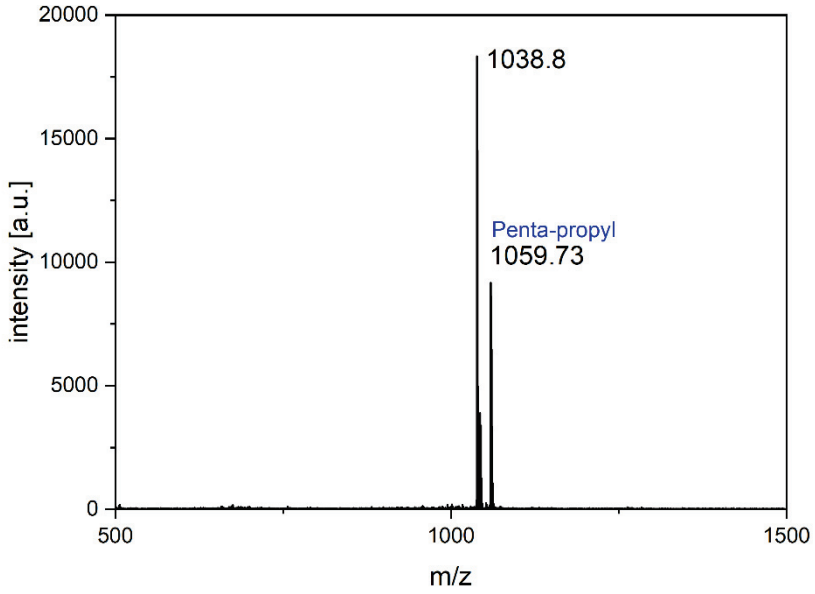

Figure 76: MALDI-TOF-MS of penta-propyl derivative obtained from alkylation of CBB2-1 with 1-iodopropane.

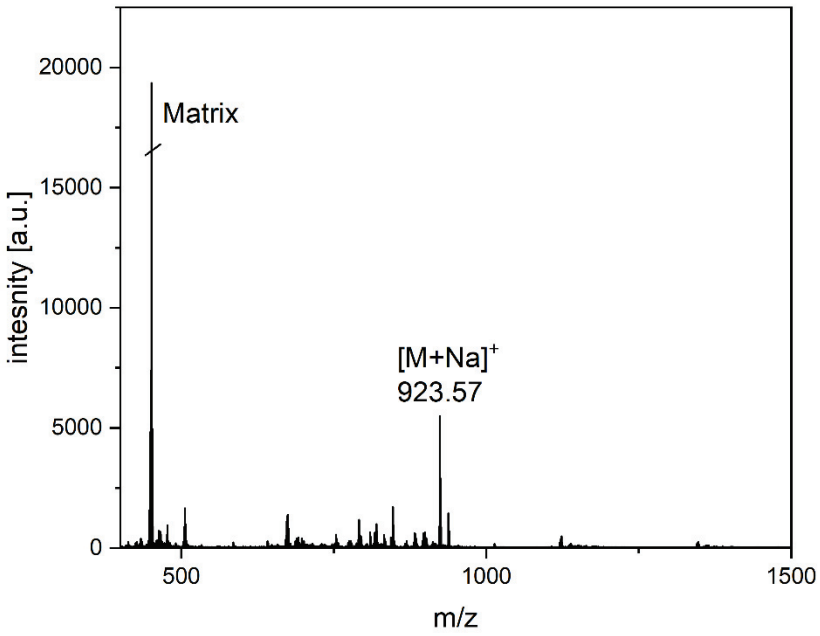

Figure 77: MALDI-TOF-MS of intermediate CBB2-2.

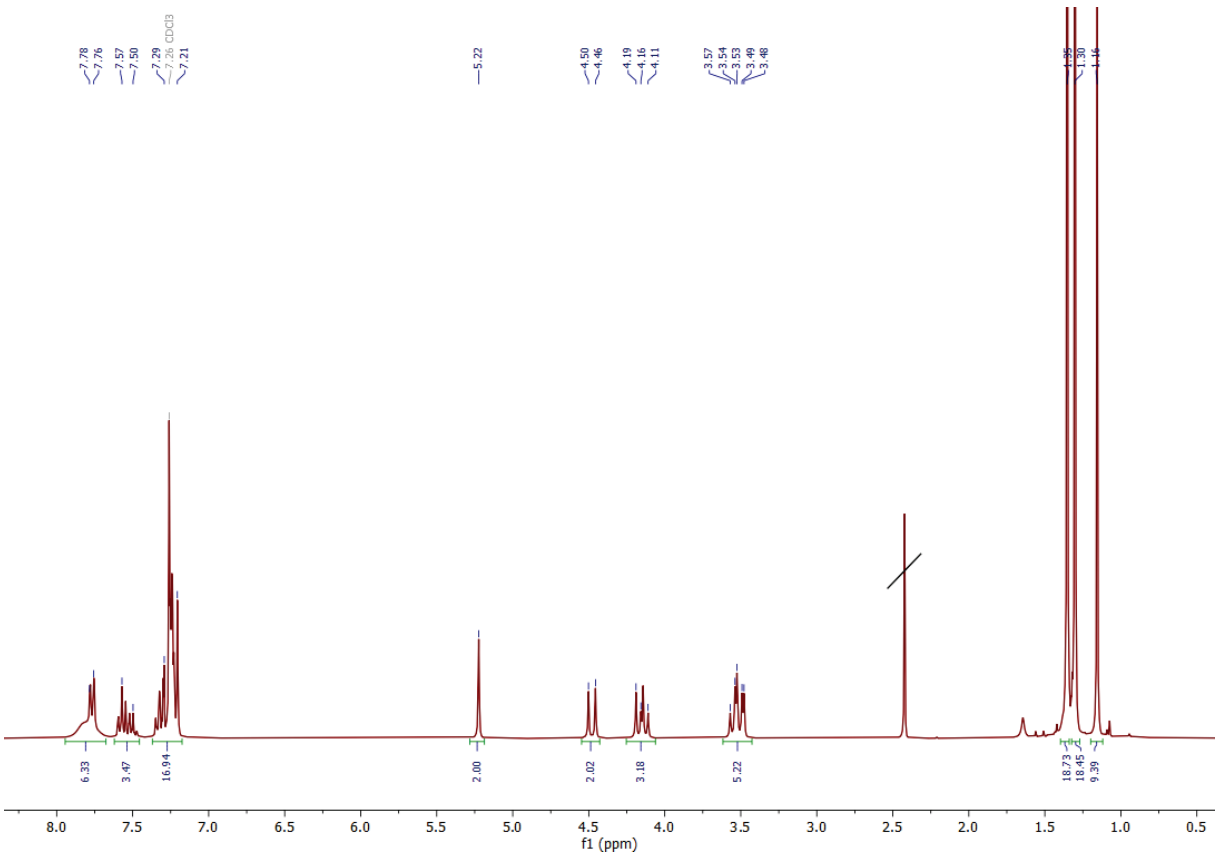

Figure 78: ^{1}H-NMR (300 MHz) of intermediate CBB2-2 in chloroform.

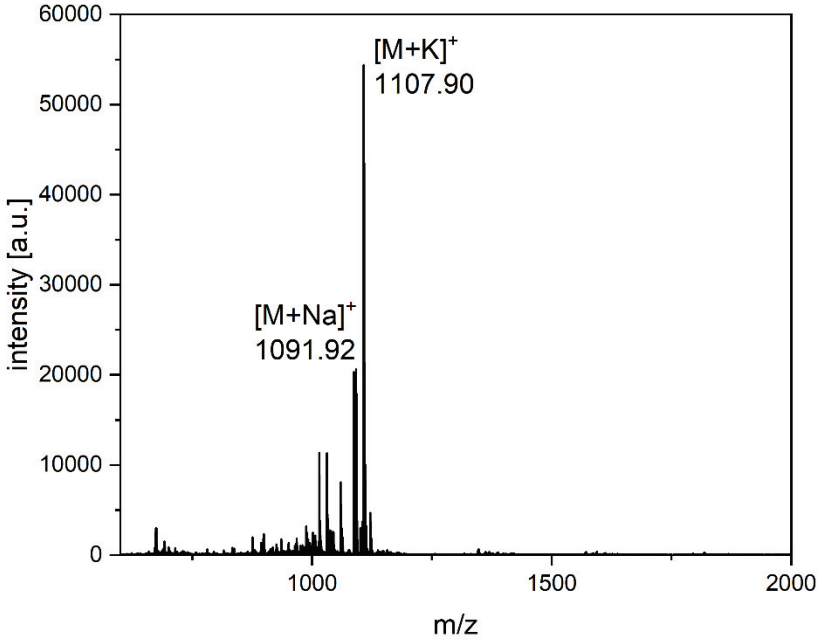

Figure 79: MALDI-TOF-MS of intermediate CBB2-3.

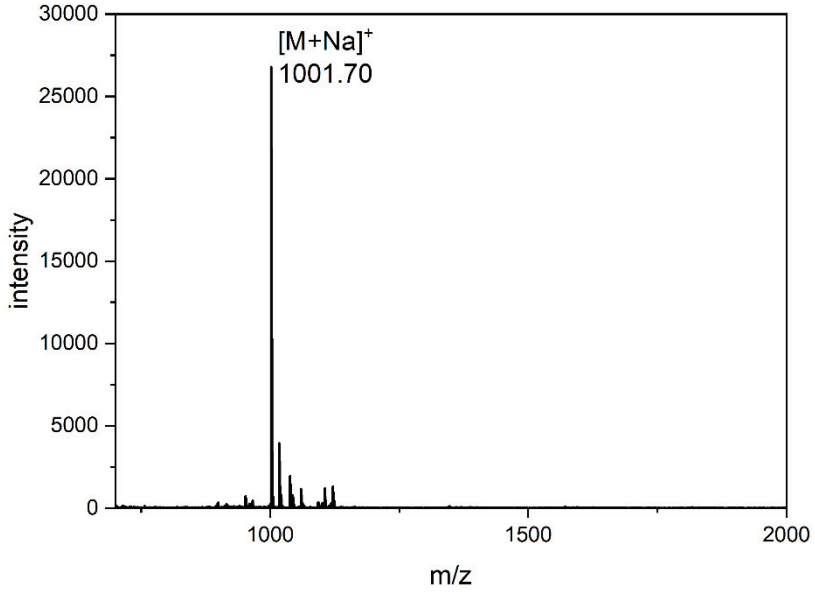

Figure 80: MALDI-TOF-MS of intermediate CBB2-4.

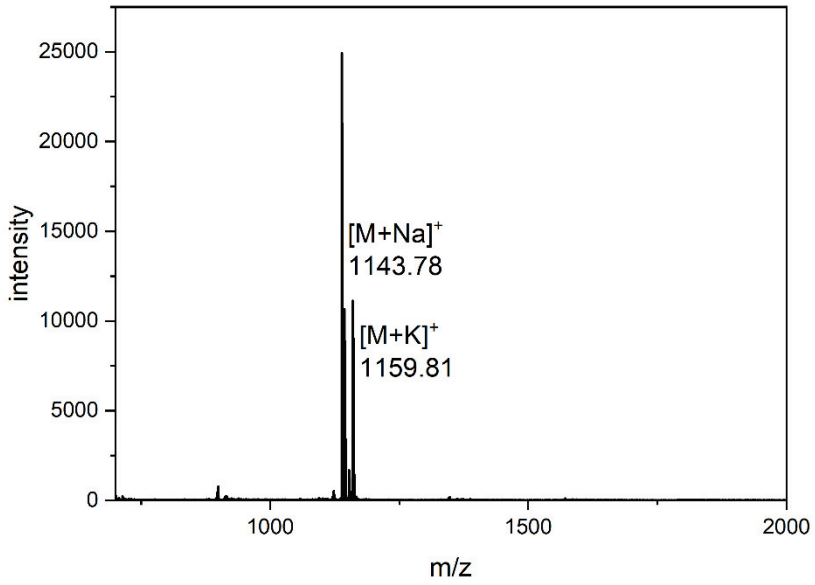

Figure 81: MALDI-TOF-MS of intermediate CBB2-5.

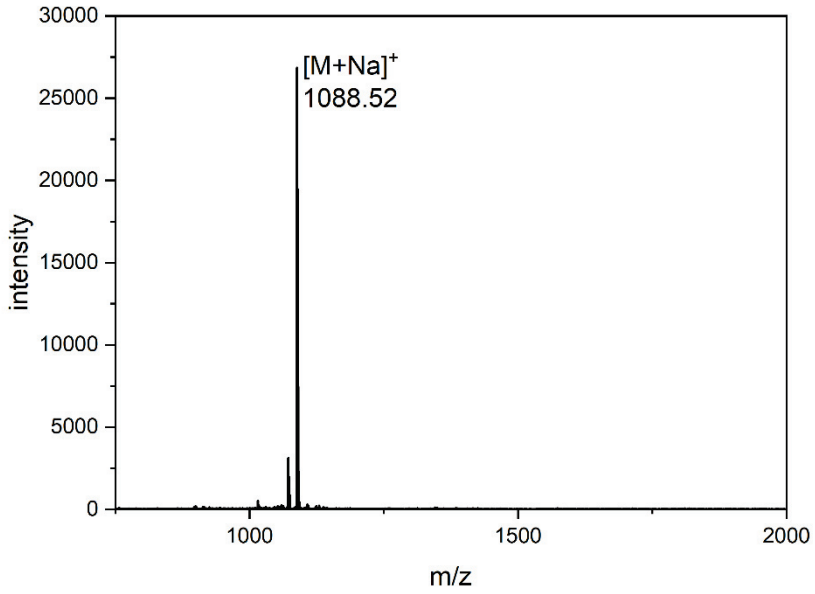

Figure 82: MALDI-TOF-MS of intermediate CBB2-6.

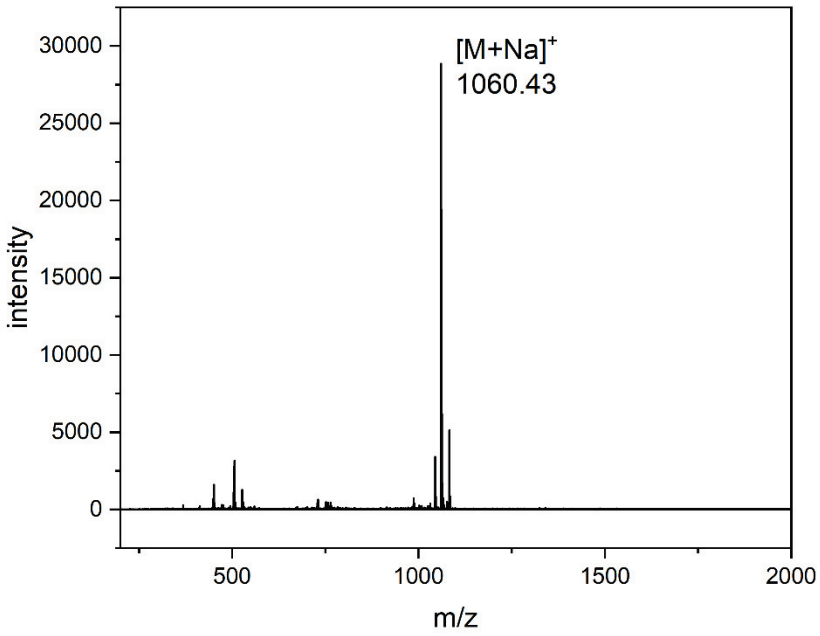

Figure 83: MALDI-TOF-MS of CBB2.

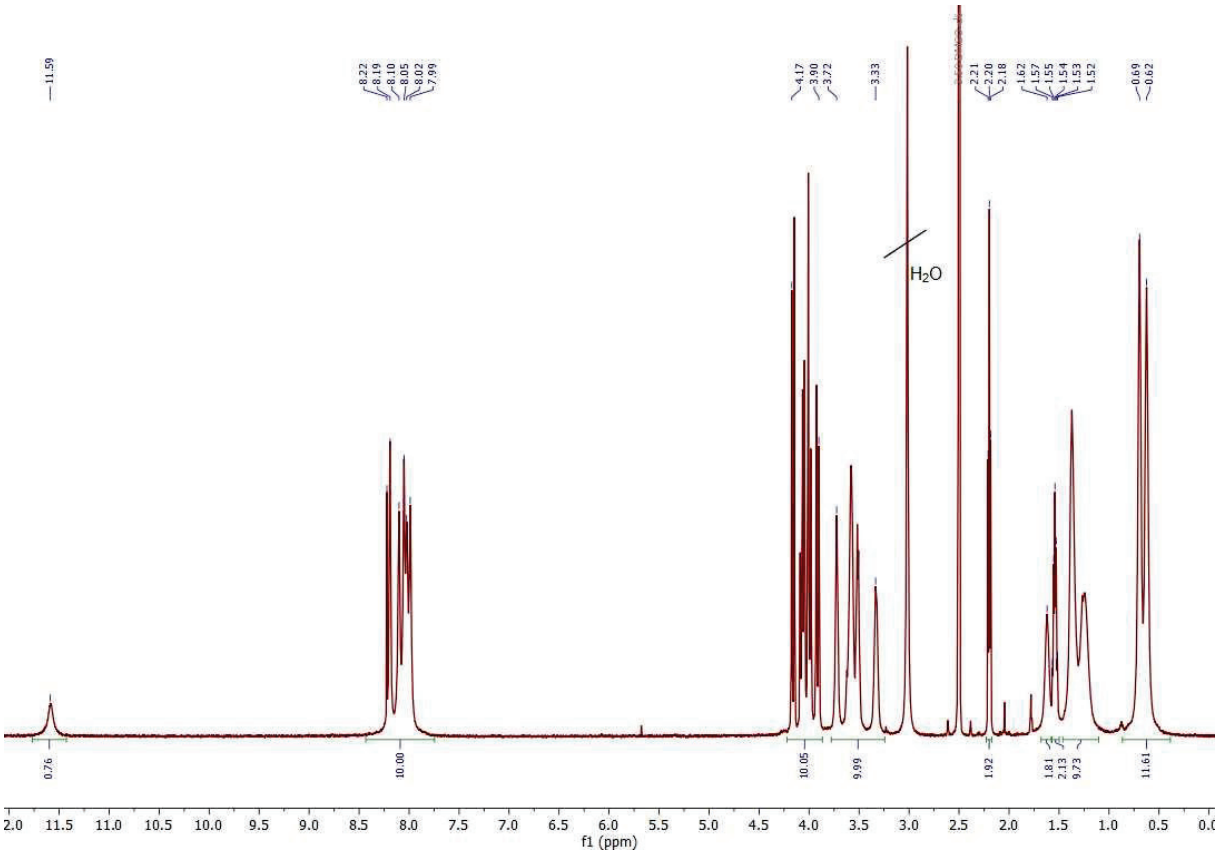

Figure 84: ^{1}H-NMR spectrum (600 MHz, 90 °C) of compound CBB2 in DMSO.

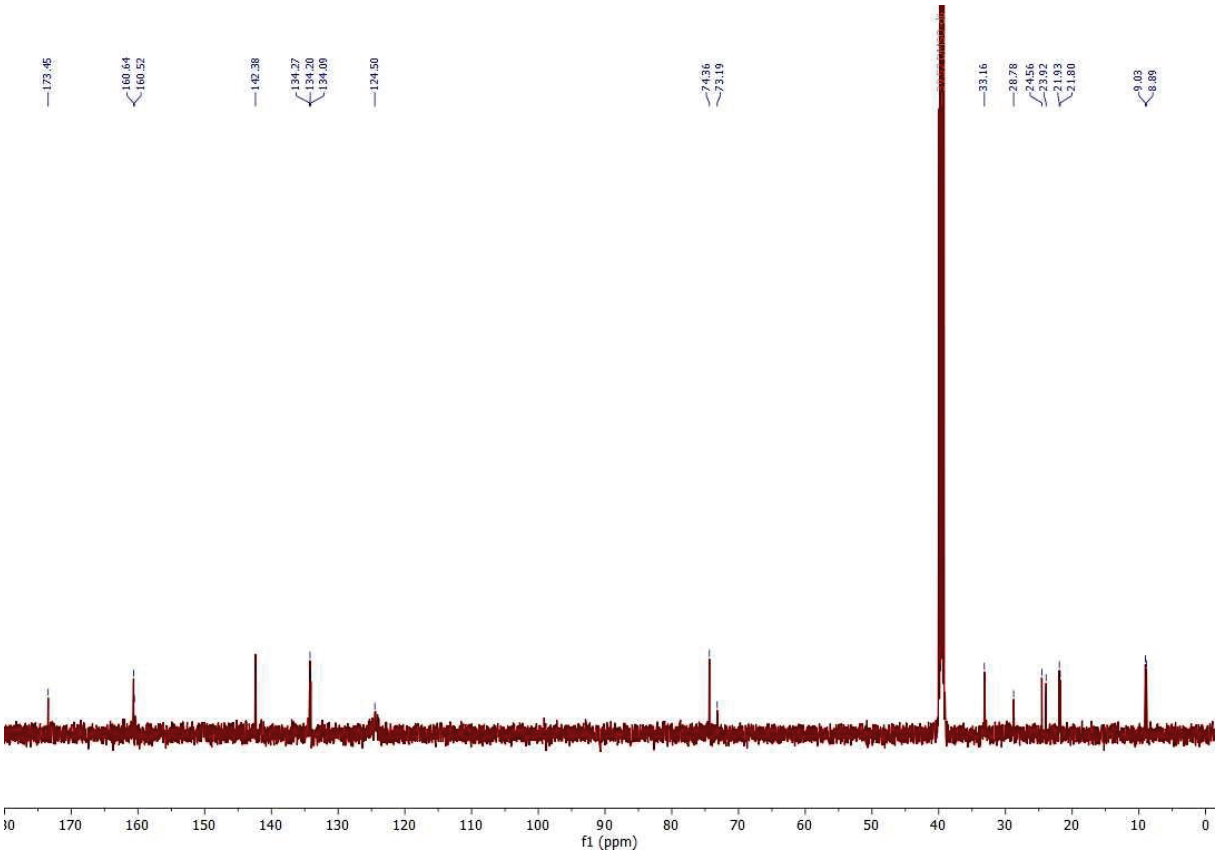

Figure 85: ^{13}C-NMR spectrum (150 MHz, 90 °C) of compound CBB2 in DMSO.

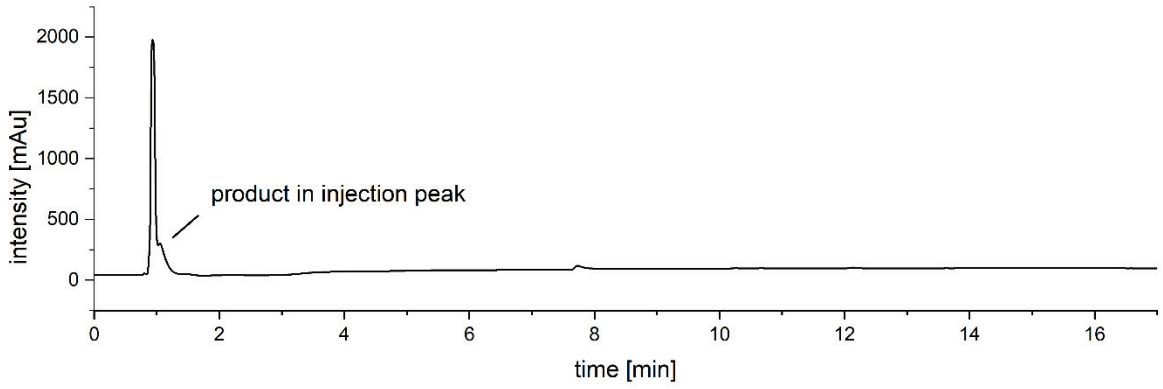

Figure 86: RP-HPLC chromatogram (100 % A to 50 % A in 17 min at 25 °C) of EDS_3-CBB2-NH_2 intermediate after reduction of nitrogen groups.

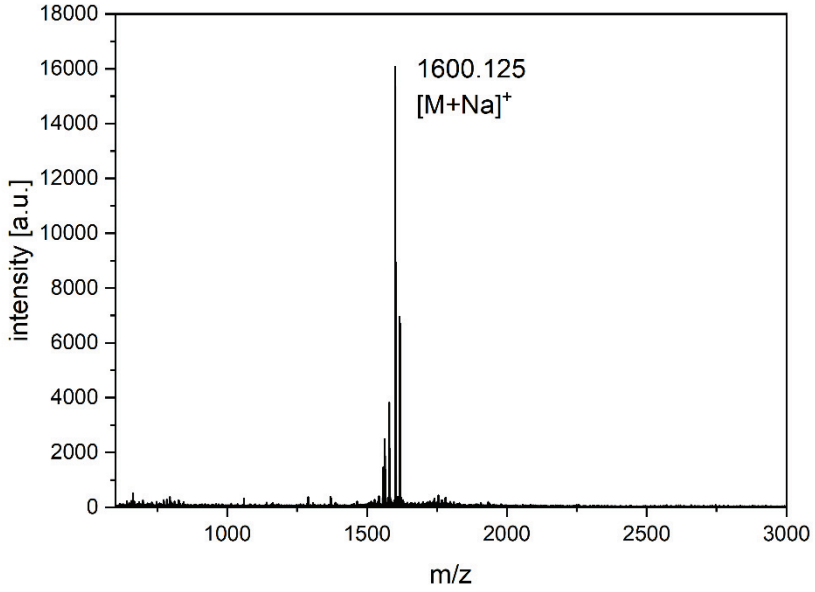

Figure 87: MALDI-TOF-MS of EDS_3-CBB2-NH_2 intermediate after reduction of nitrogen groups.

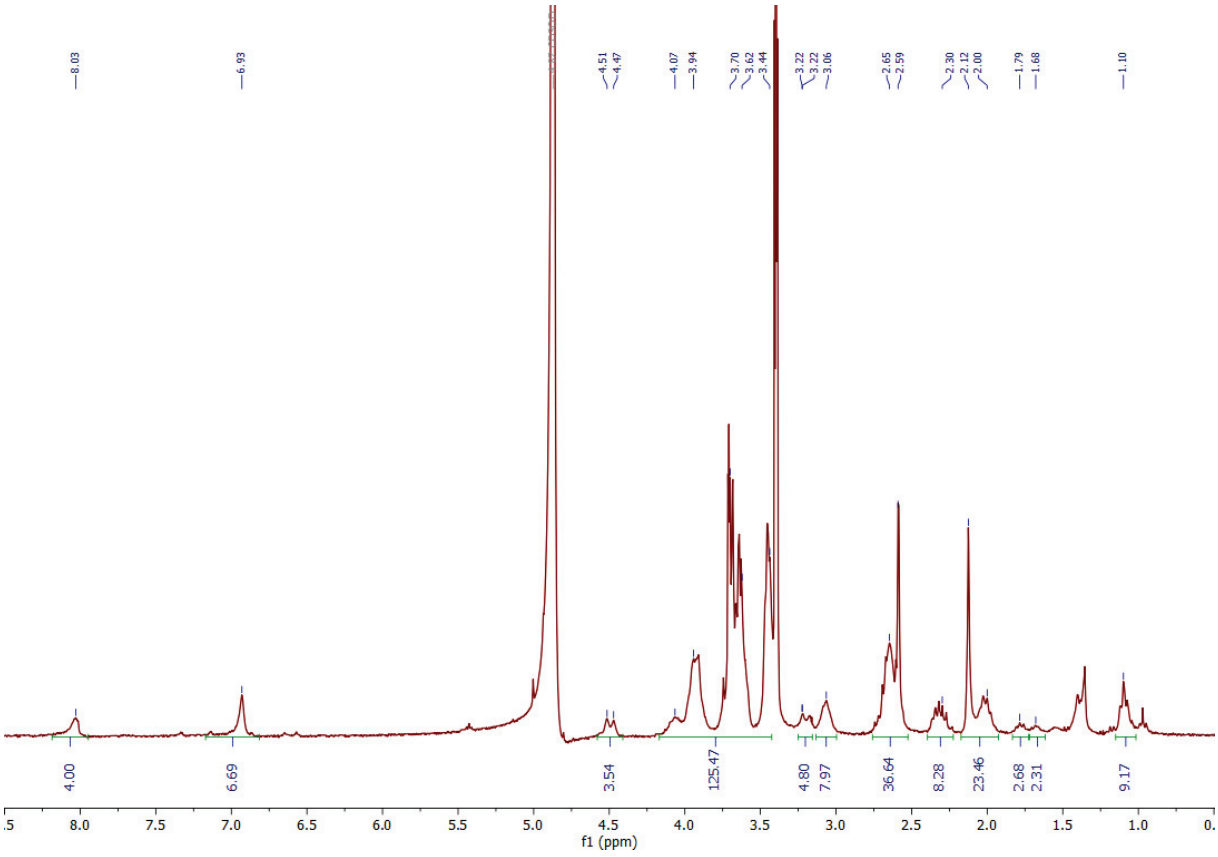

Figure 88: ^{1}H-NMR spectrum (300 MHz) of compound C16 in MeOH-d4/D_2O.

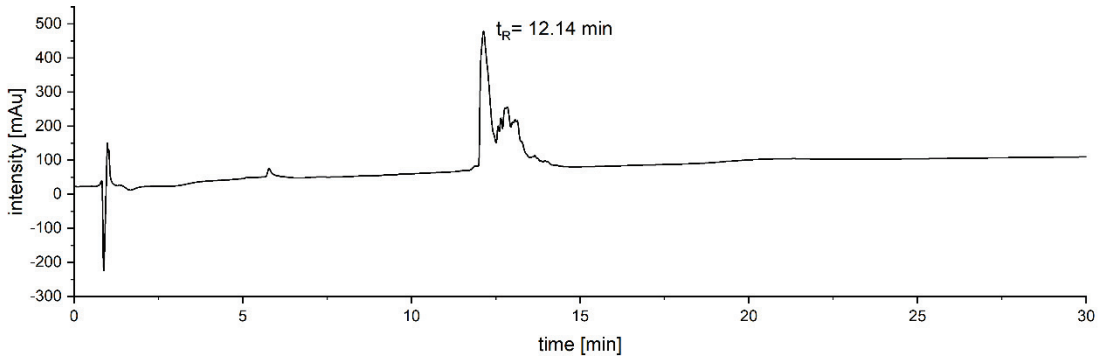

Figure 89: RP-HPLC chromatogram (100 % A to 50 % A in 30 min at 25 °C) of compound C16.

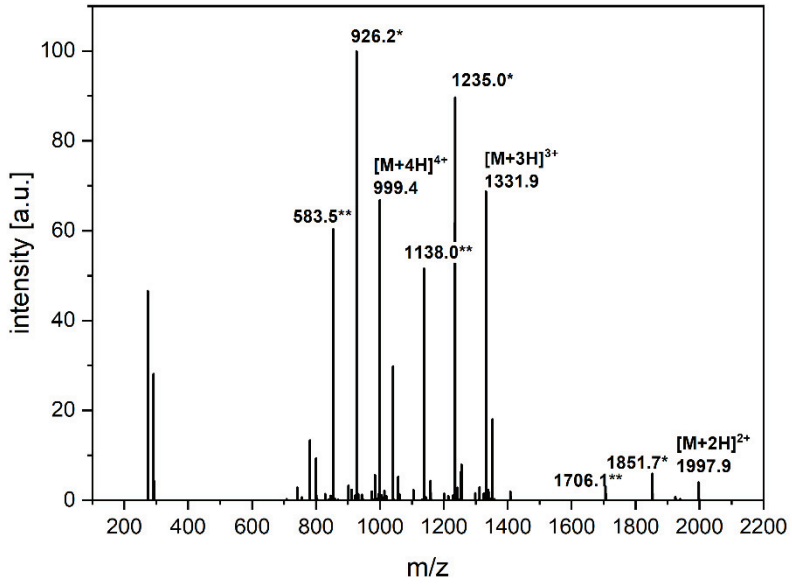

*Figure 90: ESI-MS spectrum at t_R = 12.1 min (100 % A to 0 % A in 30 min at 25 °C) of compound C16. m/z assigned to by-products due to Neu5Ac cleavage are marked with * (-1 Neu5Nac), ** (-2 Neu5Ac) or *** (-3 Neu5Ac).*

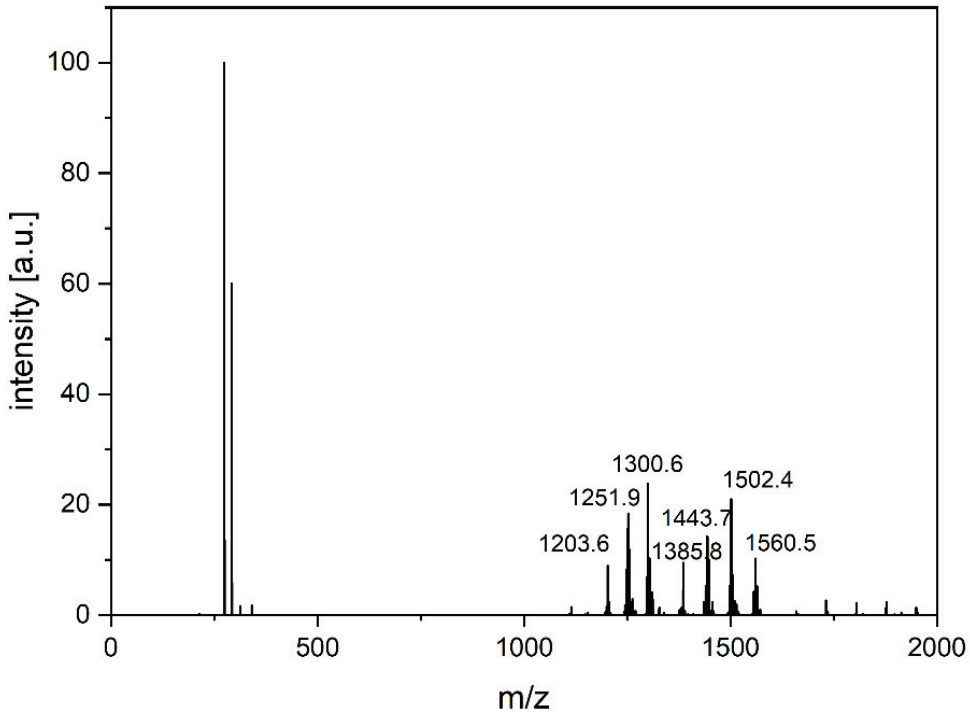

Figure 91: ESI-MS spectrum at t_R = 9.5 min (100 % A to 0 % A in 30 min at 25 °C) of compound C19.

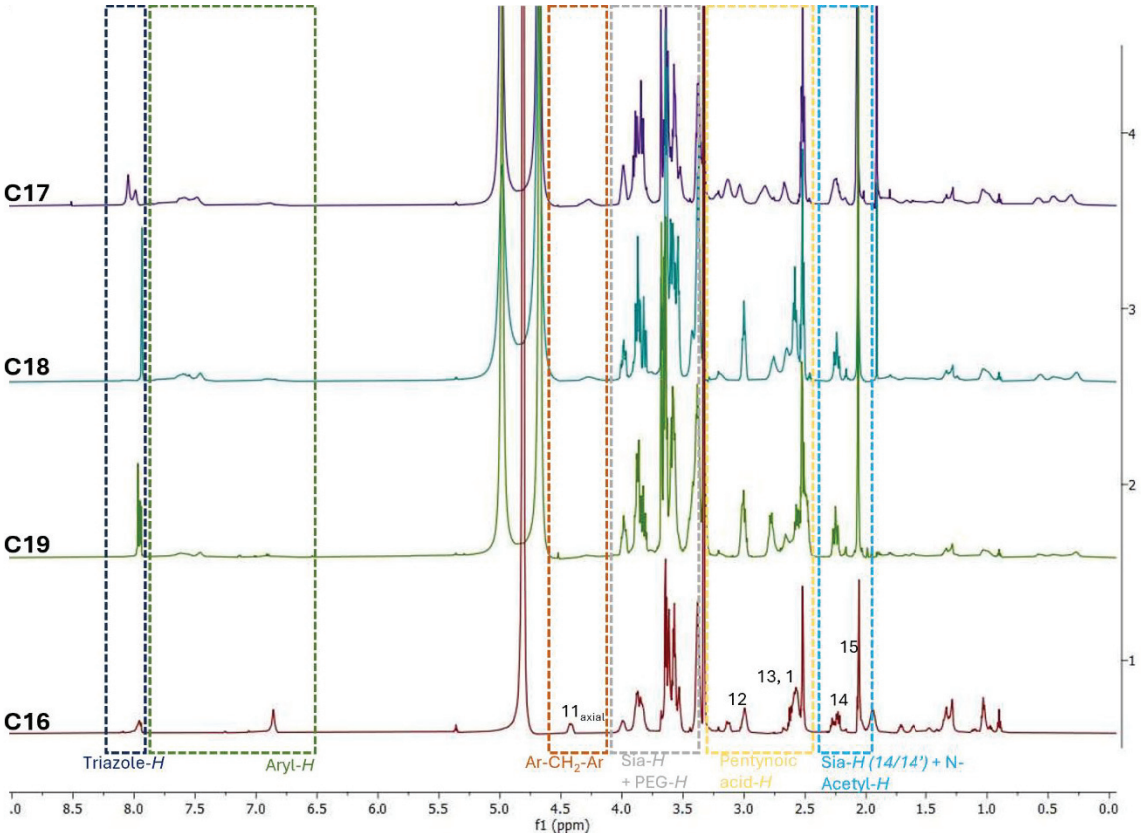

Figure 92: stack ^{1}H-NMR (600 MHz) of compound C16 (25 °C), C17, C18 and C19 (90 °C) in MeOH-d4/D_2O.

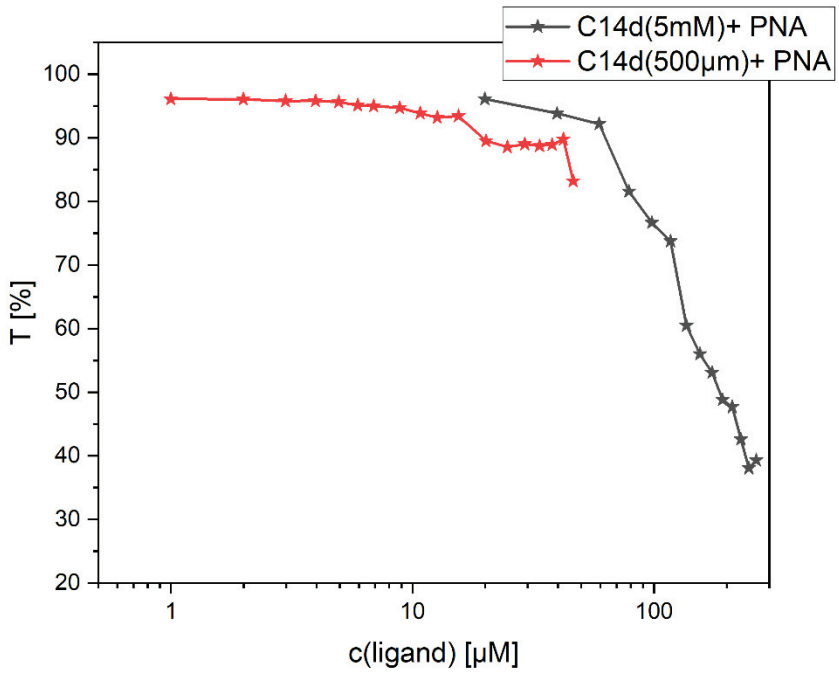

Figure 93: Transmittance values obtained from concentration-dependent turbidity assay with PNA (star) for different stock concentrations of C14d (5 mM or 500 µM).

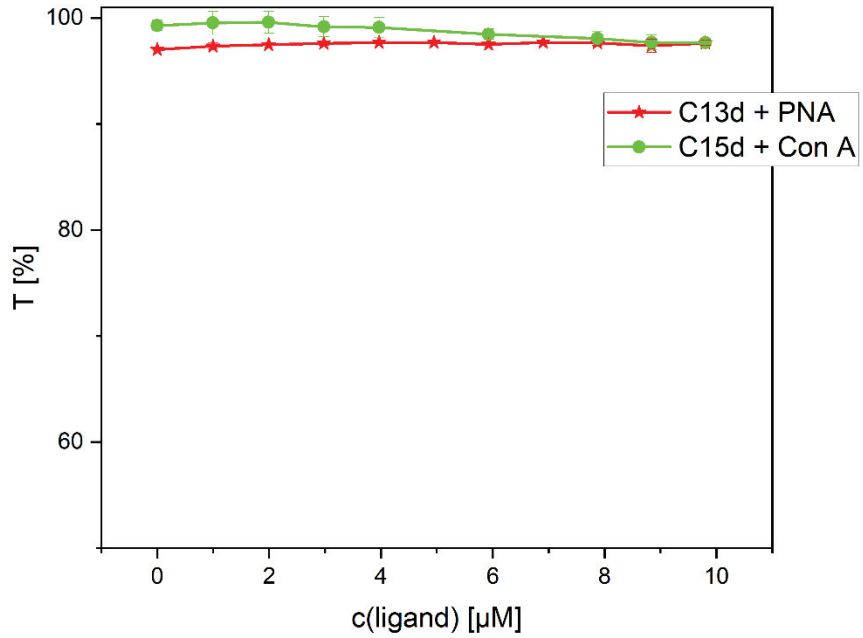

Figure 94: Transmittance values obtained from concentration-dependent turbidity assay for negative controls (C13d + PNA and C15d + Con A).

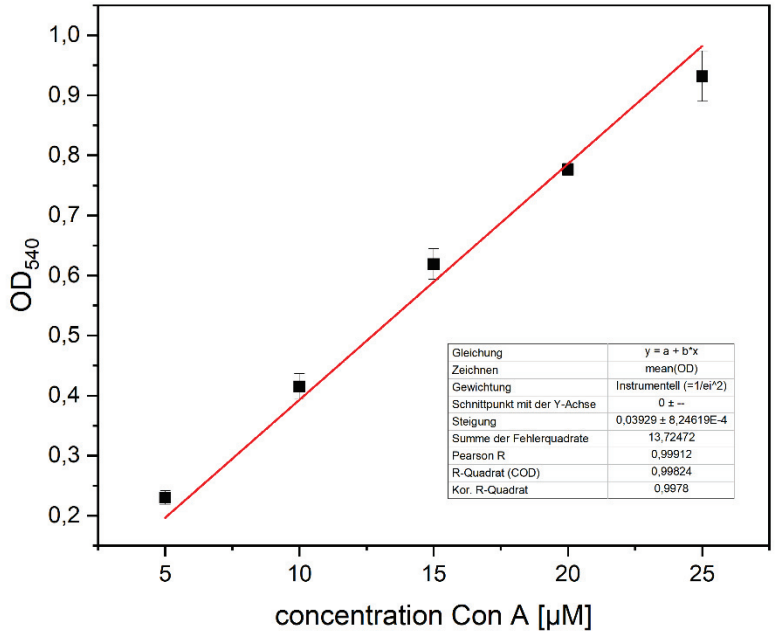

Figure 95: Calibration Curve BCA method for the protein Con A. The measurement was performed on a CLARIOstar® reader from BMG LABTECH in triplicates.

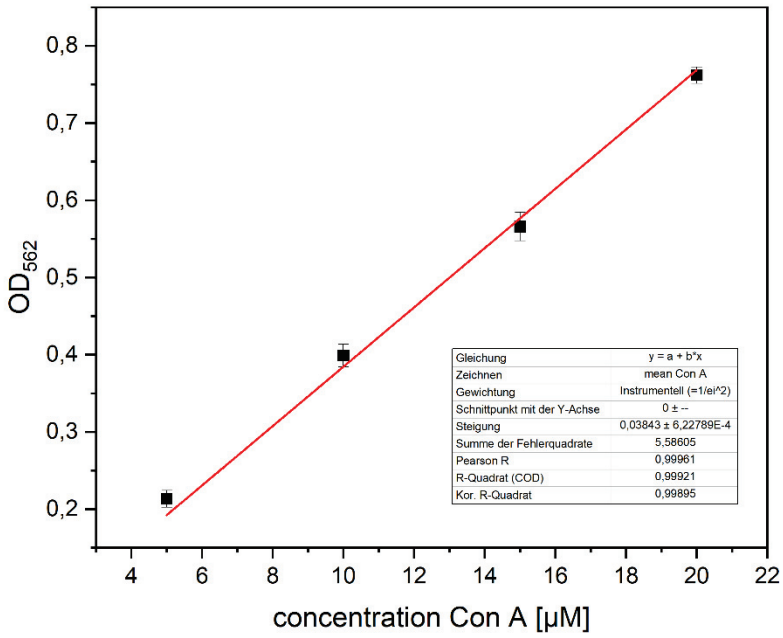

Figure 96: Calibration Curve BCA method for the protein Con A. The measurement was performed on a Multiskan Go reader from Thermo Scientific in triplicates.

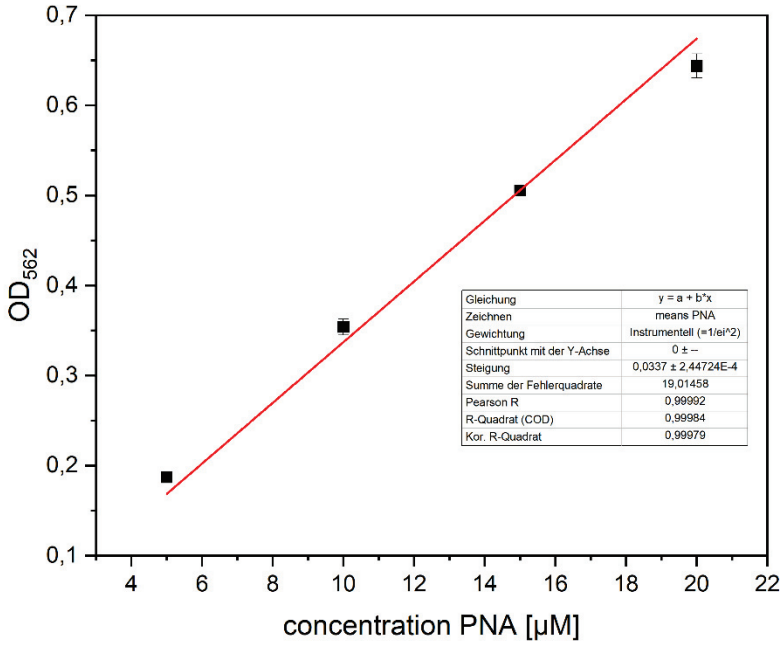

Figure 97: Calibration Curve BCA method for the protein PNA. The measurement was performed on a Multiskan Go reader from Thermo Scientific in triplicates

7 . References

1. A. Varki, *Glycobiology*, 2017, **27**, 3-49.
2. X. Zeng, C. A. Andrade, M. D. Oliveira and X.-L. Sun, *Analytical and bioanalytical chemistry*, 2012, **402**, 3161-3176.
3. R. Raman, S. Raguram, G. Venkataraman, J. C. Paulson and R. Sasisekharan, *Nature methods*, 2005, **2**, 817-824.
4. W. Burchard, in *Plant polymeric carbohydrates*, Elsevier, 1993, pp. 215-232.
5. B. Mishra, S. Manmode, G. Walke, S. Chakraborty, M. Neralkar and S. Hotha, *Organic & Biomolecular Chemistry*, 2021, **19**, 1315-1328.
6. L. L. Kiessling, J. E. Gestwicki and L. E. Strong, *Current opinion in chemical biology*, 2000, **4**, 696-703.
7. E. Köttgen, W. Reutter and R. Tauber, *Medizinische Klinik*, 2003, **98**, 717-738.
8. G. Gupta and G. Gupta, *Animal lectins: Form, function and clinical applications*, 2012, 3-25.
9. N. Sharon and H. Lis, *Lectins*, Springer Science & Business Media, 2003.
10. M. Ambrosi, N. R. Cameron and B. G. Davis, *Organic & biomolecular chemistry*, 2005, **3**, 1593-1608.
11. D. R. Bundle and N. M. Young, *Current opinion in structural biology*, 1992, **2**, 666-673.
12. S. Cecioni, A. Imberty and S. Vidal, *Chemical reviews*, 2015, **115**, 525-561.
13. G. M. Edelman, B. A. Cunningham, G. N. Reeke Jr, J. W. Becker, M. J. Waxdal and J. L. Wang, *Proceedings of the national academy of sciences*, 1972, **69**, 2580-2584.
14. S. D. Knight and J. Bouckaert, *Glycoscience and Microbial Adhesion*, 2009, 67-107.
15. M. M. Sauer, R. P. Jakob, T. Luber, F. Canonica, G. Navarra, B. Ernst, C. Unverzagt, T. Maier and R. Glockshuber, *Journal of the American Chemical Society*, 2018, **141**, 936-944.
16. J. Bouckaert, J. Berglund, M. Schembri, E. De Genst, L. Cools, M. Wuhrer, C. S. Hung, J. Pinkner, R. Slättegård and A. Zavialov, *Molecular microbiology*, 2005, **55**, 441-455.
17. F. Lehmann, E. Tiralongo and J. Tiralongo, *Cellular and Molecular Life Sciences CMLS*, 2006, **63**, 1331-1354.
18. W. I. Weis, *Current opinion in structural biology*, 1997, **7**, 624-630.
19. A. S. Dugan, S. Eash and W. J. Atwood, *Journal of virology*, 2005, **79**, 14442-14445.
20. U. Neu, H. Hengel, B. S. Blaum, R. M. Schowalter, D. Macejak, M. Gilbert, W. W. Wakarchuk, A. Imamura, H. Ando and M. Kiso, *PLoS pathogens*, 2012, **8**, e1002738.
21. Y. C. Lee and R. T. Lee, *Accounts of chemical research*, 1995, **28**, 321-327.
22. M. Mammen, S.-K. Choi and G. M. Whitesides, *Angewandte Chemie International Edition*, 1998, **37**, 2754-2794.
23. T. K. Dam, T. A. Gerken, B. S. Cavada, K. S. Nascimento, T. R. Moura and C. F. Brewer, *Journal of Biological Chemistry*, 2007, **282**, 28256-28263.
24. J. E. Gestwicki, C. W. Cairo, L. E. Strong, K. A. Oetjen and L. L. Kiessling, *Journal of the American Chemical Society*, 2002, **124**, 14922-14933.

25. C. O. Mellet, J.-F. Nierengarten and J. M. G. Fernández, *Journal of Materials Chemistry B*, 2017, **5**, 6428-6436.

26. D. Deniaud, K. Julienne and S. G. Gouin, *Organic & biomolecular chemistry*, 2011, **9**, 966-979.

27. L. L. Kiessling and N. L. Pohl, *Chemistry & biology*, 1996, **3**, 71-77.

28. J. B. Sumner and G. F. Somers, in *Chemistry and Methods of Enzymes (Third Edition)*, eds. J. B. Sumner and G. F. Somers, Academic Press, 1953, DOI: https://doi.org/10.1016/B978-1-4832-3150-1.50008-1, pp. 1-67.

29. K. Ohtsubo and J. D. Marth, *cell*, 2006, **126**, 855-867.

30. P. M. Rudd and R. A. Dwek, *Critical Reviews in Biochemistry and Molecular Biology*, 1997, **32**, 1-100.

31. L. Ellgaard and A. Helenius, *Nature Reviews Molecular Cell Biology*, 2003, **4**, 181-191.

32. X. Zhou, G. Zhao, J. J. Truglio, L. Wang, G. Li, W. J. Lennarz and H. Schindelin, *Proceedings of the National Academy of Sciences*, 2006, **103**, 17214-17219.

33. F. M. Tomlin, U. I. M. Gerling-Driessen, Y.-C. Liu, R. A. Flynn, J. R. Vangala, C. S. Lentz, S. Clauder-Muenster, P. Jakob, W. F. Mueller, D. Ordoñez-Rueda, M. Paulsen, N. Matsui, D. Foley, A. Rafalko, T. Suzuki, M. Bogyo, L. M. Steinmetz, S. K. Radhakrishnan and C. R. Bertozzi, *ACS Central Science*, 2017, **3**, 1143-1155.

34. T. Suzuki, C. Huang and H. Fujihira, *Gene*, 2016, **577**, 1-7.

35. C. Hirsch, D. Blom and H. L. Ploegh, *The EMBO journal*, 2003, **22**, 1036-1046.

36. T. Suzuki, H. Park and W. J. Lennarz, *The FASEB Journal*, 2002, **16**, 635-641.

37. G. Zhao, G. Li, X. Zhou, I. Matsuo, Y. Ito, T. Suzuki, W. J. Lennarz and H. Schindelin, *Glycobiology*, 2008, **19**, 118-125.

38. S. Walber, G. Partalidou and U. I. M. Gerling-Driessen, *Israel Journal of Chemistry*, 2023, **63**, e202200068.

39. S. L. Taylor, M. A. McGuckin, S. Wesselingh and G. B. Rogers, *Trends in microbiology*, 2018, **26**, 92-101.

40. S. V. Glavey, D. Huynh, M. R. Reagan, S. Manier, M. Moschetta, Y. Kawano, A. M. Roccaro, I. M. Ghobrial, L. Joshi and M. E. O'Dwyer, *Blood reviews*, 2015, **29**, 269-279.

41. M. M. Fuster and J. D. Esko, *Nature Reviews Cancer*, 2005, **5**, 526-542.

42. D. H. Dube and C. R. Bertozzi, *Nature reviews Drug discovery*, 2005, **4**, 477-488.

43. J. J. Lyons, J. D. Milner and S. D. Rosenzweig, *Frontiers in pediatrics*, 2015, **3**, 54.

44. B. Ernst and J. L. Magnani, *Nature reviews Drug discovery*, 2009, **8**, 661-677.

45. P. Compain, *The Chemical Record*, 2020, **20**, 10-22.

46. A. Tamburrini, C. Colombo and A. Bernardi, *Medicinal research reviews*, 2020, **40**, 495-531.

47. R. Hevey, *Pharmaceuticals*, 2019, **12**, 55.

48. C. R. Bertozzi, Kiessling and L. L, *Science*, 2001, **291**, 2357-2364.

49. A. Hölemann and P. H. Seeberger, *Current opinion in biotechnology*, 2004, **15**, 615-622.

50. S. Behren and U. Westerlind, *Molecules*, 2019, **24**, 1004.

51. P. I. Kitov, J. M. Sadowska, G. Mulvey, G. D. Armstrong, H. Ling, N. S. Pannu, R. J. Read and D. R. Bundle, *Nature*, 2000, **403**, 669-672.

52. C. C. Appeldoorn, J. A. Joosten, F. A. el Maate, U. Dobrindt, J. Hacker, R. M. Liskamp, A. S. Khan and R. J. Pieters, *Tetrahedron: Asymmetry*, 2005, **16**, 361-372.

53. S. Cecioni, R. Lalor, B. Blanchard, J. P. Praly, A. Imberty, S. E. Matthews and S. Vidal, *Chemistry–A European Journal*, 2009, **15**, 13232-13240.

54. T. K. Lindhorst, M. Dubber, U. Krallmann-Wenzel and S. Ehlers, *European Journal of Organic Chemistry*, 2000, **2000**, 2027-2034.

55. M. Gómez-García, J. M. Benito, R. Gutiérrez-Gallego, A. Maestre, C. O. Mellet, J. M. G. Fernández and J. L. J. Blanco, *Organic & Biomolecular Chemistry*, 2010, **8**, 1849-1860.

56. R. Roy, D. Page, S. Figueroa Perez and V. Verez Bencomo, *Glycoconjugate Journal*, 1998, **15**, 251-263.

57. E. A. Biessen, D. M. Beuting, H. C. Roelen, G. A. van de Marel, J. H. Van Boom and T. J. Van Berkel, *Journal of medicinal chemistry*, 1995, **38**, 1538-1546.

58. J. M. Benito, M. Gómez-García, C. Ortiz Mellet, I. Baussanne, J. Defaye and J. M. García Fernández, *Journal of the American Chemical Society*, 2004, **126**, 10355-10363.

59. C. W. Cairo, J. E. Gestwicki, M. Kanai and L. L. Kiessling, *Journal of the American Chemical Society*, 2002, **124**, 1615-1619.

60. M. Kanai, K. H. Mortell and L. L. Kiessling, *Journal of the American Chemical Society*, 1997, **119**, 9931-9932.

61. S. Cecioni, S. Faure, U. Darbost, I. Bonnamour, H. Parrot-Lopez, O. Roy, C. Taillefumier, M. Wimmerová, J. P. Praly and A. Imberty, *Chemistry–A European Journal*, 2011, **17**, 2146-2159.

62. I. Pramudya and H. Chung, *Biomaterials science*, 2019, **7**, 4848-4872.

63. S. S. Ting, G. Chen and M. H. Stenzel, *Polymer Chemistry*, 2010, **1**, 1392-1412.

64. L. Soria-Martinez, S. Bauer, M. Giesler, S. Schelhaas, J. Materlik, K. Janus, P. Pierzyna, M. Becker, N. L. Snyder, L. Hartmann and M. Schelhaas, *Journal of the American Chemical Society*, 2020, **142**, 5252-5265.

65. M. Touaibia, T. C. Shiao, A. Papadopoulos, J. Vaucher, Q. Wang, K. Benhamioud and R. Roy, *Chemical Communications*, 2007, DOI: 10.1039/B612471B, 380-382.

66. C.-C. Lin, Y.-C. Yeh, C.-Y. Yang, G.-F. Chen, Y.-C. Chen, Y.-C. Wu and C.-C. Chen, *Chemical Communications*, 2003, DOI: 10.1039/B308995A, 2920-2921.

67. C.-C. Lin, Y.-C. Yeh, C.-Y. Yang, C.-L. Chen, G.-F. Chen, C.-C. Chen and Y.-C. Wu, *Journal of the American Chemical Society*, 2002, **124**, 3508-3509.

68. S. André, F. Sansone, H. Kaltner, A. Casnati, J. Kopitz, H. J. Gabius and R. Ungaro, *ChemBioChem*, 2008, **9**, 1649-1661.

69. C. Ortiz-Mellet, J. M. Benito, J. M. García Fernández, H. Law, K. Chmurski, J. Defaye, M. L. O'Sullivan and H. N. Caro, *Chemistry–A European Journal*, 1998, **4**, 2523-2531.

70. P. Bojarová and V. Křen, *Biomaterials science*, 2016, **4**, 1142-1160.

71. J. J. Lundquist and E. J. Toone, *Chemical reviews*, 2002, **102**, 555-578.

72. Y. Miura, *Polymer journal*, 2012, **44**, 679-689.

73. M. Von Itzstein, W.-Y. Wu, G. B. Kok, M. S. Pegg, J. C. Dyason, B. Jin, T. Van Phan, M. L. Smythe, H. F. White and S. W. Oliver, *Nature*, 1993, **363**, 418-423.

74. K. McClellan and C. M. Perry, *Drugs*, 2001, **61**, 263-283.

75. P. Compain, C. Decroocq, J. Iehl, M. Holler, D. Hazelard, T. Mena Barragan, C. Ortiz Mellet and J. F. Nierengarten, *Angewandte Chemie*, 2010, **122**, 5889-5892.

76. C. Decroocq, D. Rodríguez-Lucena, V. Russo, T. Mena Barragan, C. Ortiz Mellet and P. Compain, *Chemistry–A European Journal*, 2011, **17**, 13825-13831.

77. J. F. Nierengarten, J. P. Schneider, T. M. N. Trinh, A. Joosten, M. Holler, M. L. Lepage, A. Bodlenner, M. I. García-Moreno, C. Ortiz Mellet and P. Compain, *Chemistry–A European Journal*, 2018, **24**, 2483-2492.

78. M. L. Lepage, J. P. Schneider, A. Bodlenner, A. Meli, F. De Riccardis, M. Schmitt, C. Tarnus, N. T. Nguyen-Huynh, Y. N. Francois and E. Leize-Wagner, *Chemistry–A European Journal*, 2016, **22**, 5151-5155.

79. Y. Brissonnet, C. Ortiz Mellet, S. Morandat, M. I. Garcia Moreno, D. Deniaud, S. E. Matthews, S. Vidal, S. Sestak, K. El Kirat and S. G. Gouin, *Journal of the American Chemical Society*, 2013, **135**, 18427-18435.

80. E. Howard, A. Cousido-Siah, M. L. Lepage, J. P. Schneider, A. Bodlenner, A. Mitschler, A. Meli, I. Izzo, H. A. Alvarez and A. Podjarny, *Angewandte Chemie International Edition*, 2018, **57**, 8002-8006.

81. C. Ortiz Mellet, J.-F. Nierengarten and J. M. García Fernández, *Journal of Materials Chemistry B*, 2017, **5**, 6428-6436.

82. M. Abellán Flos, M. I. García Moreno, C. Ortiz Mellet, J. M. Garcia Fernandez, J. F. Nierengarten and S. P. Vincent, *Chemistry–A European Journal*, 2016, **22**, 11450-11460.

83. C. D. Gutsche and R. Muthukrishnan, *The Journal of Organic Chemistry*, 1978, **43**, 4905-4906.

84. C. D. Gutsche, *Accounts of Chemical Research*, 1983, **16**, 161-170.

85. A. v. Baeyer, *Berichte der deutschen chemischen gesellschaft*, 1872, **5**, 1094-1100.

86. L. Baekeland, *Industrial & Engineering Chemistry*, 1913, **5**, 506-511.

87. A. Zinke, R. Kretz, E. Leggewie, K. Hössinger, G. Hoffmann, P. Weber v. Ostwalden, E. Wiesenberger, M. Sobotka and R. Kretz, *Monatshefte für Chemie und verwandte Teile anderer Wissenschaften*, 1952, **83**, 1213-1227.

88. A. Zinke and E. Ziegler, *Berichte der deutschen chemischen Gesellschaft (A and B Series)*, 1944, **77**, 264-272.

89. 1981.

90. C. D. Gutsche, B. Dhawan, K. H. No and R. Muthukrishnan, *Journal of the American Chemical Society*, 1981, **103**, 3782-3792.

91. B. Dhawan, S.-I. Chen and C. D. Gutsche, *Die Makromolekulare Chemie*, 1987, **188**, 921-950.

92. V. Böhmer, *Angewandte Chemie International Edition in English*, 1995, **34**, 713-745.

93. C. D. Gutsche, M. Iqbal and D. Stewart, *The Journal of Organic Chemistry*, 1986, **51**, 742-745.

94. C. Gutsche, *Organic syntheses*, 1990, **68**, 238.

95. J. Munch and C. Gutsche, *Organic Syntheses*, 2003, 80-80.

96. D. R. Stewart and C. D. Gutsche, *Organic preparations and procedures international*, 1993, **25**, 137-139.

97. F. Vocanson and R. Lamartine, *Supramolecular Chemistry*, 1996, **7**, 19-25.

98. A. Ninagawa and H. Matsuda, *Die Makromolekulare Chemie, Rapid Communications*, 1982, **3**, 65-67.

99. C. D. Gutsche, J. S. Rogers, D. Stewart and K.-A. See, *Pure and Applied Chemistry*, 1990, **62**, 485-491.

100. B. Hayes and R. Hunter, *Journal of Applied Chemistry*, 1958, **8**, 743-748.

101. H. Kämmerer, G. Happel, V. Böhmer and D. Rathay, *Monatshefte für Chemie-Chemical Monthly*, 1978, **109**, 767-773.

102. J. Cornforth, P. A. Hart, G. Nicholls, R. Rees and J. Stock, *British journal of pharmacology and chemotherapy*, 1955, **10**, 73.

103. C. D. Gutsche and L. J. Bauer, *Journal of the American Chemical Society*, 1985, **107**, 6052-6059.

104. C. D. Gutsche, B. Dhawan, J. A. Levine, K. H. No and L. J. Bauer, *Tetrahedron*, 1983, **39**, 409-426.

105. V. Bocchi, D. Foina, A. Pochini, R. Ungaro and G. Andreetti, *Tetrahedron*, 1982, **38**, 373-378.

106. G. D. Andreetti, A. Pochini and R. Ungaro, *Journal of the Chemical Society, Perkin Transactions 2*, 1983, 1773-1779.

107. V. Böhmer, R. Dörrenbächer, M. Frings, M. Heydenreich, D. de Paoli, W. Vogt, G. Ferguson and I. Thondorf, *The Journal of Organic Chemistry*, 1996, **61**, 549-559.

108. H. Kämmerer and G. Happel, *Die Makromolekulare Chemie: Macromolecular Chemistry and Physics*, 1978, **179**, 1199-1207.

109. H. Kämmerer and G. Happel, *Die Makromolekulare Chemie: Macromolecular Chemistry and Physics*, 1980, **181**, 2049-2062.

110. C. D. Gutsche, A. E. Gutsche and A. I. Karaulov, *Journal of inclusion phenomena*, 1985, **3**, 447-451.

111. P. Neri, J. L. Sessler and M.-X. Wang, *Calixarenes and beyond*, Springer, 2016.

112. J. Vicens and V. Böhmer, *Calixarenes: a versatile class of macrocyclic compounds*, Springer Science & Business Media, 2012.

113. C. D. Gutsche and P. F. Pagoria, *The Journal of Organic Chemistry*, 1985, **50**, 5795-5802.

114. C. D. Gutsche, J. A. Levine and P. d. Sujeeth, *The Journal of Organic Chemistry*, 1985, **50**, 5802-5806.

115. F. Arnaud-Neu, E. M. Collins, M. Deasy, G. Ferguson, S. J. Harris, B. Kaitner, A. J. Lough, M. A. McKervey and E. Marques, *Journal of the American Chemical Society*, 1989, **111**, 8681-8691.

116. C. D. Gutsche and L.-G. Lin, *Tetrahedron*, 1986, **42**, 1633-1640.

117. D. R. Stewart, M. Krawiec, R. P. Kashyap, W. H. Watson and C. D. Gutsche, *Journal of the American Chemical Society*, 1995, **117**, 586-601.

118. K. Iwamoto, K. Araki and S. Shinkai, *Tetrahedron*, 1991, **47**, 4325-4342.

119. S. Shinkai, T. Arimura, K. Araki, H. Kawabata, H. Satoh, T. Tsubaki, O. Manabe and J. Sunamoto, *Journal of the Chemical Society, Perkin Transactions 1*, 1989, 2039-2045.

120. K.-H. No and Y.-J. Noh, *Bulletin of the Korean Chemical Society*, 1986, **7**, 314-316.

121. Z. T. Huang and G. Q. Wang, *Chemische Berichte*, 1994, **127**, 519-523.

122. E. M. Collins, M. A. McKervey, E. Madigan, M. B. Moran, M. Owens, G. Ferguson and S. J. Harris, *Journal of the Chemical Society, Perkin Transactions 1*, 1991, 3137-3142.

123. F. Bottino, L. Giunta and S. Pappalardo, *The Journal of Organic Chemistry*, 1989, **54**, 5407-5409.

124. A. Arduini, A. Casnati, L. Dodi, A. Pochini and R. Ungaro, *Journal of the Chemical Society, Chemical Communications*, 1990, 1597-1598.

125. K. A. See, F. R. Fronczek, W. H. Watson, R. P. Kashyap and C. D. Gutsche, *The Journal of Organic Chemistry*, 1991, **56**, 7256-7268.

126. J.-D. Van Loon, W. Verboom and D. Reinhoudt, *Organic preparations and procedures international*, 1992, **24**, 437-462.

127. J. D. Van Loon, A. Arduini, L. Coppi, W. Verboom, A. Pochini, R. Ungaro, S. Harkema and D. N. Reinhoudt, *The Journal of Organic Chemistry*, 1990, **55**, 5639-5646.

128. S. Shirakawa, T. Kimura, S.-i. Murata and S. Shimizu, *The Journal of Organic Chemistry*, 2009, **74**, 1288-1296.

129. S. O. Kang and K. C. Nam, *BULLETIN-KOREAN CHEMICAL SOCIETY*, 2000, **21**, 167-168.

130. Y. Yang, X. Cao, D. W. Purkiss, J. F. Cannon and R. A. Bartsch, *Tetrahedron*, 2012, **68**, 2233-2244.

131. S. E. Matthews, S. Cecioni, J. E. O'Brien, C. J. MacDonald, D. L. Hughes, G. A. Jones, S. H. Ashworth and S. Vidal, *Chemistry–A European Journal*, 2018, **24**, 4436-4444.

132. S. R. Izatt, R. T. Hawkins, J. J. Christensen and R. M. Izatt, *Journal of the American Chemical Society*, 1985, **107**, 63-66.

133. M. Torvinen, R. Neitola, F. Sansone, L. Baldini, R. Ungaro, A. Casnati, P. Vainiotalo and E. Kalenius, *Organic & Biomolecular Chemistry*, 2010, **8**, 906-915.

134. M. AnthonyáMcKervey, *Journal of the Chemical Society, Perkin Transactions 2*, 1992, 1119-1125.

135. E. Sanabria Español and M. Maldonado, *Critical reviews in analytical chemistry*, 2019, **49**, 383-394.

136. V. V. Trush, S. O. Cherenok, V. Y. Tanchuk, V. P. Kukhar, V. I. Kalchenko and A. I. Vovk, *Bioorganic & medicinal chemistry letters*, 2013, **23**, 5619-5623.

137. A. M. Doolan, M. L. Rennie and P. B. Crowley, *Chemistry–A European Journal*, 2018, **24**, 984-991.

138. K. Wang, D. S. Guo and Y. Liu, *Chemistry–A European Journal*, 2010, **16**, 8006-8011.

139. L. Baldini, A. Casnati and F. Sansone, *European Journal of Organic Chemistry*, 2020, **2020**, 5056-5069.

140. R. Kumar, A. Sharma, H. Singh, P. Suating, H. S. Kim, K. Sunwoo, I. Shim, B. C. Gibb and J. S. Kim, *Chemical Reviews*, 2019, **119**, 9657-9721.

141. R. J. Forster, A. Cadogan, M. T. Diaz, D. Diamond, S. J. Harris and M. A. McKervey, *Sensors and Actuators B: Chemical*, 1991, **4**, 325-331.

142. D. Shetty, I. Jahovic, J. Raya, Z. Asfari, J.-C. Olsen and A. Trabolsi, *ACS applied materials & interfaces*, 2018, **10**, 2976-2981.

143. I. Urban, N. M. Ratcliffe, J. R. Duffield, G. R. Elder and D. Patton, *Chemical communications*, 2010, **46**, 4583-4585.

144. V. S. Bieber, E. Ozcelik, H. J. Cox, C. J. Ottley, J. K. Ratan, M. Karaman, M. Tabakci, S. K. Beaumont and J. P. S. Badyal, *ACS Applied Materials & Interfaces*, 2020, **12**, 52136-52145.

145. S. Karakurt, T. F Kellici, T. Mavromoustakos, A. G Tzakos and M. Yilmaz, *Current Organic Chemistry*, 2016, **20**, 1043-1057.

146. Y. Razuvayeva, R. Kashapov and L. Zakharova, *Supramolecular Chemistry*, 2020, **32**, 178-206.

147. Y. C. Pan, X. Y. Hu and D. S. Guo, *Angewandte Chemie*, 2021, **133**, 2800-2828.

148. A. Norouzy, Z. Azizi and W. M. Nau, *Angewandte Chemie*, 2015, **127**, 804-808.

149. H.-T. Feng, Y. Li, X. Duan, X. Wang, C. Qi, J. W. Lam, D. Ding and B. Z. Tang, *Journal of the American Chemical Society*, 2020, **142**, 15966-15974.

150. C. Chen, X. Ni, H. W. Tian, Q. Liu, D. S. Guo and D. Ding, *Angewandte Chemie*, 2020, **132**, 10094-10098.

151. A. Marra, M.-C. Scherrmann, A. Dondoni, A. Casnati, P. Minari and R. Ungaro, *Angewandte Chemie. International edition in English*, 1994, **33**, 2479-2481.

152. A. Dondoni, A. Marra, M. C. Scherrmann, A. Casnati, F. Sansone and R. Ungaro, *Chemistry–A European Journal*, 1997, **3**, 1774-1782.

153. A. Dondoni and A. Marra, *Chemical reviews*, 2010, **110**, 4949-4977.

154. U. Schädel, F. Sansone, A. Casnati and R. Ungaro, *Tetrahedron*, 2005, **61**, 1149-1154.

155. G. M. Consoli, G. Granata, V. Cafiso, S. Stefani and C. Geraci, *Tetrahedron letters*, 2011, **52**, 5831-5834.

156. R. Roy and J. M. Kim, *Angewandte Chemie International Edition*, 1999, **38**, 369-372.

157. C. Saitz-Barria, A. Torres-Pinedo and F. Santoyo-González, *Synlett*, 1999, **1999**, 1891-1894.

158. G. M. Consoli, F. Cunsolo, C. Geraci and V. Sgarlata, *Organic Letters*, 2004, **6**, 4163-4166.

159. G. M. Consoli, F. Cunsolo, C. Geraci, T. Mecca and P. Neri, *Tetrahedron letters*, 2003, **44**, 7467-7470.

160. A. Dondoni and A. Marra, *The Journal of Organic Chemistry*, 2006, **71**, 7546-7557.

161. M. Fiore, A. Chambery, A. Marra and A. Dondoni, *Organic & biomolecular chemistry*, 2009, **7**, 3910-3913.

162. I. Morbioli, V. Porkolab, A. Magini, A. Casnati, F. Fieschi and F. Sansone, *Carbohydrate research*, 2017, **453**, 36-43.

163. S. J. Meunier and R. Roy, *Tetrahedron letters*, 1996, **37**, 5469-5472.

164. A. Marra, L. Moni, D. Pazzi, A. Corallini, D. Bridi and A. Dondoni, *Organic & Biomolecular Chemistry*, 2008, **6**, 1396-1409.

165. C. Geraci, G. M. Consoli, E. Galante, E. Bousquet, M. Pappalardo and A. Spadaro, *Bioconjugate chemistry*, 2008, **19**, 751-758.

166. B. Merrifield, *Science*, 1986, **232**, 341-347.

167. R. B. Merrifield, *Journal of the American Chemical Society*, 1963, **85**, 2149-2154.

168. C. Schuerch and J. M. Frechet, *Journal of the American Chemical Society*, 1971, **93**, 492-496.

169. R. L. Letsinger and V. Mahadevan, *Journal of the American Chemical Society*, 1965, **87**, 3526-3527.

170. D. Ponader, F. Wojcik, F. Beceren-Braun, J. Dernedde and L. Hartmann, *Biomacromolecules*, 2012, **13**, 1845-1852.

171. L. Hartmann, E. Krause, M. Antonietti and H. G. Börner, *Biomacromolecules*, 2006, **7**, 1239-1244.

172. F. Wojcik, S. Mosca and L. Hartmann, *The Journal of organic chemistry*, 2012, **77**, 4226-4234.

173. M. Goodman, W. Cai and N. D. Smith, *Journal of Peptide Science: An Official Publication of the European Peptide Society*, 2003, **9**, 594-603.

174. V. T. Ivanov, E. Y. Blishchenko, O. V. Sazonova and A. A. Karelin, *Journal of Peptide Science: An Official Publication of the European Peptide Society*, 2003, **9**, 553-562.

175. J. Schneider and S. B. Kent, *Cell*, 1988, **54**, 363-368.

176. B. Gutte and R. Merrifield, *Journal of Biological Chemistry*, 1971, **246**, 1922-1941.

177. B. Marglin and R. Merrifield, *Journal of the american chemical society*, 1966, **88**, 5051-5052.

178. M. Amblard, J.-A. Fehrentz, J. Martinez and G. Subra, *Molecular biotechnology*, 2006, **33**, 239-254.

179. I. Coin, M. Beyermann and M. Bienert, *Nature protocols*, 2007, **2**, 3247-3256.

180. R. B. Merrifield, J. M. Stewart and N. Jernberg, *Analytical chemistry*, 1966, **38**, 1905-1914.

181. J. Tian, Y. Li, B. Ma, Z. Tan and S. Shang, *Frontiers in Chemistry*, 2022, **10**, 896098.

182. F. Guillier, D. Orain and M. Bradley, *Chemical Reviews*, 2000, **100**, 2091-2158.

183. E. Bayer, *Angewandte Chemie International Edition in English*, 1991, **30**, 113-129.

184. L. A. Carpino, *Accounts of Chemical Research*, 1987, **20**, 401-407.

185. L. A. Carpino and G. Y. Han, *The Journal of Organic Chemistry*, 1972, **37**, 3404-3409.

186. E. Atherton, *Bioorg. Chem.*, 1979, **8**, 351.

187. S.-S. Wang, *Journal of the American Chemical Society*, 1973, **95**, 1328-1333.

188. H. Rink, *Tetrahedron letters*, 1987, **28**, 3787-3790.

189. K. Barlos, O. Chatzi, D. Gatos and G. Stavropoulos, *Int. J. Pept. Protein Res*, 1991, **37**, 513-520.

190. D. s. M. Jaradat, *Amino acids*, 2018, **50**, 39-68.

191. G. W. Anderson and A. C. McGregor, *Journal of the American Chemical Society*, 1957, **79**, 6180-6183.

192. A. Isidro-Llobet, M. Alvarez and F. Albericio, *Chemical reviews*, 2009, **109**, 2455-2504.

193. C. D. Chang and J. Meienhofer, *International journal of peptide and protein research*, 1978, **11**, 246-249.

194. C. D. CHANG, A. M. FELIX, M. H. JIMENEZ and J. MEIENHOFER, *International Journal of Peptide and Protein Research*, 1980, **15**, 485-494.

195. O. Dangles, F. Guibe, G. Balavoine, S. Lavielle and A. Marquet, *The Journal of Organic Chemistry*, 1987, **52**, 4984-4993.

196. J. Alsina, F. Rabanal, E. Giralt and F. Albericio, *Tetrahedron letters*, 1994, **35**, 9633-9636.

197. A. Dryland and R. C. Sheppard, *Journal of the Chemical Society, Perkin Transactions 1*, 1986, 125-137.

198. C. A. Montalbetti and V. Falque, *Tetrahedron*, 2005, **61**, 10827-10852.

199. J. C. Sheehan and G. P. Hess, *Journal of the American Chemical Society*, 1955, **77**, 1067-1068.

200. J. Rebek and D. Feitler, *Journal of the American Chemical Society*, 1974, **96**, 1606-1607.

201. J. Rebek and D. Feitler, *Journal of the American Chemical Society*, 1973, **95**, 4052-4053.

202. G. Windridge and E. C. Jorgensen, *Journal of the American Chemical Society*, 1971, **93**, 6318-6319.

203. B. Castro, J. Dormoy, G. Evin and C. Selve, *Tetrahedron Letters*, 1975, **16**, 1219-1222.

204. J. Coste, D. Le-Nguyen and B. Castro, *Tetrahedron Letters*, 1990, **31**, 205-208.

205. J. Coste, E. Frerot and P. Jouin, *The Journal of Organic Chemistry*, 1994, **59**, 2437-2446.

206. D. Hudson, *The Journal of organic chemistry*, 1988, **53**, 617-624.

207. V. Dourtoglou, J.-C. Ziegler and B. Gross, *Tetrahedron letters*, 1978, **19**, 1269-1272.

208. R. Knorr, A. Trzeciak, W. Bannwarth and D. Gillessen, *Tetrahedron Letters*, 1989, **30**, 1927-1930.

209. I. Abdelmoty, F. Albericio, L. A. Carpino, B. M. Foxman and S. A. Kates, *Letters in Peptide Science*, 1994, **1**, 57-67.

210. T. Y. Chan, A. Chen, N. Allanson, R. Chen, D. Liu and M. J. Sofia, *Tetrahedron letters*, 1996, **37**, 8097-8100.

211. Y. M. Angell, C. García-Echeverría and D. H. Rich, *Tetrahedron letters*, 1994, **35**, 5981-5984.

212. L. A. Carpino, A. El-Faham and F. Albericio, *Tetrahedron letters*, 1994, **35**, 2279-2282.

213. F. Albericio, M. Cases, J. Alsina, S. A. Triolo, L. A. Carpino and S. A. Kates, *Tetrahedron letters*, 1997, **38**, 4853-4856.

214. S. C. STORY and J. V. ALDRICH, *International Journal of Peptide and Protein Research*, 1994, **43**, 292-296.

215. P. H. Seeberger and W.-C. Haase, *Chemical reviews*, 2000, **100**, 4349-4394.

216. P. Nanjan and M. Porel, *Polymer Chemistry*, 2019, **10**, 5406-5424.

217. Y. Mei, K. L. Beers, H. M. Byrd, D. L. VanderHart and N. R. Washburn, *Journal of the American Chemical Society*, 2004, **126**, 3472-3476.

218. S. A. Hill, C. Gerke and L. Hartmann, *Chemistry–An Asian Journal*, 2018, **13**, 3611-3622.

219. D. Ponader, P. Maffre, J. Aretz, D. Pussak, N. M. Ninnemann, S. Schmidt, P. H. Seeberger, C. Rademacher, G. U. Nienhaus and L. Hartmann, *Journal of the American Chemical Society*, 2014, **136**, 2008-2016.

220. F. Wojcik, S. Lel, A. G. O'Brien, P. H. Seeberger and L. Hartmann, *Beilstein journal of organic chemistry*, 2013, **9**, 2395-2403.

221. F. Wojcik, A. G. O'Brien, S. Götze, P. H. Seeberger and L. Hartmann, *Chemistry–A European Journal*, 2013, **19**, 3090-3098.

222. T. Freichel, S. Eierhoff, N. L. Snyder and L. Hartmann, *The Journal of organic chemistry*, 2017, **82**, 9400-9409.

223. S. Igde, S. Röblitz, A. Müller, K. Kolbe, S. Boden, C. Fessele, T. K. Lindhorst, M. Weber and L. Hartmann, *Macromolecular bioscience*, 2017, **17**, 1700198.

224. C. Gerke, M. F. Ebbesen, D. Jansen, S. Boden, T. Freichel and L. Hartmann, *Biomacromolecules*, 2017, **18**, 787-796.

225. M. Ebbesen, C. Gerke, P. Hartwig and L. Hartmann, *Polymer Chemistry*, 2016, **7**, 7086-7093.

226. T. Freichel, D. Laaf, M. Hoffmann, P. B. Konietzny, V. Heine, R. Wawrzinek, C. Rademacher, N. L. Snyder, L. Elling and L. Hartmann, *RSC advances*, 2019, **9**, 23484-23497.

227. K. Neuhaus, E.-C. Wamhoff, T. Freichel, A. Grafmüller, C. Rademacher and L. Hartmann, *Biomacromolecules*, 2019, **20**, 4088-4095.

228. K. S. Bücher, H. Yan, R. Creutznacher, K. Ruoff, A. Mallagaray, A. Grafmüller, J. S. Dirks, T. Kilic, S. Weickert, A. Rubailo, M. Drescher, S. Schmidt, G. Hansman, T. Peters, C. Uetrecht and L. Hartmann, *Biomacromolecules*, 2018, **19**, 3714-3724.

229. L. Baldini, A. Casnati, F. Sansone and R. Ungaro, *Calixarenes in the Nanoworld*, 2007, 233-257.

230. H. Hioki, T. Yamada, C. Fujioka and M. Kodama, *Tetrahedron letters*, 1999, **40**, 6821-6825.

231. L. Baldini, F. Sansone, F. Scaravelli, C. Massera, A. Casnati and R. Ungaro, *Tetrahedron letters*, 2009, **50**, 3450-3453.

232. S. B. Shuker, J. Esterbrook and J. Gonzalez, *Synlett*, 2001, **2001**, 0210-0213.

233. G. Granata, G. M. Consoli, S. Sciuto and C. Geraci, *Tetrahedron Letters*, 2010, **51**, 6139-6142.

234. I. J. Goldstein and C. E. Hayes, *Advances in carbohydrate chemistry and biochemistry*, 1978, **35**, 127-340.

235. S. Boden, K. G. Wagner, M. Karg and L. Hartmann, *Polymers*, 2017, **9**, 716.

236. A. G. Barrientos, J. M. de la Fuente, M. Jiménez, D. Solís, F. J. Cañada, M. Martín-Lomas and S. Penadés, *Carbohydrate research*, 2009, **344**, 1474-1478.

237. D. Goyard, B. Roubinet, F. Vena, L. Landemarre and O. Renaudet, *ChemPlusChem*, 2022, **87**, e202100481.

238. M. González-Cuesta, D. Goyard, E. Nanba, K. Higaki, J. M. G. Fernández, O. Renaudet and C. O. Mellet, *Chemical Communications*, 2019, **55**, 12845-12848.

239. L. Siukstaite, F. Rosato, A. Mitrovic, P. F. Müller, K. Kraus, S. Notova, A. Imberty and W. Römer, *Toxins*, 2021, **13**, 792.

240. N. H. Rustmeier, M. Strebl and T. Stehle, *Viruses*, 2019, **11**, 947.

241. M. I. García-Moreno, F. Ortega-Caballero, R. Rísquez-Cuadro, C. Ortiz Mellet and J. M. Garcia Fernandez, *Chemistry–A European Journal*, 2017, **23**, 6295-6304.

242. P. C. Weber, D. H. Ohlendorf, J. Wendoloski and F. Salemme, *Science*, 1989, **243**, 85-88.

243. M. Wilchek and E. A. Bayer, *Methods in enzymology*, 1990, **184**, 5-13.

244. B. Lundt, N. Johansen and J. Markussen, *International Journal of Peptide and Protein Research*, 1979, **14**, 344-346.

245. M. Hecker, M. S. H. Ting and J. Malmström, *Coatings*, 2018, **8**, 55.

246. E. Bos, A. Van der Doelen, N. v. Rooy and A. H. Schuurs, *Journal of Immunoassay and Immunochemistry*, 1981, **2**, 187-204.

247. G. E. Norris, T. J. Stillman, B. F. Anderson and E. N. Baker, *Structure*, 1994, **2**, 1049-1059.

248. A. L. Tarentino and T. H. Plummer Jr, in *Methods in enzymology*, Elsevier, 1994, vol. 230, pp. 44-57.

249. A. L. Tarentino, T. H. Plummer Jr and F. Maley, *Journal of Biological Chemistry*, 1974, **249**, 818-824.

250. A. K. H. Mirja Hartmann, Per Klemm, Thisbe K. Lindhorst, *Chemical Communications*, 2010, **46**, 330-332.

251. M. Gómez-García, J. M. Benito, D. Rodríguez-Lucena, J.-X. Yu, K. Chmurski, C. Ortiz Mellet, R. Gutiérrez Gallego, A. Maestre, J. Defaye and J. M. García Fernández, *Journal of the American Chemical Society*, 2005, **127**, 7970-7971.

252. S. P. Vincent, K. Buffet, I. Nierengarten, A. Imberty and J. F. Nierengarten, *Chemistry–A European Journal*, 2016, **22**, 88-92.

253. D. Goyard, B. Thomas, E. Gillon, A. Imberty and O. Renaudet, *Frontiers in chemistry*, 2019, **7**, 666.

254. S. M. Banik, K. Pedram, S. Wisnovsky, G. Ahn, N. M. Riley and C. R. Bertozzi, *Nature*, 2020, **584**, 291-297.

255. J. Paulk, *Nature chemical biology*, 2021, **17**, 931-933.

256. G. Ahn, S. M. Banik, C. L. Miller, N. M. Riley, J. R. Cochran and C. R. Bertozzi, *Nature Chemical Biology*, 2021, **17**, 937-946.

257. D. F. Caianiello, M. Zhang, J. D. Ray, R. A. Howell, J. C. Swartzel, E. M. Branham, E. Chirkin, V. R. Sabbasani, A. Z. Gong and D. M. McDonald, *Nature Chemical Biology*, 2021, **17**, 947-953.

258. Y. Zhou, P. Teng, N. T. Montgomery, X. Li and W. Tang, *ACS Central Science*, 2021, **7**, 499-506.

259. A. Siriwardena, M. Khanal, A. Barras, O. Bande, T. Mena-Barragán, C. O. Mellet, J. M. Garcia Fernández, R. Boukherroub and S. Szunerits, *RSC Advances*, 2015, **5**, 100568-100578.

260. M. Baier, N. H. Rustmeier, J. Harr, N. Cyrus, G. J. Reiss, A. Grafmüller, B. S. Blaum, T. Stehle and L. Hartmann, *Macromolecular Bioscience*, 2019, **19**, 1800426.

261. B. K. Chacko and P. Appukuttan, *International journal of biological macromolecules*, 2001, **28**, 365-371.

262. R. Ravishankar, K. Suguna, A. Surolia and M. Vijayan, *Acta Crystallographica Section D*, 1999, **55**, 1375-1382.

263. M. Almant, A. Mastouri, L. Gallego-Yerga, J. M. Garcia Fernandez, C. Ortiz Mellet, J. Kovensky, S. Morandat, K. El Kirat and S. G. Gouin, *Chemistry–A European Journal*, 2013, **19**, 729-738.

264. M. Ambrosi, N. R. Cameron, B. G. Davis and S. Stolnik, *Organic & biomolecular chemistry*, 2005, **3**, 1476-1480.

265. D. K. Mandal, N. Kishore and C. F. Brewer, *Biochemistry*, 1994, **33**, 1149-1156.

266. B. N. Murthy, S. Sinha, A. Surolia, S. S. Indi and N. Jayaraman, *Glycoconjugate Journal*, 2008, **25**, 313-321.

267. F. P. Schwarz, K. D. Puri, R. Bhat and A. Surolia, *Journal of Biological Chemistry*, 1993, **268**, 7668-7677.

268. P. K. Smith, R. I. Krohn, G. T. Hermanson, A. K. Mallia, F. H. Gartner, M. D. Provenzano, E. K. Fujimoto, N. M. Goeke, B. J. Olson and D. C. Klenk, *Analytical Biochemistry*, 1985, **150**, 76-85.

269. E. Johansson, R. Caraballo, N. Mistry, G. Zocher, W. Qian, C. D. Andersson, D. L. Hurdiss, N. Chandra, R. Thompson and L. Frängsmyr, *ACS Chemical Biology*, 2020, **15**, 2683-2691.

270. E. Johansson, R. Caraballo, D. L. Hurdiss, N. Mistry, C. D. Andersson, R. F. Thompson, N. A. Ranson, G. Zocher, T. Stehle and N. Arnberg, *International Journal of Molecular Sciences*, 2021, **22**, 8418.

271. R. Caraballo, M. Saleeb, J. Bauer, A. M. Liaci, N. Chandra, R. J. Storm, L. Frängsmyr, W. Qian, T. Stehle and N. Arnberg, *Organic & biomolecular chemistry*, 2015, **13**, 9194-9205.

272. W. Lu, W. Du, V. J. Somovilla, G. Yu, D. Haksar, E. de Vries, G.-J. Boons, R. P. de Vries, C. A. de Haan and R. J. Pieters, *Journal of Medicinal Chemistry*, 2019, **62**, 6398-6404.

273. S. Spjut, W. Qian, J. Bauer, R. Storm, L. Frängsmyr, T. Stehle, N. Arnberg and M. Elofsson, *Angewandte Chemie*, 2011, **123**, 6649-6651.

274. P. B. Konietzny, J. Freytag, M. I. Feldhof, J. C. Müller, D. Ohl, T. Stehle and L. Hartmann, *Biomacromolecules*, 2022, **23**, 5273-5284.

275. K. Iwamoto, K. Araki and S. Shinkai, *The Journal of Organic Chemistry*, 1991, **56**, 4955-4962.

276. K. Iwamoto, H. Shimizu, K. Araki and S. Shinkai, *Journal of the American Chemical Society*, 1993, **115**, 3997-4006.

277. O. Mogck, M. Pons, V. Böhmer and W. Vogt, *Journal of the American Chemical Society*, 1997, **119**, 5706-5712.

278. M. Baier, M. Giesler and L. Hartmann, *Chemistry–A European Journal*, 2018, **24**, 1619-1630.

279. P. Rodriguez, B. Maggio and F. Cumar, *Journal of lipid research*, 1996, **37**, 382-390.

280. A. Neuberger and W. A. Ratcliffe, *Biochemical Journal*, 1973, **133**, 623-628.

281. S. Boden, F. Reise, J. Kania, T. K. Lindhorst and L. Hartmann, *Macromolecular Bioscience*, 2019, **19**, 1800425.

282. X. Wang, O. Ramstrom and M. Yan, *Analytical chemistry*, 2010, **82**, 9082-9089.

283. L. Wu and N. S. Sampson, *ACS chemical biology*, 2014, **9**, 468-475.

284. D. Garozzo, G. Gattuso, A. Notti, A. Pappalardo, S. Pappalardo, M. Parisi, M. Perez and I. Pisagatti, *ANGEWANDTE CHEMIE. INTERNATIONAL EDITION*, 2005, **44**, 4892-4896.